



ScuDo

Scuola di Dottorato ~ Doctoral School

WHAT YOU ARE, TAKES YOU FAR

Doctoral Dissertation

Doctoral Program in Mechanical Engineering (29th cycle)

ISWEC toward the sea

Development, Optimization and Testing of the Device

Control Architecture

By

Giacomo Vissio

Supervisor(s):

Prof. Giuliana Mattiazzo

Doctoral Examination Committee:

Prof. Carlos Goedes Soares, Referee, Instituto Superior Tecnico (Portugal)

Prof. John Ringwood, Referee, Maynooth University (Ireland)

Prof. Domenico Coiro, Università degli Studi di Napoli Federico II (Italy)

Prof. Stefano Mauro, Politecnico di Torino (Italy)

Prof. Massimo Sorli, Politecnico di Torino (Italy)

Politecnico di Torino

2017

Declaration

I hereby declare that, the contents and organization of this dissertation constitute my own original work and does not compromise in any way the rights of third parties, including those relating to the security of personal data.

Giacomo Vissio
2017

* This dissertation is presented in partial fulfillment of the requirements for **Ph.D. degree** in the Graduate School of Politecnico di Torino (ScuDo).

*A mio padre e mia madre,
a mio fratello, Giulia e Agnese,
alla mia famiglia,
a Chiara,
a tutte le persone con cui ho condiviso almeno in parte questi splendidi anni,
agli incontri ed al futuro,
alla Vita.*

Acknowledgements

I would like to acknowledge Professor Giuliana Mattiazzo for the great opportunities I received, the experiences I had and the numerous talks together during these four years. Professor Ermanno Giorcelli for his simplicity and hard work attitude. Vincenzo Orlando and Mattia Rafferero for their supervision and the time they spent teaching and sharing with me different but fundamental approaches to the engineering subjects. Giovanni Bracco for his work for the group. The whole ISWEC team, without which this work would not have been possible. Biagio Passione with whom I shared my entire journey. Michele Martini for the short but valuable time spent together. The electric engineer of the group Calogero Di Carlo and the mechanical engineer Maurizio Ponzetta for the numerous technical discussion and for everything we shared. Then Ennio Prudentino for its M.Sc. dissertation and the work we did about the MPC and Antonello Sirigu for the time we spent inside and outside the university. Nicola Pozzi for his enthusiasm and love for engineering and Vito Calamusa for his serious work dedication. Andrea Gulisano for the last year collaborations. For all the other numerous people I met during this exciting, dense, challenging itinerary.

Special thanks must be paid also to Professor Duarte Valério of the Instituto Superior Técnico de Lisboa (Portugal). His knowledge and supervision has been fundamental in the application of optimal control theory to the ISWEC.

Abstract

The work performed in this thesis is part of the ISWEC project. This is a floating device devoted to the conversion of the kinetic energy owned by the sea waves. The passage between a technology readiness level (TRL) of 4 up to a TRL of 6 is covered. The existing numerical model has been revised, validated and upgraded. The experimental data used come both from previous collected data and both from the one gathered during a MARINET founded project in Hydraulics and Maritime Research Center (HMRC) in Cork, Ireland (2014). During the last year also the data coming from the full scale experiments in Pantelleria, Italy, (2015) has been processed. The design and implementation of the device Supervisory Control And Data Acquisition system has been a relevant part of the doctorate activities. Several power harvesting control strategies for the ISWEC have been investigated and their productivity for the Pantelleria installation site computed. A comparison is presented. Some preliminary results of the 2015 experimental campaign are presented and a first comparison with the data obtained with the numerical models has been carried on.

Contents

List of Figures	xi
List of Tables	xviii
1 Introduction	1
1.1 Environmental Threats and Renewable Energies	1
1.2 Ocean Energy	3
1.3 Wave Energy	5
1.4 ISWEC	10
1.4.1 Introduction and main features	10
1.4.2 ISWEC Project history	12
1.5 Contents of the Thesis and Candidate Role in the ISWEC Project . . .	19
1.6 Candidate publications	22
2 Modeling	24
2.1 Reference frames and definitions	24
2.2 Gyroscope system	26
2.3 Electro-Mechanical Power Losses	29
2.3.1 Flywheel shaft bearings	29
2.3.2 Flywheel shaft seals	29
2.3.3 Flywheel fluidodynamic friction	30
2.3.3.1 In housing configuration	31
2.3.3.2 Free configuration	32
2.3.4 Electric motor and drive efficiency	33
2.4 Hydrodynamics	36
2.4.1 Linear Cummins equation	37
2.4.2 Viscous Terms	40

2.4.3	Drift forces	41
2.4.4	Mooring system Terms	43
2.5	Hydrodynamics - 1:20 Tank Testing	44
2.5.1	Experimental tests plan	46
2.5.2	Single Degree of freedom tests	48
2.5.3	Floating moored device tests	51
2.5.4	Quadratic viscous term	53
2.6	ISWEC - Pitch DOF model	55
2.6.1	Motivations	55
2.6.2	Time Domain Model	56
2.6.3	Frequency Domain Model	57
2.6.4	State Space Pitch DOF linear model	57
2.6.5	Power Losses	59
2.7	ISWEC - Frequency Domain 6 DOF Linear Model	59
2.7.1	Hydrodynamics	59
2.7.2	Gyroscope system	63
2.7.3	ISWEC 6 DOF state space	64
2.8	ISWEC - Numerical Wave to Wire model	66
2.8.1	The Block Diagram	66
2.8.2	Time History Example	75
3	ISWEC device design	78
3.1	Installation site - Pantelleria wave resource	79
3.1.1	Irregular waves description	79
3.1.2	Occurrences scatter table	80
3.1.3	Energy scatter table	80
3.1.4	Directionality	82
3.2	The pre-design nominal sea state	86
3.2.1	The selection procedure	86
3.2.2	Examples	92
3.2.3	2013. The device pre-design wave.	97
3.2.4	2016. A novel pre-design wave.	98
3.3	Pre-design	100
3.3.1	The floater	100
3.3.2	The iso-energetic regular wave	102

3.3.3	The gyroscope system	102
3.3.3.1	The overall angular momentum	102
3.3.3.2	The flywheel size	104
3.3.3.3	The number of gyroscope units	106
3.3.4	The Power Take Off	108
3.3.5	The Bearings	109
3.3.6	The Ultracapacitors	110
3.4	Frequency Domain Analysis	112
3.5	ISWEC design tool	115
3.5.1	The Algorithm	115
3.5.2	Cost function	117
3.5.3	User Interface	120
3.5.4	Example of analysis	120
3.6	Model-Based Optimization	125
4	ISWEC Pantelleria device	127
4.1	Introduction	127
4.2	The Floater	127
4.3	The Mooring System	133
4.4	The Gyroscope	135
4.5	The PTO	142
4.6	The Electric System	143
4.7	The Cooling System	148
5	The SCADA system	151
5.1	Introduction	151
5.2	The SCADA architecture	151
5.3	State Machine and Automatic Operations	154
5.4	PTO electric motor control	156
5.5	Automatic Management	157
5.6	Human Machine Interface	159
5.7	Safety Control	161
5.8	Forecasts	163
6	Power Absorption Control	164
6.1	Introduction	164

6.1.1	Different Time Levels	164
6.1.2	Online control - Specifications	165
6.1.3	Online control - Classification	167
6.2	Proportional Derivative (PD) Control	169
6.2.1	Results - Time History Example	170
6.3	Model Free strategies	172
6.3.1	Oscillating control	172
6.3.1.1	Results - Time History Example	176
6.3.2	Continuous Rotation control	177
6.3.2.1	Results - Time History Example	178
6.4	The problem of control objective	180
6.5	Model Based strategies: Optimal Control	181
6.5.1	Time Varying Linear Quadratic Regulator and Known Distur- bance	181
6.5.2	Oscillating Linear Quadratic Regulator	185
6.5.2.1	Linear Quadratic Regulator	185
6.5.2.2	Objective function parameters design	186
6.5.2.3	Gain Scheduling	188
6.5.2.4	Results - Time History Example	190
6.5.2.5	Results - The effect of power weight	192
6.5.3	Continuous Rotation Linear Quadratic Integral Control	197
6.5.3.1	Linear Quadratic Integral Control	197
6.5.3.2	Anti Wind-Up technique	200
6.5.3.3	Gain Scheduling	200
6.5.3.4	Results - Time History Example	201
6.5.3.5	Results - The effect of power weight	202
6.6	Power Production Comparison	206
6.6.1	Optimization via Time Domain simulations	206
6.6.2	Results - Net Power optimization	209
6.6.3	Results - Gross Power Optimization	211
6.7	Conclusions	213
7	Experimental Campaign: 2015	215
7.1	Introduction	215
7.2	The installation progress	215

7.3	Experimental data	216
7.4	Validation	220
7.4.1	Controller and PTO	220
7.4.2	Mechanics	224
7.4.3	Hydrodynamics	226
7.4.4	Wave To Mechanical Power	232
7.5	Final Comments	235
8	Conclusions	236
	Bibliography	239

List of Figures

1.1	Proposal of Wave Energy Converter concepts classification.	7
1.2	ISWEC prototype and installation drawings.	11
1.3	Pantelleria, Italy, 2015. ISWEC installed prototype in operation. . . .	12
1.4	ISWEC first concept. Two degree of freedom gyroscopic system. . . .	13
1.5	Wave Energy Converter development diagram [50].	14
1.6	ISWEC prototype, 1:45 scale for Alghero site.	15
1.7	ISWEC prototype, 1:8 scale for Pantelleria site. Rome INSEAN wave tank.	17
1.8	ISWEC project stages according to OES:IA Document n°T02-0.0 . . .	18
2.1	The ISWEC floater and gyroscopic system reference frames	25
2.2	Flywheels simplified geometries for the fluidodynamic losses computation.	31
2.3	PTO efficiency map computation numerical model.	34
2.4	PTO efficiency map computation. Example of time domain simulation. . .	35
2.5	PTO efficiency map.	35
2.6	PTO losses map.	36
2.7	Mesh and example of analysis of the ISWEC floater in ANSYS® AQWA® environment.	38
2.8	Wave drift force for irregular waves. Wave envelope. [42]	42
2.9	ISWEC prototype, bow mooring system architecture.	43
2.10	ISWEC prototype, bow mooring system load vs displacement characteristic.	44
2.11	Hydrodynamics Tank Tests. Hydraulics and Maritime Research Centre, University College Cork, city of Cork, Ireland, 2014.	45
2.12	Tank Tests. 1 DOF Test Rig configurations.	45

2.13 Hydrodynamics Tank Tests. Conceptual scheme of the three test rig configurations. From left to right it is possible to see that the allowed DoFs are surge, heave, pitch.	48
2.14 Hydrodynamics Tank Tests. Pitch and Heave test rig installed in HMRC tank in Cork (Ireland), 2014.	49
2.15 Hydrodynamics Tank Tests. Time histories examples. Phase 2: pitch excitation and radiation tests.	50
2.16 Hydrodynamics Tank Tests. Time histories examples. Phase 2: pitch stiffness and uncontrolled tests.	51
2.17 Hydrodynamics Tank Tests. Floater moored to the tank floor. 6 DOF analysis.	52
2.18 Tank Tests. ISWEC 1:20 scale, design and prototype during assembly.	52
2.19 Hydrodynamics Tank Tests. Floating 6 DOF moored system. Comparison between experimental and numerical results. The Cummins fully linear model and the upgraded model are used.	54
2.20 Viscous quadratic term linearization.	61
2.21 Floater pitch RAO. Comparison RAO with and without linearized viscous forces.	62
2.22 Example of regular waves Frequency Domain Analysis performed with the state space model.	65
2.23 Numerical model - Main block diagram	68
2.24 Numerical model - Subsystem: "WAVES"	69
2.25 Numerical model - Subsystem: "FLOATER 3 DOFs"	69
2.26 Numerical model - Subsystem: "GYRO 1"	70
2.27 Numerical model - Subsystem: "Save Variables 1 Gyro"	71
2.28 Numerical model - Subsystem: "PD - Power Generation"	72
2.29 Numerical model - System Controller	73
2.30 Numerical model - Position Control Loop	74
2.31 Numerical model - Time history example - Figure A	76
2.32 Numerical model - Time history example - Figure B	77
3.1 Pantelleria occurrences scatter table (2010).	81
3.2 Pantelleria energy scatter table (2010)	82
3.3 Pantelleria installation site. Latitude $36^{\circ} 50' 2.52''$, Longitude $11^{\circ} 55' 50.40''$. Satellite view. [47]	83

3.4	Mediterranean Sea. ENEA UTMEA group. Pantelleria is highlighted by the green star. https://giotto.casaccia.enea.it/waves/ (Accessed: 06/07/2017).	83
3.5	Pantelleria directional occurrences. Period: February 2015 - February 2016.	84
3.6	Pantelleria directional power density. Period: February 2015 - February 2016.	85
3.7	Pantelleria directional energy. Period: February 2015 - February 2016.	85
3.8	Capacity factor of common generating technologies in the European Union. Source: EurElectric.	87
3.9	Pantelleria occurrences scatter table (2010). Most occurrent sea state.	88
3.10	Pantelleria energy scatter table (2010). Most energetic sea state. . . .	88
3.11	Pantelleria scatter tables (2010). Most occurrent sea state. Surrounding elliptic area analysis.	89
3.12	Pantelleria scatter tables (2010). Most energetic sea state. Surrounding elliptic area analysis.	89
3.13	Pantelleria energy scatter table (2010). Prototype 2013 predesign sea state. Surrounding elliptic area analysis.	90
3.14	Pantelleria energy scatter tables (2010). Surrounding elliptic area analysis, synthetic results: occurrences and energy.	90
3.15	Pantelleria energy scatter tables (2010). Surrounding elliptic area analysis, synthetic results: occurrences and energy. 20 kW ISWEC predesign: wave choice.	93
3.16	Pantelleria energy scatter tables (2010). Surrounding elliptic area analysis, synthetic results: occurrences and energy. 100 kW ISWEC predesign: wave choice.	95
3.17	Pantelleria energy scatter tables (2010). Surrounding elliptic area analysis, synthetic results: occurrences and energy. 60 kW ISWEC predesign: wave choice.	98
3.18	Floater main dimensions: width and length.	101
3.19	Floater longitudinal dimension and wave length.	101
3.20	Flywheel simplified geometry. Definition of parameters.	105
3.21	Poter Take Off system. Notation.	108
3.22	Frequency domain floater hydrodynamic analysis.	112

3.23	Frequency domain floater hydrodynamic analysis with gyro units. Flywheel at different speeds analysis.	113
3.24	Frequency domain ISWEC theoretical power production. Flywheel at different speeds analysis.	114
3.25	ISWEC design tool - Main functional Scheme	117
3.26	ISWEC design tool - Cost function constraining i^{th} element equation.	119
3.27	ISWEC design tool - Graphical User Interface (GUI).	120
3.28	ISWEC design tool - Example - Results of the analysis.	122
3.29	ISWEC design tool - Example of parametric study - Case A.	123
3.30	ISWEC design tool - Example of parametric study - Case B.	124
3.31	Wave to wire lumped parameters numerical model.	125
3.32	ISWEC Pantelleria 2015 - Control parameters matrices.	126
4.1	The floater final design. Side view.	128
4.2	The floater final design. Top view.	128
4.3	Floater dynamic response. The pitch RAO with fully linear BEM modeling approach.	129
4.4	The floater in the shipyard.	130
4.5	The floater: first gyroscope group installation.	131
4.6	The floater: launch and ballast filling operations.	132
4.7	The floater: mooring prow connection. Hawses design.	133
4.8	The mooring system: Pantelleria architecture scheme.	133
4.9	The mooring system: Pantelleria architecture scheme.	134
4.10	The gyroscope: flywheel design section.	136
4.11	The gyroscope: section of the first unit.	137
4.12	The gyroscope: assembly of the first unit.	138
4.13	The gyroscope: flywheel motor.	139
4.14	The gyroscope: flywheel bearings configuration.	140
4.15	The gyroscope: flywheel bearings lubricating system.	141
4.16	The gyroscope: flywheel lubricating system, oil recovery pump and rotary hydraulic joint.	141
4.17	The PTO: setup of the first unit in A.R.I.S.	143
4.18	The electric system: concept scheme.	144
4.19	The electric system: pictures of components during the SETUP.	147
4.20	The cooling system: scheme.	149

4.21	The cooling system: the group in A.R.I.S.	150
5.1	Overall SCADA system architecture.	152
5.2	Control Hardware. Components directly linked to the power conversion.	153
5.3	The ISWEC state machine.	155
5.4	Auxiliary position control loop.	157
5.5	Automatic power production operations and safety state. Flow diagram.	158
5.6	ISWEC Full Scale device. Automatic safety procedure.	158
5.7	SCADA system. Information and DATA flow diagram.	160
5.8	SCADA system. User Interface.	160
5.9	Safety control. The control architecture.	161
5.10	Safety control. The static nonlinear term in function of PTO speed.	162
5.11	Forecasts. An example of study applied to Pantelleria and the received tabulated data.	163
6.1	A proposal of control strategies classification.	168
6.2	Proportional Derivative (PD) control. Simple torque set generation scheme.	169
6.3	PD control. Time history example.	171
6.4	DeltaRef control. General architecture.	175
6.5	DeltaRef control. Time history example.	176
6.6	SpeedRef control. General architecture.	177
6.7	SpeedRef control. Time history example.	179
6.8	Optimal control with known wave disturbance. Time history example.	184
6.9	Overall LQR architecture	187
6.10	Gyroscope at different angular position for gain scheduling.	189
6.11	Interpolation method for j -th element k_j at generic position ε in the interval $[\varepsilon_i, \varepsilon_{i+1}]$ subsequent linearization points	190
6.12	LQR control. Time history example.	191
6.13	Time histories. Effect of K_N . Wave elevation and internal precession gyroscope frame axis position.	193
6.14	Time histories. Effect of K_N . Dimensionless scaled wave force, pitch rotational speed and internal precession gyroscope frame axis speed.	194
6.15	Time histories. Effect of K_N . Dimensionless scaled PTO torque and mechanical power.	195

6.16	Effect of K_N . Dimensionless scaled mean torque power in function of changing K_N	196
6.17	Effect of K_N . RMS of pitch in function of changing K_N	196
6.18	Overall LQI architecture	199
6.19	Anti Windup Strategy scheme	200
6.20	LQI control. Time history example.	201
6.21	Time histories. Effect of K_N . Floater pitch and internal precession gyroscope frame axis speed.	203
6.22	Time histories. Effect of K_N . Dimensionless scaled scaled PTO torque and mechanical power.	204
6.23	Time histories. Effect of K_N . Wave force and floater pitch angular rate.	205
6.24	Pantelleria. Italy. Occurrences and energy scatter table for 2010. Selected wave states for the comparison.	207
6.25	Adimensionalised mean net adsorbed power. Sea states describing Pantelleria site.	209
6.26	Adimensionalised mean bearing losses. Sea states describing Pantelleria site.	210
6.27	Adimensionalised mean PTO losses. Sea states describing Pantelleria site.	210
6.28	Adimensionalised PTO torque RMS. Sea states describing Pantelleria site.	210
6.29	Adimensionalized mean gross adsorbed power. Sea states describing Pantelleria site.	211
6.30	Adimensionalized mean bearing losses. Sea states describing Pantelleria site.	212
6.31	Adimensionalized mean PTO losses. Sea states describing Pantelleria site.	212
6.32	Adimensionalized PTO torque RMS. Sea states describing Pantelleria site.	212
6.33	Control strategies comparison. Productivity.	213
6.34	Control strategies comparison. Number of free parameters.	214
6.35	Control strategies comparison. Robustness against modeling and forecasts errors.	214

7.1	Experimental data. Pantelleria. Example of the floater kinematics with conversion system off.	217
7.2	Experimental data. Pantelleria. Example of the floater and conversion system behaviour.	219
7.3	Experimental data. Pantelleria. Example of the floater and conversion system behaviour.	220
7.4	Experimental data. Pantelleria. Example of the floater and conversion system behaviour.	221
7.5	Experimental data. Pantelleria. Experimental and simulation comparison. Over-voltage protection system effect.	223
7.6	Experimental data. Pantelleria. Example of the floater and conversion system behaviour.	224
7.7	Electro-mechanical system validation. Single wave internal system quantities comparison. Time histories.	225
7.8	Electro-mechanical system validation. Data Set synthetic results.	226
7.9	ISWEC sea environment installation. The wave incoming front force is predominating. The planar hypothesis are verified. Site: Pantelleria - Time 15:22 - Date: 2015.11.30	230
7.10	ISWEC sea environment installation. The wave incoming front force is predominating. The planar hypothesis are verified. Site: Pantelleria - Time 14:22 - Date: 2015.11.21	231
7.11	A proposed aft mooring architecture for solving the issues of misalignment in an high directional site.	231
7.12	Results of the wave to power comparison. Electro-mechanical system quantities and power.	234

List of Tables

1.1	Global renewable electric power installed capacity, 2016 [88].	3
1.2	Ocean Energy global potential resources.	5
2.1	Hull-fixed FCS notation	25
2.2	Gyroscope structure-fixed GCS notation	26
2.3	In housing configuration, axial friction momentum.	32
2.4	In housing configuration, plates transversal friction momentum.	32
2.5	Free configuration, transversal friction momentum.	33
2.6	Hydrodynamics Tank Tests. Full scale and scale prototype main physical parameters.	45
2.7	Comparison between different models and experimental data for irregular sea state.	62
3.1	Maximum allowable circumferential stress of some construction materials.	106
3.2	Maximum allowable peripheral speed of some construction materials.	106
3.3	Example of signs of torques exchanged by a couple of gyros and the floater.	107
3.4	ISWEC design tool - Example - Parameters setting	121
3.5	ISWEC design tool - Example - Optimization space definition.	121
3.6	PTO configurations	123
4.1	Floater properties	129
4.2	The floater: mass distribution.	131
4.3	The moorings system: parameters.	135
4.4	Flywheel properties	136
4.5	Flywheel motor, SIEMENS 1FW3154-1BP.	139
4.6	Generator, SIEMENS 1FW3285-2E.	142

6.1	Selected wave state for comparison.	206
7.1	All the logged data and system parameters.	216
7.2	Pantelleria. Experimental and simulated comparison. 25 th November 2015. Average power fluxes of [240 260] s range.	222
7.3	Electro-mechanical system validation. Single wave internal system quantities comparison (Site: Pantelleria - Time 16:03 - Day 2015.11.28). Synthetic results.	226
7.4	Data set used for a first hydrodynamic comparison between experimental and numeric data. Site: Pantelleria, Year: 2015.	228
7.5	Results of the hydrodynamic comparison between experimental and numeric data. Site: Pantelleria, Year: 2015.	229
7.6	Data set used for a first wave to mechanical power comparison between experimental and numerical data. Site: Pantelleria, Year:2015.	232
7.7	Results of the wave to power comparison. Floater hydrodynamic quantities.	233
7.8	Results of the wave to power comparison. Electro-mechanical system quantities and power.	233

Chapter 1

Introduction

1.1 Environmental Threats and Renewable Energies

The thirst of energy of the modern World [54] combined with the climate change threat [30, 94] is one of the contemporary greatest challenges for humanity. The causes of the global warming phenomenon are widely recognized and shared among the scientific community [29, 69]. In particular, the current global warming trend is found to be related with intense human consumption of fossil fuels, being used as primary energy source for different activities such as industrial production, goods and people transportation and electricity generation. In fact the combustion of fossil fuels causes the emission of several gases, carbon dioxide and methane among the others. These gases, once released in the atmosphere, increase the Earth natural greenhouse effect, thus generating an anthropic-led, uncontrolled and unpredictable increase of our planet surface temperatures. The situation is worsen by the developing countries -eager of Western comfort and consumerism-, and by others large scale human actions against the environment, amongst which an important role has the forests clearing. All these facts heavily disturb world environment equilibrium.

In 1992 the International Community, aware of this problem, shared the United Nations Framework Convention on Climate Change (UNFCCC), an international treaty that recognizes the "anthropogenic interference with the climate system" [98] and in which the signatory States commit themselves in reducing greenhouse gas emissions. Some years later, in 1997, the Kyoto Protocol quantitatively stated the objectives of gases emission reduction for each single State [99]. Nowadays these agreements are in force and regulate and point the objectives for the 2020 time horizon. For what concern the post 2020 time frame, the 2015 Paris climate agreement is and will be the reference

for the actions that the countries are going to undertake. All these agreements plan the reduction of fossil fuels utilization through the improvement of buildings and processes efficiency and the utilization of alternative, renewable, energy sources.

As suggested by Sørensen [92], a large part of the human history has been characterized by renewable energy sources: at first the power provided by humans and animals, and then the technical solutions realized exploiting flowing water and wind. When the industrial revolution begun, fossil fuels started to be massively exploited. These are classified as non-renewables because their regenerating time is much longer than the time the humanity takes to run them out. It is estimated that the time needed for carbon formation is million of years. Fossil fuels led to the extraordinary technology development that characterized the last two centuries and brought prosperity to industrialized countries population. Although the combustion engines polluting action has always been clear, the possibilities given by this technology were immediately understood. It was during the Seventies of the XX^{th} Century, before the environmental costs of oil became evident, that another of the major drawbacks of this resource appeared clear. It was with the 1973-1974 Middle East War crisis and the following oil embargo. Europe faced the lack of oil and gas rationing. The fragility of an economic system completely based on fossil fuels appeared clear: the whole society was completely dependent on a single technology managed by very few major players. After this experience OECD States decided to establish the International Energy Agency (IEA), an organization devoted to foster international co-operation, energy sources diversification and long-term policy development related to energy themes. The quest for alternatives to fossil fuels fostered the research about new ways for producing energy, both looking at old technologies, e.g. the wind turbines or geothermal energy, and venturing in new fields like the untapped oceans resources, e.g. waves and currents. The modern interest to renewable energy sources was main subject of numerous initiatives, both public and private. Several years of development, industrialization and commercialization of these technologies followed, creating a fast-growing industrial field. In 2004 REN21 was founded, the *Renewable Energy Policy Network for the 21st Century*. Its main aim is to coordinate and speed up the transition to a carbon-free society, powered by renewable energies. According to their 2017 annual report [88], the total renewable power capacity in 2016 was equal to 2,017GW, with an increase with respect to the previous year of 161.4GW. In Table 1.1 the 2016 total installed capacity per each technology is presented. Renewable energy sources could provide several times the present world demand [97]. In 2014 the overall renewable energies sources (hydroelectric included)

Table 1.1 Global renewable electric power installed capacity, 2016 [88].

Technology	Installed Capacity [GW]
Bio-power	112
Geothermal power	13.5
Hydropower	1,096
Ocean power	0.5
Solar PV	303
Concentrating solar thermal power (CSP)	4.8
Wind power	487
Total Renewable power capacity	2,017

produced in total the 22.8% of the 23,480 TWh world electricity production [27].

Apart from the more mature hydropower, extensively widespread around the world, among these renewables wind turbines and solar Photo Voltaic panels are the most developed and diffused. In particular, the case of wind is particularly interesting, since its development started just after the oil-crisis period like the wave power and its development path has been difficult and not straight-forward, similarly to ocean energy technologies. Nonetheless, after years of research it rightfully entered in the energy mix as a reliable and cost-effective source of clean energy.

Wave energy also started in the Seventies, but on completely different and unexplored basis. It was in fact the first time that the human beings were starting to develop serious efforts for harvesting it. The path to become part of the renewable energies mix has been difficult and it is not yet completed, but it also confirms a slow, steady development, revealing the potentialities of the exploitation of this untapped resource.

1.2 Ocean Energy

Among alternative energy resources, Oceans represent a vast, predictable and renewable potential. Moreover they are well distributed across the earth, since the 70% of our planet surface is covered by water and roughly the 44% of the world population lives within 150 kilometers from the coasts [95].

The increased activity in the ocean technologies field at the end of the XXth Century led to the foundation in 2001 of the Ocean Energy Systems Technology Collaboration Programme (OES), an intergovernmental agency established by the International Energy Agency (IEA) and initially signed by three active countries: Denmark, Portugal

and United Kingdom. Main aim of the organization was to coordinate countries in order to advance research, development and demonstration of all the ocean renewable conversion technologies. Every year the IEA-OES Annual Report contains the state of play of the technology development [23] and inform about the active and expected policies dedicated to the field.

In 2012 the European Commission published the Blue Growth communication [36], which contains definitions and indications about the opportunities for marine and a maritime sustainable growth. This document is in general transversely dedicated to all the activities related to sea and coasts economy, and an entire section is dedicated to the wider category of *Blue Energy*. Among these technologies a special mention to the offshore wind energy has to be done. Despite the numerous challenges that it shares with wave power, at the time of the writing this industrial field reached its first commercial installation: the 6 MW Hywind floating offshore wind farm in Scotland [57]. For what concern the Ocean Energies, in the Commission communication it is stated that the challenge is to *accelerate its path to commercialization*. In the following 2014 Blue Energy communication [38], the parallel with the successful offshore wind sector is drawn, and policies and vision for the field development are more deeply enunciated. The challenges that still need to be faced are nonetheless outlined, underlying in particular the technology cost, the electrical transmission grid infrastructure, the complex licensing and consenting procedures, the assessment of the environmental impacts and the lack of grant and revenue support due to the current economic climate.

All these interests and efforts are explained by the nature and size of the ocean resource and the fact that Europe is one of the best spots to harvest this energy. Even if it is difficult to quantify the potential of this resource and data from different authors varies considerably [60, 59, 58, 70, 48, 67], in Table 1.2 it is possible to find some ranges of exploitable potentials of the different physical forms of energy contained into the sea. Currently, the identified and studied technologies are wave, tidal and ocean currents, the emerging ocean thermal energy conversion and osmotic power (salinity gradient).

Tidal current energy is caused by the periodic gravitational pull of the moon and sun on the oceans' water. Tidal technology captures the kinetic energy of the water current motion in and out of the tidal areas. Common installations consist of submerged turbines lying on the seabed. Even if with a lower overall potential, it is more mature with respect to wave energy, and will likely contribute to the energy mix within the 2030 time horizon.

Table 1.2 Ocean Energy global potential resources.

Resource	Potential [TWh]
Tidal Energy	300 - 1,200
Marine Current Power	>800
Osmotic Power	2,000 - 5,177
Ocean Thermal Energy	10,000 - 85,000
Wave Energy	8,000-80,000

Ocean Thermal Energy Conversion (OTEC) exploits the temperature differential between sea warmer surface and cooler deep water. The heat extracted from the warm seawater is used to produce a vapor that acts as a working fluid for a turbine. On the other hand, the cold water is used to condense the vapor and ensure the pressure difference that drives the turbine. This heat cycle can be realized both in open and close architectures, and it can exploit different working fluids. The power plants can be land-based, moored to the sea-bed or floating.

Marine current energy is related to the oceans currents, where huge masses of water move below the sea surface. The technologies studied to exploit this motion converts the kinetic energy of the fluxes through axial turbines, analogously to wind energy.

Osmotic power, also called salinity gradient power, is the energy present in the difference of salt concentration between fresh and seawater. A common generation station is at the estuary of a river, where the fresh river water is used and then returns to the sea in the form of brackish water.

Another potential resource owned by oceans is that of the waves. Citing two works completely devoted to the wave energy resource [48, 67], the world wave average power resource should be in the range of 2 or 3 TW, meaning a theoretical available energy resource between 17,520 and 26,280 TWh. The relevance of this value is obtained when compared to the overall world energy consumption in 2014, equal to 159,320 TWh [88].

This noticeable value, also coupled with the zero land consumption, makes this resource interesting to be explored.

1.3 Wave Energy

The technology having as first aim to harvest the kinetic and potential energy owned by sea and ocean surface waves is called *wave energy*.

The first patent ever registered dates back to 1799, by a father and his son named Girard in France. Japanese Yoshio Masuda can be considered as the father of modern wave energy, given his studies started 1940s that brought to the development of floating oscillating water column solutions [39]. During the Seventies, in Europe, Kjell Budal and Stephen Salter pioneered this field in Norway and UK. In particular, a paper by Stephen Salter of the University of Edinburgh published in "Nature" in 1974 [83] is also usually regarded as an important milestone for the growth of the technology. In 1975 Budal and Falnes published on the same journal a paper introducing the concept of point absorbers wave energy converters [25]. As already mentioned in section 1.2, this was a first period of public interest for the research and development of this alternative energy, with funds guaranteed by UK, Sweden and Norway. Throughout 1980s, apart from two shoreline full-scale devices built in Norway, the activity in Europe predominantly remained at the academic level, with smaller prototypes being realized, mostly of the oscillating water column type. A lot of effort in this period was devoted to the development of different hydrodynamic modeling approaches, as basis for the design of the technology. In 1991 the situation changed, it was when the European Commission introduced wave energy in the R&D program on renewable energies. At that time already more than one thousand of different concepts and prototypes were already invented [41]. Under different funding frameworks the European Commission financed more than thirty projects, giving the spark that started the growth of several developing teams around Europe. Since then, a lot of innovative devices were developed and tested, both from university and from industrial players [67, 8], [104] that have enhanced the wave energy technology readiness level up to pre-commercialization levels.

More recently, the Department Of Energy (USA) and Wave Energy Scotland (UK) proposed grant programs with a competition based on a multiple-gate structure, with the aim of selecting the best technologies to enter the next funding step. This incremental funding scheme revealed to be effective to avoid the waste of public money and to assure that the money goes to the best teams/projects. These programmes fund R&D activities both about device sub-systems (PTO, control systems, materials) and for the development of novel WEC concepts.

Wind and hydroelectric power have reached a considerable convergence about the final conversion concept. This is a crucial point for the costs reduction and it is a sign of technology maturity. On the contrary, the number of different solutions for harvesting wave energy remains huge. At this time almost no convergence has been reached in

the sector. An introduction to the different solutions and possible classifications are presented in [34], [39], [67], [104] but also in [11],[78]. Starting from the previous sources, a matrix classification is proposed in Figure 1.1.

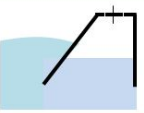
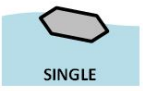
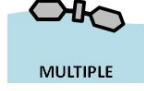
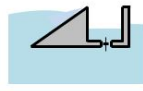
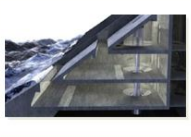
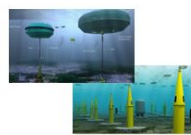
		PRIMARY CONVERSION WORKING PRINCIPLE			
		OWC	WAVE ACTIVATED BODY		OVERTOPPING
			 SINGLE	 MULTIPLE	
LOCATION	ONSHORE				
	NEARSHORE 10 - 25m deep				
	OFFSHORE > 40m deep				

Figure 1.1 Proposal of Wave Energy Converter concepts classification.

Starting from the top of the matrix, WECs can be classified using their primary conversion working principle. In this classification they are categorized in three groups: Oscillating Water Columns (OWC), wave activated body and overtopping devices.

Oscillating Water Columns (OWC) essential structure is a semi-submerged chamber open on the bottom to the sea. Following the waves' action, the enclosed water starts a vertical oscillating motion that pressurizes the air trapped above. An air flow is thus formed in the duct connecting this superior chamber to the outer environment. The power extraction happens by mean of an air turbine, usually of the Wells typology. Examples of installations of this type are the LIMPET, the installation in Mutriku, the OE buoy and the Sparbuoy-OWC.

Wave Activated Bodies (WAB) are all those WECs that have as first conversion chain a floating element that transforms the pressure and kinetic energy contained in waves into mechanical energy owned by the buoy. These are divided in those that have a single body acting against a fixed reference frame (shore, seabed or an internal inertial

system) or those that have a relative motion with respect to other floating elements. The Brazilian Research and Technological Development Program of the Brazilian ANEEL prototype, the Oyster, CETO and Seabased WEC S2.7 are part of the first group. Power Buoy, Langlee and the Pelamis can fit the second definition.

Overtopping devices are characterized by a water storage basin with a water level higher than the mean sea level. This is filled by waves filling in by overtopping the lateral reservoir walls. The captured water is then returned to the sea by a low-head hydraulic turbine. Different examples of this concept are the SeaWave Slot-Cone Generator (SSG), the WavePlane and the WaveDragon.

Another widespread classification, also based on the typology of the first absorption step, is the one differentiating the WECs relative size and direction in comparison with the incoming wave. This method divides the devices in three main branches: point absorbers, attenuators and terminators.

Point Absorbers (PA) have small dimensions in comparison with wavelength. They can thus be considered as points and can work independently to the wave direction.

Attenuators are characterized by structures with a relevant size in the longitudinal direction, parallel to the incoming wave. They generally work attenuating the amplitude of the waves going through them.

Terminators also have long structures and are usually placed parallel to the wave front direction, perpendicular to the predominant direction of the wave propagation.

Another straightforward method for classifying WECs is their deployment location. This classification gives information about availability, installation and operational costs and the kind of technology expertise involved.

Onshore devices can be located at the shore and mounted above the sea surface, integrated in civil infrastructures like a breakwater or a dam, fixed to a cliff. Advantages are reduced installation and maintenance costs, given the easy accessibility and the lack of mooring systems nor electric infrastructure. Disadvantages are that waves contain less energy and the high disruptive power of breaking waves during storms.

Nearshore devices are installed in water from 10 to 25 meters, in moderate water depths. They can be moored systems or directly fixed to the seabed.

Offshore devices are located in deep waters, with more than 40 meters of water depth. They are floaters or submerged structures moored to the seabed. Advantages are the higher power that they can access, on the other hand the distance from the coast

makes the electric grid infrastructure and every kind of operation, installation and maintenance, very expensive.

As presented, forty-years-old wave energy produced a great variety of devices and technology developments, forming a complete, wide, literature of papers, publications and industrial reports. An interesting history of this itinerary is presented in [39]. In the following some review papers from different subjects helpful for this work are cited.

A good theoretical introduction to wave energy converters modeling and control can be found in the classical book by Falnes: *Ocean Waves and Oscillating Systems* [40]. Other more recent works covering main fundamental topics are *Numerical Modelling of Wave Energy Conversion* [43] and *Ocean Wave Energy - Current Status and Future Perspectives*[31].

Given the oscillatory, dynamic, nature of the converters, appropriate control system architectures are fundamental for the maximization of the wave energy absorption. Extended overviews of different control techniques applied to different devices can be found in [82], [104], [51] and [61]. The correct phase between floater and waves can be obtained with latching and declutching techniques, applied to floating point absorber converters in [53],[5], [84] and[6]. The research of optimal absorption soon led to the need of knowing future waves elevation. Some paper addressing the problem of online estimation are [46], [71]. Optimal control has straightforward application in the field for its way of dealing with the objective function, as discussed in section 6.4. Its application with Model Predictive Control strategies, in order to deal with the motion and force constraints, is often proposed as a control method in wave energy conversion [49],[1],[86],[22],[19]. As a simplification, Linear Quadratic Regulator infinite-horizon, continuous-time forms are proposed by [87] and [56].

Reviews of hydrodynamic modeling of wave energy farms is in [33] and [66]. An analysis of electrical configurations and subsystems is presented in [89]. An example of the investigation over the effects caused by the presence of a farm over the sea resource is in [55]. The DTOcean (Design and Optimization Tool for Ocean Arrays) project [37], funded by the European Commission, aims at accelerating the industrial development of wave energy converters farms by the creation of tools dedicated to the design of wave energy converter arrays.

Concluding, nowadays full-scale demonstrator projects driven both by public [44] and private funding are trying to challenge the reduction of levelized cost of electricity generation (LCOE), in order to become a viable technology, economically sustainable and competitive with other energy sources. An updated description of the actual landscape can be found in [24] and [23].

The device object of this thesis, the ISWEC, is one of the technologies that are going to face this challenging mission.

1.4 ISWEC

1.4.1 Introduction and main features

The ISWEC, Inertial Sea Wave Energy Converter, is an offshore, single body, floating wave energy converter. A schematic of the concept is presented in Figure 1.2. It consists of a monolithic hull, with an inner equipment room completely sealed with respect to the outer ocean environment. In the internal volume two gyroscopic units are installed. Also the electric PTO and the power conditioning system are completely enclosed into the floater. The only component that have continuity from the inside out is the electric cable, following the idea of a "deploy and plug" device.

During the development of the ISWEC concept a key feature was the removal of any seal, joint or part in relative motion into the harsh sea environment. This perspective was adopted with the first aim of reducing problems related to corrosion and thus decrease maintenance expenses. This is believed to be an asset of this device and sea tests are expected to prove it.

In normal energy production operation mode the device is aligned with the wavefront direction and the waves make the floater pitching around the δ axis. The floater pitch motion combines with the internal flywheel spinning velocity ψ , thus originating an inertial gyroscopic torque acting on the internal precession axis ε . An electric motor is mounted on this shaft, and electricity is generated braking its motion.

The exploitation of the gyroscopic effect enables the exchange of torques through the gyroscopic frame to the hull to the waves, providing the conditions for the power absorption. On the other hand, another fundamental feature of this technology is that its angular momentum is function of the flywheel speed and it can be consequently easily tuned. In this way it is possible to actively change the natural resonant frequency of the system in accordance with the foreseen incoming wave climates.

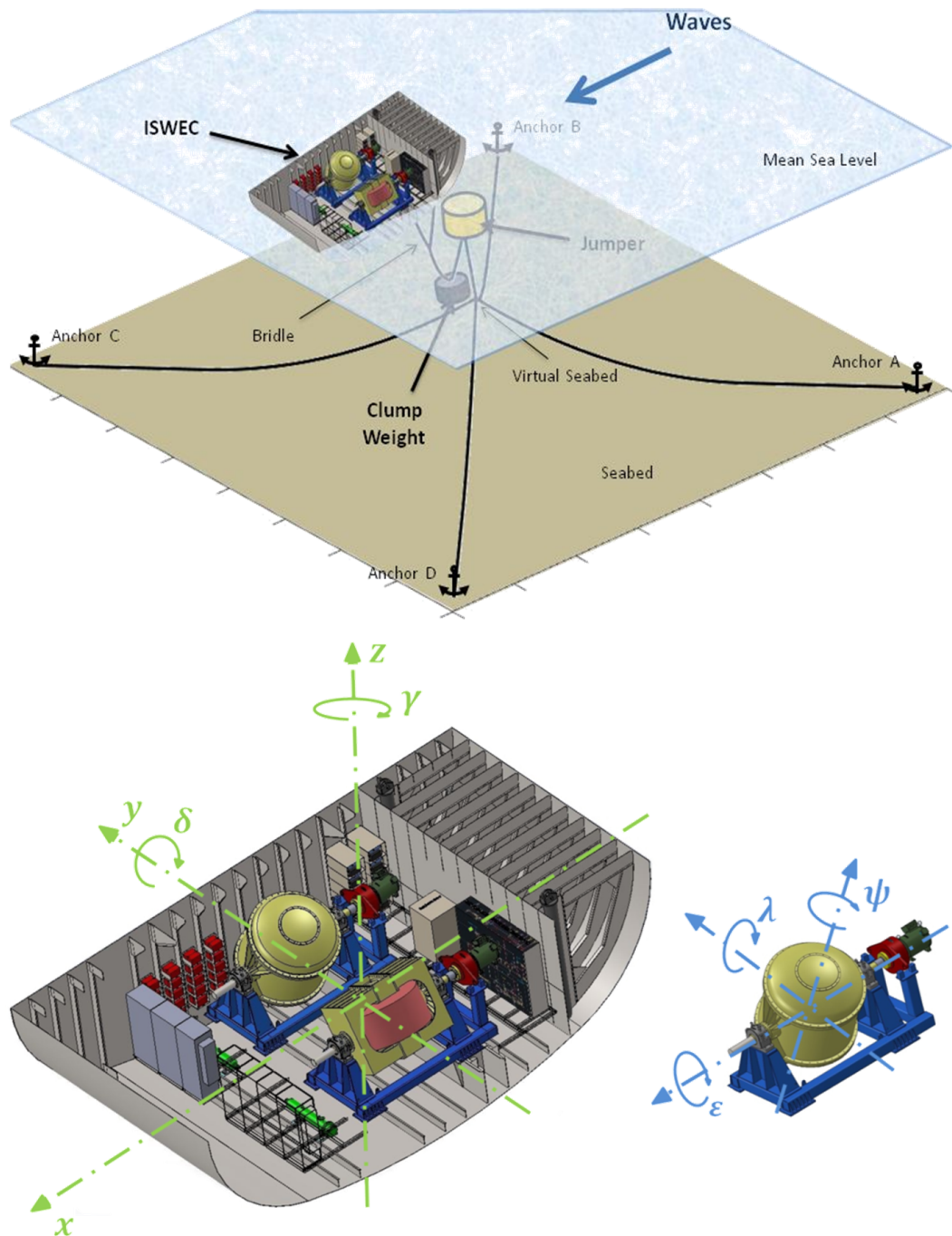


Figure 1.2 ISWEC prototype and installation drawings.

Another important feature of the gyroscopic system power conversion is the transmission multiplication that happens during the passage from the floater pitch oscillations (usually around 10 deg) to the oscillations of the internal gyroscope frame axis on which the PTO is mounted (about 60 deg). This side effect positively influences the design and choice of the next elements in the conversion chain, the mechanical gearbox and the electric torque motor.

The floater mooring system has conceived with a slack mooring configuration, with a single line interrupted by a jumper and a clump weight that is connected to the floater bow with a bridle. In this way the hull is passively self-aligning with respect to the incoming waves main direction.

Due to the gyroscopic working principle, the ISWEC is mainly conceived for working in the enclosed sea climates with reduced fetches, as the Mediterranean Sea, characterized by waves of considerable steepness and high frequency.



Figure 1.3 Pantelleria, Italy, 2015. ISWEC installed prototype in operation.

1.4.2 ISWEC Project history

The first concept can be traced back to 2005. It was conceived by the renewable group of the Mechanical and Aerospace Engineering department of the Politecnico di Torino (Italy). The idea was to exploit the gyroscopic effect created by the combined motion of a hull and a flywheel spinning speed for harvesting the wave energy and convert it to electricity. This kind of conversion principle were originally thought for working in the Mediterranean Sea, characterized by waves of high steepness, with high frequency and considerable height [78]. First concept is dated to 2005. It was a 2

degree of freedom (DOF) gyroscope system, as represented in Figure 1.4. It has been studied completely in the university framework at Politecnico di Torino Department of Mechanical and Aerospace Engineering (DIMEAS). A first proof of concept of the system was developed by the research group in 2007, in order to test the effectiveness of the conversion principle and to validate the developed models [68, 11]. First qualitative water tests were then performed in the Department of Environment,

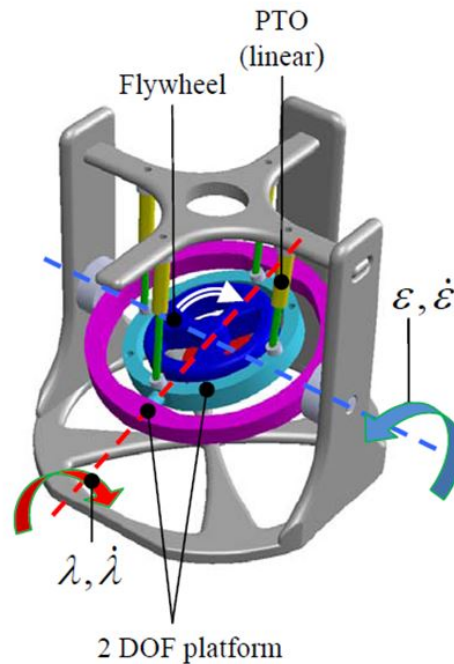


Figure 1.4 ISWEC first concept. Two degree of freedom gyrosopic system.

Land and Infrastructure Engineering (DIATI) always at Politecnico di Torino, where a flume with a wave maker is available. After this first experience the simplification of the overall system was decided, and the internal gyroscope system lose one DOF, with the final internal gyrosopic system constrained to precession motion only. The PTO was mounted on this internal gyrosopic frame oscillating shaft. The idea of the ISWEC was born. The whole research program about this device followed a development path generally seen as a standard in the wave power field. This was presented in the wave power development and evaluation protocol, by HMRC, in 2003 [50] also cited in [72]. A table of the proposed development program is shown in Figure 1.5.

Thereafter in 2009 the first ISWEC prototype was developed. Always quoting the HMRC report, "*within ocean engineering there is a tradition for model testing in order to provide valuable information on loads and movements required to finalize the*

DEVELOPMENT	PHASE 1: Validation Model (lab)			PHASE 2 Design Model (lab)	PHASE 3: Process Model		PHASE 4 Prototype	PHASE 5 Demonstration
	Concept	Performance	Optimisation		Lab. Tests	Sea Trials		
Objectives / Investigations	Op. Verification Design Variables Physical Process Validate/Calibrate Maths Model Damping Effect Signal Phase	Real Generic Seas Design variables Damping PTO Natural Periods Power Absorption Wave to Devise Response Phase	Hull Geometry Components Configurations Power Take-Off Characteristics Design Eng. (Naval Architects)	Final Design Accurate PTO [Active Control] Mooring system Survival Options Power Production Added mass	Scale effects of Overall Performance PTO Method Options & Control Environmental Influences & Factors Inst. Power Absorption Characteristics Electricity Production & Quality Mooring & Anchorage Security	Ops Procedures Electrical Quality Grid Supply PTO Performance Control Strategy Survival	Grid Connection Array Interaction Maintenance Service Schedules Component Life Economics	
Output/ Measurement	Vessel Motion Pressure / Force, Velocity, RAOs with Phase Diagrams Power Conversion Characteristic Time Histories Hull Seaworthiness: Excessive Rotations or Submergence Water Surface Elevation Ahead of Devices	Vessel Motion Response Amplitude Operators & Stability Pressure / Force, Velocity, RAOs with Phase Diagrams Power Conversion Characteristic Time Histories Hull Seaworthiness: Excessive Rotations or Submergence Water Surface Elevation Ahead of Devices	Motion RAOs Phase Diagrams Power v Time Wave Climates @ <i>head,beam,ftail</i>	Incident Wave Field 6 D of F Body Motion & Phase PTO Forces & Power Conversion Seaworthiness of Hull & Mooring [Survival Strategies]	Full On-Board Monitoring Kit for Extended Physical Parameters	Service, Maintenance & Production Monitor, Telemetry for Periodic checks & Evaluation		
Primary Scale (λ)	$\lambda = 1 : 25 - 100$ ($\therefore \lambda_s = 1 : 5 - 10$)	$\lambda = 1 : 25 - 100$ ($\therefore \lambda_s = 1 : 5 - 10$)	$\lambda = 1 : 10 - 25$	$\lambda = 1 : 10 - 15$	$\lambda = 1 : 1 - 2$	$\lambda =$ Full size		
Tank	2 D Flume or 3 d Basin	2 D Flume or 3 d Basin	3 -d Basin	3 - D Basin	Benign Site	Open Location		
Duration -inc Analysis	1-3months	1-3months	6 - 12 months	3 - 6 months	6 - 18 months	12 - 36 months		
Typical No. Tests	250 - 750	250 - 500	100 - 250	50 - 100	50 - 250	Continuous		Statistical Sample
Budget (€000)	1 - 5	25-75	25-50	500 - 1,000	1,000 - 2,500	5,000 - 10,000		2,500 - 7,500
Model	Idealised with Quick Change Options Simulated PTO (0-∞ Damping Range) Std Mooring & Mass Distribution	Distributed Mass Minimal Drag Design Dynamics	Final design (internal view) Mooring Layout	Advanced PTO Simulation Special Materials	Full Fabrication True PTO & Elec Generator	Grid Control Electronics Emergency Res		First Fully Operational Device
Excitation / Waves	Monochromatic Linear (10-25Δf) (25-100 waves)	Panchromatic Waves (20min scale) +ve 15 Classical Seaways Spectra Long crested Head Seas	Deployment -Pilot Site Sea Spectra Long, Short Crested Classical Seas Select Mean wave Approach Angle	Extended Test Period to Ensure all Seaways inc.	Full Scatter Diagram for initial Evaluation Continuous Thereafter			
Specials	DofF (heave only) 2-Dimensional Solo & Multi Hull As Required	Storm Seas (3hr) Finite Regular As required	Power Take-Off Bench Test PTO & Generator	Device Output Repeatability Survival Forces	Salt Corrosion Marine Growth Permissions	Quick Release Connections Service Ops	Solo or Small Array (Up-grade to Generating Station)?	
Maths Methods (Computer)	Hydrodynamic, Numerical Frequency Domain to Solve the Model Undamped Linear Equations of Motion	Finite Waves Applied Damping Multi Freq Inputs	Time Domain Response Model & Control Strategy Naval Architects Design Codes for Hull, Mooring & Anchorage System. Economic & Business Plan			Array Interaction Economic Model Electrical Stab.	Int Market Projection for Devise Sales	

Figure 1.5 Wave Energy Converter development diagram [50].

structural design". It was designed to be in a 1:45 scale with a device to be installed in Alghero site (Sardinia, Italy). Possible installation sites were in fact starting to be studied. The attention to finalize the whole research activities to a possible final, full scale, commercially viable, wave energy converter technology was in fact continuous during the whole project.

The choice of an installation site is in fact a key point both for the choice and detailed development of the device, both to realize an assessment of the economic viability of the proposed solution at early stages of the project.

This 1:45 scale prototype, Figure 1.6, was tested both at Politecnico di Torino and at the wave tank of University of Edinburgh (UK). Also a simple test rig was built and used for performing dry tests on a moving platform, simulating the pitch motion of the device floater (DIMEAS Servo-systems Laboratories).

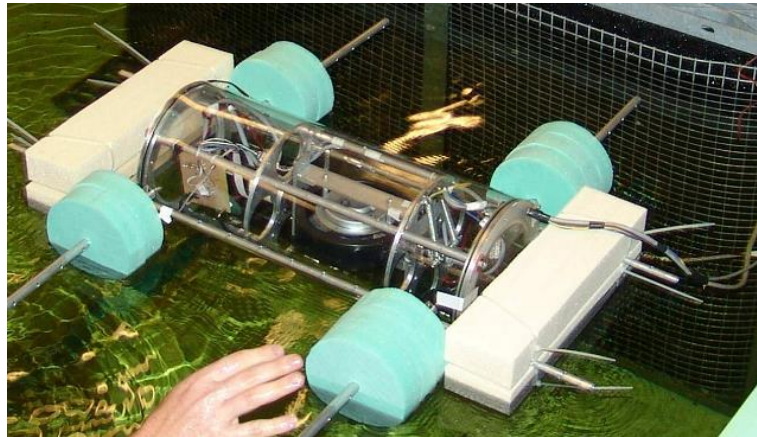


Figure 1.6 ISWEC prototype, 1:45 scale for Alghero site.

During this early phase, a preliminary comprehension of the system was gained and some interesting solutions and system configurations were hypothesized and tested ([16, 17, 20]). Results of wave tank experimental campaigns were compared to the mathematical and numerical models, creating knowledge and experience about the use of this tools fundamental for following phases. Nevertheless, some problems remained unstudied or unknown, because of scale issues and the not real installation environment. It was in fact impossible to assess the actual real contribution of friction, aerodynamic losses and electric efficiency, thus making impossible to scale up these effects to the final device.

The following fundamental step was the design and construction of a bigger scale prototype. It was initially financed with an Italian Regional project named SPOSD-DET (Self Powerd Floating Device for Sea Traffic - Detection and Transmission) in 2009. Always referring to the HMRC protocol, this part of the ISWEC project can be defined as both phase 2 and 3. The objective was identified in designing a 1:8 scale prototype with respect to a device for Pantelleria site (Sicily, Italy). In 2010 a waves and currents sensor was in fact installed near the port of Pantelleria, in the identified installation point. It is an Acoustic Waves and Currents (AWAC) sensor, commercialized by Nortek (www.nortek-as.com). The measurement campaign started in January 2010 and ended in December 2011. With post processing activities on gathered data, occurrences scatter tables of the installation site were obtained. This was useful both for the statistical characterization of the waves states in the installation sites, both for the wave height profiles record logged. More reliable time-domain simulations could be run with the wave-to-wire developed model, starting from real wave profile.

During the study and design of this new prototype the group decided to start a university's spin-off called "Wave for Energy S.r.l.". This company main mission was the realization and commercialization of the ISWEC.

The 1:8 prototype, Figure 1.7, was realized in collaboration with Aris S.p.a. In 2012 it was completed and tested at INSEAN wave tank in Rome. In the meanwhile a dry hardware in the loop test rig was also realized [18].

The experience and results obtained from the 1:8 scaled prototype has been proved fundamental for building a skilled team and to draw the main guidelines for the ISWEC design. After the evaluation of the several power conversion losses, the pre-design phase was improved taking into account of the electro-mechanical power losses and the hull hydrodynamic conversion capabilities.

In 2012 an important project named PROMO was funded by the Poles of Innovation, a public structure of the Italian Regione Piemonte. The objective of this program was to design a 60 kW rated power ISWEC full scale prototype to be installed in Pantelleria island (Sicily, Italy) and to launch it in Summer 2014. Objective of the project was to demonstrate the device energy production capabilities. Besides Politecnico di Torino and Wave for Energy Srl, other project partners were ARIS S.p.a. for the realization and setup of the internal electro-mechanical gyroscopic groups, LANDRA S.r.l. for the design of the floater and the mooring system, SIRIUS S.r.l. for the provision of custom electric components, UP Design for the visual impact and

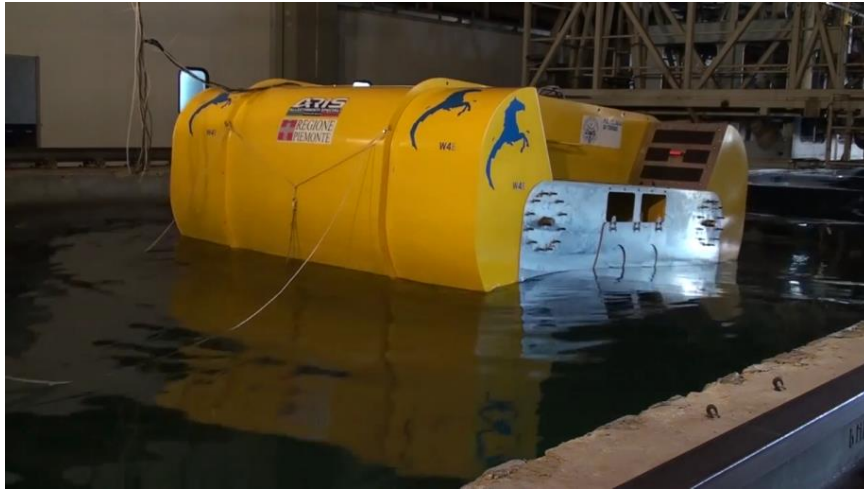


Figure 1.7 ISWEC prototype, 1:8 scale for Pantelleria site. Rome INSEAN wave tank.

advertising management.

The specification procurement, the main design and optimization of this device has been mainly carried out up to 2014. The whole procedure is exhaustively described in Raffero doctoral thesis "Design of a Wave Energy Converter. A case of application: ISWEC" [78].

The realization of the several subsystems constituting the device started in Autumn 2014 and was concluded in the Summer 2015. In August 2015 the ISWEC was launched and installed on the near shore of Pantelleria, not far from the port. The first experimental campaign began.

In Figure 1.8 a synthesis of the overall project is presented. The period covered by this Doctorate is the final part of the full scale design and the construction, deployment, test and data post-processing analysis.

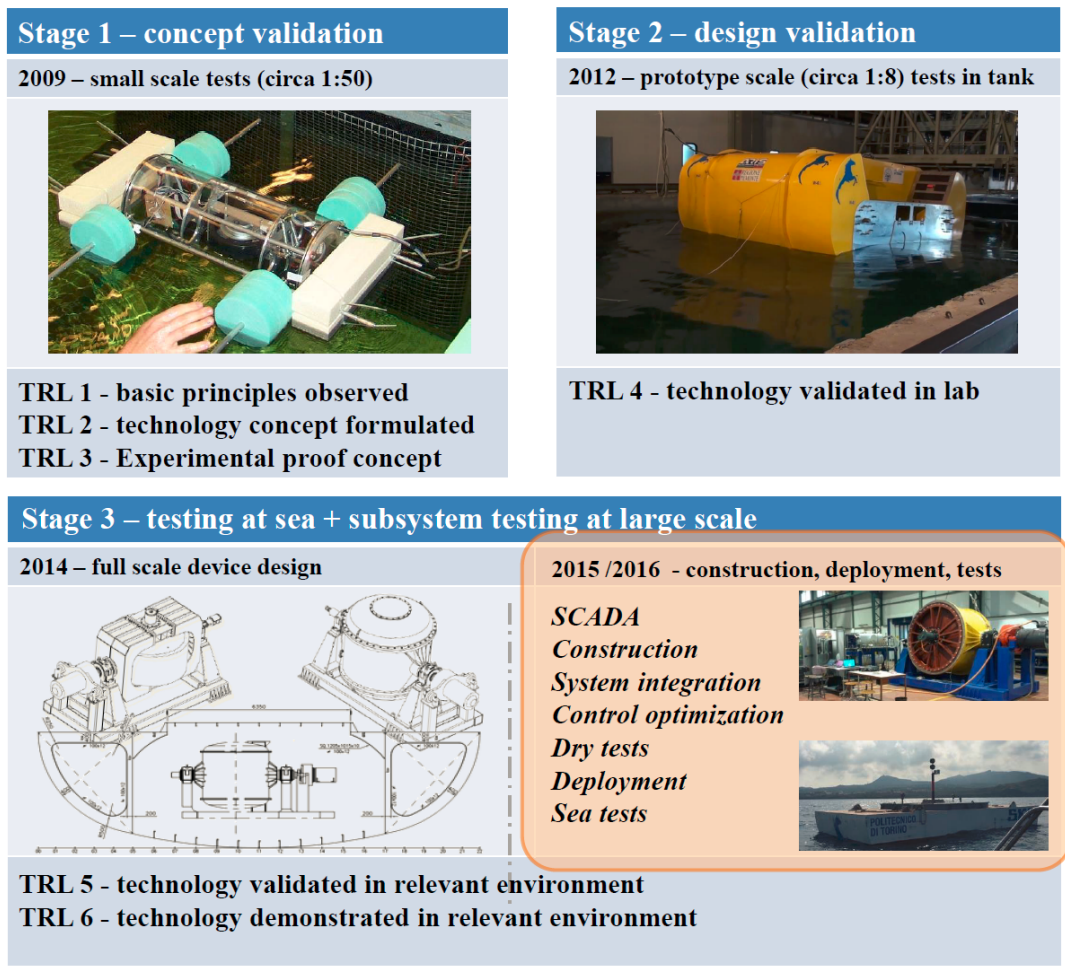


Figure 1.8 ISWEC project stages according to OES:IA Document n°T02-0.0

1.5 Contents of the Thesis and Candidate Role in the ISWEC Project

As stated, this thesis work places in the domain of the ISWEC development program. As described in section 1.4, during the doctorate period the project reached the full scale sea demonstration stage, with the launch of the device into the sea. Objective of the candidate activity has been the design, the implementation and the operation of the ISWEC control system for the full scale device during its first experimental campaign. This main objective involved different activities at various levels of the entire ISWEC design process. The need of constantly improving the modeling approach is a constant in wave energy field. Various typologies of models respond to different needs: for the description of different sea state conditions, for reducing the computational time in the pre-design phase or for implementing model-based control strategies. A description of the several models developed for the ISWEC is presented in Chapter 2. While dealing with the description of the behavior of the device, has been natural to deal also with the device design procedures. This was also due to the need of identifying the limits of the devices, both kinematics and electric, and with the consequent safety procedures. While the limitations of the device were found, it came also evident that some corrections of the design procedure should have been implemented. In Chapter 3 design procedures are described. In Chapter 4 the construction of the ISWEC Pantelleria device is described. In parallel to the electro-mechanical development of the prototype, also the SCADA system coding started. This is described in Chapter 5. It has been a relevant part of the candidate work and it involved numerous dry and wet tests. The first were carried out in the company where the device has been built, the others after the device launch both in port and offshore. The overall research activity about the development of the power absorption control is presented in Chapter 6. Given the timing of these activities in the project, first specification was that the developed strategies should have been feasible with the already predisposed SCADA hardware. In Chapter 7 some preliminary results from the 2015 experimental campaign are presented. In the last Chapter 8, some conclusion of the overall work are drawn.

In order to specify the activities carried out specifically by the candidate, his main contributions in the project are hereafter highlighted for each thesis chapter.

- **Chapter II - Modeling.**

- Introduction of the flywheel shaft seals losses.
- Development of the flywheel fluidodynamic friction losses analytical model.
- Development of the electric drive numerical model jointly with Wave for Energy electric Eng. C. Dicarlo. Implementation of the quasi static modeling in the overall model.
- Experimental campaign with 1:20 scale prototype for hydrodynamic validation at HMRC in Cork, Ireland. Marinet project carried out with PhD M. Raffero (Polito).
- Transition to pitch DOF to complete planar modeling.
- Identification of a viscous term for the pitch DOF and integration in the numerical model.
- Integration of the ISWEC mooring system with MoorDyn mooring modeling tool. Work with M. Hall (UMaine) and B. Passione (Polito)
- Development of the single hydrodynamic DOF state space linear model. This has been the basis for the development of the advanced model based controllers.
- Development of the frequency domain 6 DOF model with the linearization of the pitch quadratic viscous term.
- Development and maintenance of new part of the nonlinear lumped parameters model. In particular the subsystem related to the control system

- **Chapter III - ISWEC device design.**

- Site characterization. Data analysis of data gathered by the AWAC for obtaining the directional resource distribution.
- Development of a method for analyzing the selection of a WEC sea state pre-design nominal point in an occurrences scatter table.
- Proof for the choice of an even number of gyroscopes
- Development of a method for computing the specifications for the size of the electric systems ultra-capacitors

- Development of the ISWEC design tool software. Also supervising the S.A. Sirigu MsC Thesis.
- **Chapter IV - ISWEC Pantelleria device.** Given the deep insight in the device specifications and functionalities, obtained through the extensive use of the numerical models and the development of the device control systems architecture, the candidate has had an active role during the setup of the system in the ARIS company. In particular for what concerned the selection of the dry tests to be performed and the specifications for important steps, as for example the maximum angular speed at which the flywheel had to be equilibrated. He also had a consultancy, problem solving, role for several technical challenges. Some adaptations to the SCADA code came from experiences gained on the field, as for example the confidence of using higher PTO saturation torques and linking them to the actual thermal state of the inverter and the motor, or the possibility to choke the interval of utilization of the cooling system and the procedure of splitting its operations in order to save power. Also, the development of the automatic procedures for the start-up and the safety stop has been implemented during tests on the field.

Last part of the involvement in the tests has been in Mazara del Vallo (Sicily) first and Pantelleria (Sicily) after, where numerous tests of the complete system were performed, before the final installation of the device.
- **Chapter V - The SCADA system.** This part of work has been a relevant portion of the time spent during the PhD. It has been supervised by Vincenzo Orlando, system and control Engineer of Wave for Energy. The part mainly related to the candidate are reported below.
 - Development of the high level software architecture. Identification of different load cases and development of the state machine.
 - Development of the position control loop of the gyroscope frame axis.
 - Identification of the safety procedure and its implementation.
 - Development of the Human-Machine Interface
 - Development of the safety control strategy
 - Development of logics related to the choice of control parameters starting from the sea state forecasts

- **Chapter VI - Power Absorption Control.** The entire work of this chapter has been carried out by the candidate. The sections related to the optimal control have been supervised by D. Valerio (Instituto Superior Tecnico, Lisbon).
- **Chapter VII - Experimental Campaign: 2015.**
 - Computation of the control matrices that schedule the regulators parameters via numerical model optimizations.
 - Direct operation of the device in sea during power harvesting. Manual choice of the control parameters and supervision. This has been realized remotely using the remote HMI interface.
 - Post processing of the data gathered.

1.6 Candidate publications

The candidate publications during the doctorate period reflects his involvement in the different areas of the ISWEC project. Internal reports or the control code developed for the SCADA cannot be reported for intellectual and industrial properties claims by Wave for Energy srl.

The list of publications in which the candidate has been involved is hereafter presented:

- Modeling
 - Modeling and optimization of a Wave Energy Converter using ANSYS AQWA [12]
 - Expanding ISWEC Modelling with a Lumped-Mass Mooring Line Model. Conference [102].
 - Identification of the hydrodynamic parameters of a wave energy converter. Conference [79].
 - MARINET access technical report: Hydrodynamic model validation [80].
 - Experimental validation of different hydrodynamic modelling techniques applied to the ISWEC [77].
- Design procedures
 - Performance assessment of the full scale ISWEC system [15].

-
- ISWEC design tool. Selected among the best published paper at EWTEC 2015 and published in journal [101].
 - ISWEC design tool [90].
 - A performance assessment methodology for floating pitching WEC arrays [91].
 - Control
 - ISWEC: linear quadratic regulator oscillating control [103].
 - Application of Linear Model Predictive Control to the ISWEC [19].
 - Application of sub-optimal control techniques to a gyroscopic Wave Energy Converter [14].
 - Use of wave forecast for the regulation of ISWEC [13].
 - Tuning a linear quadratic regulator for point absorber wave energy converters [100].
 - ISWEC control tuning: Lessons learned. Conference [21].
 - Application of a passive control technique to the ISWEC [10]

Chapter 2

Modeling

In this chapter the modeling of the ISWEC is presented. It covers the different phenomena involved in the power conversion: the hydrodynamic interaction between the floater and the sea surface, the gyroscope system and the electric systems. Several numerical models have been developed, responding to the different needs characteristic of the different design and optimization phases of the project. A special attention is given in order to highlight all the assumptions used for the different modeling approaches.

This chapter starts from the work previously done and presented in [11, 78].

2.1 Reference frames and definitions

In Figure 2.1 some definitions about the ISWEC reference frames are given. Also the three main components of the internal gyroscopic system are shown: the flywheel (red), the gyroscopic structure (blue) and the PTO (green).

The reference frames are thus defined as follow:

- ECS: earth-fixed coordinate system (x_0, y_0, z_0) ;
- FCS: floater-fixed coordinate system (x_1, y_1, z_1) ;
- GCS: gyroscopic structure-fixed coordinate system (x_2, y_2, z_2) ;

As a first simplification, both the ECS and FCS origins are set in the center of gravity of the system and with x_1 and x_2 axes that are coincident with the bow direction.

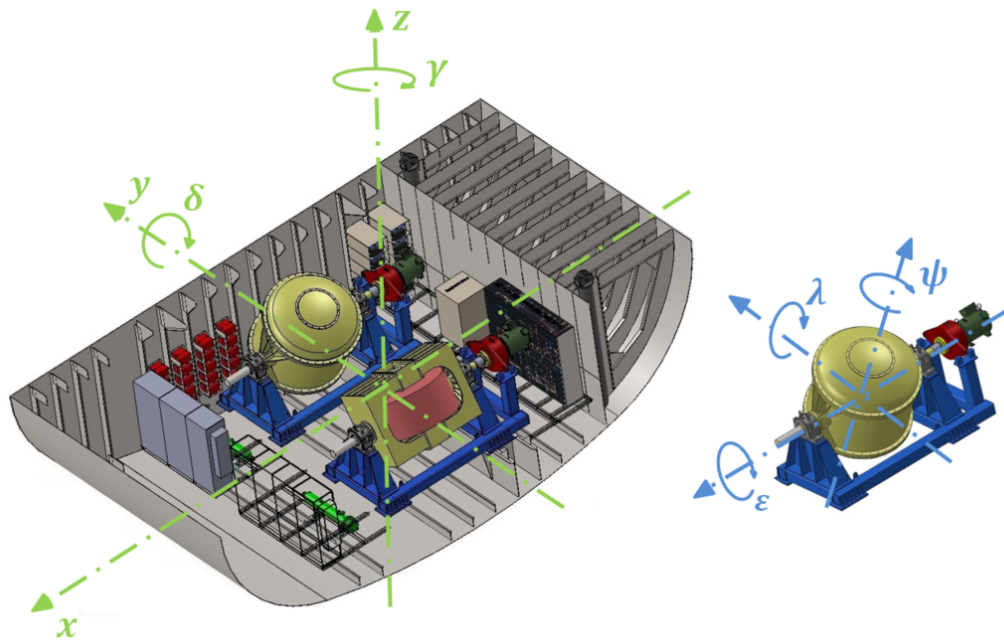


Figure 2.1 The ISWEC floater and gyroscopic system reference frames

Table 2.1 Hull-fixed FCS notation

DOF	Name	Comment	Symbol
1	surge	motions in the x_1 -direction	x
2	sway	motions in the y_1 -direction	y
3	heave	motions in the z_1 -direction	z
4	roll	rotations about the x_1 -axis	rx
5	pitch	rotations about the y_1 -axis	ry, δ
6	yaw	rotations about the z_1 -axis	rz, γ

Table 2.2 Gyroscope structure-fixed GCS notation

DOF	Name	Comment	Symbol
1	-	$x_2 \parallel x_1$	-
2	-	-	-
3	-	-	-
4	precession axis	rotations about x_2 -axis	ε
5	-	rotations about y_2 -axis	λ
6	-	rotations about the z_2 -axis	ψ

As can be seen in Figure 2.1 the FCS is the classical notation used for marine vehicles (Table 2.1):

The hull rotation around the y_1 axis (δ) is called pitch and it is due to the wave-floater-gyro interaction.

In Table 2.2 GCS variables are also better defined. Of course not all the DOF are free, since the gyroscope structure is fixed to the hull.

The rotating PTO system is mounted on the precession ε -axis shaft. The flywheel is linked to the gyroscope structure with a revolute joint, so it is free to rotate around the z_2 -axis with a $\dot{\phi}$ speed.

2.2 Gyroscope system

The gyroscopic system is the core of this technology and it represents the tool with which the kinetic energy of the floater can be turn in available mechanical energy on the internal precession axis. On the same internal shaft is mounted the PTO, which converts the mechanical energy into electricity. In this section the equation describing the gyroscopic dynamic behavior are presented. For the detailed proof of the results and notation, please refer to [78].

The analysis is carried out with the Newtonian approach. Thus, starting from the Newton's Second Law (*the change in momentum of a body is proportional to the force applied on it along the line on which the impulse is impressed*), the mechanical momentum generated on the COG of the system by the angular momentum variation in time is evaluated. As known it is equal to the external generalized forces applied on the system:

$$\vec{M}_E = -\frac{d\vec{L}}{dt} = \sum_{i=0}^N \vec{T}_{E,i} \quad (2.1)$$

Which is the expression of the angular momentum conservation theorem. It must be noticed as vector are involved in this formulation.

Then, we can express the absolute angular velocities of the GCS, $\vec{\omega}_{GCS}$, and the flywheel, $\vec{\omega}_{fw}$, with respect to the GCS ("fw" is the abbreviation of flywheel):

$$\vec{\omega}_{GCS} = \dot{\varepsilon} \hat{i}_2 + \dot{\lambda} \hat{j}_2 + \dot{\psi} \hat{k}_2 \quad (2.2)$$

$$\vec{\omega}_{fw} = \vec{\omega}_{GCS} + \dot{\phi} \hat{k}_2 = \dot{\varepsilon} \hat{i}_2 + \dot{\lambda} \hat{j}_2 + (\dot{\phi} + \dot{\psi}) \hat{k}_2 \quad (2.3)$$

Where $\hat{i}_2, \hat{j}_2, \hat{k}_2$ are the GCS three mutually orthogonal unit versors. The flywheel angular momentum \vec{L}_{fw} is then equal to:

$$\vec{L}_{fw} = \hat{I}_{fw} \cdot \vec{\omega}_{fw} \quad (2.4)$$

Where, since this reference is constituted by principal axes of inertia, the inertia tensor of the flywheel \hat{I}_{fw} can be written as

$$\hat{I}_{fw} = \begin{bmatrix} I_{fw} & 0 & 0 \\ 0 & I_{fw} & 0 \\ 0 & 0 & J \end{bmatrix} \quad (2.5)$$

Looking at eq. 2.1, the expression of the dynamic behavior of the gyroscope related to the external generalized force can be obtained. In scalar components, with respect to GCS:

$$M_{Efw,x_2} = \vec{M}_E \cdot \hat{i}_2 = I_{fw} \ddot{\varepsilon} + (J - I_{fw}) \dot{\lambda} \dot{\psi} + J \dot{\phi} \dot{\lambda} \quad (2.6)$$

$$M_{Efw,y_2} = \vec{M}_E \cdot \hat{j}_2 = I_{fw} \ddot{\lambda} - (J - I_{fw}) \dot{\varepsilon} \dot{\psi} - J \dot{\phi} \dot{\varepsilon} \quad (2.7)$$

$$M_{Efw,z_2} = \vec{M}_E \cdot \hat{k}_2 = J(\ddot{\phi} + \ddot{\psi}) \quad (2.8)$$

It is now time to translate these equations in the hull reference frame (FCS). First passage is to rewrite λ and ψ and their derivatives in function of δ and ε . Next

operation is doing the dot product of \vec{M}_E by $\hat{i}_1, \hat{j}_1, \hat{k}_1$. Thus the dynamic equations due to the gyroscopic effect of the flywheel in FCS are shown:

$$M_{Efw,x_1} = \vec{M}_E \cdot \hat{i}_1 = \vec{M}_E \cdot \hat{i}_2 = M_{E,x_2} = \quad (2.9)$$

$$I_{fw}\ddot{\epsilon} - (J - I_{fw})\dot{\delta}^2 \sin \epsilon \cos \epsilon + J\dot{\phi}\dot{\delta} \cos \epsilon$$

$$M_{Efw,y_1} = \vec{M}_E \cdot \hat{j}_1 = \quad (2.10)$$

$$(I_{fw} \cos^2 \epsilon + J \sin^2 \epsilon)\ddot{\delta} + 2(J - I_{fw})\dot{\delta}\dot{\epsilon} \sin \epsilon \cos \epsilon - J\dot{\phi}\dot{\epsilon} \cos \epsilon - J\ddot{\phi} \sin \epsilon$$

$$M_{Efw,z_1} = \vec{M}_E \cdot \hat{k}_1 = \quad (2.11)$$

$$- (J - I_{fw})\ddot{\delta} \sin \epsilon \cos \epsilon + [(J - 2I_{fw}) \sin^2 \epsilon - J \cos^2 \epsilon]\dot{\delta}\dot{\epsilon} - J\dot{\phi}\dot{\epsilon} \sin \epsilon + J\ddot{\phi} \cos \epsilon$$

In order to complete the dynamic description of the gyroscopic group, the term due to the gyroscopic structure has to be considered as well. The angular momentum of the gyroscope structure is:

$$\vec{L}_{gs} = \hat{I}_{gs} \cdot \vec{\omega}_{GCS} \quad (2.12)$$

Where, since this reference is constituted by principal axes of inertia, the inertia tensor of the gyroscopic structure is:

$$\hat{I}_{gs} = \begin{bmatrix} I_{gs,x} & 0 & 0 \\ 0 & I_{gs,y} & 0 \\ 0 & 0 & I_{gs,z} \end{bmatrix} \quad (2.13)$$

With the same procedure as above, the equations governing the behavior of the structure are very similar except for the fact that there is not any spinning flywheel here. So terms with $\dot{\phi}$ do not appear.

In conclusion, full gyroscopic equations can be likely considered equal to the previous ones, except for the momentum of inertia. When the gyroscopic structure is added, we obtain the expression of the overall external generalized forces in GCS:

$$\begin{aligned} \vec{M}_{E,tot} = & I_x \ddot{\epsilon} \hat{i}_2 + I_x \dot{\epsilon} (\dot{\psi} \hat{j}_2 - \dot{\lambda} \hat{k}_2) + I_y \ddot{\lambda} \hat{j}_2 + I_y \dot{\lambda} (\dot{\epsilon} \hat{k}_2 - \dot{\psi} \hat{i}_2) + \\ & + (I_z + J) \ddot{\psi} \hat{k}_2 + (I_z + J) \dot{\psi} (\dot{\lambda} \hat{i}_2 - \dot{\epsilon} \hat{j}_2) + J \dot{\phi} \hat{k}_2 + J \dot{\phi} (\dot{\lambda} \hat{i}_2 - \dot{\epsilon} \hat{j}_2) \end{aligned} \quad (2.14)$$

where the momentum of inertia I_x, I_y and I_z are obtained adding to the flywheel momentum of inertia I_{fw} those of the gyro structure $I_{gs,x}, I_{gs,y}$ and $I_{gs,z}$.

2.3 Electro-Mechanical Power Losses

2.3.1 Flywheel shaft bearings

Losses caused by friction of the flywheel shaft bearings are modeled using the SKF catalogue method. The time-varying friction moment is computed using the following:

$$M_{b,L} = \frac{1}{2} \mu_b P_{b,eq} d_s \quad (2.15)$$

where μ_b is the friction coefficient, depending on the bearing family; d_s is the shaft diameter.

$P_{b,eq}$ is the equivalent dynamic load and it is computed starting from radial $F_{b,R}$ and axial forces $F_{b,A}$ with the following:

$$P_{b,eq} = X_b F_{b,R} + Y_b F_{b,A} \quad (2.16)$$

Where X_b and Y_b depend on the bearing type and load combination.

Even if this torques and forces are not involved in the dynamic behavior of the system, they are important to be modeled in order to asses the net power production of the device, the most important outcome of the model.

The corresponding power losses term is then proportional to the flywheel speed:

$$P_{losses,bearings} = P_{b,eq} \dot{\phi} \quad (2.17)$$

2.3.2 Flywheel shaft seals

Two radial shaft seals are mounted on the flywheel shaft. This power losses contribution is shown in the next:

$$P_{losses,seals} = \frac{F_r \pi d^2}{2} \dot{\phi} \quad (2.18)$$

F_r is a constant term given by the seal manufacturer. For the gyroscope group equipped with the vacuum chamber, this constant term is strongly dependant on the pressure inside the chamber. Also this term is proportional to the flywheel speed $\dot{\phi}$.

2.3.3 Flywheel fluidodynamic friction

The flywheel fluidodynamic losses represent an important part of the overall power losses in the system. These are the main reason for the choice of the use of a vacuum chamber and they are one of the key parameters to be taken into account during the design of the flywheel. Also the choice of using or not a vacuum chamber is based on a quantitative evaluation of this term.

In this section a semi-analytic model for the computation of the friction moment in the case of flywheel with a vacuum chamber (in-housing) or without (free) is presented. The Navier-Stokes equations are written in cylindrical polar coordinates r, ϕ, z , with the z – axis along the rotation axis of the flywheel [85]:

$$\frac{dp}{dr} = \frac{\rho v^2}{r}$$

$$\frac{d^2v}{dr^2} + \frac{1}{r} \frac{dv}{dr} - \frac{v}{r^2} = 0$$

where v is the fluid velocity, p its pressure and ρ its density. Since the domain is axial symmetrical, the following boundary conditions for the solution of the problem are used:

$$v_z = v_r = 0$$

$$v_\phi = v(r)$$

$$p = p(r)$$

Other hypothesis are: flywheel infinite axial length, steady state flow, Newtonian and incompressible fluid. The simplified geometry used is shown in Figure 2.2.

The axial and transversal contributions friction are evaluated and summed, assuming the superposition principle valid.

In the following the computation of the friction momentum is presented for the two different flywheel design cases.

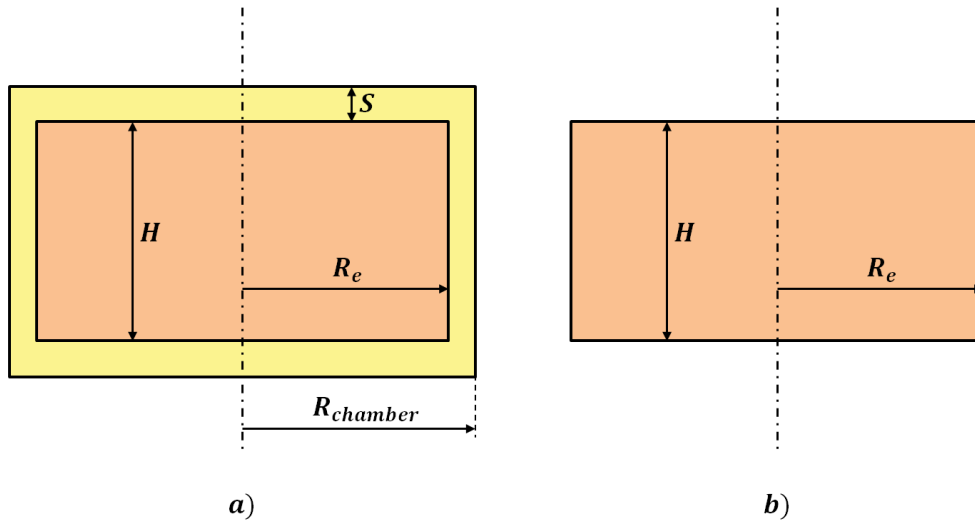


Figure 2.2 Flywheels simplified geometries for the fluiddynamic losses computation.

2.3.3.1 In housing configuration

The in-housing configuration is modeled with an inner and an outer cylinder. See Figure 2.2 image a). The internal represents the flywheel and is supposed to rotate at a constant speed. The air inside the housing is driven by the viscous drag force of the flywheel rotating wall. The chamber wall is fixed. The model thus results in a shear flow phenomenon. At low flywheel angular velocities, the fluid regime is laminar and the flow is steady and azimuthal. Under such conditions, the fluid assumes a two-dimensional motion named Couette flow. When the spinning speed reaches a threshold value, the flow becomes unstable and significant mass transport on the azimuthal momentum is observed. This phenomenon is named Taylor instability (or vortex).

Cylinder contribution

A semi-analytic expression for evaluating the friction momentum for an annulus with the rotating inner cylinder and no axial pressure gradient has been proposed by Bilgen and Boulos [9]. The momentum of a vacuum chamber axial contribution $M_{vc,ax}$ is formulated as follows:

$$M_{vc,ax} = \frac{1}{2} C_M \pi \rho \dot{\phi}^2 R_e^4 H \quad (2.19)$$

where ρ is the air density and it is function of the chamber temperature and pressure, $\dot{\phi}$ is the flywheel speed, R_e is the flywheel outer radius and H is the flywheel height.

The moment coefficient C_M is function of the d/R_e ratio and the Couette Reynolds number:

$$Re_{\phi m} = \frac{R_e \omega d}{\nu} \quad (2.20)$$

where ν is the kinematic viscosity of the fluid.

In table 2.3 the two relationships for low turbulent and high turbulent flows are presented.

Table 2.3 In housing configuration, axial friction momentum.

$$\begin{array}{ll} \text{Low Turbulent} & Re_{\phi m} \leq 10^4 \quad C_M = 1.03 \left(\frac{d}{R_e}\right)^{0.3} Re_{\phi m}^{-0.5} \\ \text{High Turbulent} & Re_{\phi m} > 10^4 \quad C_M = 0.065 \left(\frac{d}{R_e}\right)^{0.3} Re_{\phi m}^{-0.2} \end{array}$$

Plates contribution

For computing the vacuum chamber transversal moment $M_{vc,tr}$ the next Schlichting model is used.

$$M_{vc,tr} = \frac{1}{2} C_M \rho \phi^2 R_e^5 \quad (2.21)$$

The dimensionless torque coefficient C_M is evaluated differently [26] in function of the following adimensionalised coefficient.

$$Re_{disk} = \frac{R_e^2 \phi}{\nu} \quad (2.22)$$

In Table 2.4 the formulas are presented.

Table 2.4 In housing configuration, plates transversal friction momentum.

$$\begin{array}{lll} \text{Laminar} & Re_{disk} \leq 10^4 & C_M = \frac{\pi R_e}{s} \frac{1}{Re_{disk}} \\ \text{Low Turbulent} & 10^4 < Re_{disk} \leq 2 \cdot 10^5 & C_M = \frac{1.334}{Re_{disk}^{1/2}} \\ \text{High Turbulent} & Re_{disk} > 2 \cdot 10^5 & C_M = \frac{0.0311}{Re_{disk}^{1/5}} \end{array}$$

2.3.3.2 Free configuration

Without the vacuum chamber, the flywheel can be analyzed as a simple rotating cylinder in air. See Figure 2.2 image b).

Cylinder contribution

The fluid around the cylinder is brought in rotation by the flywheel via viscous drag. In this case, since there is not an outer wall, the fluid is subjected to centrifugal forces and motion. According to [85] the friction torque is defined as in previous equation 2.21 and the Reynolds number as in 2.22. For this configuration the flow regime are all considered turbulent. In this case the instabilities experienced before are no more present. The following empirical correlation by Theodorsen and Regier is used [93]:

$$\frac{1}{C_M} = -0.8572 + 1.25 \ln \left(Re_\phi \sqrt{C_M} \right) \quad (2.23)$$

The equation needs an iterative procedure to be solved.

Plates contribution

The same model for the in housing configuration is used. The friction moment formula is the same of 2.21. This time the friction coefficient is distinguished as function of the Reynolds number 2.22 as proposed in the following table 2.5.

Table 2.5 Free configuration, transversal friction momentum.

$$\begin{array}{ll} \text{Low Turbulent} & Re_{\phi m} \leq 3 \cdot 10^5 \quad C_M = \frac{1.935}{\sqrt{Re_{disk}}} \\ \text{High Turbulent} & Re_{\phi m} > 3 \cdot 10^5 \quad C_M = \frac{0.073}{Re_{disk}^{1/5}} \end{array}$$

2.3.4 Electric motor and drive efficiency

The PTO efficiency is also heavily affecting the net power production of the system and it depends on the PTO technology. The ISWEC device has a full electric conversion system, so it is not straightforward to model the losses with accuracy without increasing too much the computational costs. The quasi-static approach is chosen. A numerical time-domain model has then been built. Objective of this tool is to obtain the PTO quasi static efficiency map. The Matlab/Simulink environment realized model is shown in Figure 2.3. The "*PM Synchronous Motor Drive*" block in Electric Drives/AC drives of Simulink Simscape is used. According to MATLAB Documentation this high-level block is made of six blocks: the Permanent Magnet Synchronous Motor vector control drive, the three-phase inverter, the three-phase diode rectifier, the speed controller,

the braking chopper and the vector controller. This PTO electric machine is forced to rotate at a certain speed and different torques are actuated. After a transient, the system stabilizes around the steady state condition. Given the electric nature of the electric system this transient is very short, in the order of a few tenths of second. For this reason in the final ISWEC model a quasi static approximation can be adopted.

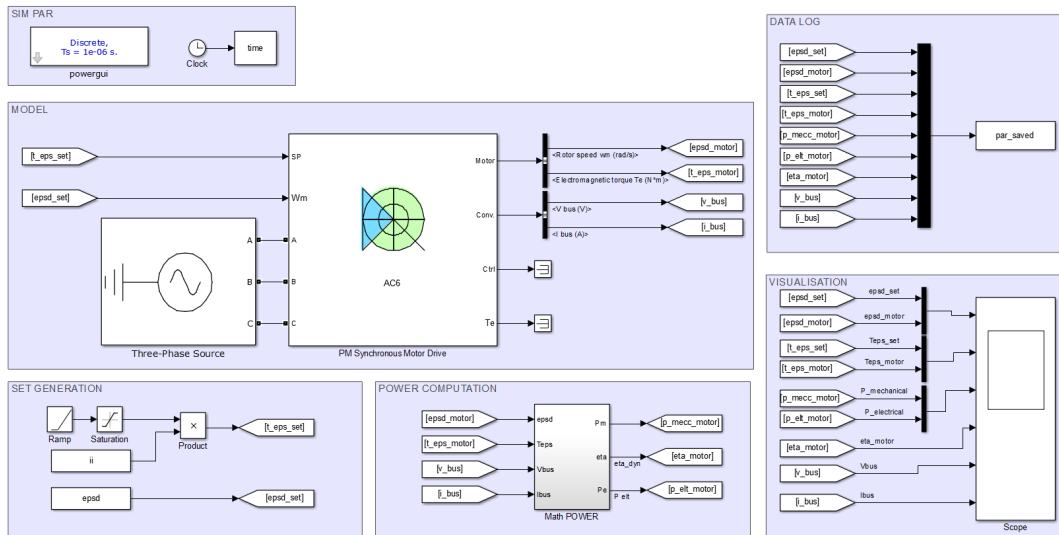


Figure 2.3 PTO efficiency map computation numerical model.

An example of simulation in time domain is presented in Figure 2.4. The speed reference is constant. After a short transient also a mechanical torque load is given. The bus voltage and current is also shown, but it is dependant on the system in which the PTO is installed. For the sake of this analysis it is not used. The interesting data to be logged are the difference between the mechanical and the electric power in the steady state condition and its correspondent efficiency value "eta motor".

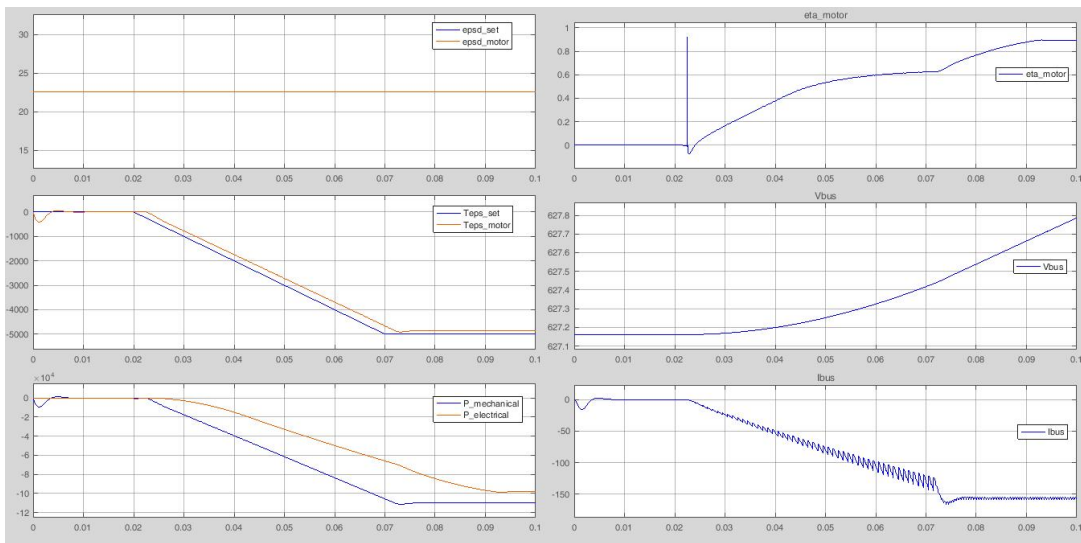


Figure 2.4 PTO efficiency map computation. Example of time domain simulation.

The efficiency and the power losses are then mapped for all the four quadrants representing the different load conditions of the PTO electric machine 2.5,2.6.

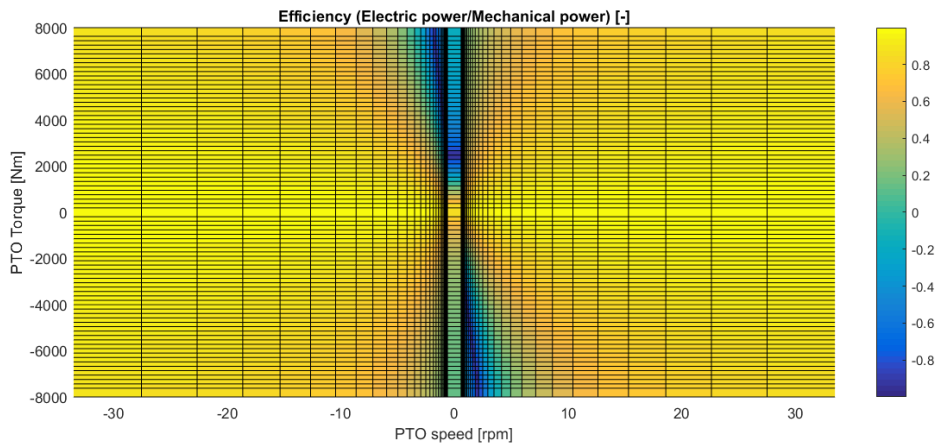


Figure 2.5 PTO efficiency map.

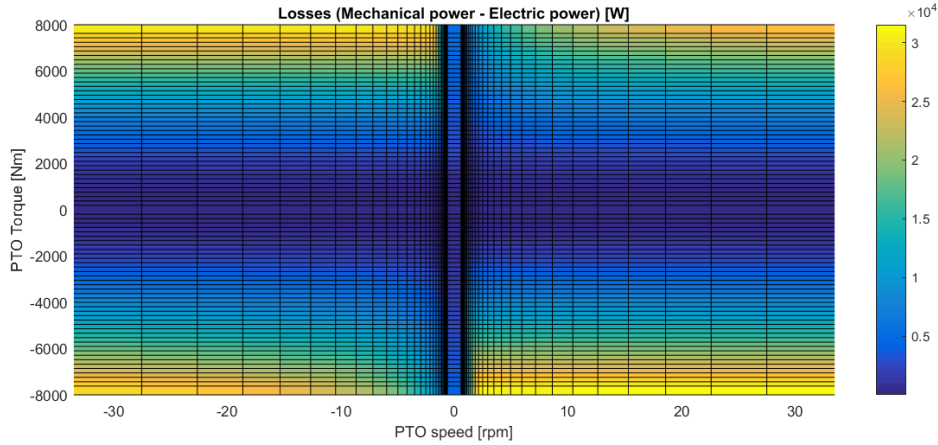


Figure 2.6 PTO losses map.

Analytically, the PTO efficiency formulation is thus a static term. Following equations can be used:

$$\begin{aligned} P_{electrical,PTO} &= P_{mechanical,PTO} \eta, & \text{generator mode} \\ P_{electrical,PTO} &= P_{mechanical,PTO} / \eta, & \text{motor mode} \end{aligned} \quad (2.24)$$

2.4 Hydrodynamics

The interaction between hull and waves represents the very first stage in power conversion and a correct modeling of this phenomenon is fundamental for the description of the overall system behavior. In general fluid dynamics phenomena are known to be difficult to be treated, both from an analytical and a numerical point of view, where computational power is still a limitation [45].

Ideally, the wave-body interaction could be studied solving the entire set of Navier-Stokes equations. Given that these equations cannot be solved analytically, the studied domain must be discretized and solved through numerical methods. Software packages able to carry out these evaluations are known as Computational Fluid Dynamics (CFD) codes. Even though it is possible to reach high-fidelity results with this approach, its main limitation is related to the extremely high computational time required.

Other compromise solutions have been developed through years, having different trade-offs between modeling precision and required time [106, 81, 73, 35]. Linear, partially non-linear and nonlinear potential flow methods have been widely studied and used in the field, being part of commercial and open-software suites [77]. Linear potential flow codes enable the computation of the matrices required in the fast-running Cummins

lumped parameter equation. This method is at the basis of ISWEC hydrodynamic modeling.

In this section this low-computational cost lumped parameters model used in the model-based design loop is introduced. It is a combination of the already mentioned Cummins hydrodynamic linear integro-differential equation with a couple of viscous non linear terms and the contribution of some potential flow second order terms, as the mean drift forces.

2.4.1 Linear Cummins equation

The equation describing the motion of the floater used in the model is the linear time-domain Cummins equation. This is considered a standard tool for the modeling of the behavior of marine structures in waves [74]. It is a linear time-invariant integro-differential equation [32]. The same equation can also be written in frequency domain, with frequency dependent parameters. In the frequency domain it is easy to explore the main resonance properties of a floater and having first draft designs.

Hypothesis of the model

The representation given by this model exploits the results of potential flow theories. Outcome of this theory is the pressure distribution around the floating body in steady-state condition, both in rest and perturbed by waves. This leads to the computation of the wave-floater exchanged forces and torques. In particular Cummins dealt with first order linear potential flow theory. Main hypothesis are:

- The fluid is incompressible.
- The fluid is inviscid.
- The fluid velocity field is irrotational. This means that there are no vortices.
- The body has zero or very slow forward motion.
- The body motions have small amplitude starting from the body equilibrium position, corresponding to a mean wetted surface.

The calculation of the forces acting on the body can be splitted into three sub-problems. The first one consists in the analysis of the forces acting on the static body in still water.

- Hydrostatic restoring force. It represents the overall contribution of gravity and buoyancy forces on the floater in a static situation with a still water surface.

The second one consists in the analysis the forces acting on the oscillating body in still water. Two effects are here evaluated:

- Added mass contribution. This term considers the acceleration of the fluid surrounding the hull.
- Radiation forces. These forces are effect of the waves generated by the hull motion. This is a dissipative effect and is related to the velocity vector of the body. For these reasons it is also called a damping term.

The third sub-problem consists in the calculation of the forces acting on a still body under monochromatic waves. In this case two effects are evaluated:

- Froude-Krylov forces. These actions represent the waves forcing term for the whole dynamic equation. They are obtained by the integration over the hull submerged surface of the pressure field generated by the undisturbed waves.
- Diffraction forces. These are complementary to the previous ones. The introduction of of the floating body alters the wave surface, some waves are diffracted. The pressure field is consequently influenced and so the forces obtained by its spatial integration over the floater wetted surface.

The flow potential theory software used for the analysis and computation of all the required matrices and terms is ANSYS® AQWA®. In Figure 2.7 the ISWEC floater with a used mesh configuration is illustrated.

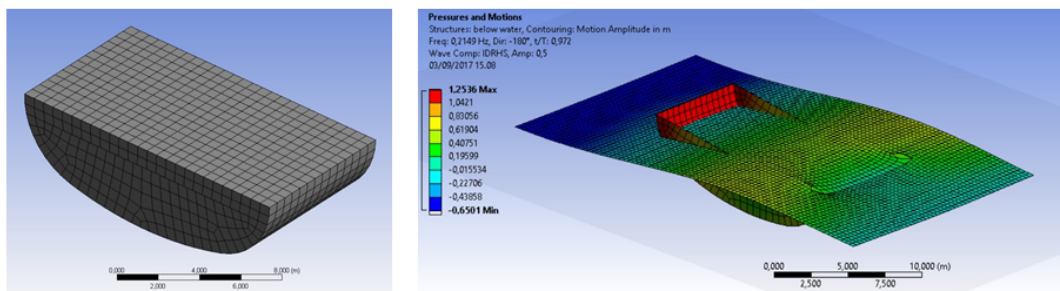


Figure 2.7 Mesh and example of analysis of the ISWEC floater in ANSYS® AQWA® environment.

Frequency-domain representation

The first form to be presented is in frequency-domain. It is a frequency-dependent

coefficients, second order, differential equation:

$$[-\omega^2[\mathbf{M} + \mathbf{A}(\omega)] + j\omega\mathbf{B}(\omega) + \mathbf{K}]X(\omega) = F_w(\omega) + F_m(\omega) \quad (2.25)$$

This is a matrix equation, where the $\vec{X}(j\omega_w)$ vector contains the 6 DOFs of the floater (see Table 2.1):

$$\bullet X = [x, y, z, r_x, r_y, r_z]^T = [surge, sway, heave, roll, pitch, yaw]^T$$

And where:

- \mathbf{M} : Floating body inertia matrix [6x6];
- $\mathbf{A}(\omega)$: Frequency dependent added mass matrix [6x6];
- $\mathbf{B}(\omega)$: Frequency dependent radiation matrix [6x6];
- \mathbf{K} : Hydrostatic stiffness matrix [6x6];
- $F_w(\omega)$: Frequency dependent wave force vector [6x1];
- $F_m(\omega)$: Mooring line actions [6x1].

It must be noticed that coefficients are dependent either on the wave frequency and direction. The hypothesis in this analytic model is that the system is aligned with the incoming water front direction. This hypothesis is strongly dependent also from the installation site and the mooring system chosen. In Pantelleria this hypothesis can be considered reasonable, as is presented later in Chapter 7.

Time-domain representation

The second form in which the Cummins equation can be used is in time-domain. It is an integro-differential equation with a convolution integral that describes the fluid memory effects associated with the radiation phenomena.

$$(\mathbf{M} + \mathbf{A}_\infty)\ddot{\vec{X}} + \int_0^t \mathbf{h}_r(t - \tau)\dot{\vec{X}}d\tau + \mathbf{K}\vec{X} = F_w(t) + F_m(t) \quad (2.26)$$

This is a matrix equation, where the $\vec{X}(j\omega_w)$ vector contains the 6 DOFs of the floater (see Table 2.1):

$$\bullet \vec{X} = [x, y, z, r_x, r_y, r_z]^T = [surge, sway, heave, roll, pitch, yaw]^T$$

And where:

- \mathbf{M} : Floating body inertia matrix [6x6];
- $\mathbf{A}(\infty)$: Infinite frequency added mass matrix [6x6]. This is a constant positive definite matrix, obtained with the following limit:

$$\mathbf{A}_\infty = \lim_{\omega \rightarrow \infty} \mathbf{A}(\omega) \quad (2.27)$$

- Dissipative term in the form of a convolution integral:

$$\int_0^t \mathbf{h}_r(t - \tau) \dot{\mathbf{X}} d\tau \quad (2.28)$$

It represents the fluid memory effects due to the radiated waves caused by the motion of the floater. The kernel of the convolution is the impulse response of the body.

- \mathbf{K} : Hydrostatic stiffness matrix [6x6];
- $F_w(t)$: Wave force vector [6x1];
- $F_m(t)$: Mooring line actions [6x1].

2.4.2 Viscous Terms

It is well known in wave power field that the linear Cummins equation is reliable for the slow and small amplitude floater motions. This kind of modeling is used for multiple marine applications however, since wave energy devices are designed for working in resonance conditions, it reveals its intrinsic weakness in the modeling of a converter. It is then quite common in literature [81] to add some viscous terms, in order to overcome such issues. Another viscous contribution is needed for damping the forward motion of the floater. ISWEC owns a slack mooring architecture so some freedom in surge motion is allowed. In next two paragraphs solutions to these issues are presented.

Pitch viscous term

The ISWEC is a floating pitching device. Thus it is designed to have pitch DOF resonance frequency near the most energetic one of the installation site. A viscous

damping force is then added. It takes the form:

$$F_{viscous,\delta} = -\beta \dot{\delta} |\dot{\delta}| \quad (2.29)$$

Where $\dot{\delta}$ is the pitch rotative speed and the β coefficient is identified starting from experimental data or fully nonlinear CFD analysis. In the ISWEC full scale application, the parameter has been identified starting from 1:20 scale prototype HMRC wave tank tests (see [79, 80]) then scaled with Froude relationships to the full scale system. Results are definitely positive even for the modeling of the full scale device in real sea environment, as showed in section (see section 7.4.3).

Surge viscous term

For what concern the surge DOF, the viscous action is evaluated according to the drag force contribution of the classical Morison equation. The hypothesis of zero or very low forward speed is used.

$$F_{viscous,x} = -\frac{1}{2} \rho C_d A \dot{x} |\dot{x}| \quad (2.30)$$

Where:

- ρ : is the water density.
- C_d : is the drag coefficient. It is a dimensionless coefficient found in literature for simple geometries.
- A : is the cross section area with respect to incoming water front direction of the hull submerged part.
- \dot{x} : is the body surge speed.

2.4.3 Drift forces

This kind of forces are fundamental in the modeling of a moored floating body. Theoretically they are also obtained starting from the Bernoulli's equation and from flow potential theory. The novel contribution here introduced is instead due to the 2nd order order approximation of the obtained equations. The two main contributions are hereafter presented.

Mean drift forces

These induce a mean surge displacement of the floater, in equilibrium between forces mean value and the mooring system ones. This can be computed directly from 1st order linear solution and for regular waves it is proportional to the square of the wave amplitude multiplied by the correspondent drift frequency-dependent coefficient. The equation for the regular wave is the next:

$$\bar{F}_{drift,x} = \left(\frac{H}{2}\right)^2 f_{drift}(\omega), f_{drift}(\omega) \in \mathbb{R} \quad (2.31)$$

For an irregular wave, the mean value is computed starting from the spectrum distribution. The sum of the different components in frequency constituting the irregular wave spectrum is presented:

$$\bar{F}_{drift,x} = \sum_{n=1}^N 2 f_{drift}(\omega_n) S_{\eta}(\omega_n) \Delta\omega \quad (2.32)$$

Low frequency drift forces

The low frequency, with respect to waves, oscillating drift forces cause a low frequency motion along the surge axis. These are due to 2nd order pressure fluctuations around the hull [42, 76]. These fluctuations are caused by variations of the wave amplitude. So for a regular wave, these are null. The contribution becomes instead notable for irregular waves.

For evaluating the time variation of the amplitude of an irregular wave, the concept of wave envelope must be introduced:

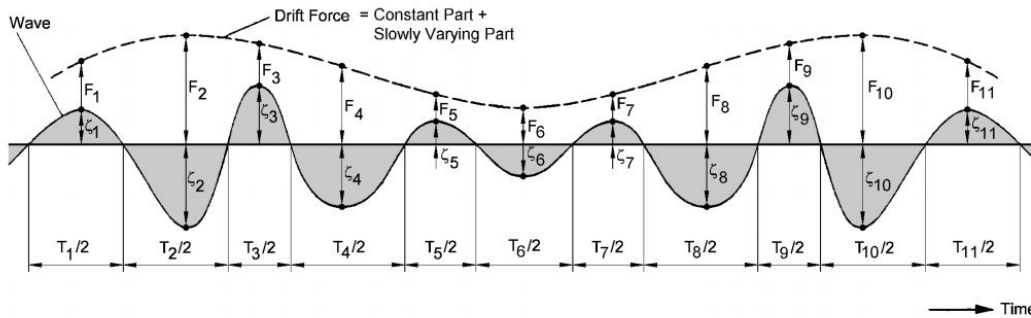


Figure 2.8 Wave drift force for irregular waves. Wave envelope. [42]

The approach used for this application is the Neuman's approximation. This choice is justified because it has definitely lower computational time with respect to quadratic transfer functions, and results are considered as acceptable. This method uses only

mean drift force coefficients while dropping all the combined effects coefficients. The mathematical formulation is the following:

$$F_{drift,x}(t) = 2 \left(\sum_{n=1}^N \eta_{a,n} \sqrt{f_{drift}(\omega_n)} \cos(\omega_n t + \phi_n) \right)^2 \quad (2.33)$$

2.4.4 Mooring system Terms

The mooring system architecture designed for the ISWEC floating device is characterized by a jumper and a clump weight. An image of the solution is showed in Fig.2.9. An insight in this configuration and its modeling is given in [102].

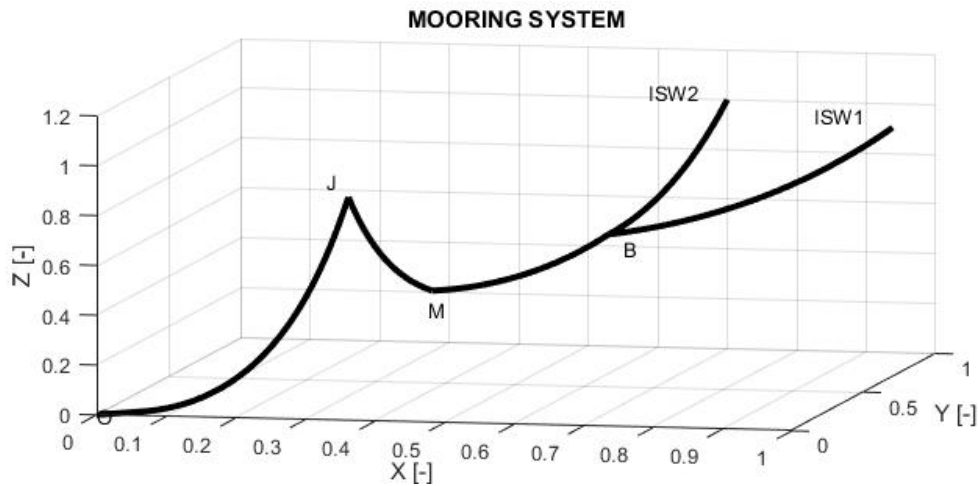


Figure 2.9 ISWEC prototype, bow mooring system architecture.

Where in J stays for jumper, M for the clump weight, B is the start of the bridle and ISW1, ISW2 are the connection points on the floater.

The quasi-static modeling approach is chosen. The steady positions of the overall system are computed for different positions of ISW1, ISW2. The corresponding loads are then function of their X and Z coordinates in the working plane. The characteristic presented in Fig.2.10 is used.

As can be noticed, such an architecture involves very small loads for small displacements, thus reducing the interaction with the floater dynamic. For high displacement loads increase with a smooth exponential trend. This avoid impulsive loads on the catenary, in order to reduce mechanical stresses faults.

In conclusion, from a dynamical point of view, the F_m force is thus a nonlinear static term, function of the floater motions:

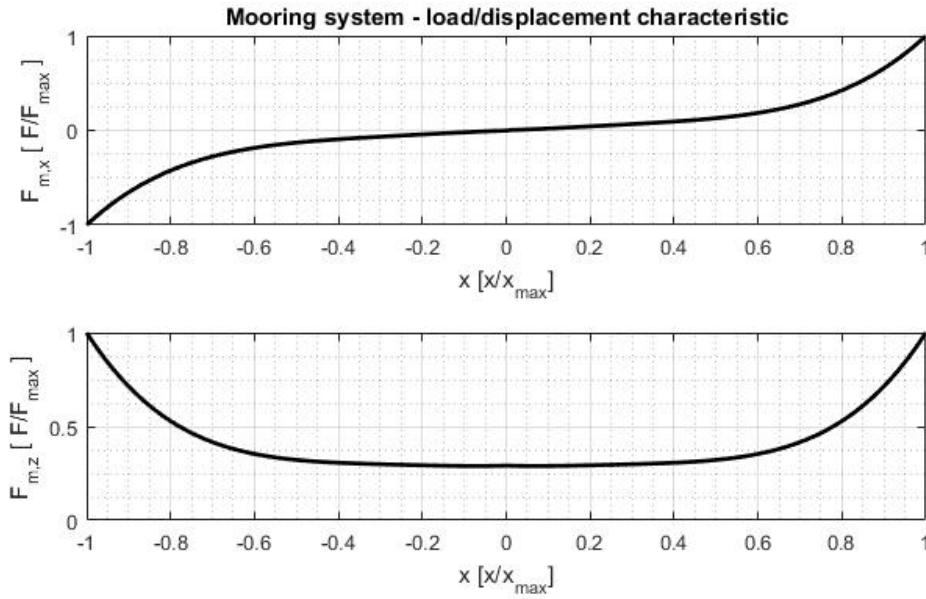


Figure 2.10 ISWEC prototype, bow mooring system load vs displacement characteristic.

$$F_{moorings} = f(X) \quad (2.34)$$

Where X is the complete floater state (surge,sway,heave,roll,pitch,yaw).

2.5 Hydrodynamics - 1:20 Tank Testing

During the last phase of ISWEC design and specification procurement, in 2014, it was clear that some studies for enhancing the ISWEC hydrodynamic behavior description were required. The first aim was to reduce the unrealistic pitch motions given by the resonance phenomena of the linear Cummins equation. An experimental campaign was thus carried out at UCC HMRC Wave Tank in Cork (Ireland) (Figure 2.11) in order to verify the accuracy of the used hydrodynamic model and to identify unmodelled dynamics. The access was financed under the EU MARINET project framework [28].

A Pantelleria floater 1:20 scale prototype was realized. In Figure 2.12 the 3D CAD of the realized prototype is shown. It has been designed in order to match the computed scale properties of the full scale device, as illustrated in next Table 2.6. Tests have been organized in two main stages: as a first stage surge, heave and pitch have been studied independently using a re-configurable test rig attached to the tank bridge. In a



Figure 2.11 Hydrodynamics Tank Tests. Hydraulics and Maritime Research Centre, University College Cork, city of Cork, Ireland, 2014.

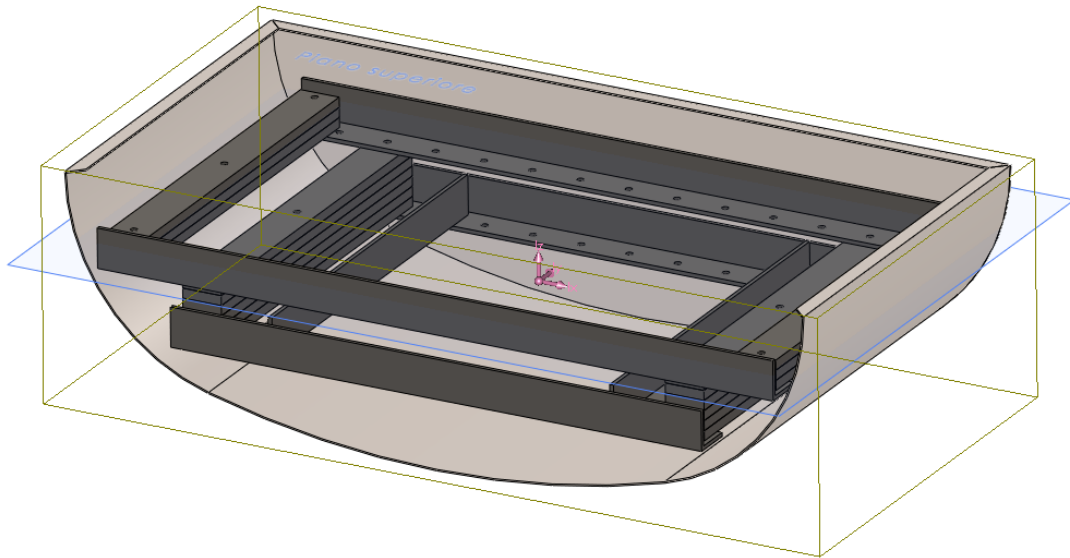


Figure 2.12 Tank Tests. 1 DOF Test Rig configurations.

Table 2.6 Hydrodynamics Tank Tests. Full scale and scale prototype main physical parameters.

Parameter	Froude	ISWEC1:1	ISWEC 1:20	Prototype
Length [m]	1	15,00	0,75	0,76
Width [m]	1	8,00	0,40	0,40
Mass [m]	3	300000	37,5	37,5
Ixx [kg m ²]	5	2046000	0,639	0,750
Iyy [kg m ²]	5	9500000	2,969	3,020
Izz [kg m ²]	5	10810000	3,378	2,420
Design Wave Period [s]	0,5	6,7	1,498	-
Design Wave Height [m]	1	1,60	0,080	-
Center Of Gravity [m]	1	-0,250	-0,013	-0,05

second step the device has been moored and the complete 6 DOF floating system has been analyzed.

2.5.1 Experimental tests plan

The overall experimental campaign was three week long, and it was composed by 5 phases:

1. **Phase 1:** Mass calibration and definitions of the hull parameters (Mass, Center Of Gravity, Momentum of Inertia)
2. **Phase 2:** Pitch configuration
 - (a) Excitation forces. The hull is locked in all its DOFs, with the pitch constrained by means of a load cell sensor on the pitch DOF. Excitation torque is thus directly measured.
 - i. Regular waves
 - ii. Irregular waves
 - (b) Radiation forces. The linear actuator is controlled to perform sinusoids.
 - (c) Hydrostatic stiffness. The hull is actuated at different position. The force on the actuator is recorded. Two tests have been performed: in the first test the hull pitch was set to a constant value and the torque was acquired, in the second a continuous motion has been given to the floater. The hull was guided with a sinusoidal motion whose parameters was: 0,01Hz frequency and 15deg amplitude.
 - (d) Uncontrolled response. The linear actuator is dismantled, thus enabling the rotation around the pitch axis. The response of the hull is measured with respect to different waves generated with the wave maker. The movements of the hull are measured with an inertial motion unit sensor.
 - i. Regular
 - ii. Irregular
3. **Phase 3:** Surge configuration
 - (a) Excitation forces

- i. Regular waves
 - ii. Irregular waves
 - (b) Radiation forces
- 4. **Phase 4:** Heave configuration
 - (a) Excitation forces
 - i. Regular waves
 - ii. Irregular waves
 - (b) Radiation forces
 - (c) Hydrostatic stiffness
- 5. **Phase 5:** Floater 6 DOFs moored configuration
 - (a) No PTO action. The floater is moored to the tank floor and waves are generated by the paddle. The flywheel is at zero speed and there is no interaction with the floater kinematics.
 - i. Regular waves
 - ii. Irregular waves
 - iii. Multi directional waves
 - iv. Three dimensional waves
 - (b) PTO action. The floater is moored to the tank floor and waves are generated by the paddle. The flywheel is spinning at different speeds and the internal gyroscopic system is influencing the hull motions.
 - i. Regular waves
 - ii. Irregular waves

The detailed description of the tests and their elaboration can be found in [80] and [79]. For each single DOF the evaluation of the different hydrodynamic phenomena has been done: excitation, radiation and stiffness are separately studied. Uncontrolled response tests are then used to verify the completeness of the analysis.

2.5.2 Single Degree of freedom tests

A modular, re-configurable test rig is required for the experiments carried out in phases 2, 3 and 4. In the following Figure 2.13 the structure concept is shown. The floater (orange) is connected to a structure (blue) that allows only one DOF at a time. The allowed motion is controlled using a linear actuator (green) and the force is measured by a force gauge (red).

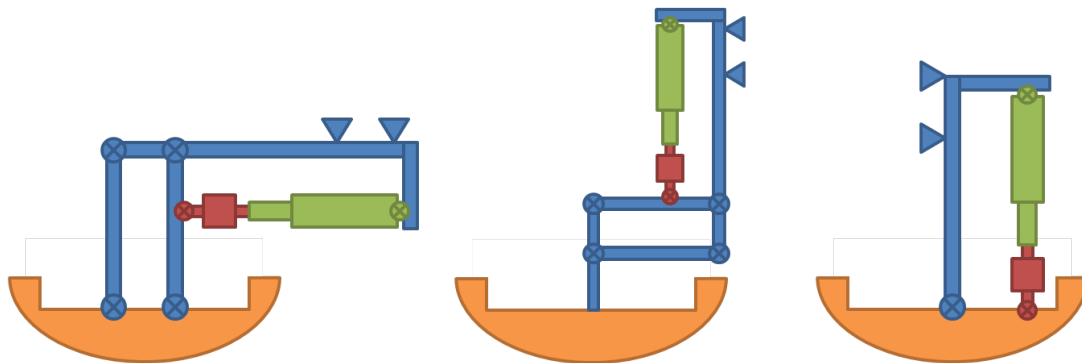


Figure 2.13 Hydrodynamics Tank Tests. Conceptual scheme of the three test rig configurations. From left to right it is possible to see that the allowed DoFs are surge, heave, pitch.

In Figure 2.14 pitch and heave test rigs are shown. They are mounted on the bridge at HMRC in Cork during the experimental campaign. The structure was designed following a functional modular approach. In this way it was possible to reduce the number of components and to reuse them. In particular the linear actuator and the load cell. By controlling the linear position of the actuator is possible to obtain the desired linear or angular position of the floater. On the other hand, controlling the actuator in the starting position, while waves hits the floater loads are measured by the load cell, thus enabling the measurement of the overall torque acting on the floater.

Some time histories examples of phase 2, pitch tests, are presented below in Figures 2.15 and 2.16. Starting from the top, an example of test devoted to the computation of excitation forces is shown. The floater is kept fixed by the linear actuator and the corresponding force is measured through the load cell. The floater is hinged in its COG and the corresponding moment arm enables the measure of the overall acting torque on the hull. The tank paddles are activated in order to create different waves into the tank. In the plot the wave elevation measured by wave probe 6 (WP6) is shown. When the resultant moving water hits the hull a net torque is



Figure 2.14 Hydrodynamics Tank Tests. Pitch and Heave test rig installed in HMRC tank in Cork (Ireland), 2014.

generated. This generalized force is also shown.

In the second subplot a radiation time history is presented. This time the tank paddles are held and the tank water surface at the beginning of each test is still. The actuator is controlled in position to realize sinusoidal motions. The torque exerted is measured. With some post-processing analysis (cleaning inertia and stiffness components) it is possible to evaluate the floater radiation term.

In Figure 2.16 some data coming from stiffness tests (configuration "c") and an

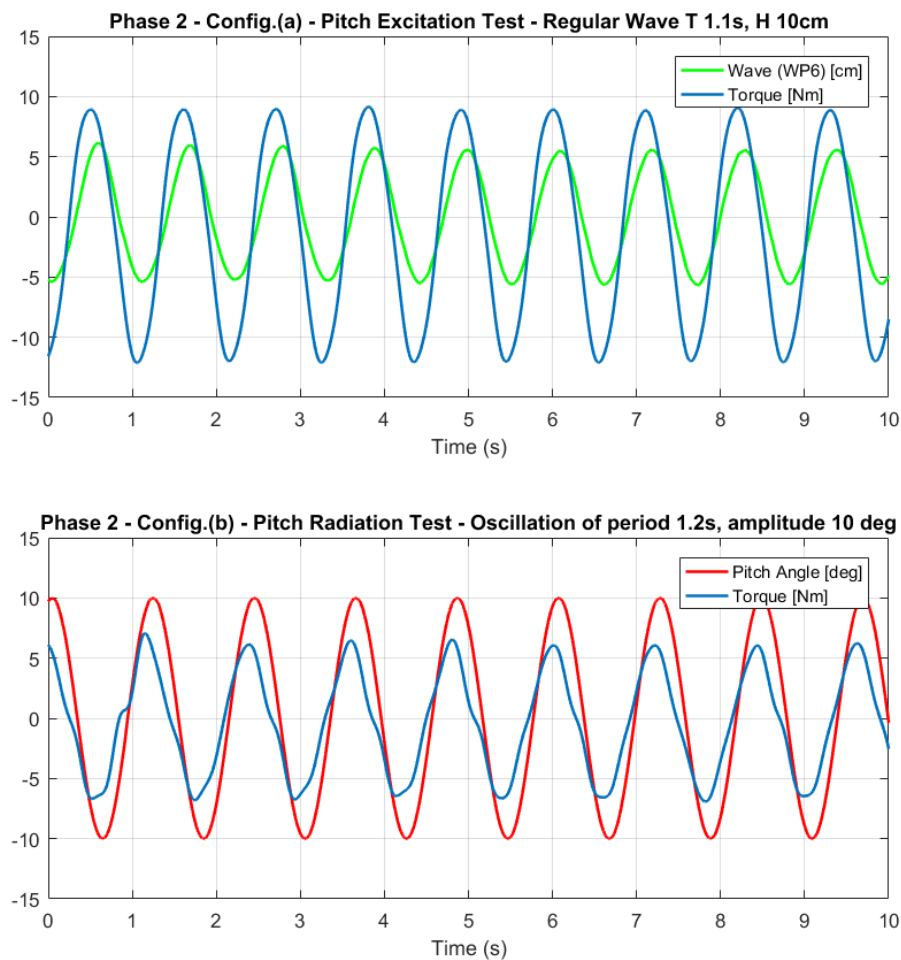


Figure 2.15 Hydrodynamics Tank Tests. Time histories examples. Phase 2: pitch excitation and radiation tests.

example of uncontrolled response (configuration "d") are presented. In the top subplot the stiffness, restoring, torque is represented in function of the pitch angle. This was controlled by the linear actuator. In this picture it is interesting to observe the stiffness nonlinear behavior when pitch is greater than 10 deg and the floater deck goes

underwater.

In the bottom subplot an example of irregular waves uncontrolled response is illustrated. In these tests the linear actuator is removed and the floater is free to rotate around the pitch axis centered into its COG. Both regular and irregular waves are explored. In this case a unidirectional irregular wave is reported.

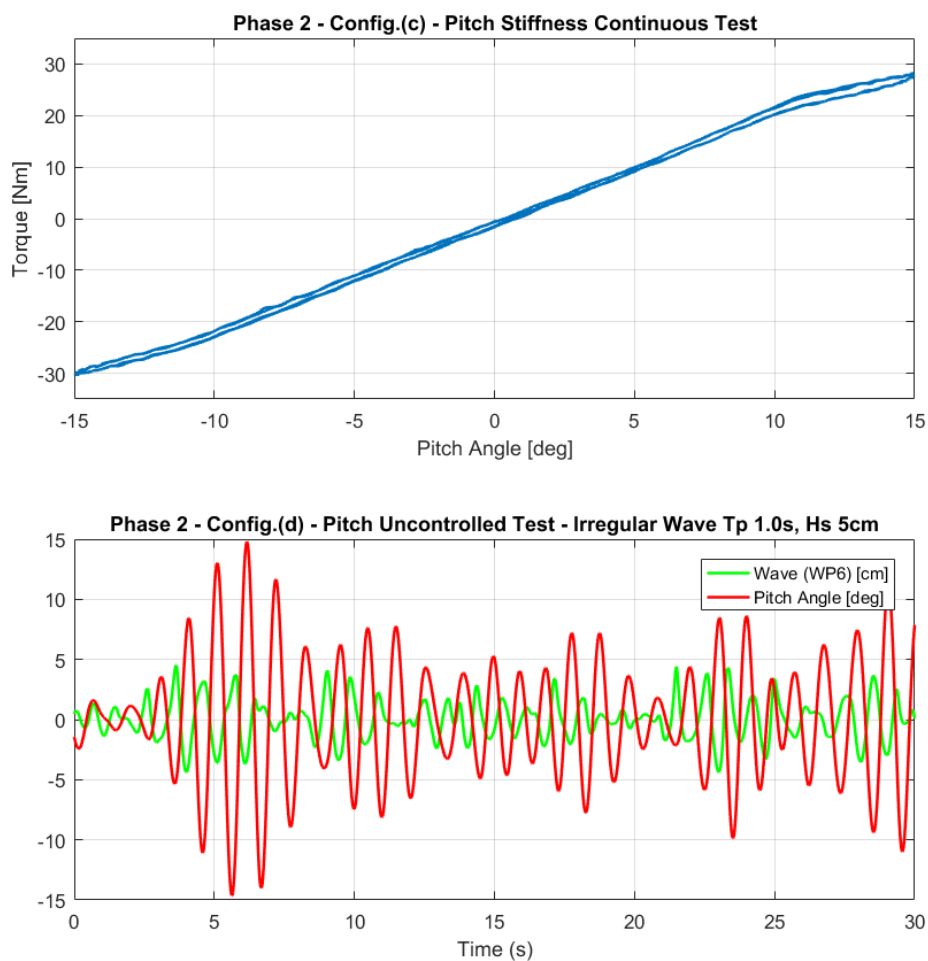


Figure 2.16 Hydrodynamics Tank Tests. Time histories examples. Phase 2: pitch stiffness and uncontrolled tests.

2.5.3 Floating moored device tests

In phase 5 the floater is moored in the center of the tank, in front of the paddles in a previously calibrated area. Four wave probes have been installed around. In Fig-

Figure 2.17 the test setup is shown. The mooring system has also been scaled according to the 1:20 ratio.



Figure 2.17 Hydrodynamics Tank Tests. Floater moored to the tank floor. 6 DOF analysis.

Tests have been carried out both with the uncontrolled floater and with a controlled one. In Figure 2.18 the complete device used for the tests is shown. The prototype owns a complete SCADA system on-board, with a cRIO running an acquisition and control software with external PC user interface. A small DC electric motor works as PTO. It is equipped with a 4 quadrants power electronic drive and it can perform full reactive control on the axis. A small torque motor is mounted on the flywheel spinning axis and controls its speed. A set of batteries and a wi-fi model complete the setup.

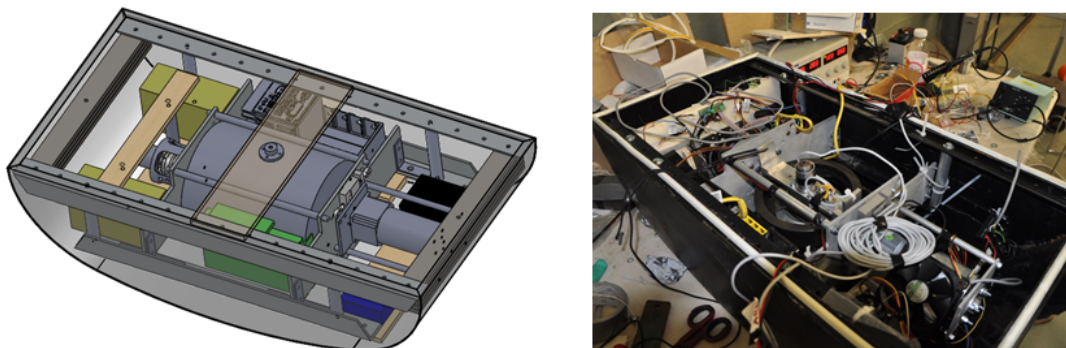


Figure 2.18 Tank Tests. ISWEC 1:20 scale, design and prototype during assembly.

From this series of tests a lot of information and experiences were gained. Both of a quantitative or qualitative form. Some of the most important result are hereafter mentioned:

- some tests were performed with regular and irregular waves changing the main direction (0 deg to 30 deg) of the incoming wave front. The self-alignment properties of the system were thus verified.
- some tests were also performed with fully 3D waves field, both with the PTO both without. These tests were important in observing the reaction of the floater to the multidimensional problem, otherwise not deeply studied with the numerical model.
- an important outcome was an observation about the functionality of the mooring system. Sometimes happened that during the surge oscillations of the floater, the hull overcame the jumper chains node, thus bridling itself. This problem was effectively solved by reducing the length of the chains to the main body and elevating the jumper position. This solution was also adopted for the ISWEC installation in Pantelleria.

2.5.4 Quadratic viscous term

Different results coming out from data post processing are presented in [79]. The identification of a quadratic viscous term proportional to the pitch angular rate was the most important result, because it made the overall ISWEC numerical model definitely more credible and reliable. The parameter β has been identified minimizing the root mean square error between the pitch amplitudes of experiments and simulations.

$$F_{viscous,\delta} = -\beta \dot{\delta} |\dot{\delta}| \quad (2.35)$$

In Figure 2.19 the comparison between experimental results and those obtained with two numerical models, one fully linear and the other with the viscous quadratic term are shown. As expected for a quadratic term, its influence is less for waves with smaller amplitude, where the floater motion are also confined. For higher waves, the effect is more important. The quadratic term in fact reduces the resonance effects of the linear model.

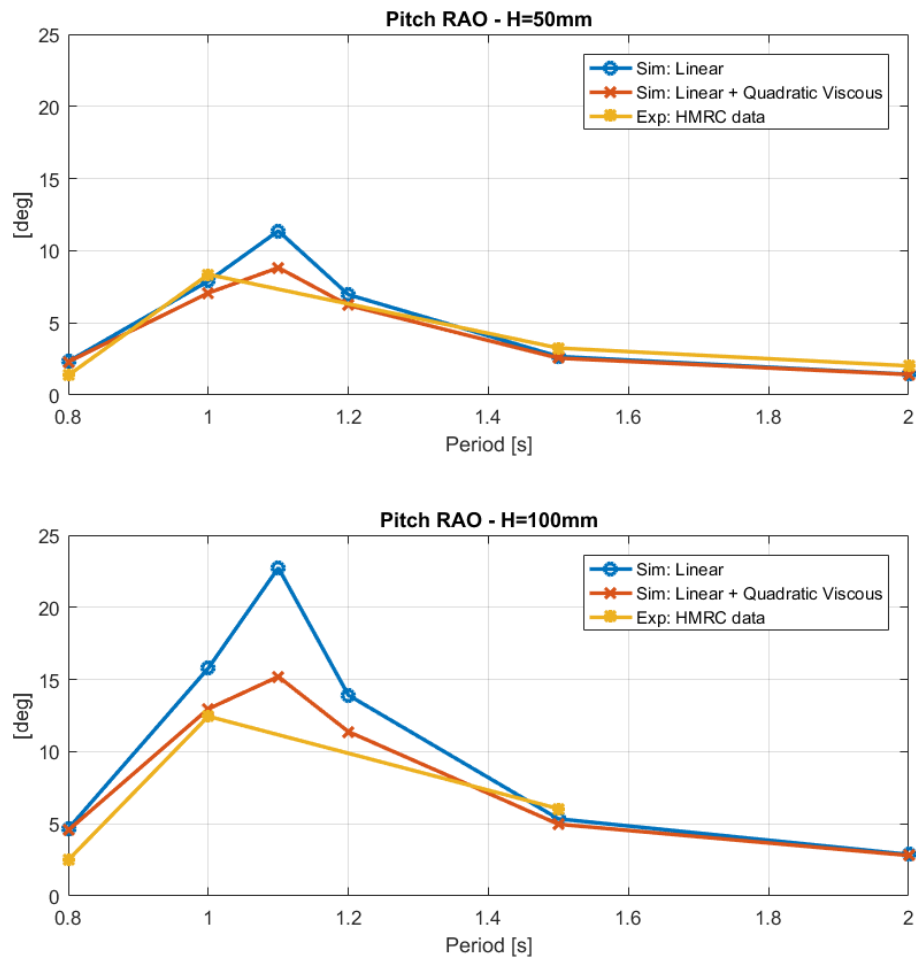


Figure 2.19 Hydrodynamics Tank Tests. Floating 6 DOF moored system. Comparison between experimental and numerical results. The Cummins fully linear model and the upgraded model are used.

2.6 ISWEC - Pitch DOF model

The design of the 1:8 Pantelleria scale prototype and the Pantelleria full scale prototype has been completely carried out with a pitch, one degree of freedom model. Objective of this paragraph is to introduce the reasons of this choice and some of the drawbacks and advantages that such a modeling approach involve.

2.6.1 Motivations

First reason lies in the historic development of the model. Starting from regular-waves standard Cummins equation, the study moved steps toward the modeling of irregular waves. This was possible in particular through the state space approximation of the Cummins time-domain convolution term [74]. The main problem at that time was the modeling of the irregular drift forces. The research started, but a viable solution had to be found in order to go further with the design. The solution found was to start an hydrodynamic experimental campaign with a 1:20 Pantelleria floater, in order to validate this simplified hydrodynamic or at least to assess its modeling capabilities. This experimental campaign is presented in Chapter 7. Outcome of the work was the identification of the pitch viscous term, previously shown. The searched coefficient was independent from frequency and amplitude. Results were acceptable.

A second reason, that can be both a drawback or an advantage, is that without the surge motion it was possible to do simulations and obtaining results without upgrading the model with a non-standard modeling of the mooring system. In such a way the specification procurement phase could carried out, having info about the hydro and electro-mechanical loads of the ISWEC.

A drawback was the quality of the results, but at that time was not clear the real possible improvement of a 3 DOF plane model. Some experimental campaign had to carried out.

An advantage of such a modeling is the possibility to linearize it. This can be used both for frequency analysis and the development of model based observers or control strategies, as is proposed in Chapter 6. The final main advantage is the extremely low computational demand of this model. It has been considered extremely quick to be run in extensively numerical time-domain parameters optimizations with millions of runs per campaign. Making it a suitable tool for the model-based design procedures used.

2.6.2 Time Domain Model

For simplicity the device interaction with waves is reduced to a planar problem, with the work plane defined by the vertical gravity axis and the direction of the incoming wave, since the system is self-orientating toward the incoming wave front direction. Another simplification consists in dropping lower-magnitude terms, see [78]. For hydrodynamic modeling, the planar approximation and the pitch only model, make the hydrodynamic linear [6x6] matrix problem to collapse into a scalar one, where the variable is the pitch δ and its derivatives.

The gyroscopic modeling also becomes a single differential equation governing the internal precession axis ε .

At the end all the dynamic relationships can be reduced to a system of one differential and one integro-differential equations given in equation 2.36: the first describing the dynamic behavior of internal precession PTO axis and the second the floater pitch degree of freedom (DOF).

$$\begin{cases} T_{\varepsilon} = I_g \ddot{\varepsilon} + J\dot{\phi} \dot{\delta} \cos(\varepsilon) \\ \tau_w = (I_{eq} + \mu_{\infty}) \ddot{\delta} + \int_0^t \dot{\delta}(\tau)h(t - \tau) d\tau + \\ \quad + \beta |\dot{\delta}| \dot{\delta} + K_w \delta - J\dot{\phi} \dot{\varepsilon} \cos(\varepsilon) \end{cases} \quad (2.36)$$

In the first equation T_{ε} is the PTO torque, I_g is the overall momentum of inertia around the PTO ε -axis, J is the gyroscope axial momentum of inertia, $\dot{\phi}$ is the flywheel velocity. In the second equation, τ_w represents the wave induced torque on the floater, I_{eq} is the device momentum of inertia around the pitch DOF, μ_{∞} is the instantaneous added mass and $\mu = \int_0^t \dot{\delta}(\tau)h(t - \tau) d\tau$ is the convolution integral representing the radiation force memory effects, having the impulse response in the kernel [32], K_w is the linear hydrostatic stiffness. β is a quadratic term added after being identified in 1:20 tank tests campaign at HMRC(2014) and scaled up using Froude similitude relation [81]. It is used in order to mitigate unreal linear resonance effects. The gyroscopic effect owed to inertial momentum quantity $J\dot{\phi}$ dynamically links the two equations with nonlinear coupling terms. It can be easily noticed that the two axis become independent when the flywheel velocity $\dot{\phi}$ equals zero.

The last missing element is the description of the T_{ε} contribute. This is the torque applied by the Power Take Off electric generator. In order to keep the flywheel axis oscillating around the vertical, the control law presented in equation(2.37) was

designed. It is made of a stiffness component proportional to the angular distance from vertical ε , and a damping component proportional to the same axis speed $\dot{\varepsilon}$.

$$T_{\varepsilon PTO}(t) = -k\varepsilon(t) - c\dot{\varepsilon}(t) \quad (2.37)$$

A reactive power flux between the PTO and the sea surface is expected, due to the presence of the stiffness component. This control belongs to reactive control techniques and it is then close to impedance matching approach.

2.6.3 Frequency Domain Model

Equation (2.38) shows the system of equations (2.36) after being linearized around $\varepsilon = 0$ and then brought in frequency domain using the Laplace transform:

$$\begin{cases} \bar{T}_{\varepsilon} = I_g \bar{\varepsilon} s^2 + J\dot{\bar{\phi}} \bar{\delta} s \\ \bar{\tau}_w = (I_{eq} + \mu_{\infty}) \bar{\delta} s^2 + F_{rad}(s) \bar{\delta} s + K_w \bar{\delta} - J\dot{\bar{\phi}} \bar{\varepsilon} s \end{cases} \quad (2.38)$$

If it is desired to study the effect of the wave over the system, the dynamic relationship between the wave elevation and the wave force must be made explicit:

$$\bar{\tau}_w = \bar{a}_w F_{h2f}(s) \quad (2.39)$$

The closed loop proportional-derivative control law is transformed in Laplace domain as well:

$$\bar{T}_{\varepsilon PTO} = -k\bar{\varepsilon} - c\bar{\varepsilon} s \quad (2.40)$$

After some manipulations with these equations, it is possible to find the relationship (eq.2.41) between the wave elevation and the pitch amplitude for different wave periods in regular sea states.

$$\frac{\bar{\delta}}{\bar{a}_w} = \frac{F_{h2f}(s)}{(I_h s^2 + F_{rad}(s)s + K_w) + \frac{J_g^2 \dot{\phi}^2 s^2}{I_g s^2 + cs + k}} \quad (2.41)$$

2.6.4 State Space Pitch DOF linear model

Starting from the system of equations 2.36, the problem is hereafter reformulated in a state space form.

Previously, a required step is to reformulate the convolution integral term μ can be

reshaped in an approximated state space shape [64].

$$\mu = \int_0^t \dot{\delta}(\tau)h(t-\tau)\dot{\delta} d\tau \approx \begin{cases} \dot{x} = \mathbf{A}_{rad}x + \mathbf{B}_{rad}\dot{\delta} \\ \mu = \mathbf{C}_{rad}x \end{cases} \quad (2.42)$$

It is then possible to rewrite the overall system in a set of first order linearized differential equations, know as state space representation. The general form is then proposed:

$$\dot{\mathbf{X}} = \mathbf{A}\mathbf{X} + \mathbf{B}u + \mathbf{B}_d w \quad (2.43)$$

where

\mathbf{X} is the state vector containing the gyro frame position and speed for modeling the precession axis dynamics, the pitch angle and its rate for describing the floater motion and the n states required by the approximation of the wave radiation convolution integral.

$$\mathbf{X} = [\dot{\epsilon} \ \epsilon \ \dot{\delta} \ \delta \ \rho_{rv1} \ \dots \ \rho_{rvn}]^T \quad (2.44)$$

u is the controllable input. It is the PTO electric motor torque (T_{PTO}) after being multiplied by the gearbox ($T_{\epsilon PTO}$).

\mathbf{B} is the controllable input matrix.

$$\mathbf{B} = \left[\frac{1}{I_g} \ 0 \ 0 \ 0 \ 0 \ \dots \ 0 \right]^T \quad (2.45)$$

w is the uncontrollable, unknown input. It is the wave disturbance. This is the torque exerted by the waves on the floater pitch degree of freedom.

\mathbf{B}_d is the wave disturbance input matrix.

$$\mathbf{B}_d = \left[0 \ 0 \ \frac{1}{I_{eq} + \mu_{\infty}} \ 0 \ 0 \ \dots \ 0 \right]^T \quad (2.46)$$

\mathbf{A} is the system matrix. It is linearized around $\epsilon = 0$, that is for having the flywheel rotational axis inside the ISWEC longitudinal plane. For sake of simplicity the

following substitution is made: $I_{eq*} = I_{eq} + \mu_{\infty}$.

$$\begin{bmatrix} 0 & 0 & \frac{J_g \dot{\phi}}{I_g} & 0 & 0 & 0 & 0 & \dots & 0 \\ 1 & 0 & 0 & 0 & 0 & 0 & 0 & \dots & 0 \\ \frac{-J_g \dot{\phi}}{I_{eq*}} & 0 & 0 & \frac{-K_w}{I_{eq*}} & \frac{-c_1}{I_{eq*}} & \frac{-c_2}{I_{eq*}} & \frac{-c_3}{I_{eq*}} & \dots & \frac{-c_n}{I_{eq*}} \\ 0 & 0 & 1 & 0 & 0 & 0 & 0 & \dots & 0 \\ 0 & 0 & 1 & 0 & a_1 & a_2 & a_3 & \dots & a_n \\ 0 & 0 & 0 & 0 & 1 & 0 & 0 & \dots & 0 \\ 0 & 0 & 0 & 0 & 0 & 1 & 0 & \dots & 0 \\ \vdots & \vdots & \vdots & \vdots & \vdots & \vdots & \ddots & 0 & 0 \\ 0 & 0 & 0 & 0 & 0 & 0 & 0 & 1 & 0 \end{bmatrix} \quad (2.47)$$

The linearized viscous term can also be added. It is presented in next section 2.7 .

2.6.5 Power Losses

For what concern the power losses, these are the introduced in the model in the same way as those already described in section 2.3.

2.7 ISWEC - Frequency Domain 6 DOF Linear Model

A linear frequency domain model can be useful after the floater is designed and Cummins parameters identified. It can be used in the pre-design phase for the correct choice of the parameters to be explored in the following detailed model-based, design phase. A state space approach for writing the equations is used.

2.7.1 Hydrodynamics

Most restrictive hypotheses concern the hydrodynamics model. The floater is free to move in all its 6 DOFs. Second order effects are neglected. The only second order contribution that is taken into account is the pitch viscous term, that is linearized as explained in the following.

The first step is to write the state space matrices of the 6 DOFs hydrodynamics. Looking at equation 2.25, it is elaborated in the equation:

$$[\mathbf{M} + \mathbf{A}(\omega)]\ddot{\mathbf{X}}_{hyd}(\omega) + \mathbf{B}(\omega)\dot{\mathbf{X}}_{hyd}(\omega) + \mathbf{K}\mathbf{X}_{hyd}(\omega) = \mathbf{F}_w(\omega) \quad (2.48)$$

Where the :

$$\bullet X_{hyd} = [x, y, z, r_x, r_y, r_z]^T = [surge, sway, heave, roll, pitch, yaw]^T$$

And where:

- \mathbf{M} : Floating body inertia matrix [6x6];
- $\mathbf{A}(\omega)$: Frequency dependent added mass matrix [6x6];
- $\mathbf{B}(\omega)$: Frequency dependent radiation matrix [6x6];
- \mathbf{K} : Hydrostatic stiffness matrix [6x6];
- $F_w(\omega)$: Frequency dependent wave force vector [6x1];

Next step is to define $\mathbf{A}_{eq}(\omega) = [\mathbf{M} + \mathbf{A}(\omega)]$. And to compute the acceleration from the equation above:

$$\ddot{X}_{hyd}(\omega) = -\mathbf{A}_{eq}(\omega)^{-1} \mathbf{B}(\omega) \dot{X}_{hyd}(\omega) - \mathbf{A}_{eq}(\omega)^{-1} \mathbf{K} X_{hyd}(\omega) + \mathbf{A}_{eq}(\omega)^{-1} F_w(\omega) \quad (2.49)$$

The state vector is then defined as:

$$X_{SS,hyd} = \begin{bmatrix} \dot{X}_{hyd} \\ X_{hyd} \end{bmatrix} \quad (2.50)$$

And the previous equation is written as a system of first order equations in a matrix form:

$$\begin{bmatrix} \dot{X}_{hyd} \\ \dot{X}_{hyd} \end{bmatrix} = \begin{bmatrix} -\mathbf{A}_{eq}(\omega)^{-1} \mathbf{B}(\omega) & -\mathbf{A}_{eq}(\omega)^{-1} \mathbf{K} \\ I & 0 \end{bmatrix} \begin{bmatrix} \dot{X}_{hyd} \\ X_{hyd} \end{bmatrix} + \begin{bmatrix} -\mathbf{A}_{eq}(\omega)^{-1} F_w(\omega) \\ 0 \end{bmatrix} H \quad (2.51)$$

$$\dot{X}_{SS,hyd} = \mathbf{A}_{SS,hyd}^* X_{SS,hyd} + \mathbf{B}_{SS,hyd} H \quad (2.52)$$

Where I is the ones diagonal identity matrix and H is the wave height.

It is common that such linear models return exaggerate values of motion amplitudes, mainly in the proximity of resonance values. In order to increase the reliability of the model, a quadratic damping term is added, as explained in section 2.4.2. The pitch damping factor is linearization procedure is hereafter introduced.

The pitch oscillating speed amplitude in regular waves can be evaluated with the simple relationship:

$$\dot{\delta}_0 = \frac{2\pi}{T_{max\ pitch\ RAO}} \delta_0 \quad (2.53)$$

For the ISWEC Pantelleria floater, the maximum amplitude of the pitch RAO is at 5 s. Keeping this value constant, the pitch speed can be evaluated for different amplitude of oscillations δ_0 . The viscous quadratic term can be computed using its relationship:

$$T_{viscous,\delta,0} = -\beta \dot{\delta}_0 |\dot{\delta}_0| \quad (2.54)$$

The term can thus be linearized for different δ_0 amplitudes, as shown in Figure 2.20. The linearization point amplitude value is identified from CFD or experimental analy-

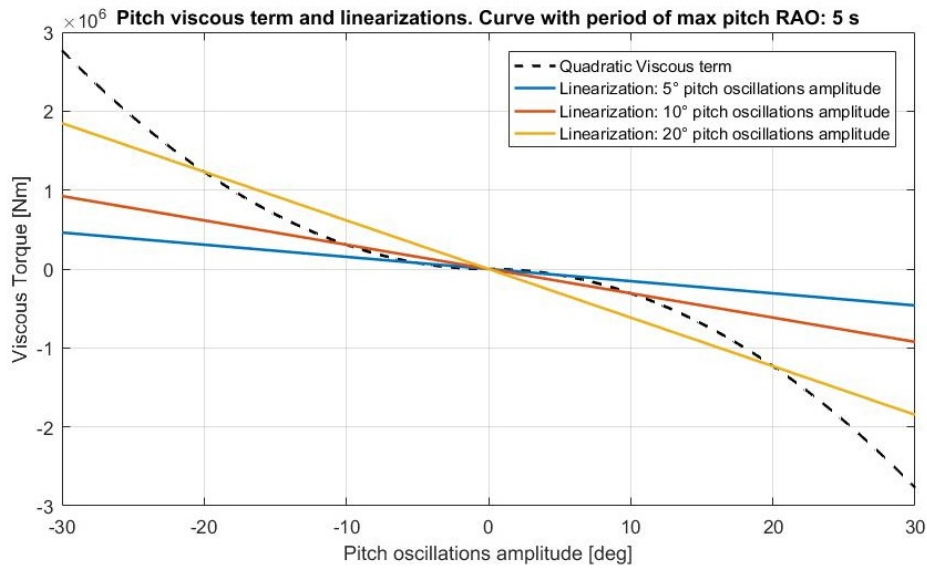


Figure 2.20 Viscous quadratic term linearization.

sis. In the present document, the linearization point is chosen using sea experimental data coming from the 2015 ISWEC experimental campaign. The nonlinear planar model presented in this chapter has good match with experimental data, thus the linearization point is identified in order to match this data. In table 2.7 an example is presented. More experimental tests with the system orientated are needed, as explained in Chapter 7, at this stage $\delta_0 = 10$ is chosen for the following.

This β_{lin} coefficient is frequency independent. It is summed to all the $\mathbf{B}(\omega)_{(5,5)}$ elements. After this sum, the $\mathbf{A}_{SS,hyd}^*$ system matrix assumes its final version defined $\mathbf{A}_{SS,hyd}$.

$$\mathbf{A}_{SS,hyd} = \mathbf{A}_{SS,hyd}^* + \beta_{lin} @ \mathbf{B}(\omega)_{(5,5)} \quad (2.55)$$

In Figure 2.21 the comparison between the two RAO plots is presented.

Table 2.7 Comparison between different models and experimental data for irregular sea state.

Test		
14:22 30th Nov 2015		
Te (s)	Tp (s)	Hs (m)
6.48	7.54	2.05
Experimental	3DOF nonlinear model	1DOF nonlinear model
δ rms (deg)	δ rms (deg)	δ rms (deg)
5.42	5.28	6.48
6DOF linear model (viscous lin 5deg)	6DOF linear model (viscous lin 10deg)	6DOF linear model (viscous lin 20deg)
δ rms (deg)	δ rms (deg)	δ rms (deg)
6.49	5.47	4.34

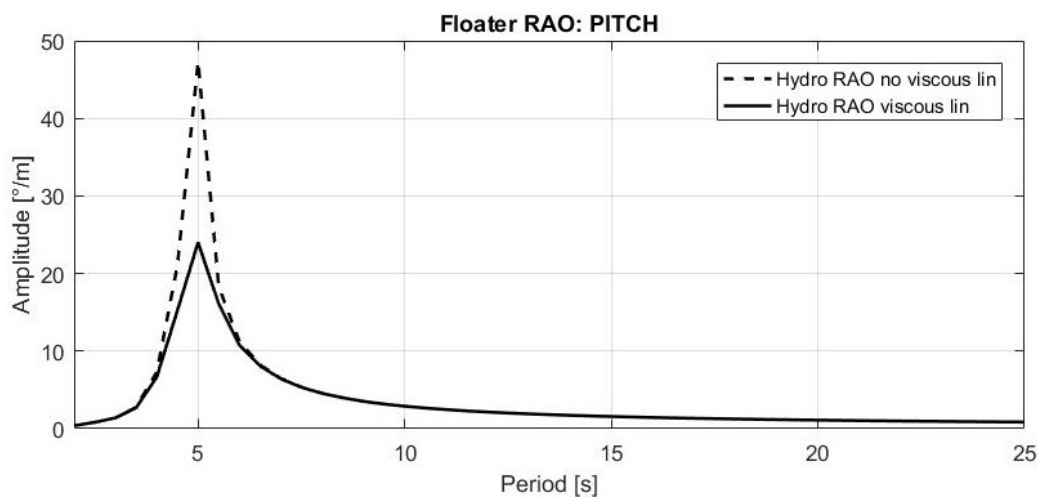


Figure 2.21 Floater pitch RAO. Comparison RAO with and without linearized viscous forces.

2.7.2 Gyroscope system

The 6DOF gyroscopes equations are simplified considering an even number of gyroscopes, as presented in section 3.3.3.3. Thus the starting nonlinear equations come from the simplified planar model, also found in equation 2.36. Masses and inertia moments are reduced to an equivalent gyroscope, since the only resulting effect is on the pitch degree of freedom and a symmetric behavior is assumed. Then, this equivalent gyroscope is linearized around the vertical, $\varepsilon = 0$, position. All efficiencies are ideally chosen equal to 1.

Two more states are added: the equivalent gyroscope frame angular position ε_{gyro} and the equivalent gyroscope frame angular velocity $\dot{\varepsilon}_{gyro}$.

$$X_{SS,gyro} = \begin{bmatrix} \dot{\varepsilon} \\ \varepsilon \end{bmatrix} \quad (2.56)$$

The regulation used for writing this equations is the proportional-derivative (PD) control law. The linearized equation governing the axis behavior is:

$$I_g \ddot{\varepsilon}_{gyro} = c\dot{\varepsilon}_{gyro} + k\varepsilon_{gyro} - J\dot{\phi}\dot{\delta} \quad (2.57)$$

This can be written as a system of first order equations:

$$\begin{cases} \ddot{\varepsilon}_{gyro} = \frac{c}{I_g}\dot{\varepsilon}_{gyro} + \frac{k}{I_g}\varepsilon_{gyro} - \frac{J\dot{\phi}}{I_g}\dot{\delta} \\ \dot{\varepsilon}_{gyro} = \dot{\varepsilon}_{gyro} \end{cases} \quad (2.58)$$

Some matrices have to be defined. The first is the precession ε axis dynamic equation matrix.

$$A_{gyro} = \begin{bmatrix} -c/I_g & -k/I_g \\ 1 & 0 \end{bmatrix}, [2x2] \quad (2.59)$$

The second is the $A_{floater \rightarrow gyro}$ matrix, describing the action torque caused by the floater speed on the internal ε axis:

$$A_{floater \rightarrow gyro} = \begin{bmatrix} 0 & 0 & 0 & 0 & -J\dot{\phi}/I_g & 0 & \dots & 0 \\ 0 & 0 & 0 & 0 & 0 & 0 & \dots & 0 \end{bmatrix}, [2x12] \quad (2.60)$$

The third matrix is the matrix that models the torque discharged by the gyroscope systems motion on the floater, the reaction torque $J\dot{\phi}\dot{\epsilon}$:

$$A_{gyro \rightarrow floater}(\omega) = \begin{bmatrix} 0 & 0 & 0 & 0 & J\dot{\phi} / (M_{5,5} + A_{5,5}(\omega)) & 0 & \dots & 0 \\ 0 & 0 & 0 & 0 & 0 & 0 & \dots & 0 \end{bmatrix}^T, [12 \times 2] \quad (2.61)$$

2.7.3 ISWEC 6 DOF state space

The complete frequency domain representation is obtained by the combination of the two above presented. The system is thus modeled with a 6DOF linear hydrodynamics and a frequency independent damping term. The gyroscopes are described with a single equivalent group. The mechanic-electrical conversion is considered as ideal. The state space is shown in equation 2.62.

$$\begin{bmatrix} \dot{X}_{SS,gyro} \\ \dot{X}_{SS,hyd} \end{bmatrix} = \begin{bmatrix} A_{gyro} & A_{floater \rightarrow gyro} \\ A_{gyro \rightarrow floater}(\omega) & A_{SS,hyd} \end{bmatrix} \begin{bmatrix} X_{SS,gyro} \\ X_{SS,hyd} \end{bmatrix} + \begin{bmatrix} 0 \\ B_{SS,hyd} \end{bmatrix} H \quad (2.62)$$

An example of analysis that can be carried out with this linear model is presented in Figure 2.22. An algorithm looks for the optimal c and k control parameters in order to optimize the power adsorbed at a desired wave period (6.5 s) while keeping the internal axis oscillations within a specified range (in this example the maximum amplitude of oscillations is 40°). Using the RAOs of the floater motions and of the internal shaft parameters it is possible to look insight the behavior of the system. From the figure on the top left corner, it is straightforward to see that the ISWEC harvests energy through the damping of the pitch hull motion. The floater has a dominant effect, as can be seen in other frames. The gyroscope frame motion is linked to the floater response and the peak is near the peak of the pitch RAO. Nonetheless, it is broader and nearer the wave period of interest, 6.5 s. The power adsorption also has a similar shape, with the peak in between 5 s and 6.5 s. As last information, also a preliminary quantitative idea of the RCW is given (with efficiency equal to 1).

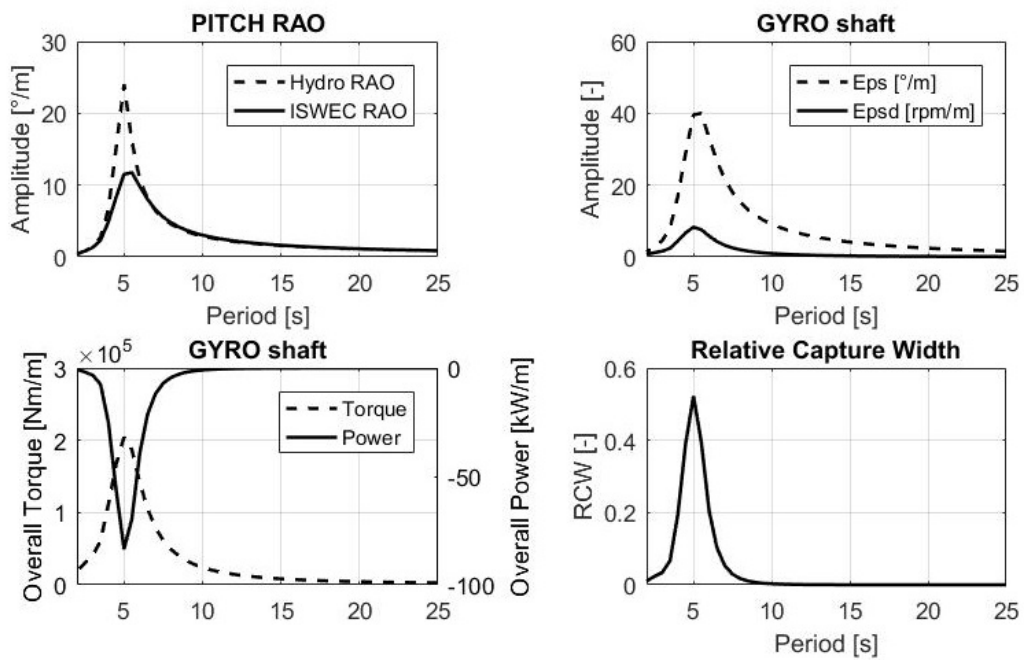


Figure 2.22 Example of regular waves Frequency Domain Analysis performed with the state space model.

2.8 ISWEC - Numerical Wave to Wire model

Wave to wire models (W2W) are common instruments in wave power for the evaluation of power conversion capabilities of a technology. They are fundamental tools for techno-economical evaluations and for functional simulations and specification procurement. Usually these models require short time to simulate minutes of WEC sea operations. ISWEC wave to wire model consists of a Matlab/Simulink Time Domain numerical model. The main block diagram and some of its main subsystems are presented in this chapter. The development, upgrade and maintenance of this model has been a key element during the doctorate program activities. Several versions have been produced depending on the functionalities required. The model hereafter presented is the one that has been used for some main activities: the components specifications procurement, the estimation of final device life, the computation of control matrices and the productivity/LCOE estimation of the device in Pantelleria installation site.

2.8.1 The Block Diagram

In Figure 2.23 the main block diagram is shown. Starting from the left, the first subsystem is the one dedicated to waves. This is the real input of the system, containing the waves loads that are forcing the dynamics of the whole device. The wave forces then enters the block "Floater 3DOFs", in which hydrodynamics relationships are implemented. Other inputs for the hydrodynamic subsystem are the mooring forces, obtained by the "Mooring" block, and the generalized reaction forces received as a feedback by the internal gyroscopic system. The floater kinematics is then directly linked as input to the two gyros subsystems. The torques acting on the internal axis are in fact proportional to floater rotational velocities. The Power Take Off torque is also acting on the same axis and thus each gyro block has also the input port devoted to this term. The control system is composed by the elements in the central part of the model. The first two blocks, in orange, are the ones that generate the power production set points for the two groups. The second, in red, is a higher level controller that manages the passage between different operation cases, the synchronization of the two gyroscopic groups, some safety controllers and the position control loop shared between different cases. At the left bottom there are two subsystem dedicated to data log and some post processing operations, as the computation of losses due to the electric drive efficiencies and the gyroscopes bearings.

In the following, a brief look inside the different subsystems is proposed.

In Figure 2.24 the waves internal block diagram is illustrated. The Froude-Krylov and diffraction forces for the DOFs are given: surge, with both excitation and drift forces, heave and pitch. For what regards the surge, also the wave drift forces are fed. At the bottom also the wave elevation is logged.

The "Floater 3DOFs" block is shown in Figure 2.25. At the top left three input terms are algebraically summed into the summation block: the gyroscope system reaction torques, the wave generalized forces and the mooring forces. Also hydrodynamic retroaction terms are fed back: radiation, viscous and stiffness components come into summation block with minus sign. The algebraic sum of all these forces is then divided per the overall floater inertia and the added mass matrix. From these operation, the accelerations for all the DOFs are computed. The three DOFs characterizing the planar problem are then fed through, while other DOFs are multiplied by zero. Two integrals compute then velocities and positions. In Figure 2.26 the gyroscope system subsystem is explored. This model extensively uses the mechanical blocks of the "Simscape" Simulink toolbox. The hull kinematics are given as input to the planar and rotation joints of zero-inertia bodies. This imposed kinematics forces the gyroscope system internal rotational joint. This is linked to the gyroscope frame body and also receives as input the torque exerted by the PTO electric motor. On this body is connected the revolute joint that enables the spinning motion of the flywheel body. This last axis (ϕ) also is forced by a kinematic input: the constant flywheel speed. Simscape library is very effective in the simulation of such a phenomenon, positively simplifying the complexity of the model at the expenses of a slight increase in calculus time. Fundamental output of the block are the computed reaction torques, the loads discharged by the gyroscope system on the three floater DOFs.

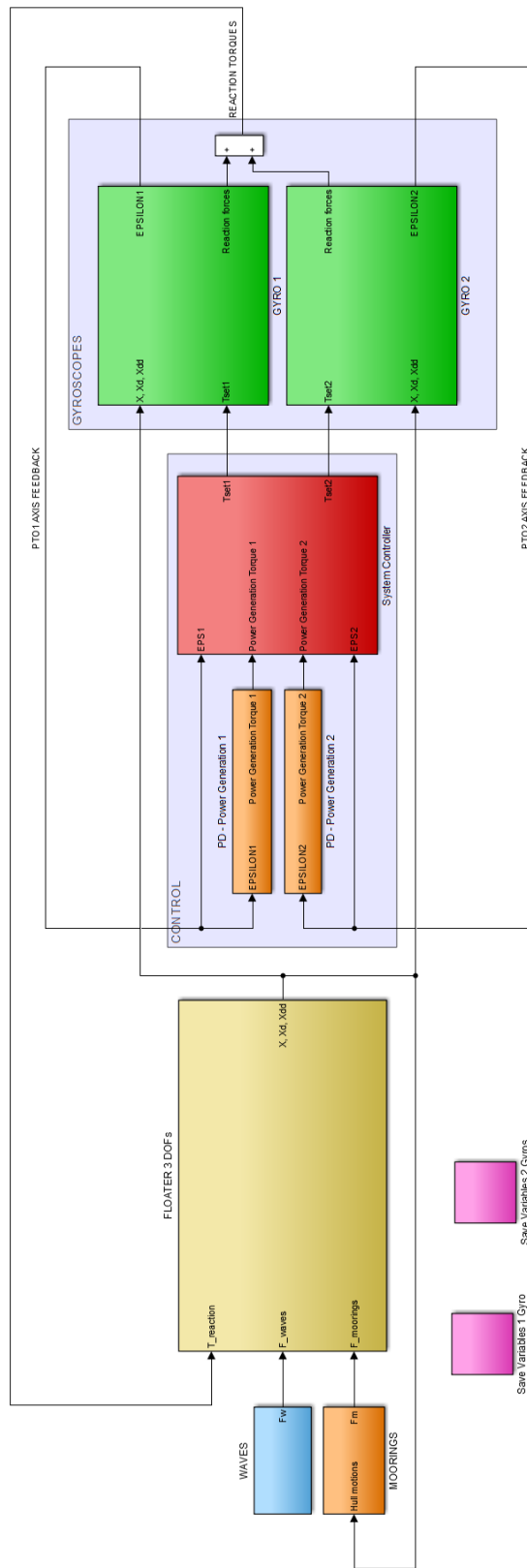


Figure 2.23 Numerical model - Main block diagram

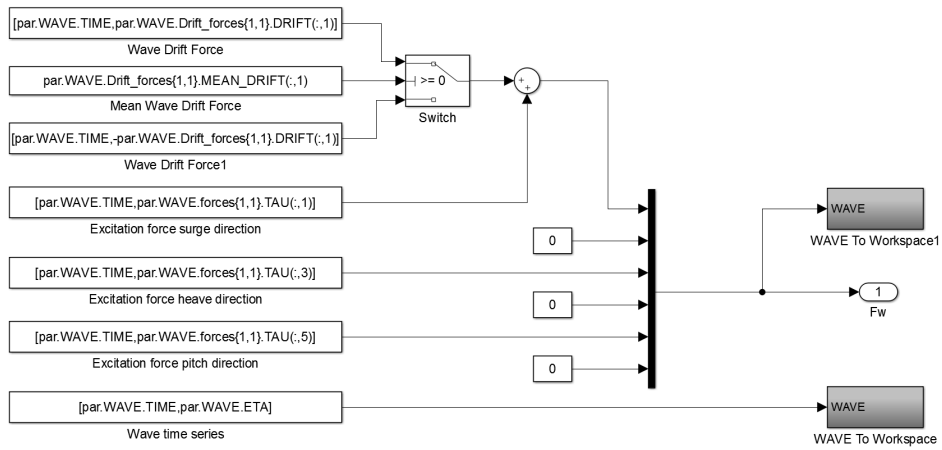


Figure 2.24 Numerical model - Subsystem: "WAVES"

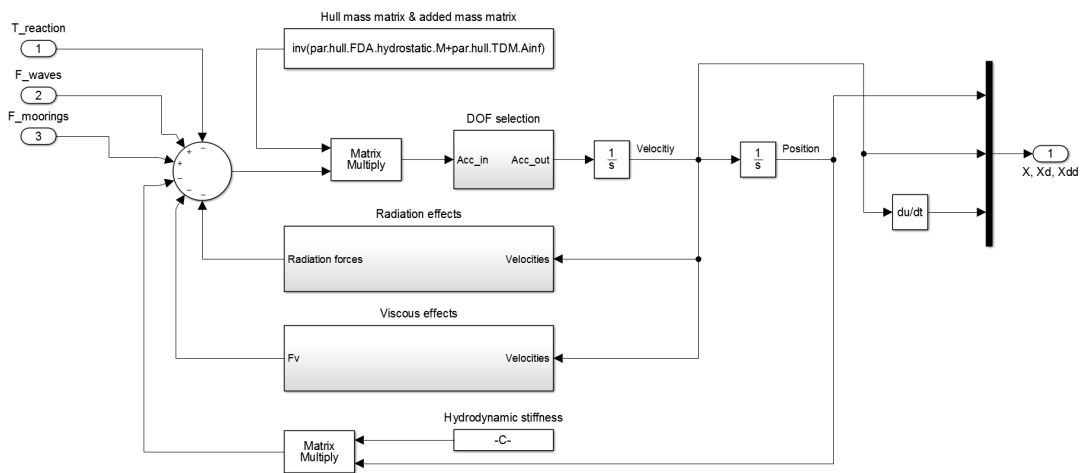


Figure 2.25 Numerical model - Subsystem: "FLOATER 3 DOFs"

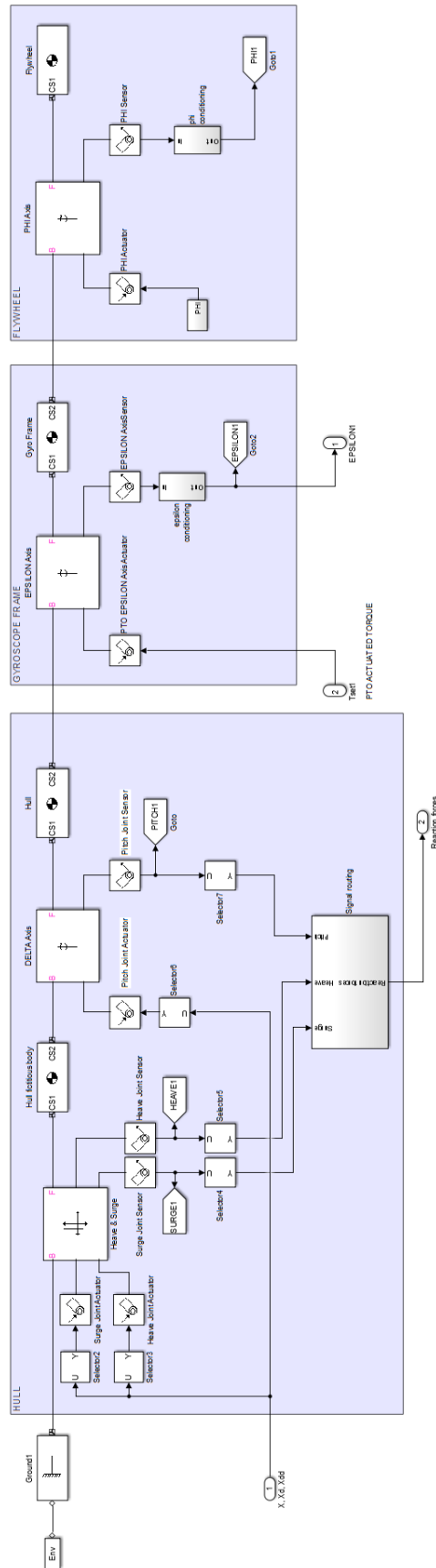


Figure 2.26 Numerical model - Subsystem: "GYRO 1"

Power losses are not affecting the dynamics of the system. They are computed using system states time histories and can even be computed offline in post processing operations. Despite this, in order to reduce memory effort and the amount of data and signals to be stored, these are computed online, in the "log and save" subsystem. In Figure 2.27 the block containing the static lookup tables of power losses is shown.

Two subsystems that have been central in the development of the ISWEC SCADA

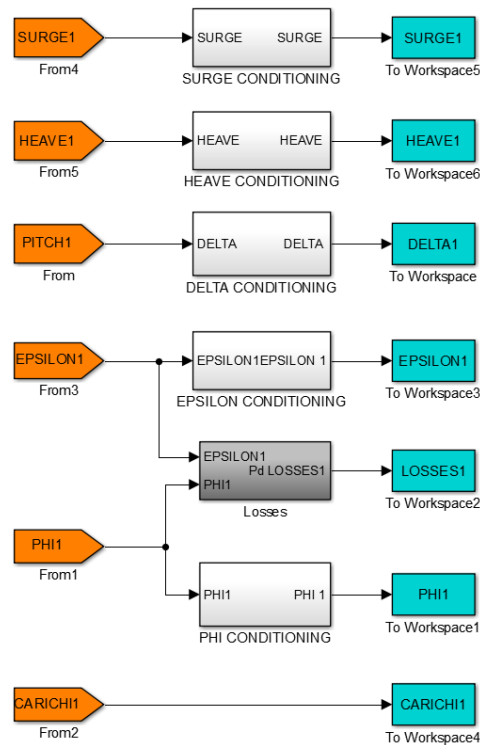


Figure 2.27 Numerical model - Subsystem: "Save Variables 1 Gyro"

system are the "Power Generation Control" and the "System Controller". These are the center of the system management, containing the logic for the state machine operations and the creation of the set point for the PTO electric motor. These two subsystems grew together with the device SCADA software, in an iterative procedure of development and coding. It was in fact fundamental to have the same logic developed and tested on the two different environments. In Figure 2.28 the first subsystem to be presented is the "Power Generation". This is the responsible of the computation of the PTO torque reference, in order to maximize the energy harvesting. In this example, the proportional derivative controller is presented. At the left of the scheme, the signal conditioning mimicking the units of the real SCADA system. On the right the computation of the torque reference happens with the same numerical gains as in the real Pantelleria

device. This is fundamental for the portability of code and parameters and avoid mistakes and incidents.

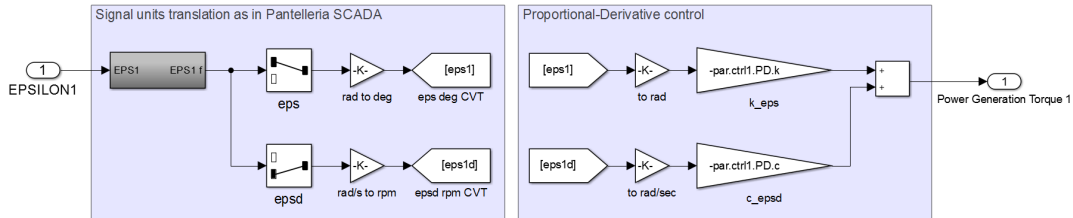


Figure 2.28 Numerical model - Subsystem: "PD - Power Generation"

In Figure 2.29 the system controller subsystem is presented. This block receives both the set point generated by the two gyroscopic groups, both the kinematics of the respective frames. Several other fundamental blocks are part of this architecture:

- **Position Controller.** The Power generation torque enters this block with the gyro group kinematics. This system is the responsible of the device state machine, choosing and managing the operational states. Moreover, in case of testing, safety or transition cases, in which the position controller takes over the generation control, it is controlling the axis position with a closed loop feedback architecture.
- **The synchronizing controller.** This controller corrects the actions given as set to the PTO gyro group 2 in order to keep in "synchronized", in phase, with the first "master" gyro group 1.
- **Torque Saturation Safety.** These two blocks, one per each gyro, are the responsible of the torque constraints, both related to the maximum saturation in order to avoid overloads, both for what concern the most common constraint management, with strategies that are presented in the following.
- **Power Saturation.** This subsystem is responsible for the torque limitation with respect to the maximum power achievable by the PTO. This security system is also present into the electric motor drive, but it is put here for redundancy and because in this way the maximum power can be changed from the human machine interface, via internet connection, during operations.

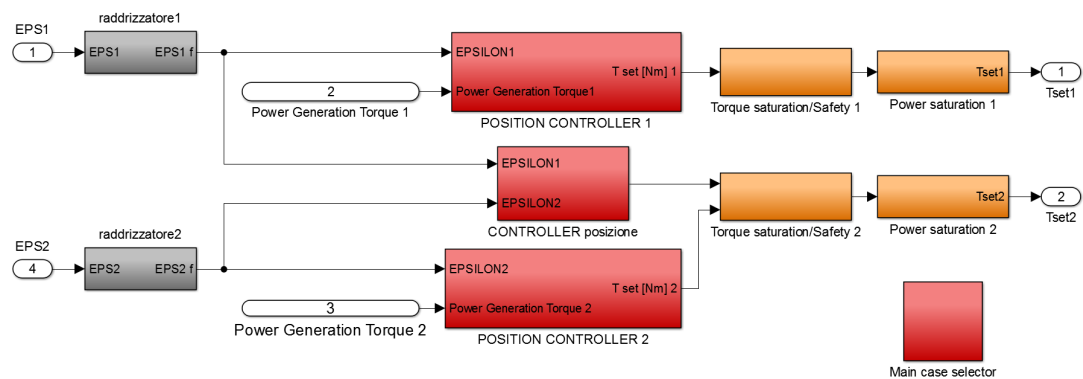


Figure 2.29 Numerical model - System Controller

In this subsystem two main architectures are present: the "Case Selector" subsystem and the "Position Control Loop". The case selector gives as output the current operational state of the machine: if it is in normal operation, in safety case or in transition between them. It mainly receives input related to the controlled PTO. The strategies involved in case selection are presented in section 5. The position control loop is an always operational system, even if often the torque reference it generates is excluded. It consists of the controller of a predominantly inertial under-actuated system. This makes this axis not of simple control, in particular during storms, when the system is safety case. The first specification for this controller was stability, then a weighted derivative gain was added to the standard proportional term. Also rate limiters in velocity set-point generation and torque actuation are included. Another particularity present in this system is the bump-less transition, which avoids discontinuities in the torque actuation even if the set-point are instantaneously changed (normal power harvesting to safety conditions change). On the right of the scheme, the selector is feeding through the power harvesting torque or the position controller computed reference.

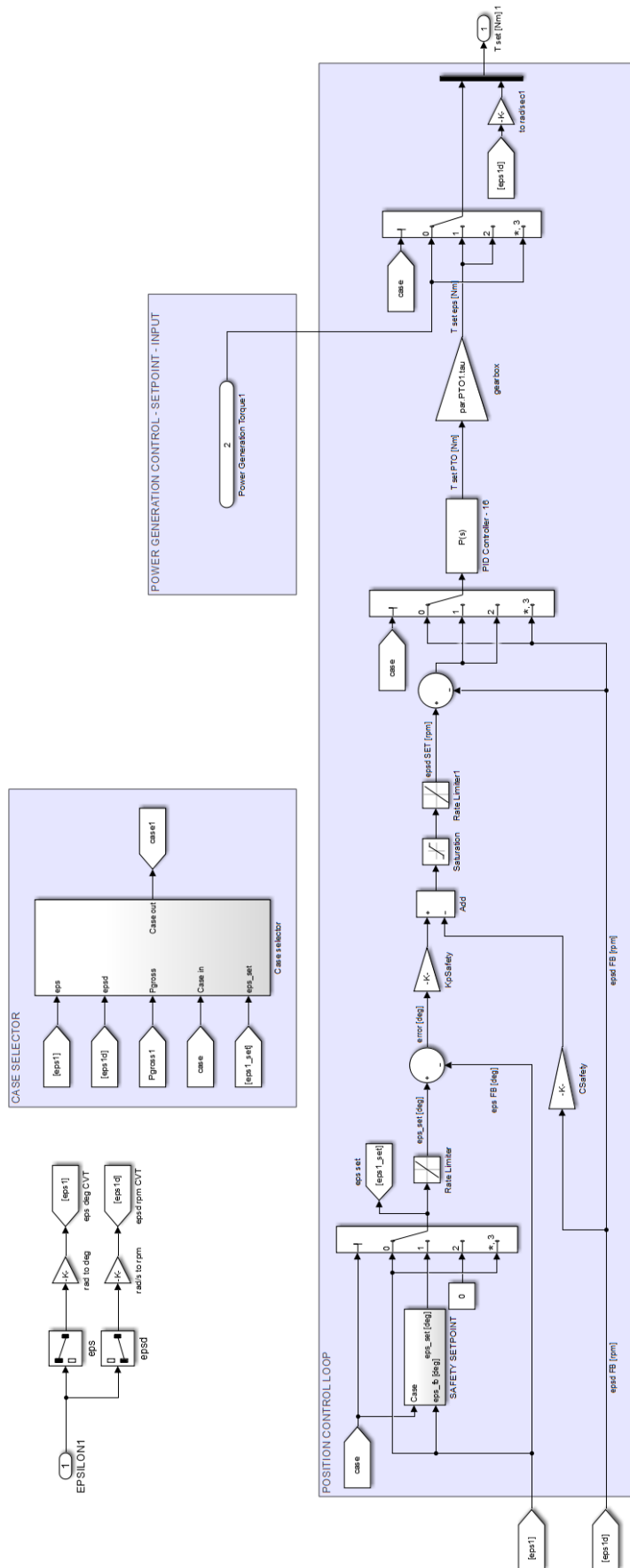


Figure 2.30 Numerical model - Position Control Loop

2.8.2 Time History Example

In the following Figures 2.31,2.32 an example of time domain outcomes is proposed. Even if it includes numerous non-linearities, the time required for this simulations, with an overall simulated time of 900s, is of 50s. This low value enables the use of the model for parametric analysis, both orientated to the design both for the optimization of control parameters. Starting from the top of Figure A, wave elevation and the floater pitch are shown. The forcing wave is very energetic and steep, considering Pantelleria wave climate. These are the conditions in which the device is working at its best. It must be noticed that the pitch motions have a maximum amplitude less the 15 degrees. It means that it remains in a valid, reasonable, area of operations. This kind of behavior is strongly due to the non-linear quadratic viscous term, otherwise it would be easy to find unrealistic oscillations greater than 30 or even 40 deg. The second subplot is well illustrating one of the main features of the ISWEC device: the pitch to gyro frame axis motion amplification. Both the internal mechanical ε and the floater δ are angles, and the ratio between the root mean square value for this time history is of about 6. So during this first power conversion step the angular velocities are increased and torque is reduced, thus simplifying the loading conditions for the further conversion chain element: the PTO. In the bottom plot the PTO torque and mechanical absorbed power are illustrated. Looking at the power, it is clear to see the functioning of the reactive control and the mean negative value, meaning an average energy absorption is happening.

Figure B is completely devoted to the illustration of power fluxes. It is thus possible to observe the relative available power decrements characteristics of this power conversion system. In the top plot the PTO mechanical and electric power are plotted together. The difference is due to the PTO efficiency. These losses are then plotted in the middle figure together with the flywheel bearings mechanical losses. Even if the absolute values are not plotted, they have been adimensionalized with respect to the peak maximum absorbed mechanical power. It is thus possible to observe their relative value in relation to the power absorption. Values are about the 10-15% for the electric losses and less than 5% for the mechanical ones. In the bottom graph the net electric power going into the DC bus is plotted with the mechanical harvested one.

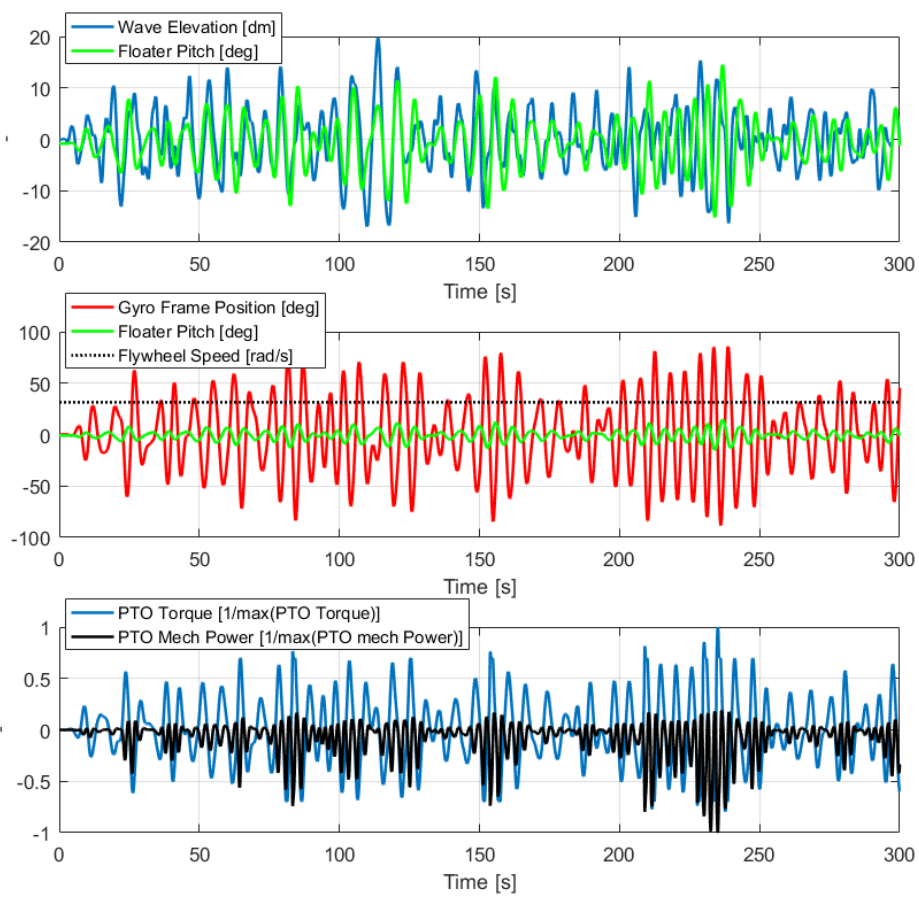
ISWEC Pantelleria - Wave: $T_e=6.7s$, $H_s=2,5m$ - Fig.A

Figure 2.31 Numerical model - Time history example - Figure A

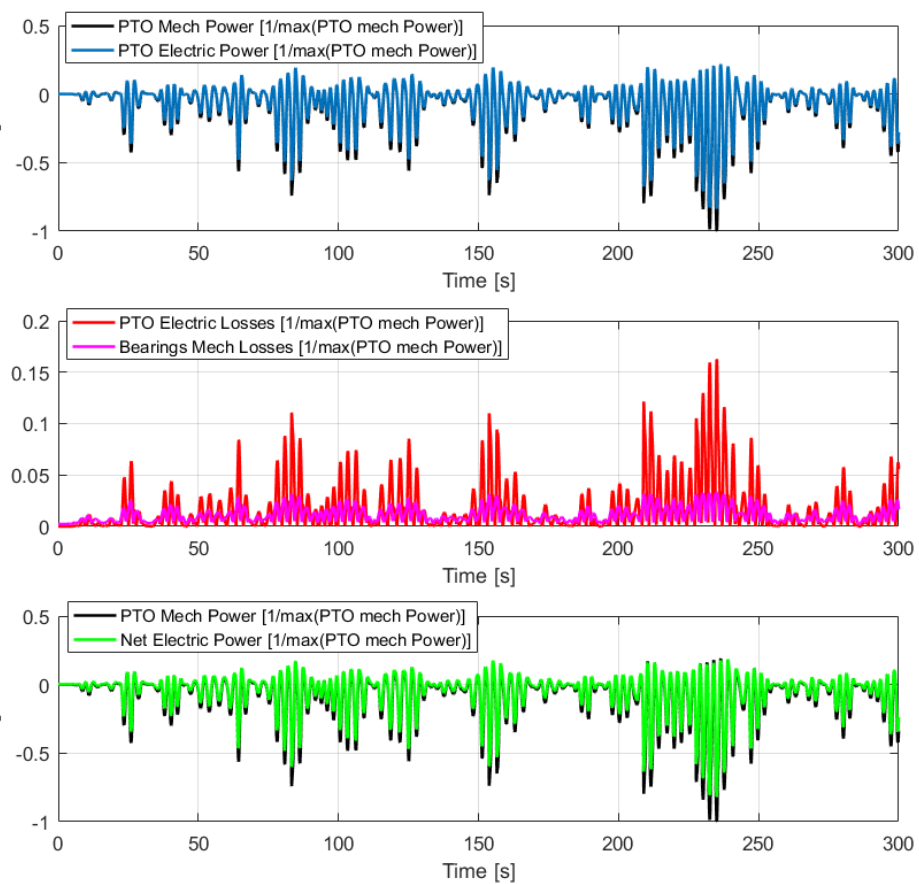
ISWEC Pantelleria - Wave: $T_e=6.7s$, $H_s=2.5m$ - Fig.B

Figure 2.32 Numerical model - Time history example - Figure B

Chapter 3

ISWEC device design

The purpose of this chapter is to present the method that have to be used to design an ISWEC device. This procedures are originally described in Chapter 5 of the Raffero thesis [78]. Nevertheless several contributions are completely original and some choices previously adopted are here further clarified or proved.

Among the novel contents in this chapter:

- The selection of the pre-design nominal sea state, as a fundamental step for the minimization of ratio between installed capacity to power factor. The introduction of a scalar parameter indicating the neighboring quantities of occurrences and energy for each sea state on the scatter is an unpublished concept in literature. Some examples of applications to different ISWEC devices are proposed.
- The need of an even number of gyroscope units is explored and proved.
- The pre-design of ultracapacitors is introduced with an analytical formulation, starting from the admissible DC BUS voltage fluctuations.
- A pre-design tool, the "ISWEC design tool", has been developed. This software uses some hypothesis and a cost function constraint methods in order to use a fully linear ISWEC model for the simulations. In this way it is possible to reduce the computational time needed for calculating a whole optimized power matrix. This tool helps the system engineer to have a quantitative feedback already from the very first phases of the project about the productivity, the life of main components, the size and number of gyroscopic groups and PTOs.

Finally quite a few improvements in the analysis and design methods have been introduced, also starting from considerations risen with the experiences gained with the ISWEC Pantelleria device.

3.1 Installation site - Pantelleria wave resource

3.1.1 Irregular waves description

As introduced in the project overview section 1.4, in 2010 there has been a wave profile data acquisition campaign, with an AWAC sensor. A 20 minutes data record was logged every hour, sampled at 2 Hz frequency.

Irregular waves can be described as the sum of a number of regular waves. They thus can be described a frequency domain representation. The distribution of the wave elevation in function of frequencies is normally defined as wave spectrum. Thus, a wave profile time history can be studied and defined using some scalar indexes, in particular starting from the so-called moments of the distribution [105].

In general, the n th-order moment m_n is computed as:

$$m_n = \int_0^{\infty} f^n E(f) df \quad (3.1)$$

Where f is the frequency measured in Hz and $E(f)$ is the energy variance density.

At least a couple key-defining sea state parameters can be evaluated using different order moments:

- **Significant wave height.** This value is defined as the average of the highest one-third of the wave heights, $\bar{H}_{1/3}$. It is possible to accurately estimate it also starting from the zero order momentum of the wave distribution.

$$H_{m_0} = 4\sqrt{m_0} \quad (3.2)$$

In general the approximation is correct for narrow spectra, but even if not, in most cases the difference is small, with an average of $H_{m_0} = 1.05\bar{H}_{1/3}$ [105]. So, when the significant wave height is indicate with H_s , it is always better to indicate whether it is H_{m_0} or $\bar{H}_{1/3}$. In the present work, $H_s = H_{m_0}$ is used.

- **Wave energy period.** This parameter gives information about the energetic content of the analyses irregular wave. It is calculated using the following relationship:

$$T_e = \frac{m-1}{m_0} \quad (3.3)$$

These two parameters are fundamental for the computation of the energy content of a wave, its power density. They thus consist in the first step in the characterization procedure for the resource present in an installation site.

3.1.2 Occurrences scatter table

Each single wave elevation time record of the complete 2010 dataset is then analyzed with the previous methods. In this way each wave is identified with a couple of parameters: H_s and T_e . The data is then clustered in what are called scatter tables. Rows (heights) and columns (periods) entries for the table have fixed intervals. Each wave position is then automatically identified in order to stay inside both intervals of periods and heights. Each matrix element is the sum of the hours that a particular sea state happened during the analyzed year.

Occurrences scatter tables obtained with the previously presented method are shown in Fig. 3.1.

Observing the occurrence scatter table, some comments have to be given. The first is that the most occurrent sea state is about H_s 0.5m and T_e equal to 5.75s. Starting from this maximum occurrences point, the time distribution of waves goes on a diagonal, with a trend common to almost all installation sites. Despite being a Mediterranean site, there is still an area characterized by $T_e = 8s$, $H_s = 3.2m$ with quite interesting occurrences that have to be explored in the design phase.

For completing the site screening, the energy content of the waves must also be explored.

3.1.3 Energy scatter table

In this section wave energy available power basic theoretical assumptions are stated and the Pantelleria installation site resource is evaluated. As a first step, the wave power density power has to be defined. This quantity indicates the time average power

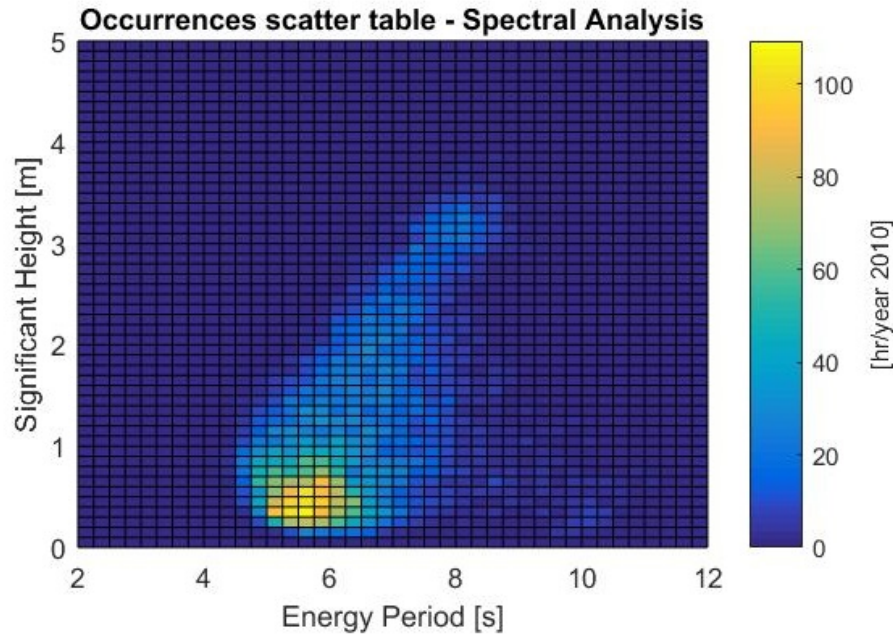


Figure 3.1 Pantelleria occurrences scatter table (2010).

that one meter of wave front owns. It is commonly indicated with kW/m unit. There are different equations for the evaluation of this quantity for regular and irregular gravity waves [96]. The one used in this thesis are those with the deep water hypothesis, for areas with a water depth larger than half the wavelength.

- **Regular waves power density.** The equation is:

$$J_{reg} = H^2 T \quad (3.4)$$

Where J is the power density in kW/m , H is the height in m and T is the period in s .

- **Irregular waves power density.** The equation is:

$$J_{irreg} = 0.49 H_s^2 T_e \quad (3.5)$$

Where J is the power density in kW/m , H_s is the significant wave height in m and T_e is the wave energy period in s .

The energy scatter table is then obtained multiplying each occurrences scatter table matrix element (hours per year) by its correspondent power density (kW/m). For the

design of the ISWEC the energy scatter table is computed with the irregular waves power density formula.

The resulting matrix is presented in Fig. 3.2.

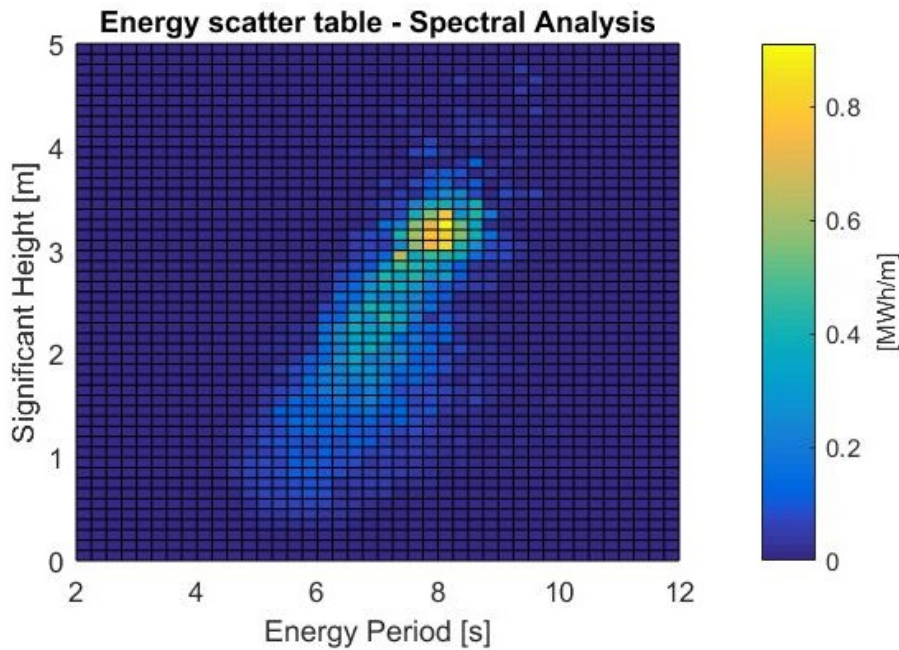


Figure 3.2 Pantelleria energy scatter table (2010)

The energy maximum in the year is in an area of sea states near $H_s = 3.2m$, $T_e = 8s$. This seems to imply that it is preferable to design the device for working in this point. In reality, the choice of the installation point must necessarily be a trade-off choice between the most energetic point and the most occurrent, in order to reduce the maximum installed capacity over the yearly mean absorbed power and to increase the capacity factor of the WEC. The choice of a suitable design point is discussed in section 3.2.

3.1.4 Directionality

Another waves key property in the characterization of an installation site is the wave front spreading direction. In the analysis carried out for the design of the ISWEC, Pantelleria resulted to be a site characterized by a prevalent direction. The system is in fact installed in the north west side of the island (Fig. 3.3, the red circle), the most energetic one. Looking at Figure 3.4 it is possible to understand why, given that it is

open to the west Mediterranean fetch. Moreover, it is close to the island port and on the shore of the industrial area, thus reducing visual and environmental impact.

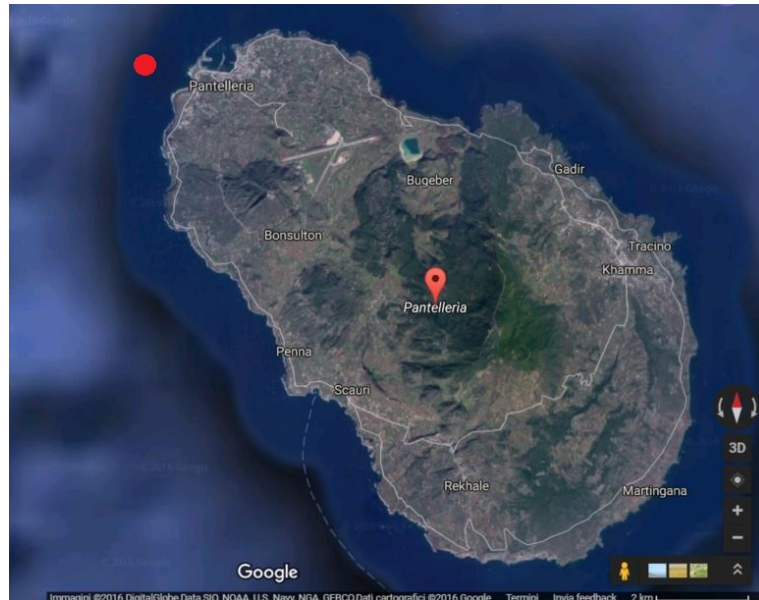


Figure 3.3 Pantelleria installation site. Latitude $36^{\circ} 50' 2.52''$, Longitude $11^{\circ} 55' 50.40''$. Satellite view. [47]

Forecast valid for 06 Sep 2017 at 07h
Init 06 Sep 2017 at 00h

whole Mediterranean sea

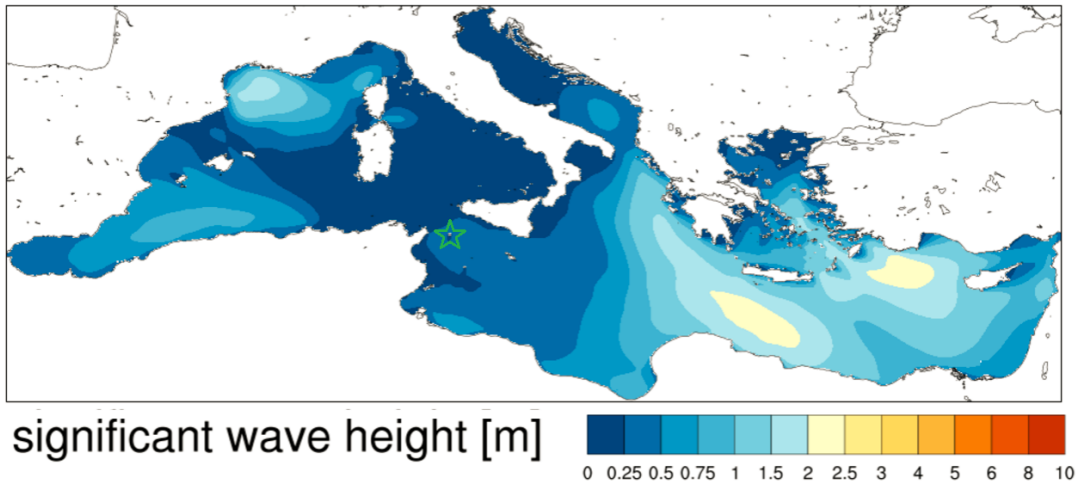


Figure 3.4 Mediterranean Sea. ENEA UTMEA group. Pantelleria is highlighted by the green star. <https://giotto.casaccia.enea.it/waves/> (Accessed: 06/07/2017).

As can be seen in Figure and knowing that in that area of the Mediterranean Sea the main wave propagation direction is from North-West to South-East, it can be easily understood the early reasons of the following project hypothesis: in the selected

installation site the waves direction distribution has a strong prevalent North-West to South-East behavior.

Nonetheless, after the experimental campaign started, a constant monitoring and analysis of the incoming waves direction in the site has been carried on. The results of the period elapsed from 18 February 2015 up to 18 February 2016 are summarized in next Figure 3.5, 3.6, 3.7.

From the occurrences distribution, a prevalent direction can be identified from 270° up to 330° . However also a minor but not negligible part of the waves is coming from East, at about 90° . These have to be considered during the mooring configuration design.

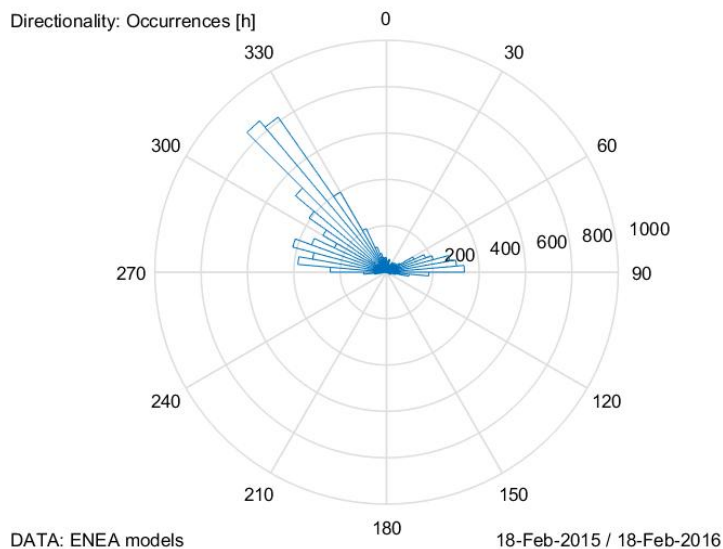


Figure 3.5 Pantelleria directional occurrences. Period: February 2015 - February 2016.

Looking at the power content, the site is even more directional. In fact all the waves arriving from the island, the 90° direction, are characterized by a very low height. This fact makes this distribution narrower, from about 305° up to about 340° .

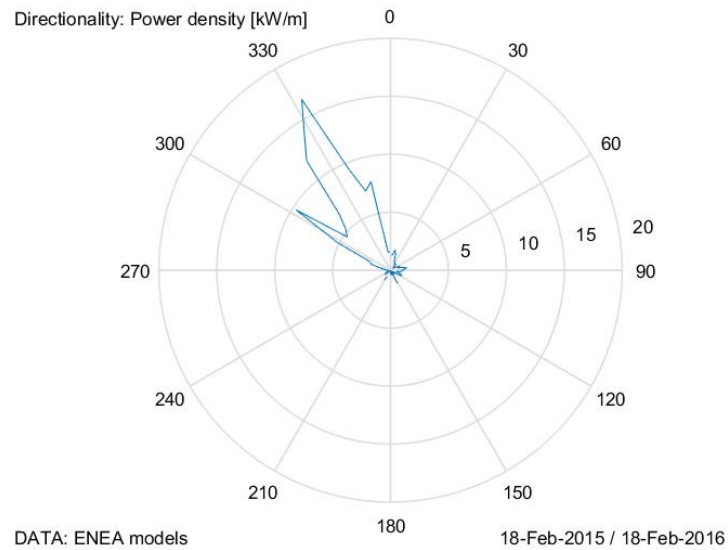


Figure 3.6 Pantelleria directional power density. Period: February 2015 - February 2016.

The last step is to verify the directionality of the energy content. After the multiplication of the occurrences direction distribution by the power density direction distribution, the situation is even more clear. Almost all the energy in the site is coming from about 320°, North-West direction.

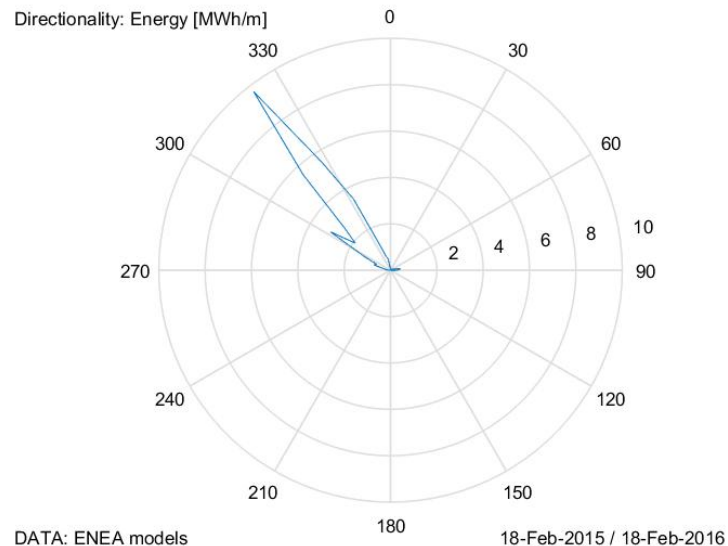


Figure 3.7 Pantelleria directional energy. Period: February 2015 - February 2016.

The conclusion of all these observation is that the early hypothesis of considering the site directional can be considered truthful.

3.2 The pre-design nominal sea state

After the Pantelleria installation site resource has been characterized, what is called a *design point* must be chosen. This is a reference, nominal sea state used in the pre-design phase for the identification of a first-attempt configuration of the device. Starting from this configuration, an extensive parametric optimization is performed. However, the choice of the design point can change the whole project direction and represents a crucial phase in the design process.

3.2.1 The selection procedure

There is not a straightforward way to choose the optimal design point at this time. A standard will probably be defined with research and experience in the field. In next lines a procedure draft with some observations and open points is presented.

Pre-design point - Nominal sea state - Choice

- **Plant Nominal Power.** The nominal power of the plant can have different meanings. The first definition is the one that has been used in the design of the Pantelleria device. The following two are instead two novel suggestions based on the experience gained in these years. Those are useful for a site-depending design for a new device.
 - 1) It can be the mean net power output in nominal sea state conditions.

$$P_{nom} = P @ \textit{nominal sea state} \quad (3.6)$$

- 2) It is the minimum desired mean net power output in the year.

$$P_{nom} = \frac{(\textit{year net productivity [kW h]})}{(365 \textit{ days}) (24 \textit{ hours/day})} \quad (3.7)$$

- 3) A third option, the most complete, is that it is the nominal power plant power to be used when computing the capacity factor. The desired capacity factor has also to be chosen in this phase.

$$P_{nom} = \frac{(\textit{year net productivity [kW h]})}{(365 \textit{ days}) (24 \textit{ hours/day}) (\textit{CapacityFactor} [\%])} \quad (3.8)$$

It is recalled that here the capacity factor is the ratio of the energy delivered to the grid in an year, to the potential energy output if it were possible for the device to operate continuously at nominal power for the whole year.

In next Fig. 3.8, some reference values for different technologies are presented [52].

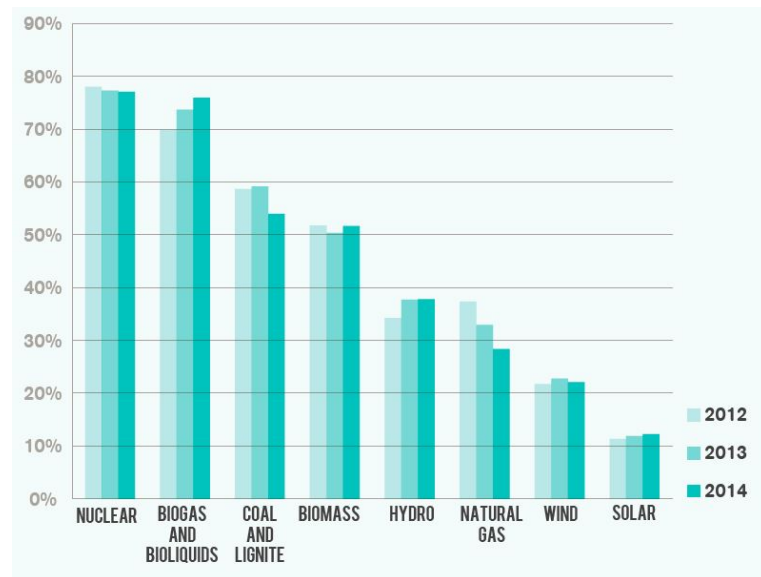


Figure 3.8 Capacity factor of common generating technologies in the European Union.
Source: EurElectric.

For what concern the current status of the wave power technology, it is difficult to indicate a capacity factor, because of its link to the nominal power of the plant. It is thus suggested to use them both in order to explain the performances of the plant.

- **Resource sea states.** Looking at the occurrences scatter table and at the energy scatter table, two primary sea states can be identified:

1) *Most occurrent.* This is obtained looking for the maximum of the occurrences scatter table. Marked in green in Fig. 3.9.

2) *Most energetic.* This is obtained looking for the maximum of the energy scatter table. Marked in red in Fig. 3.10.

This can be done easily for Pantelleria, because here the occurrences scatter table is substantially convex, and maxima can be found easily in both the tables. For other installation sites, these statements have to be reviewed.

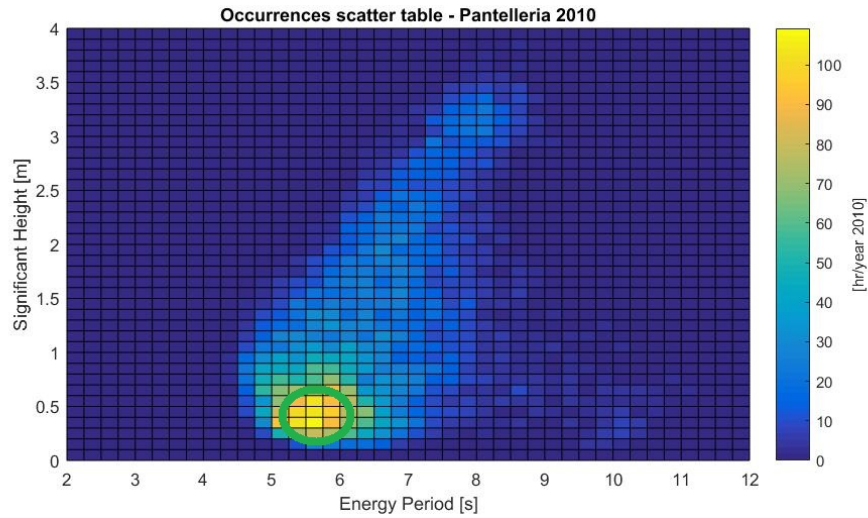


Figure 3.9 Pantelleria occurrences scatter table (2010). Most occurrent sea state.

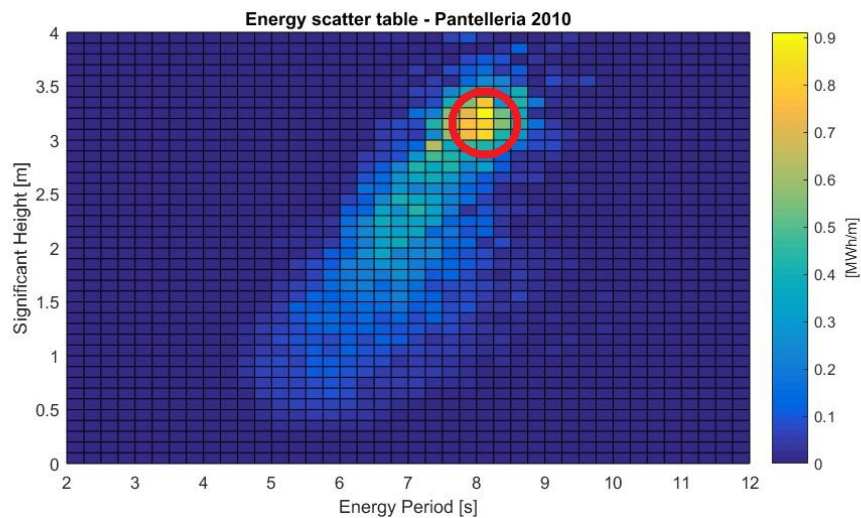


Figure 3.10 Pantelleria energy scatter table (2010). Most energetic sea state.

These two points are here manually identified as local maxima. Of course these are not singularities in the table, but are representative of most occurrent and most energetic set of sea states.

3) *Intermediate*. A more analytic criteria, could be identify the point computing the sum of the occurrences/energy in an elliptic area around a chosen nominal sea state, described by a ΔT_e , ΔH_s parameters:

$$\left(\frac{x - T_{enom}}{\Delta T_e}\right)^2 + \left(\frac{y - H_{snom}}{\Delta H_s}\right)^2 \leq 1 \quad (3.9)$$

Such an analysis method gives more information about the chosen state. It describes the surrounding area, in terms of total occurrences in the year and their percentage, the total amount of energy in that area and its percentage. Some images are shown, in order to explain better the concept and proposing solutions to the pre-design wave sea state choice (Figure 3.11, 3.12 and 3.13).

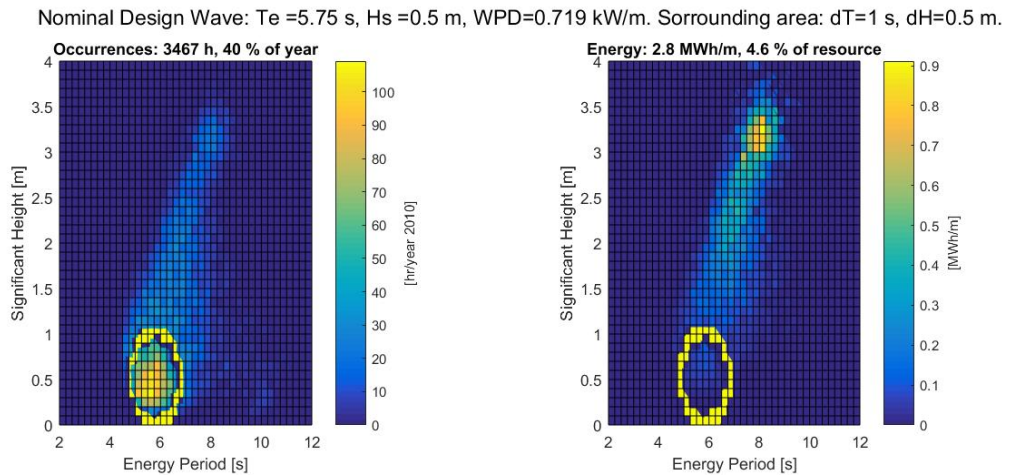


Figure 3.11 Pantelleria scatter tables (2010). Most occurring sea state. Surrounding elliptic area analysis.

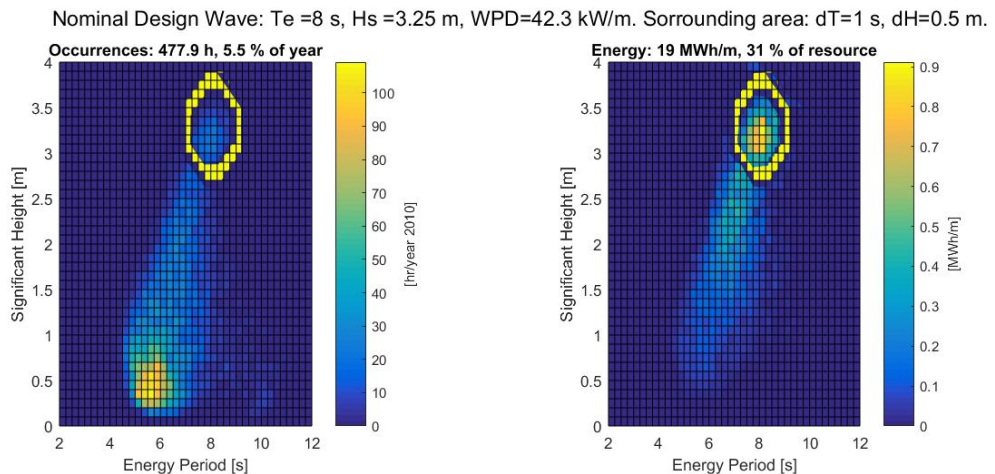


Figure 3.12 Pantelleria scatter tables (2010). Most energetic sea state. Surrounding elliptic area analysis.

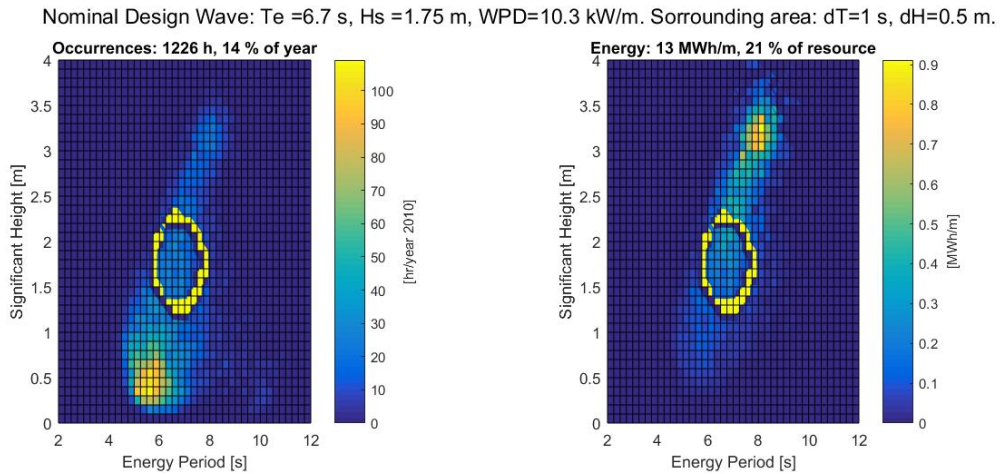


Figure 3.13 Pantelleria energy scatter table (2010). Prototype 2013 predesign sea state. Surrounding elliptic area analysis.

As last observation of this paragraph, it must be noticed that each sea state can be described with these two scalar numbers. Therefore two new synthetic scatter tables can be presented 3.14:

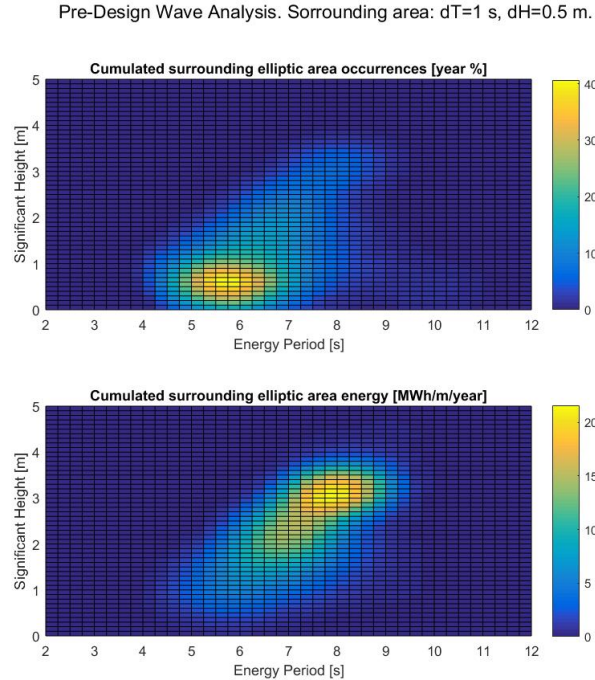


Figure 3.14 Pantelleria energy scatter tables (2010). Surrounding elliptic area analysis, synthetic results: occurrences and energy.

These two maps are extremely useful to the choice of the most suitable pre-design point.- A method like this could also help in more difficult installation sites, where the resource owns for example different local maxima.

4) *Directionality*. In general directionality has to be considered. How and how much the waves are spread in direction. This have to be considered already starting from first phases of the project. This point is not important for Pantelleria site, see 3.1.4.

- ***Pre-design point - Nominal Wave - Choice***. The selection of the design point is a mixture of information presented in the previous points and the experience of the designer. Of course, if during the following phases of the project problems rise (high mechanical loads, expensive floater, low productivity, high costs, etc.), the pre-design point can be changed. In this paragraph some suggestions are proposed.

1) *Most occurrent*. The first natural choice is to design the device for the sea state that more often is present in the site. Unfortunately almost always this is not coincident with the most energetic state. This means that in that place the installed WEC works for a lot of time during the year, but it is not designed for working well with the most energetic wave. This may lead to an inferior quantity of energy production, but on the other hand to a more continuous power output. This is a great advantage for the electric grid system.

2) *Most energetic*. A second choice is to design the device for the most energetic sea state. This seems to be the most reasonable solution, but it also presents some drawbacks. In fact as seen before, the power density goes with the square of the height and linearly with period, meaning that the system it is designed for working with the most powerful waves. This, depending on the device, can result in huge costs in the equipment, PTO system and so on. Moreover, the waves become longer and the device length increase accordingly, resulting in very high costs. As a last drawback, working outside the most occurrent area, means that the system will give peaks of power production in some part of the year, and will reasonably work bad in the others. This can provoke problems in the interface with the island grid, even if combined with other renewable energy sources and energy buffers solutions.

3) *Intermediate site*. There may be different ways of choosing an intermediate point. Infinite solutions can be identified based on a lot of variables. The next

paragraph 3.2.2 showed some examples. In general the designer has to deal with some criteria: plant nominal power, floater maximum size, equipment costs, looking for a constant power output delivered to the grid but many other aspects could be cited. All these depend on the wave energy technology to be deployed and the installation site characteristics.

3.2.2 Examples

- ***A 20 kW ISWEC for Pantelleria.***

The nominal power here is considered in couple with a capacity factor, in order to assess the minimum expected energy production of the year.

Looking at others renewable energy sources, a first attempt can be to indicate the maximum value in the group: about $CF = 50\%$ is characterizing the biomass technologies.

So the minimum net year productivity desired is:

$$E_{net\ min} = (20\ kW) (365\ days/year) (24\ hours/day) (50\%) = 87.6\ MWh/year \quad (3.10)$$

Some parameters of the device has to be roughly estimated: a mean relative capture width in the surrounding area equal to $RCW = 0.5$ is taken, a PTO overall efficiency of $\eta_{PTO} = 0.7$ and a hull width of 10 meters. Thus using the synthetic results tables presented in Figure 3.14 a suitable point where to design the WEC can be chosen: $T_e = 6.75\ s$, $H_s = 2.1\ m$ (see Figure 3.15) is identified.

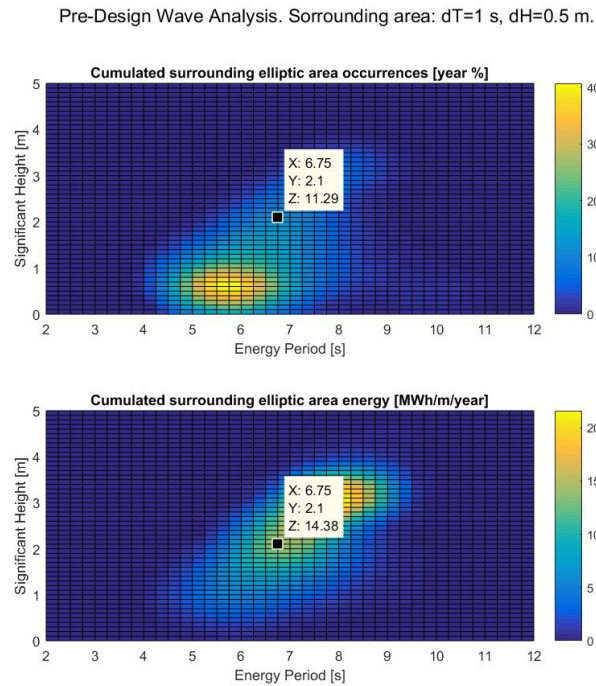


Figure 3.15 Pantelleria energy scatter tables (2010). Surrounding elliptic area analysis, synthetic results: occurrences and energy. 20 kW ISWEC predesign: wave choice.

The wave power density (WPD) of the nominal wave and the correspondent expected power output P_{nomexp} are:

$$WPD = 0.49 T_e H_s^2 = 0.49 (6.75 \text{ s}) (2.1 \text{ m})^2 = 14.59 \text{ kW/m} \quad (3.11)$$

$$\begin{aligned} P_{nomexp} &= (WPD [\text{kW/m}]) (Hull \text{ width [m]}) (RCW) (\eta_{PTO}) = \\ &= (14.38 \text{ kW/m}) (10 \text{ m}) (0.5) (0.7) = 50.33 \text{ kW} \end{aligned} \quad (3.12)$$

The net power output at the design wave is then higher than the nominal power requested. This is understandable, because for assuring the performances requested on a widespread set of different sea states, statistically distributed, the device as to be of a greater size. Anyway, this values have to be verified in the next specification procurement, detailed design.

The net minimum annual energy delivered to the grid is then computed:

$$E_{net \min} = (14.59 \text{ MWh/m/year}) (10 \text{ m}) (0.5) (0.7) = 51.07 \text{ MWh/year} \quad (3.13)$$

Such a value represents almost the 60% of the energy production required with only the 11.3% of the year time and the 24% of the whole site available energy:

$$\begin{aligned} \text{Time utilization ratio} &= \frac{E_{net\ min\ surrounding\ nominal\ wave}}{E_{net\ min\ required}} = \\ &= \frac{(51.07\ MWh/year)}{(86.7\ MWh/year)} = 0.59\% \end{aligned} \quad (3.14)$$

This last value is of course only a first estimation of the minimum production of the device. But all these values together give instantaneously a feedback on the type of device that is going to be sized and on the power fluxes involved.

- **A 100 kW ISWEC for Pantelleria.**

The nominal power here is considered as in the previous example in couple with a capacity factor in order to assess the minimum expected energy production of the year. The capacity factor is also the same as before, $CF = 50\%$.

The energy production is then computed:

$$E_{net\ min} = (100\ kW) (365\ days/year) (24\ hours/day) (50\%) = 438\ MWh/year \quad (3.15)$$

For such a big power plant for the installation site, the design wave directly goes to the most energetic point (Figure 3.16).

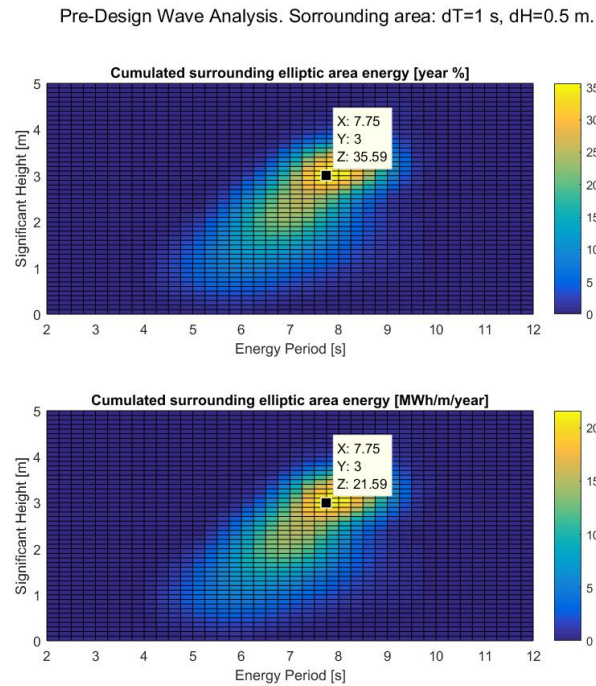


Figure 3.16 Pantelleria energy scatter tables (2010). Surrounding elliptic area analysis, synthetic results: occurrences and energy. 100 kW ISWEC predesign: wave choice.

Always using a $RCW = 0.5$ and a PTO efficiency as $\eta_{PTO} = 0.7$, the first value of the hull width that can satisfy such a production is:

$$E_{net\ min} = (21.59\ MWh/m/year) (30\ m) (0.5) (0.7) = 227\ MWh/year \quad (3.16)$$

With a hull of 30 meters width, the device is taking into account the 35.6% of the available energy but only the 7% of occurrences. The percentage of the required production is:

$$\begin{aligned} \text{Time utilization ratio} &= \frac{E_{net\ min\ surrounding\ nominal\ wave}}{E_{net\ min\ required}} = \\ &= \frac{(227\ MWh/year)}{(438\ MWh/year)} = 0.52\% \end{aligned} \quad (3.17)$$

It is difficult to imagine that this device is going to achieve the objective of 438 MWh net energy production delivered to the grid.

Moreover the hull is likely going to be too large and expensive and the device to be designed for giving an electricity production too much concentrated in some periods of the year.

This is a case in which the productivity request to the site can't be satisfied. A solution can be to reduce the capacity factor to a wind power plant value: $CF = 20\%$.

$$E_{net\ min} = (100\ kW) (365\ days/year) (24\ hours/day) (20\%) = 175\ MWh/year \quad (3.18)$$

With this new value, a 15 m wide hull is enough.

$$E_{net\ min} = (21.59\ MWh/m/year) (15\ m) (0.5) (0.7) = 113\ MWh/year \quad (3.19)$$

And a production ratio in near the design sea state of:

$$\begin{aligned} \text{Time utilization ratio} &= \frac{E_{net\ min\ surrounding\ nominal\ wave}}{E_{net\ min\ required}} = \\ &= \frac{(113\ MWh/year)}{(175\ MWh/year)} = 0.65\% \end{aligned} \quad (3.20)$$

Thus, the WPD associated to this predesign wave is:

$$WPD = 0.49\ 7.75s\ (3m)^2 = 34.18\ kW/m \quad (3.21)$$

And the net power extracted at the design, nominal, wave is:

$$P_{nomxp} = WPD\ (width\ m)\ (RCW) = (34.18\ kW/m) (15\ m) (0.5) (0.7) = 179\ kW \quad (3.22)$$

3.2.3 2013. The device pre-design wave.

In this paragraph the choice of the design sea state for the full scale ISWEC prototype for Pantelleria is presented.

Objective of the PROMO project was the construction and deployment of a 60 kW rated power device. The rated power was considered as the net power given by the device working in the nominal sea state conditions. At that time the criteria chosen for selecting the nominal wave was looking at the occurrences and energy scatters and taking a compromise wave. However the scatters used were those obtained with the zero crossing-equivalent regular wave analysis. The identified wave state was: $T = 6.7s$, $H = 1.6m$. This was chosen in order to be in between of the maximum energy and maximum occurrences points of the 2010 scatter table. It must be noticed that this is a regular wave. In fact the analysis outcome was a scatter of equivalent regular waves. When computing the power density and the width of the hull, this turns to be extremely important.

The wave power density, WPD, is computed with the following regular wave formula:

$$WPD = 6.7s (1.6m)^2 = 17.15kW/m \quad (3.23)$$

An overall efficiency of the system equal to 0.35 was chosen ($RCW = 0.5$, $\eta_{PTO} = 0.7$) and the floater width computed:

$$P_{nom,xp} = (WPD [kW/m]) (width [m]) (RCW) (\eta_{PTO}) = (17.15kW/m) (10m) (0.5) (0.7) = 60kW \quad (3.24)$$

When the scatter tables started to be obtained with the spectral analysis methods, some problems in this pre-design assumptions appeared.

Indeed the wave $T_e = 6.7s$, $H_s = 1.6m$ has about half of the available power:

$$WPD = 0.496.7s (1.6m)^2 = 8.4kW/m \quad (3.25)$$

Looking at the Pantelleria 2010 tables in Figure 3.1, 3.2, an iso-energetic wave state keeping the same wave period is: $T_e = 6.7s$, $H_s = 2.4m$. This irregular wave sea state has in fact a WPD of:

$$WPD = 0.49 6.7s (2.3m)^2 = 17.37kW/m \quad (3.26)$$

This point is reasonably inside the occurrences area of the Pantelleria site. But of course the methodology that brought this choice is far from being optimal. In next paragraph the procedure is repeated with the new method presented above.

3.2.4 2016. A novel pre-design wave.

The nominal power of the ISWEC could be of 60kW with a capacity factor $CF = 30\%$. The productivity request becomes:

$$E_{net\ min} = (60\text{kW}) (365\ \text{days/year}) (24\ \text{hours/day}) (30\%) = 158\text{MWh/year} \quad (3.27)$$

For such a specification, an updated design point for the Pantelleria device could be $T_e = 7.75\text{ s}$, $H_s = 3\text{ m}$. This sea state has the properties shown in Figure 3.17.

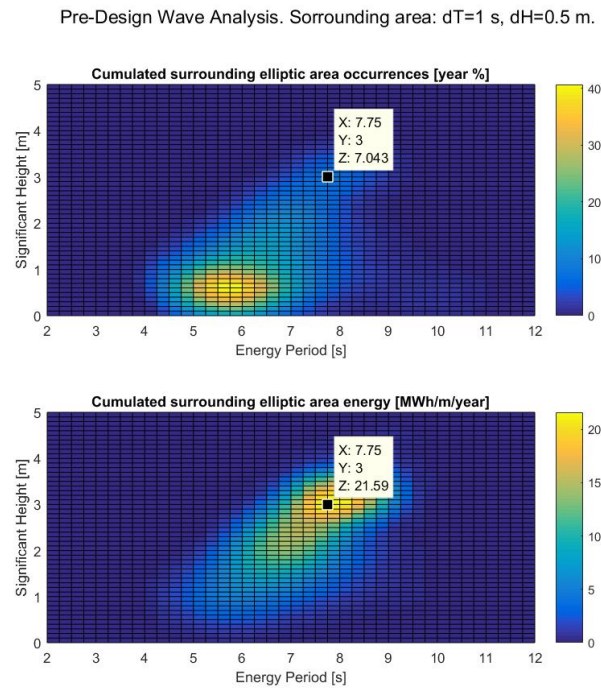


Figure 3.17 Pantelleria energy scatter tables (2010). Surrounding elliptic area analysis, synthetic results: occurrences and energy. 60 kW ISWEC pre-design: wave choice.

With a wave like this, the energy production in the surrounding elliptic area is:

$$E_{net\ min} = (21.59\text{MWh/m/year}) (14\text{ m}) (0.5) (0.7) = 106\text{MWh/year} \quad (3.28)$$

Reaching the 67% of the objective energy to be given to the grid.

$$\begin{aligned} \text{Time utilization ratio} &= \frac{E_{net\ min\ surrounding\ nominal\ wave}}{E_{net\ min\ required}} = \\ &= \frac{(106\ MWh/year)}{(158\ MWh/year)} = 0.67\% \end{aligned} \quad (3.29)$$

The wave power density associated to the sea state and its respective power production are:

$$WPD = 0.49775s (3m)^2 = 34.2\ kW/m \quad (3.30)$$

$$P_{nomxp} = WPD (width [m]) (RCW) (\eta_{PTO}) = (34.18\ kW/m) (14m) (0.5) (0.7) = 167\ kW \quad (3.31)$$

3.3 Pre-design

The pre-design begins from assumptions based on the prior knowledge about the device and exploits frequency domain analysis methods. The objective of this phase is to obtain a first device configuration to be used as starting condition in the following more detailed model-based design optimization. Information obtained at the end of this phase are the floater size, the number and sizing of gyroscopes, the flywheel speed, the gearbox ratio, the PTO torque and speed specifications, an estimation of the power flow, the losses of the flywheel shaft bearings and others.

It must be pointed out that the whole pre-design phase can be carried out without using any other software or numerical simulations. Where needed, assumptions coming from the designer experience are used. This makes the pre-design a quick and versatile tool for having useful information at the very start of the project of a new machine.

In this section the method is presented.

3.3.1 The floater

The first step in the pre-design procedure is the determination of the hull main dimensions: the width and length 3.18. In this thesis the floater shape is in fact given. For more information about the study and research about the optimized version see [11], [78] and [12].

The width is linked to the nominal power specifications for the device, as introduced in the previous paragraphs. In particular it is computed with the following:

$$W_{\text{floater width}} = \frac{P_{\text{nomxp}} [\text{kW}]}{(WPD [\text{kW}/\text{m}]) (RCW) (\eta_{PTO})} \quad (3.32)$$

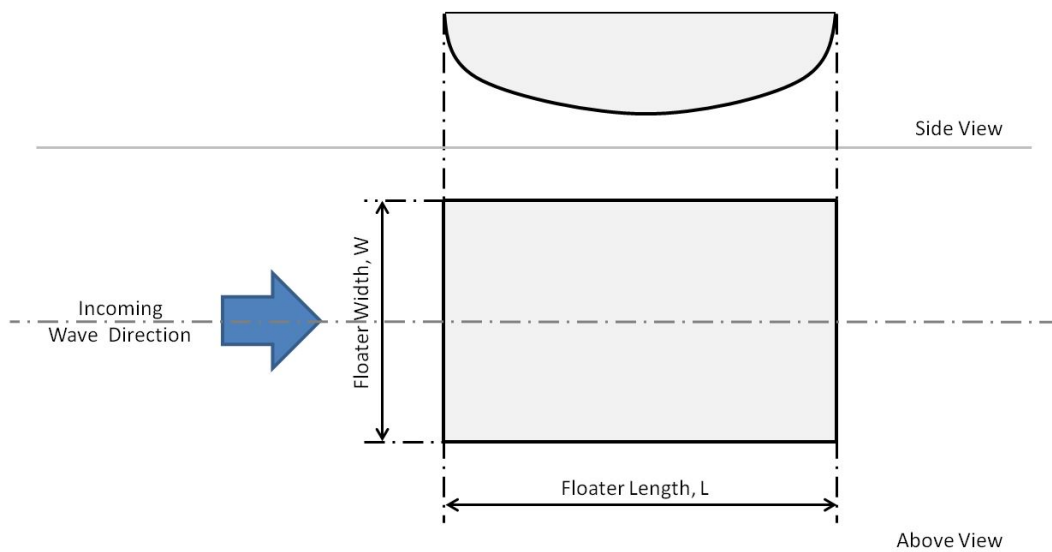


Figure 3.18 Floater main dimensions: width and length.

The length of the device is dependent to the working principle of the device. The ISWEC is in fact a pitching device, so the length and shape of the hull should enable and facilitate the pitch motion. A floater length between $1/2$ and $1/3$ of the design wavelength is then chosen. A smaller geometric size in fact enables a mainly heave motion, meanwhile a longer device has filtering effects on short waves for what concern the pitch DOF, Figure 3.19.

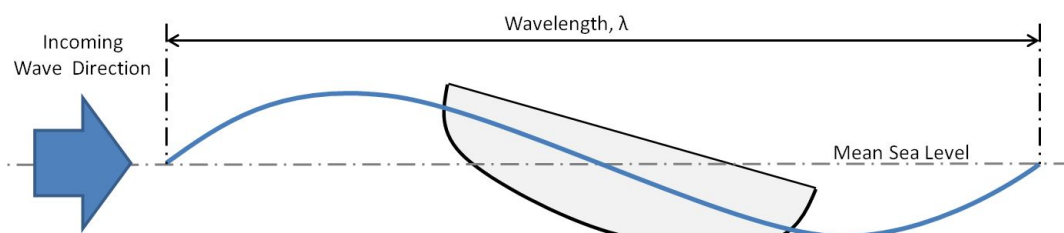


Figure 3.19 Floater longitudinal dimension and wave length.

The wavelength λ is computed using the linear Airy wave theory with the deep water hypothesis:

$$\lambda = \frac{(g [m/s^2]) (T^2 [s])}{2\pi} \quad (3.33)$$

where g is the gravity acceleration and T is the regular wave period. The value of the wavelength and the considerations above bring constraints for the choice of the hull length:

$$\frac{\lambda}{3} \leq L_{floaterslength} \leq \frac{\lambda}{2} \quad (3.34)$$

For choosing the length optimal final value belonging to this range, other considerations are involved. Some more detailed analysis with a BEM software and a preliminary estimation of the costs would be required but at the pre-design level such a detail is not required.

3.3.2 The iso-energetic regular wave

In order to use the frequency analysis method, a regular wave is required. The idea here is to introduce a wave that is iso-energetic with respect to the nominal irregular sea state. The wave period is chosen equal to the wave energy period and the wave height is scaled in order to obtain the same power density.

The wave power density for both regular and irregular waves is hereafter shown:

$$\begin{aligned} WPD_{reg} &= T H^2 \\ WPD_{irreg} &= 0.49 T_e H_s^2 \end{aligned} \quad (3.35)$$

Consequently, the iso-energetic regular wave parameters are:

$$\begin{cases} T = T_e \\ H = H_s \sqrt{0.49} \\ WPD_{reg} = WPD_{irreg} \end{cases} \quad (3.36)$$

3.3.3 The gyroscope system

The objective of the next section is to determine the gyroscopes overall angular momentum, the number of gyroscope units, its size and their speed at the nominal design point.

3.3.3.1 The overall angular momentum

In order to ensure the nominal net power production at this sea state, the gross mechanical power acquired by the WEC must be higher:

$$\begin{aligned} P_{captured} &= (W_{floaterswidth} [m]) (WPD [kW/m]) (RCW) = \\ &= \frac{P_{nomxp} [kW]}{\eta_{PTO}} \end{aligned} \quad (3.37)$$

This is the power that the system must be able to convert. In order to compute the overall angular momentum required for the conversion, some analytic steps have to be done.

Combining the first equation of 2.40 and the basic proportional-derivative control of equation 2.38, with some passages the following relationship is obtained:

$$-k\bar{\varepsilon} - c\bar{\varepsilon}s = I_g\bar{\varepsilon}s^2 + J\dot{\phi}\bar{\delta}s \quad (3.38)$$

The equation is then transformed from Laplace to frequency domain, remembering that $s = j\omega$:

$$(-I_g\omega^2 + cj\omega + k)\varepsilon_0 = J\dot{\phi}j\omega\delta_0 \quad (3.39)$$

$$\varepsilon_0 = \frac{J\dot{\phi}j\omega}{-I_g\omega^2 + cj\omega + k}\delta_0 \quad (3.40)$$

If now the natural frequency of the internal PTO axis is defined as $\omega_n = k/I_g$, then the stiffness factor can be rewritten as $k = \omega_n I_g$. Substituting this in the equation above:

$$\varepsilon_0 = \frac{J\dot{\phi}j\omega}{I_g(\omega_n^2 - \omega^2) + cj\omega}\delta_0 \quad (3.41)$$

The power that the system is able to convert is equal to the internal PTO axis speed $\dot{\varepsilon}$ by the damping coefficient c . In frequency domain the average of this product can be computed. Thus the next equation of the average power absorbed can be presented:

$$P_{captured} = \frac{c}{2}\omega^2\varepsilon_0^2 = \frac{c}{2}\frac{(J\dot{\phi}\omega^2\delta_0)^2}{I_g^2(\omega_n^2 - \omega^2)^2 + c^2\omega^2} \quad (3.42)$$

Then, since the system is controlled in order have this internal axis resonant to the incoming wave, the hypothesis is that k is such that $\omega_n = \omega$. With this simplification the mean extractable power becomes:

$$P_{captured} = \frac{c}{2}\omega^2\varepsilon_0^2 = \frac{(J\dot{\phi}\omega\delta_0)^2}{2c} \quad (3.43)$$

With a little manipulation of the latter, the *overall angular momentum required for the power conversion* analytical relationship can be found:

$$(J\dot{\phi})_{overall} = \frac{2P_{captured}}{\omega^2\varepsilon_0\delta_0} \quad (3.44)$$

This value can be evaluated starting from the expected kinematic of the overall system in nominal conditions: the internal PTO axis oscillation amplitude and the floater pitching amplitude. These are chosen according to previous experience. Typical values are 60 for the PTO angular position and about 10 for the floater pitch DOF.

3.3.3.2 The flywheel size

After the overall angular momentum has been computed, the axial momentum of inertia of the single flywheel can be easily computed:

$$J = \frac{(J\dot{\phi})_{overall}}{\dot{\phi}_{nom} n_{gyros}} \quad (3.45)$$

where $\dot{\phi}_{nom}$ is the flywheel speed at the nominal design sea state and n_{gyros} is the number of units inside the floater. The flywheel speed is chosen according to the experience of the designer and the physical limit imposed by the technical implementation of big flywheels, as explained in the following of this paragraph. The choice of gyroscopes number is further detailed in next paragraph.

Some observations about the flywheel design have to be presented. The centripetal acceleration stress and the hydrodynamic power losses increase as the flywheel speed increases. On the other hand, the mass and cost, its geometric dimensions and its moment of inertia increase if the flywheel speed decreases and the overall momentum has to be maintained. The choice of the optimal configuration is then a compromise between all these different aspects. In the following, the design procedure is illustrated. Starting from the obtained flywheel single momentum of inertia J , with the help of some parameterization is possible to estimate its geometry and footprint.

The selected geometry is a cylinder (Figure 3.20). Some parameters, useful for the simplification of the problem, have to be introduced:

- **height/external diameter, χ_h .** This is the ratio between the flywheel height, i.e. the dimension along the rotation axis, and the external diameter.

$$\chi_h = H/D_e \quad (3.46)$$

Since the PTO axis is designed free to the rotation, a starting value of 1 is usually adopted.

- **internal diameter/external diameter, χ_d .** This parameter affects the distribution of the masses of the final geometry.

$$\chi_d = D_i/D_e \quad (3.47)$$

- **density, ρ_{fw} .** It is function of the chosen material. A standard $7700\text{kg}/\text{m}^3$ proper of commercial stainless steel is used.

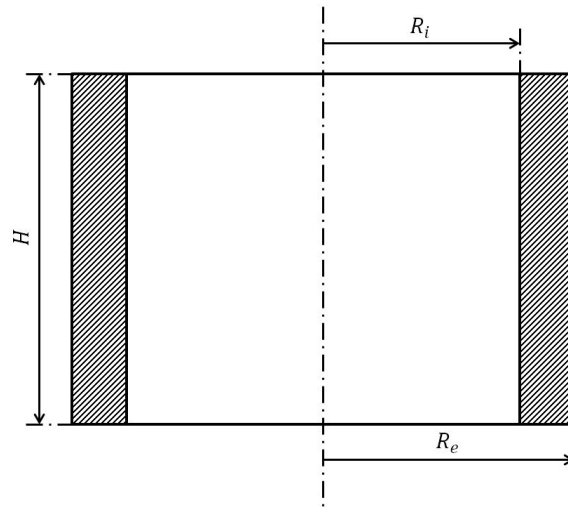


Figure 3.20 Flywheel simplified geometry. Definition of parameters.

The angular momentum of a cylinder can be computed with the following expression:

$$J = \frac{1}{2} \rho_{fw} \pi H (R_e^4 - R_i^4) \quad (3.48)$$

Substituting the parameterisation and looking for the expression of the external diameter in function of the desired angular momentum, the following relationship is found:

$$D_e = 2 \sqrt[5]{\frac{J}{\rho \pi \chi_h (1 - \chi_d)}} \quad (3.49)$$

The internal diameter and the height can be easily directly computed via parameterisation.

The flywheel mass can be then easily computed

$$m = \rho_{fw} \pi H (R_e^2 - R_i^2) \quad (3.50)$$

Table 3.1 Maximum allowable circumferential stress of some construction materials.

Material	Maximum allowable stress, σ_{adm} [MPa]
Cast iron	12
Steel	63
High quality steel	78

Table 3.2 Maximum allowable peripheral speed of some construction materials.

Material	Maximum allowable peripheral speed [m/s]
Cast iron	35/40
Steel	70/90
High quality steel	100

An interesting consideration is that the mass goes with the square of the radius while the momentum of inertia with the fourth. Since the mass linearly affects the cost of the flywheel, bigger radius are preferred. The problem with bigger radius, at the same angular speed, are the higher centrifugal forces. One of the most important constraint in the design of an ISWEC is due to the technological limits imposed to the construction of big flywheels. In the last part of this paragraph, a simple model for the computation of the stresses and the constraints imposed by the materials are presented. The maximum circumferential stress of a homogeneous and isotropic thin ring flywheel can be computed with the next equation 3.52. This value must be less than a number characterizing each construction material, here named σ_{adm} :

$$\sigma_{max} = \rho \dot{\phi}^2 R_e^2 \leq \sigma_{adm} \quad (3.51)$$

Some standard literature values are shown in table 3.1. Another constraint that is involved in the sizing of a flywheel is the maximum peripheral speed (table 3.2). It is computed with:

$$V_p = \dot{\phi} \frac{D_e}{2} [m/s] \quad (3.52)$$

3.3.3.3 The number of gyroscope units

The decision of installing more than a gyroscope unit inside the floater has multiple reasons: technological, economic and related to the system working principle. In this paragraph these will be briefly introduced.

The first motivation for having an even multiple units configuration is to compensate the undesired three dimensional gyroscopic torques. Recalling equations 2.9, 2.10

Table 3.3 Example of signs of torques exchanged by a couple of gyros and the floater.

	$\dot{\phi}$	$\dot{\delta}$	M_{Efw,x_1}	$\dot{\epsilon}$	ϵ	M_{Efw,y_1}	M_{Efw,z_1}
gyro 1	→	→	→	→	→	←	←
gyro 2	←	→	←	←	←	←	→

and 2.11, dropping lower magnitude order terms, the torques exchanged by a single flywheel over the floater are:

$$M_{Efw,x_1} = I_{fw}\ddot{\epsilon} + J\dot{\phi}\dot{\delta}\cos\epsilon \quad (3.53)$$

$$M_{Efw,y_1} = -J\dot{\phi}\dot{\epsilon}\cos\epsilon \quad (3.54)$$

$$M_{Efw,z_1} = -J\dot{\phi}\dot{\epsilon}\sin\epsilon \quad (3.55)$$

A configuration with two gyroscopes is taken as example and the three torques contributions are analyzed.

The two flywheels are counter rotating:

$$\dot{\phi}_1 = -\dot{\phi}_2 \quad (3.56)$$

Looking at the first contribution M_{Efw,x_1} , exchanged on the internal PTO axis, since $\dot{\delta}$ is the pitch motion of the floater and it is the same for both the groups and the *cosine* function is even, this torque has two different signs over the two different groups. This means that for a positive rotation $\dot{\delta}$, the gyro group 1 receives a positive torque and the group 2 a negative one.

The power conversion fundamental torque over hull pitch DOF, M_{Efw,y_1} , is now examined. The $\dot{\epsilon}$ has different signs for the two groups, as seen before. The *cosine* trigonometric function is even. The flywheels opposite angular speeds combine with the opposite PTO rotations and generate two torques that have that are concordant.

The third torque M_{Efw,z_1} is computed using the opposite flywheel speed and PTO speed, but this time the *sine* function is odd. This time the torques have different direction. This means that a odd number of gyroscopes causes undesired torques on the yaw DOF. This phenomenon can have very different order of magnitude depending on the relative size of the gyroscope and the floater, but has to be taken into account.

Summarizing, the torques over roll and yaw are compensated with an even number of gyros, meanwhile the torque over pitch are additive, as shown in Table 3.3.

The second motivation is to split the big loads involved in the power conversion. As just explained, with more than a gyroscopic unit, the overall angular momentum can

be divided between different gyroscopes.

Lastly, this enables to build smaller groups, reducing the costs of construction of big steel flywheels and the associated logistics. Also the technological problems related with the maximum allowable stresses can be managed.

3.3.4 The Power Take Off

At this point of the pre-design, all the loads and kinematics are defined. With some elaborations it is possible to estimate the maximum PTO speed and torque, main specifications for an electric motor choice.

In Figure 3.31 the Power Take Off scheme and its notation are presented.

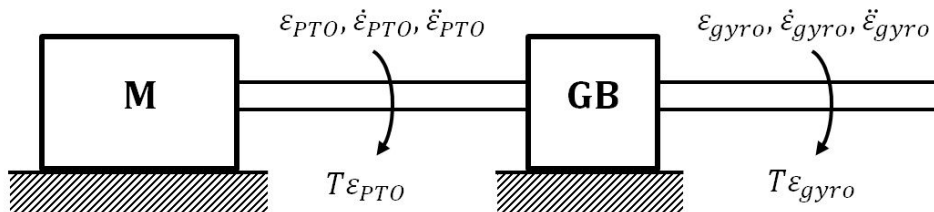


Figure 3.21 Poter Take Off system. Notation.

"M" is the electric generator, a permanent magnet DC motor is chosen for the Pantelleria device. "GB" is the gearbox, that is reducing torques and increasing speed from gyro side to the PTO one. The choice of the gear box ratio is in fact made with the determination of the electrical machine.

The quantities from the gyro side are completely determined. The maximum gyro speed is:

$$\dot{\varepsilon}_{gyro\ max} = \frac{2\pi}{(TK_T)} (\varepsilon_0 K_\varepsilon) \quad (3.57)$$

Where T is the period of the nominal regular wave, K_T is a coefficient considering the working interval, ε_0 is the amplitude of the oscillations of the gyro group at the nominal design wave and K_{max} is a coefficient for increasing the required speed. Usually $K_T < 1$ for accounting the situation in which waves have the lowest period and the highest frequency meanwhile $K_\varepsilon = 120/\varepsilon_0$, considering 120 the maximum expected amplitude of oscillations.

The maximum PTO torque is computed starting from Equation 3.53. The maximum contribution for both terms is used, considering them in phase, even if it is not real.

This hypothesis is adopted for safety sake, for not downsizing the component. The torque is then evaluated with the following:

$$T_{gyro\ max} = I_{fw}\omega^2\varepsilon_0 + J\dot{\phi}\omega\delta_0 \quad (3.58)$$

Wave power resource is characterized by very high torques and low frequencies, consequently a gearbox is commonly introduced. Its ratio is one of the parameters to be sized during the pre-design. The PTO speed and torque hence become:

$$\dot{\varepsilon}_{PTO\ max} = \dot{\varepsilon}_{gyro\ max} \tau \quad (3.59)$$

$$T_{PTO\ max} = \frac{T_{gyro\ max}}{\tau} \quad (3.60)$$

3.3.5 The Bearings

Some specifications about the flywheel bearings can be obtained at this level. These are a crucial component in the overall system, since they are bearing the highest mechanical loads in the system and great part of the mechanical losses are due to the resulting friction. The procedure for the sizing of radial and thrust bearings is described in this paragraph. First components to be studied are the radial bearings. These consist of a couple of roller bearings sustaining the torque acting on the y_2 - axis, $M_{E\ fw,y_2}$, referred to the gyroscope structure and called T_λ . The exhaustive description is reported in section 2.2.

$$M_{E\ fw,y_2} = \vec{M}_E \cdot \hat{j}_2 = I_{fw}\ddot{\lambda} - (J - I_{fw})\dot{\varepsilon}\dot{\psi} - J\dot{\phi}\dot{\varepsilon} \quad (3.61)$$

With the linearization around $\varepsilon = 0$ and dropping the lower-magnitude terms, the next simplified relationship can be written:

$$T_\lambda = M_{E\ fw,y_2} = -J\dot{\phi}\dot{\varepsilon} \quad (3.62)$$

Dividing this torque for the distance between the components d_b , the radial force F_R is obtained:

$$F_R = \frac{T_\lambda}{d_b} \quad (3.63)$$

The bearings are one of the most critical components in the system, so they are designed and chosen according to some duration specification. Input of this phase is the L_{10h} bearing life. In this pre-design phase the duration is computed with the

constant load conditions formula:

$$L_{10h} = \frac{10^6}{60 \dot{\phi}_{nom} \frac{30}{\pi}} \left(\frac{C_b}{F_{b,eq}} \right)^{p_b} \quad (3.64)$$

where p_b is a bearing type dependent parameter, $\dot{\phi}_{nom}$ is the flywheel speed at the design wave state, C_b is the dynamic equivalent load coefficient and $F_{b,eq}$ is the equivalent bearing load, obtained with the following:

$$F_{rb,eq} = \frac{F_R}{\sqrt{2}} \quad (3.65)$$

Since all the parameters are known but the C_b characteristic of the chosen bearing, the minimum value required for satisfying the life time request at design load conditions can be computed:

$$C_{rb,min} = F_{rb,eq}^{p_b} \sqrt[10h]{L_{10h} \frac{60 \dot{\phi}_{nom} \frac{30}{\pi}}{10^6}} \quad (3.66)$$

The radial bearing that is selected must have a dynamic equivalent load coefficient higher than the minimum computed value, $C_b > C_{b,min}$.

For the thrust bearings the procedure is the same, but the load is represented by the flywheel weight:

$$F_{tb,eq} = m_{flywheel} (9.81 \text{ m/s}^2) \quad (3.67)$$

Thus the $C_{rb,min}$ parameter is computed, and the thrust bearing can be chosen.

3.3.6 The Ultracapacitors

The ultracapacitors are the elements in the system providing the smoothing effect of the power output. Starting from the mechanical power captured by the device at the nominal period, see equation 3.43, the nominal entrant energy in the DC BUS in half a cycle can be evaluated. The whole PTO efficiency is taken equal to 1, thus the capacitors are sized with confidence. Computing the inverse of the mean power captured relationship, it is possible to evaluate the respective damping coefficient.

$$c = \frac{(J\dot{\phi}\omega\delta_0)^2}{2P_{captured}} \quad (3.68)$$

Thus, given that the desired nominal oscillations amplitude ε_0 is an input of the pre-design, it is possible to evaluate the speed amplitude $\dot{\varepsilon}_0$ and with the damping

coefficient the torque T_{ε_0} .

$$\dot{\varepsilon}_0 = \varepsilon_0 \frac{2\pi}{T_{nom}} \quad (3.69)$$

$$T_{\varepsilon_0} = c \dot{\varepsilon}_0 \quad (3.70)$$

Since the speed and torque are in phase, it is possible to evaluate the maximum amplitude value of the mechanical power oscillations, given the mean adsorbed power value, $P_{captured}$.

$$P_{\varepsilon_0} = T_{\varepsilon_0} \dot{\varepsilon}_0 \quad (3.71)$$

The power flow is thus modeled with a simple sinusoid, with the amplitude above computed and the frequency deriving from the nominal wave period. If the PTO efficiency is equal to 1, this is also the electric power flow flowing into the DC BUS. The DC BUS tension is assumed as constant, that means as a first hypothesis an infinite capacity. The entrant electric energy is computed with the following time integral:

$$E_{el} = \int_0^{T_{nom}/2} VI dt = V_0 \int_0^{T_{nom}/2} I dt \quad (3.72)$$

The amplitude of the current oscillation is computed as $I_0 = P_0/V_0$, and the current equation in time is:

$$I = I_0 \sin\left(\frac{2\pi}{T_{nom}} t\right) \quad (3.73)$$

Calculating and evaluating the integral, the final simplified equation is:

$$E_{el} = \frac{P_0 T_{nom}}{\pi} \quad (3.74)$$

This energy is then used for the computation of the capacitance C . The energy stored in the ultracapacitors can be evaluated using the expression:

$$E_{UC} = \frac{1}{2} CV^2 \quad (3.75)$$

The specification to be given at this step is the desired tension increment ΔV for the incoming energy flux. Thus it is possible to equalize the energy introduced in the BUS with the one accumulated by the ultracapacitors for a given voltage variation of the BUS to which they are directly connected.

$$E_{el} = \Delta E_{UC} = \frac{1}{2} C ((V_0 + \Delta V)^2 - V_0^2) \quad (3.76)$$

$$C = \frac{2E_{el}}{(V_0 + \Delta V)^2 - V_0^2} \quad (3.77)$$

3.4 Frequency Domain Analysis

The frequency domain analysis is often used in wave energy in order to have some feedback about the dynamic properties of a system at the earliest phase of the design procedure, with very low expenditure of time and costs. In case of the ISWEC design procedure, this is the first step in which dynamics enter the work-flow. In fact the previous pre-design procedures is based on assumptions, without any dynamic analysis.

Input of the frequency domain analysis are the hydrodynamic parameters of the floater, obtained using flow potential theory solvers software, like WAMIT[®], ANSYS[®] AQWA[®] or NEMOH[®].

Looking at the floater Response Amplitude Operator (RAO) in pitch, it is possible to understand if the system configuration can be suitable to the installation site, thus evaluating the effect of several design parameters like the hull length, width or draft, its mass and momenta of inertia as functions of the ballast masses and materials, the hull metacentric height or the center of buoyancy. A typical linear frequency domain analysis of the floater hydrodynamic behavior is presented in Figure 3.22. The 6DOF linear model used is described in section 2.7 with the gyroscope speed equal to zero. In this way it is possible to study the hydrodynamics independently.

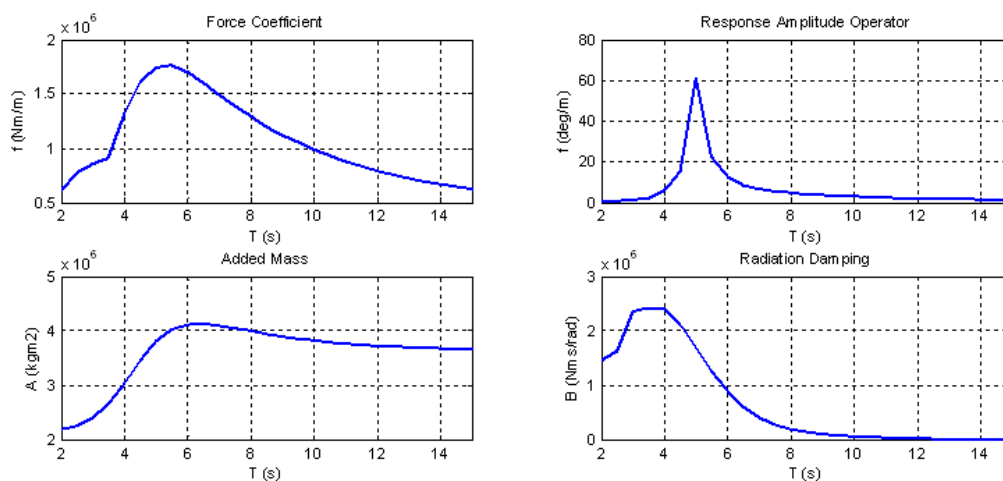


Figure 3.22 Frequency domain floater hydrodynamic analysis.

Once that the selected floater is fulfilling the given specifications, the next step is to include the gyroscope units. The parameters that identify the gyroscopes are also coming from the previous pre-design phase. Flywheel geometry, material and range of rotating speeds, the gearbox ratio, the bearing distance and PTO maximum torque and speed with which is possible to evaluate a range of stiffness and damping control parameters.

It is then possible to choose a configuration of PTO control values and to explore the floater RAO in function of different values of flywheel speed. In Figure 3.23 an example of this analysis is shown.

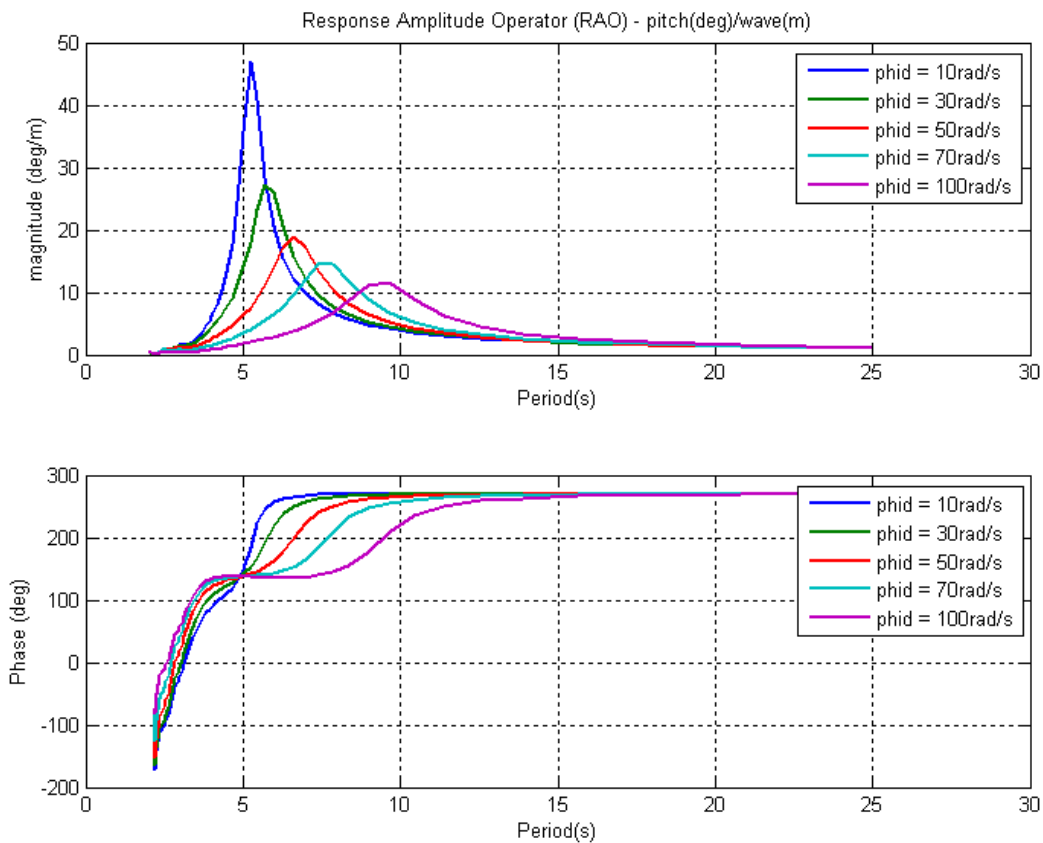


Figure 3.23 Frequency domain floater hydrodynamic analysis with gyro units. Flywheel at different speeds analysis.

As a consequence, it is also possible to evaluate the theoretical power generated by the system and having an idea of the range of frequencies over which the devices should be effective. This kind of outcome comes in the form shown in Figure 3.24.

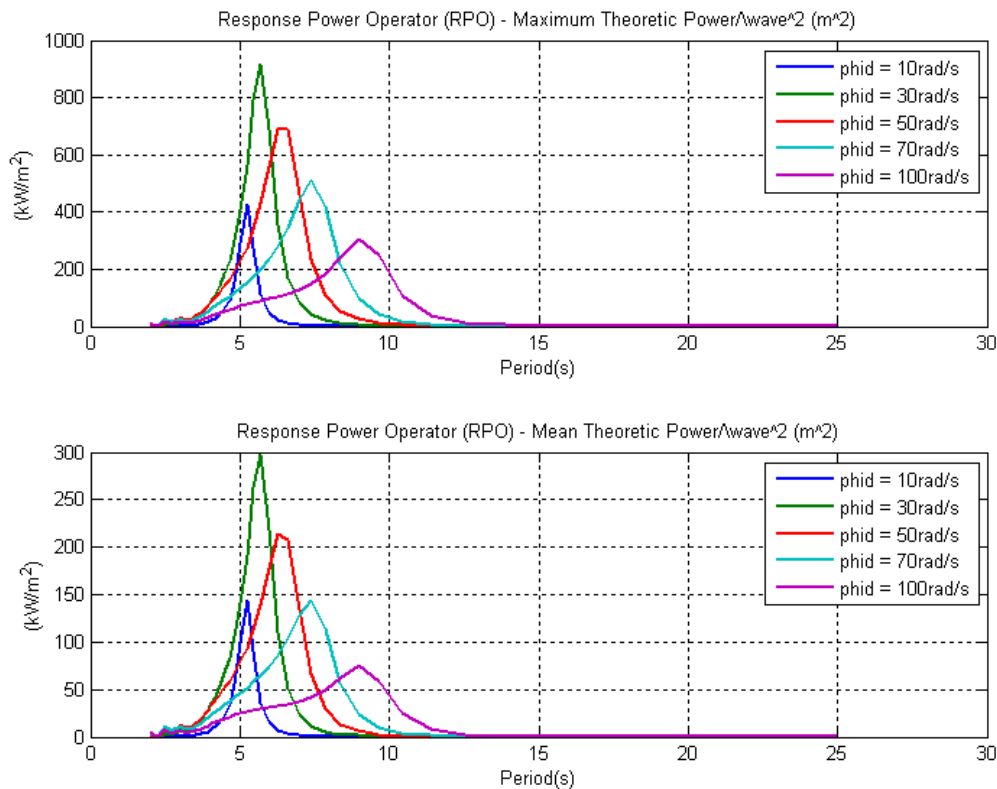


Figure 3.24 Frequency domain ISWEC theoretical power production. Flywheel at different speeds analysis.

It can be observed that some clear information about the frequency working range of the device can be obtained. Another relevant outcome of this kind of analysis is the possibility of tune the system by changing the flywheel speed. Looking at the graph in Figure, a great difference of power absorption response for different flywheel speed is seen. This means that the gyroscope systems have been correctly designed, and they are not too big nor too small for the floater. In fact in the case of small gyroscopes, the floater RAO would not be affected, on the other hand the pitch amplitude would be completely damped.

Looking at the maximum power absorption in Figure 3.24, it is possible to observe that value have very different order of magnitude for the different flywheel speeds. These turn to overcome the maximum PTO power threshold several times. This fact is due to the misleading choice of the control parameters. In fact, in this simple analysis, one parameter of control is varied, while the other two are kept constant and the constraints are verified once the graphs are drawn.

Some more detailed modeling tools with time-domain simulations are thus required.

3.5 ISWEC design tool

In this paragraph the "ISWEC design tool" is presented. This consists in an intermediate step between the preliminary frequency domain analysis and the most detailed time domain model numerical optimizations. More detailed references can be found in [90]. The main purpose of this software is to allow to the system engineer in charge of making the first specifications for a new ISWEC to compute the annual electrical productivity using a simplified model, taking into account several considerations such as system geometrical and electrical configurations, numerous physical constraints, the hull properties or the installation site. To obtain this result, an automatic optimization of control parameters is implemented and a very short computational time is required (1-2 minutes). A cost function is minimized under various system constraints (e.g. PTO torque and power, flywheel speed) and the absorbed power of the system is evaluated for each sea state of a user define scatter table. Output of the software is the device productivity, along with considerations about structural loads, PTO utilization, floater and mass properties. The software helps to draw preliminary decisions and to check the adaptability of this WEC technology to the desired sea site. This kind of methodology can be generalized to other applications and problems, especially in wave energy field, where severe constraints and time consuming simulations are common, and the use of a tool with simplified hypothesis and a controllable constraint management procedure can reduce develop time, giving different information from the very start of projects of different nature.

3.5.1 The Algorithm

Aim of this section is to explain how the tool works and under which hypothesis. The first motivation of coding such an algorithm is related to the time needed for performing a complete matrix optimization with the complete ISWEC nonlinear lumped parameters model. In fact, as described in section 2.8, the time required for running a 900s simulation is of about a 50s, and thus a complete optimization over a scatter table with a considerable number of sea states usually takes some hours/days of CPU time. On the other side, a time domain simulation of the linear version of the single hydrodynamic DOF model, described in section 2.6.4, can be run in 0,5s. The problem, as is well known, is that linear model cannot includes nonlinearities such saturation, quadratic terms or discontinuities, and thus the results they give must be carefully checked in order to assess if they remain in their validity domain. The idea

behind this algorithm is to use the fully linear model for quickly computing ISWEC operations time histories. From these results, several synthetic physical quantities are computed and then weighted by mean of a cost function. This expression considers the power production and also if the outcomes respect a whole set of desired constraints. A non-linear minimum constrained multi-variable algorithm is then used in order to minimize the cost function. In particular the Nelder-Mead simplex search method with boundaries is used [62]. The power sign conversion is in fact negative in case of energy harvesting. In case of violation of one of the constraints, a big positive number is summed. In this way the optimization algorithm change direction and excludes the search area. In Figure 3.25 the main input and output of the tool are outlined. The first required input is the installation site characterization, given in the occurrences scatter table form. This reflects the need of tightly optimize each single WEC for the installation site where it is supposed to be installed. The second arrow input gathers together the complete set of electro-mechanical parameters describing the internal gyroscope units. These parameters can be easily changed and their values explored (number of units, radius of the flywheels, electric motors size and others). The third input is actually the most delicate, since it involves the data coming from the hydrodynamic flow potential theory analysis for the hull. This kind of analysis requires considerable time and must be performed previously, with a different software. From this point of view, the "ISWEC design tool" is a tool that helps the early evaluation of performances of the overall system and enables the quick evaluations only for the inner electro-mechanical system configuration. The first output is the annual energy productivity (AEP). Performance parameters are of two different nature: the first are synthetic kinematics and loads scattered in matrices in function of the sea states (H_s and T_e couples). Others are simple scalars, providing information about floater and gyroscope kinematics, mechanical and electrical loads, utilization factors and bearings life (bearings represent the reason for the first main maintenance operation which requires the ISWEC to be brought into the port).

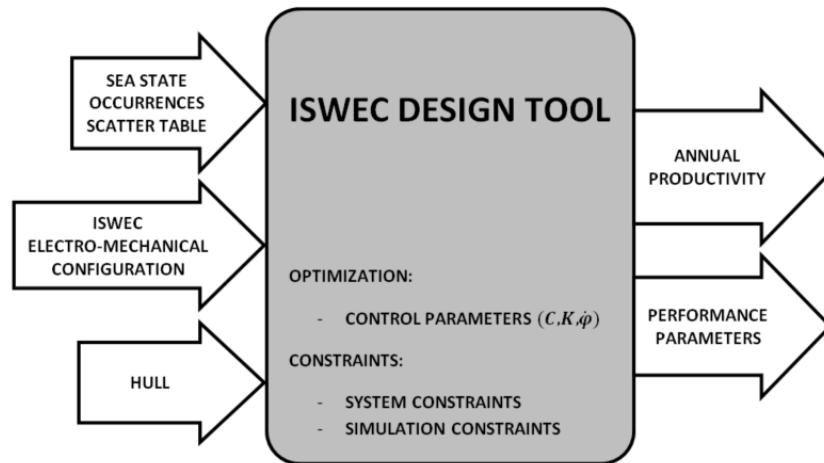


Figure 3.25 ISWEC design tool - Main functional Scheme

3.5.2 Cost function

The cost function to be optimized by the minimization algorithm aims at maximizing the device energy production for each sea state. The parameters to be explored are those acting on the control system parameters: C, K, ϕ . While looking at the optimal configurations for each sea state, it must insure the respect of different nature constraints. All these requirements must enter the cost function " J ". This consists mainly of two parts, the net average power and the system constraints terms. At this point a consideration must be done: when considering the terms of a cost function it is important to opportunely adimensionalize or scale them. In this way it is possible to control the relative order of magnitude of the terms and to tune the function itself. In the following, term with * are pointed all the adimensionalized quantities.

The cost function overall expression is:

$$J = P_{netmean}^* + \sum_i J_{constraints_i} \quad (3.78)$$

As already stated before, absorbed power has a negative mean value. In case of constraint violation, J_i elements add a positive value, thus directing the optimization search to different areas of the optimization space.

The scaling of the different contributes is hereafter discussed.

Average absorbed power is scaled accordingly to the overall ISWEC electric motors installed capacity. In this way, different sizes of the devices can be managed by the software through very different range of devices.

$$P_{net\,mean}^* = \frac{P_{net\,mean}}{P_{nom\,PTO}} \quad (3.79)$$

Among kinematics constraints, both gyroscope and floater are considered. For what regards the gyroscope, the maximum epsilon value and its root mean square value are constrained. This is required for different reasons. Firstly, given that a linearized model is used, the gyroscope frame maximum oscillation amplitude must be constrained in order to reduce the errors coming from the nonlinear gyroscopic torque miscalculation. Moreover normal operations of the system are bounded by a maximum oscillation amplitude of about 60deg. The maximum rms value is introduced in order to enhance the coherence and stability of the results coming from simulations.

$$\epsilon_{max}^* = \frac{\epsilon_{max}}{\epsilon_{max\,constr}} \quad (3.80)$$

$$\epsilon_{rms}^* = \frac{\epsilon_{rms}}{\epsilon_{rms\,constr}} \quad (3.81)$$

The limitations imposed to the floater kinematics are due to the respect of the Cummins hydrodynamic laws hypothesis of small amplitudes oscillations. This means that simulations in which the amplitude of oscillations overcomes certain values are discarded.

$$\delta_{max}^* = \frac{\delta_{max}}{\delta_{max\,constr}} \quad (3.82)$$

$$\delta_{rms}^* = \frac{\delta_{rms}}{\delta_{rms\,constr}} \quad (3.83)$$

Another fundamental term is the one related to the PTO electric motor maximum torque. In order to keep the system linear in fact torque saturation have been deleted. Since as known this is affecting noticeably the power absorption, causing an overestimation of the final productivity, the control parameters are tuned in such a way that the maximum available torque is of about 1.5 times the maximum PTO available value (this usually happens only a couple of times in a 20 minutes history) and its rms value is constrained to the PTO nominal torque, in order to respect the electric machine and inverter thermal specifications and ensure overheating phenomena.

$$T_{PTO\,max}^* = \frac{T_{PTO\,max}}{T_{PTO\,max\,constr}} \quad (3.84)$$

$$T_{PTO\,rms}^* = \frac{T_{PTO\,rms}}{T_{PTO\,rms\,constr}} \quad (3.85)$$

The last value to be constrained is the gyroscope axis maximum angular velocity. This in fact must be strictly controlled to be under the maximum speed that the PTO can handle, in order to avoid hazardous overvoltages.

$$\omega_{PTOmax}^* = \frac{\omega_{PTOmax}}{\omega_{PTOmax_{constr}}} \quad (3.86)$$

$$\omega_{PTOrms}^* = \frac{\omega_{PTOrms}}{\omega_{PTOrms_{constr}}} \quad (3.87)$$

Each of these adimensionalized quantities is then given as input to a purposely built function. Calling x^* a generic dimensionless term value, its related cost is thus defined by:

$$J(x^*) = \frac{1 + \tanh(x^* - 1)}{2} + H(x^*) \cdot (x^* - 1)^2 \quad (3.88)$$

Where $H(x^*)$ is the Heaviside function:

$$H(x^*) = \begin{cases} 0 & x^* \leq 1 \\ 1 & x^* > 1 \end{cases} \quad (3.89)$$

The behavior of this equation is shown in Figure 3.26

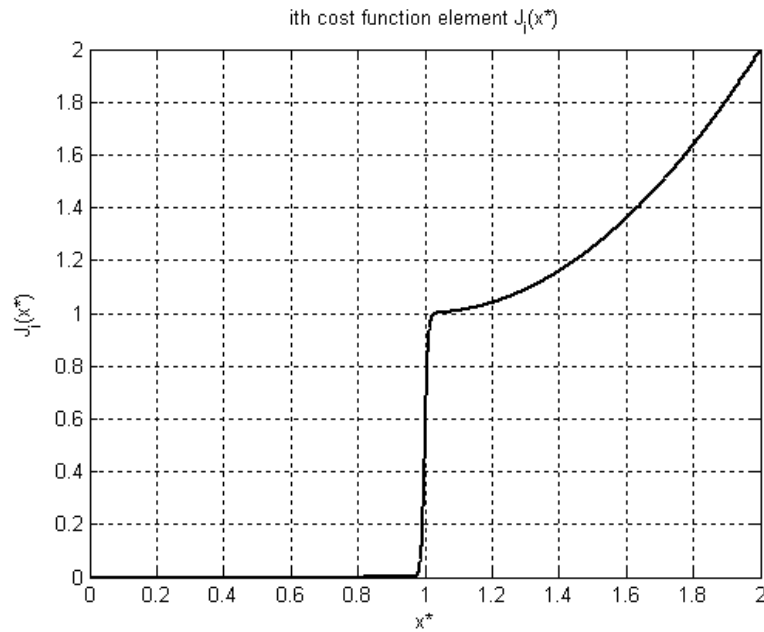


Figure 3.26 ISWEC design tool - Cost function constraining i^{th} element equation.

3.5.3 User Interface

A graphical user interface has been developed in order to enable an immediate use of the software. From this it is possible to load input data, as hull hydrodynamic parameters, the electro-mechanical configuration or installation site data, and to save the analysis results. Moreover, gyroscope units parameters can be changed directly from the user interface and results can be visualized both in tables or in scatter tables form. In Figure 3.27 the Matlab developed GUI is shown.

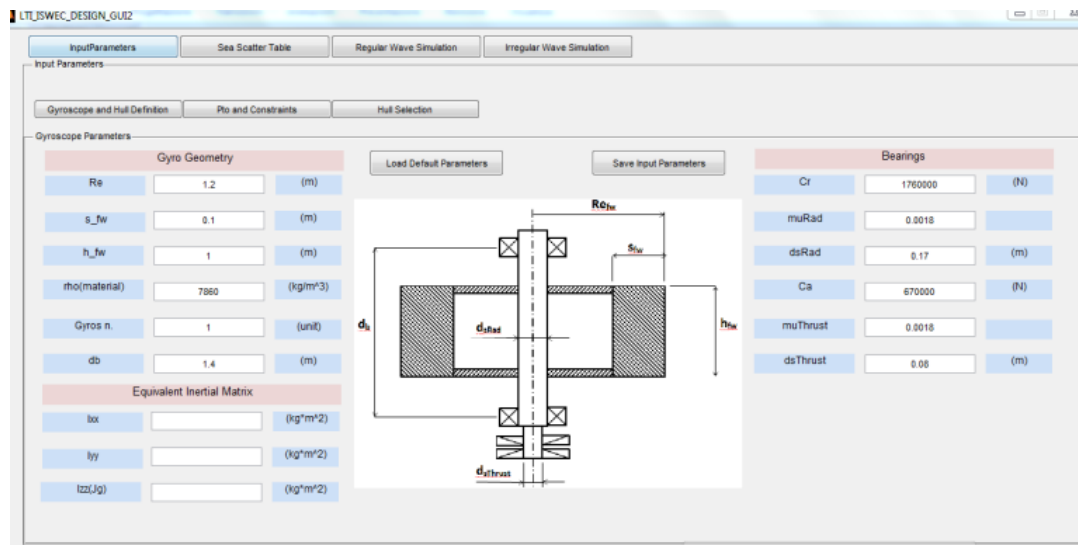


Figure 3.27 ISWEC design tool - Graphical User Interface (GUI).

3.5.4 Example of analysis

In this section an example of the results obtainable from the software is presented. Pantelleria installation site is chosen. The hull parameters and analysis are those presented section 4.2. The electro-mechanical parameters and the constraints used in the analysis are presented in Table 3.4. The parameters shown are those on which it is possible to quickly act, thus easily verifying the impact of their variation on the device. It is possible to change the gyroscope dimensions, the number of gyro units, the electric motor size and the gearbox ratio.

The choice of simulation constraints is more challenging and actually the choice of the optimal values comes with the experience gained using the tool and comparing it with results coming from the nonlinear model. In particular, the acceptable maximum values seems to be exaggerated. This is explained by the irregular nature of waves. The single peak value of ε or δ in a 20 minutes time history is about 3/4 times the

Table 3.4 ISWEC design tool - Example - Parameters setting

Mechanical parameters			
Flywheel external radius [m]	1,2	Flywheel height [m]	1
Flywheel thickness [m]	0,1	Flywheel material density [kg/m]	7800
Gearbox ratio [-]	10		
Electrical parameters			
PTO nominal torque [Nm]	5000	PTO maximum torque [Nm]	10000
PTO maximum speed [rpm]	250		
Simulation constraints			
Gyro frame maximum angle [deg]	150	Floater pitch maximum angle [deg]	50
Gyro frame rms angle [deg]	50	Floater pitch rms angle [deg]	10

Table 3.5 ISWEC design tool - Example - Optimization space definition.

Control parameter boundaries		
C [Nms/rad]	0	10^5
K [Nm/rad]	0	10^5
phid [rpm]	0	1000

common peaks of the other remaining oscillations. Limiting this value to a reasonable number would actually highly damp the system dynamics, thus almost blocking the system. Then the choice has been that of accepting some unrealistic data and keeping the others in a more reasonable range. The maximum rms value comes in help and combined with the previous works fine for the performances prediction.

Others important user settings are related to the definition of the optimization space, the bounded area in which the optimization function must search for the results. For the current analysis, the control parameter in Table 3.5 are selected.

In Figure 3.28 the results of the analysis are illustrated. These consist of matrices with different kind of synthetic data and parameters, optimized minimizing the cost function for each sea state condition. A critical analysis of the results must be performed, starting from the matrices at the top left, in which the kinematics rms and maximum values are plotted. The epsilon rms values are in a good range, with the maximum values below the 50deg threshold. The maximum values are relevant, but for areas of the scatter with very low occurrences and thus they have very low or zero impact on the final productivity computation. The delta rms values are sometimes overcoming the 10deg threshold, but they are all realistic values. Maximum pitch angles are sometimes big, but also in this case they are in very low populated areas of the scatter. At the top right there are the matrices with results showing the PTO performances. The rms maximum torque is always below the nominal value of the chosen electrical

machine. On the other hand the maximum torque is almost always reached. Also the maximum velocities of the PTO are often close to the maximum admissible value, even if they never overcome it. Productivity and the power net matrices give an overview of the device conversion capabilities. A final comment must be spent about the white not-filled points. In this points it was not possible to find any viable working condition, and the system was completely out of bounds. This is due to waves with a combination of frequencies in a range close to the resonance of the floater and with high wave amplitudes.

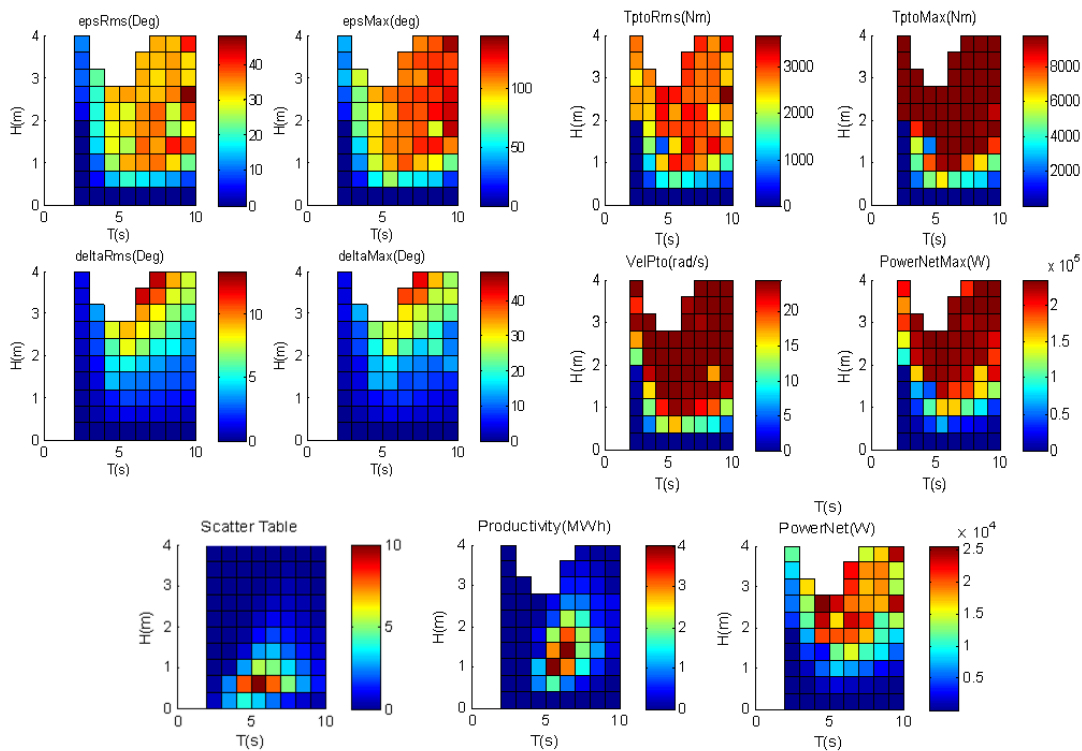


Figure 3.28 ISWEC design tool - Example - Results of the analysis.

This single analysis of a configuration can be reiterated for slightly changing configurations. Two synthetic results from [90] are proposed.

In Figure 3.29 an analysis regarding the gyroscope size is carried out. The flywheel radius has been varied from 0.75m up to 1.9m. The annual energy production has been evaluated for the case of a single and two gyroscope units. Both curves present a maximum and the relative increment of power absorption between the two can be computed. An analysis like this can be coupled with an economic evaluation of the

device construction for the different cases.

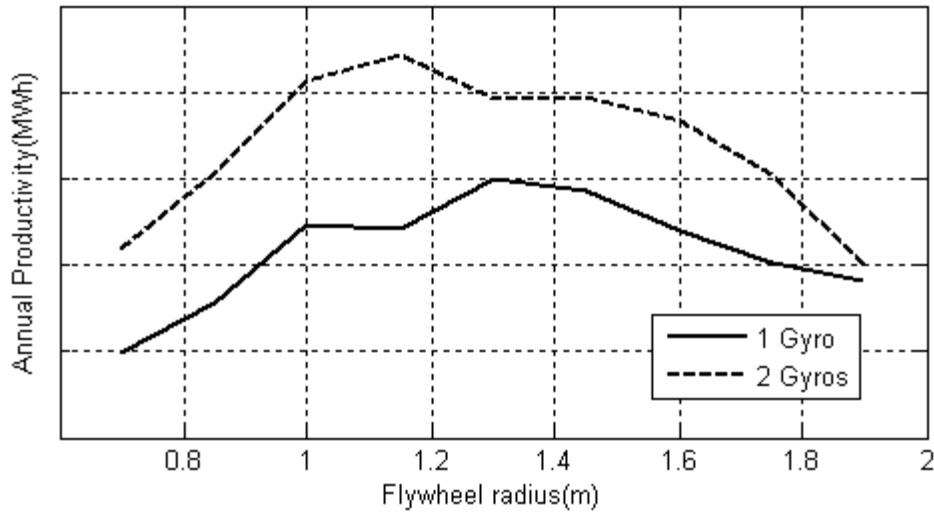


Figure 3.29 ISWEC design tool - Example of parametric study - Case A.

In Figure 3.30 a second example of analysis is proposed. This time three parameters are changing: the gearbox ratio, the gyroscope numbers and the kind of PTO. PTO configurations refer to the parameters listed in Table 3.6. This kind of analysis can be important for optimizing the cost through the reduction of the size requested to the electric PTO or for trying to understand if a direct drive option is viable.

Table 3.6 PTO configurations

PTO conf.	Max Torque [Nm]	Nominal Torque [Nm]	Nominal Speed [rpm]
1	6000	3750	250
2	8000	5000	250
3	10000	6250	250

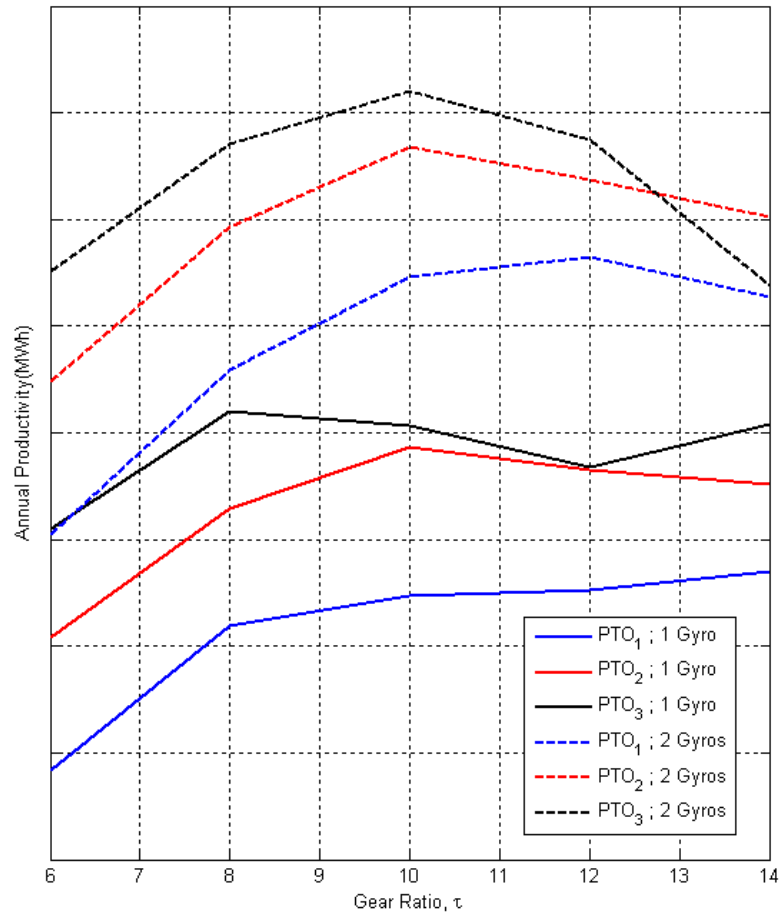


Figure 3.30 ISWEC design tool - Example of parametric study - Case B.

3.6 Model-Based Optimization

Once the pre-design configuration is found, a more detailed optimization is performed. In particular here the objective is to compute the productivity of the device in the installation site. The target is attained by Time Domain simulations, using the lumped-parameters numerical model in MATLAB[®]/Simulink[®] environment described in section 2.8: the wave to wire model.

Starting from the occurrences scatter table of the installation site, for each sea state the control parameters c, k and the flywheel speed ϕ are optimized using a cost function that weighs the net annual productivity, the electro-mechanical loads, the mooring forces and the bearings life. This analysis is repeated for different device configurations varying single subsystem starting from the pre-design one. With the productivity and the estimation of the maintenance procedures, the plant LCOE can be assessed. If the result is not enough interesting, the procedure can be repeated. The design optimization phase is then an iterative procedure, where the output are the specifications of the most important subsystems of the ISWEC.

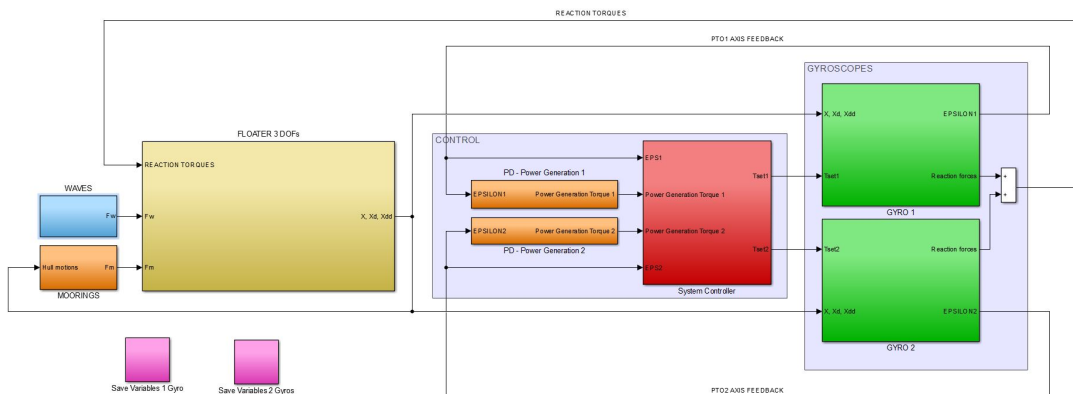


Figure 3.31 Wave to wire lumped parameters numerical model.

Examples of the output and analysis performed with the help of this model are presented in Chapter 6.

Another fundamental outcome of the use of this nonlinear numerical model is the identification of functional specifications and operation load cases. For example, it has been through numerical time-domain simulations that the need of a safety state for the machine was identified. Its controller was then designed and tested numerically, prior the dry and wet tests on the prototype could be performed.

Final objective of the model-based optimization is to find the control parameters to be used for each sea state and the mean power harvested. This optimization mainly

consists in the exploration of a wide set of control parameters configurations and then in the choice of "optimal" configurations according to different indexes and criteria. For example, in the first experimental campaign the control matrices used were designed looking at a trade-off between the minimization of the electro-mechanical loads and a good power production capability.

The matrices obtained from this optimization and that have been implemented for the utilization during the first experimental campaign in Pantelleria in 2015 are presented in Figure 3.32. The first controller to be tested into the sea was the simplest proportional-derivative, spring-damper, controller. In this case the regulator has three parameters over which is possible to act: the flywheel speed, the internal precession axis damping and stiffness coefficients.

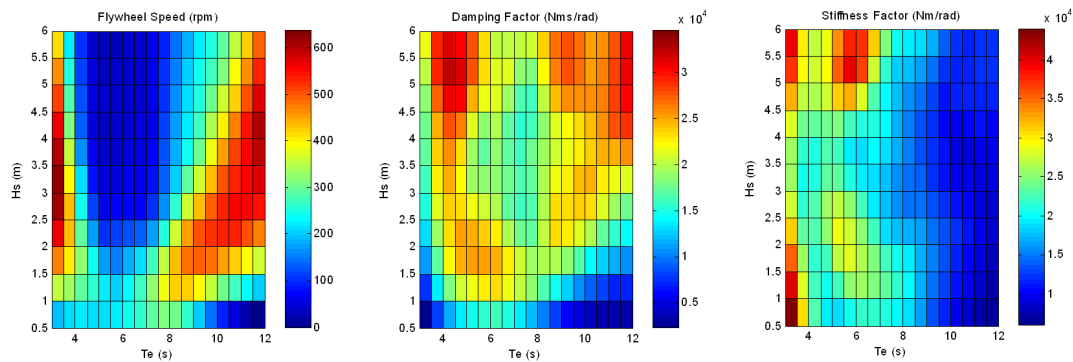


Figure 3.32 ISWEC Pantelleria 2015 - Control parameters matrices.

Chapter 4

ISWEC Pantelleria device

4.1 Introduction

A wave energy converter is a complex system and its construction requires expertises and knowledge in disparate fields. Wave for Energy S.r.l. has been responsible of the coordination of companies involved in the project. Politecnico di Torino offshore renewable group assisted the whole procedure with consultancy, design and procurement activities.

Objective of this chapter is to present the final realisation of the fundamental ISWEC subsystems. The assembly of the final configuration launched and tested during the first experimental campaign in second part of 2015 is presented.

In the last section system upgrades for next campaign are exposed.

4.2 The Floater

The final designed version consists of a monolithic steel hull with a semi elliptic shape. The objective of the floater of an ISWEC device is to maximize the pitch response in the range of frequencies characteristic of the installation site, not forgetting the possibility to regulate the system overall response through the control of the internal gyroscopic groups. However, the maximization of production performances alone does not represent the optimal solution for the design: a complete cost analysis has to be made. In order to reduce expenses, the overall shape remained as simple as possible and longitudinal dimensions were minimized. In fig. 4.1 and 4.2 the final design is presented. The machinery room is situated in the centre of the device and

the gyroscopic groups are positioned such that the two flywheels center of gravity lie on the lateral median plane of the hull and they are symmetric with respect to the longitudinal plane. The forepeak and the aftpeak are designed to store the ballast required for reaching the specified inertia momentum.

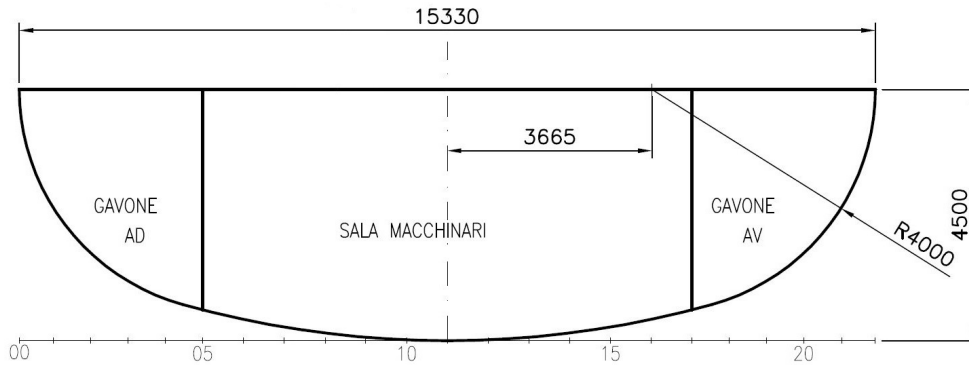


Figure 4.1 The floater final design. Side view.

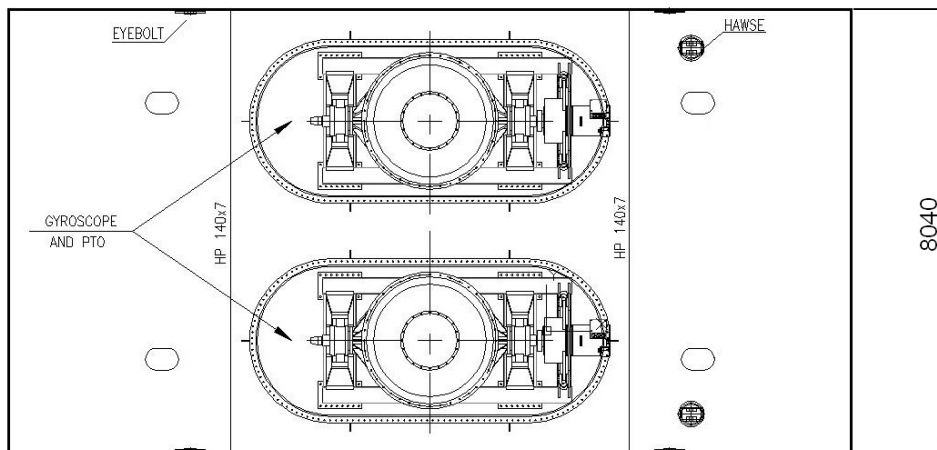


Figure 4.2 The floater final design. Top view.

The hydrodynamic properties of the floater can be presented using the linear model hypothesis already presented in chapter 2 and whose synthetic result is the response amplitude operator, the RAO. This is a common instrument for the analysis of stability in the ship industry and for designing floaters in wave energy field. The pitch response peak was set the nearest possible to the desired design point, also following some techno-economic evaluations as explained before. Thus, the wave period in which the floater is designed to maximise the oscillations is $T = 5s$. The mass, geometric and hydrostatic properties are summarised in table 4.1:

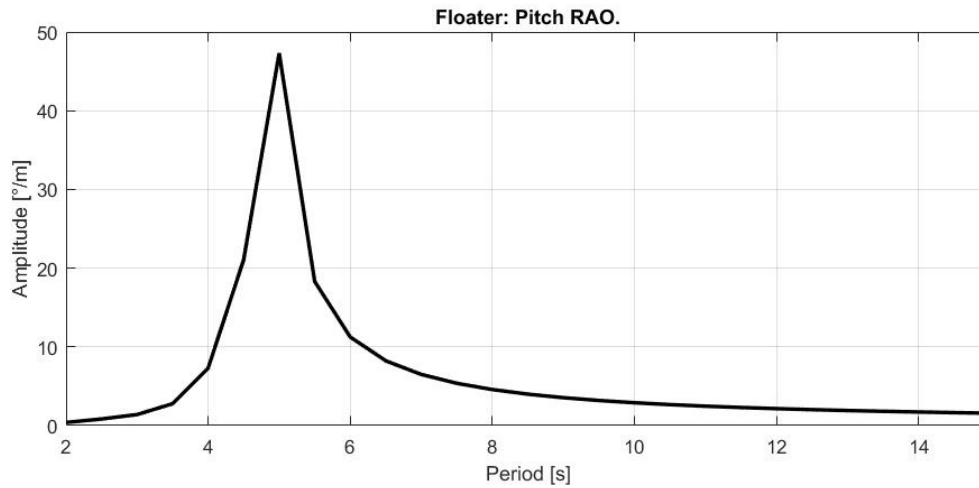


Figure 4.3 Floater dynamic response. The pitch RAO with fully linear BEM modeling approach.

Table 4.1 Floater properties

Properties group	Quantity	Unit	Value
Geometry	Floater Length	[m]	15
	Floater Height	[m]	4.5
	Floater Width	[m]	8
Overall Mass properties	Overall system Mass	[ton]	288
	Momentum of Inertia about longitudinal axis x	[kg m ²]	1.92 10 ⁶
	Momentum of Inertia about transversal axis y	[kg m ²]	8.49 10 ⁶
	Momentum of Inertia about vertical axis z	[kg m ²]	7.15 10 ⁶
	Center of Gravity distance from Deck	[m]	2.03
Hydrostatic properties	Waterplane Area	[m ²]	119.17
	Water Level distance from Deck	[m]	1.5
	Submerged Volume	[m ³]	280



Figure 4.4 The floater in the shipyard.

The floater construction and assembly was pursued by Cantiere Navale F.lli Gicalone S.p.a. shipyard in Mazara del Vallo (Sicily, Italy) under the coordination of Wave for Energy S.r.l. The beams and plates composing the floater are made of FE430B steel. These are curved and welded in order to making up the Desired shape. As last step they were properly coated with two painted layers of bi-component polyurethane in order to have a sufficient resistance to the corrosion caused by the harsh sea environment.

In Fig. 4.4 the floater waiting for the launch is shown. After the hull is completed, the first gyroscope group is installed inside. In place of the second unit a concrete clump weight is allocated in order to balance the overall mass distribution. In Fig. 4.5 some pictures of the process are shown.

Table 4.2 The floater: mass distribution.

Mass	Units	Value
Hull	ton	56
Ballast x 2	ton	86 x 2
Gyroscope x 2	ton	30 x 2



Figure 4.5 The floater: first gyroscope group installation.

After the internal electro-mechanical system was completed and some preliminary dry tests were done, the system is launched.

The ballast tanks in the prow and aft are then filled with sand. Thanks to this operation the planned momentum of inertia is reached. In next Fig. 4.6 two images showing the floater before and after this operation are shown. In Table 4.2 the mass distribution is shown and it is possible to see the significant mass of the ballast.

The connection with the mooring system is realised with a couple of hawses in the prow side. In Figure 4.7 a section showing the solution found is presented. The mooring line in red is going through the hawsehole in the bottom hull wall, below the



Figure 4.6 The floater: launch and ballast filling operations.

mean sea level. The chain then ascends vertically up to the hawse joint. The function of these connections is better explained in the mooring section 4.3.

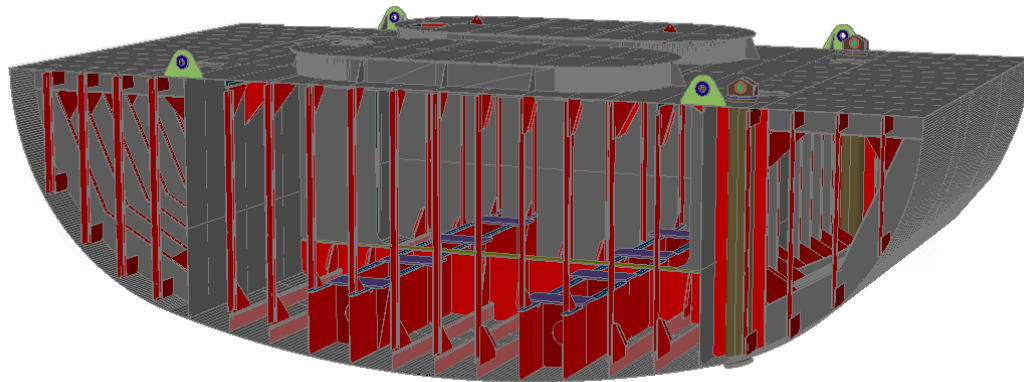


Figure 4.7 The floater: mooring prows connection. Hawses design.

4.3 The Mooring System

The mooring system final design is related to the installation point on the 800 m far from the Pantelleria shore. The resource in this site is directional, the energy is mostly concentrated coming from 320 deg North-West direction. The selected mooring configuration has self-aligning properties, and it is free to rotate around a central point. It was decided to test in real sea environment such characteristic. Main objective for such an application is to reduce the influence of the moorings on the dynamic behaviour of the device, in the case of the ISWEC the most important degree of freedom not to be influenced is the pitch. A mass-jumper configuration is chosen for this purpose. The final architecture is introduced in Figure 4.8.

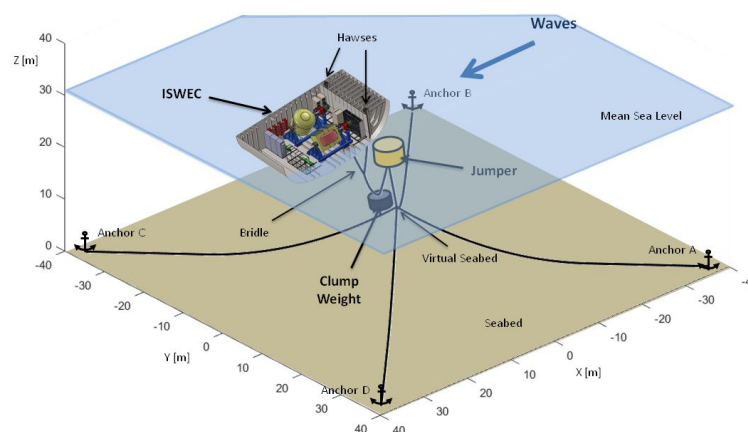


Figure 4.8 The mooring system: Pantelleria architecture scheme.

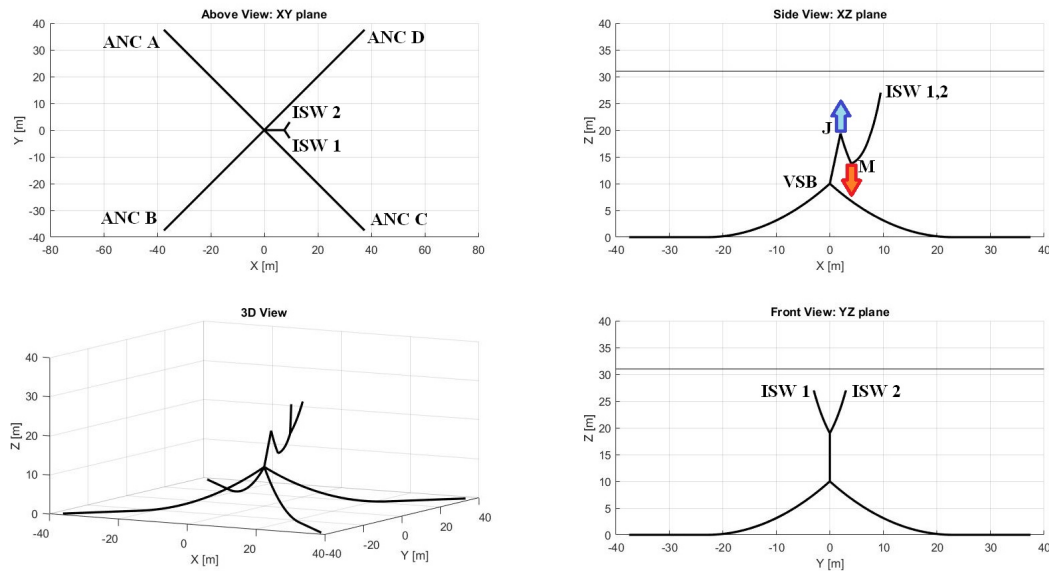


Figure 4.9 The mooring system: Pantelleria architecture scheme.

The mean sea level in the selected installation point is at 31 m from the seabed. Four 4 tons Hall type anchors by Italmet are installed in a axisymmetric configuration. From these ones, four catenary lines are linked to a single point, the virtual seabed, 10 m above the seabed. This point is taken as the center of the reference system of the mooring architecture. From this point a chain line is connected to the jumper, a body with a positive buoyancy of $12,9\text{ tons}$. After this, another chain line reaches the clump weight, a negative buoyancy of 8 tons . From this body a line starts toward the hull, it is then split in a bridle shape and the two lines reach the hull in proximity of the two hawseholes.

In Figure 4.9 some orthogonal views of the system are presented and key points are defined. Referring to these definitions, the properties of all catenary lines involved are presented in Table 4.3.

Table 4.3 The moorings system: parameters.

Clump Weigth	Volume [m3]	Net Buoyancy [kg]
Steel and concrete element	5.4	-8000
Anchor	Type	Mass [kg]
4 x Italmet - AHN4320	Hall	4000
Jumper	Volume [m3]	Net Buoyancy [kg]
Floatex BOEORM	19.4	12600
Line	Length [m]	Diameter [mm]
ANC xx- VSB	55	40
VSB - J	9.5	48
J - M	6	48
M - Bri	6.5	48 / 32
Bri - ISW xx	8.8	48

4.4 The Gyroscope

The gyroscopic groups are the key subsystems enabling the power conversion. The Pantelleria ISWEC device is designed with two units, an even number for the reasons explained in section 3.3.3.3. During the first experimental campaign only one group was installed. The construction and assembly was carried on at A.R.I.S. SpA, a company devoted to defence and special applications settled in Lombardore, near Turin in Italy. Main aim of this section is to introduce its main features.

Main specification of a gyroscope unit is the angular momentum. This is equal to the product of the flywheel axial momentum and its spinning velocity. Given the high inertial torques that have to be exchanged, components have noticeable size and heavy load duty conditions.

First component to be presented is the flywheel. It is composed by a central element called crown and two short shafts sections on both sides. The crown is made of an external cylindrical element that is reinforced by two side plates and a central one. An hollow shaft enables the connection with the main rotation elements. This configuration allows the use of smaller bearings and constitutes a stiff structure with small distortions. A section of the final design is shown in Figure 4.10. The top and bottom elements are obtained from steel plates, where the central holes are made by flame cutting and then all lateral surfaces are processed at the lathe. The two semi-shaft are made of 39NiCrMo3 hardened steel, forged and then then machined at lathe. The ring

Table 4.4 Flywheel properties

Properties group	Quantity	Unit	Value
Geometry	Ring external diameter	[m]	2.15
	Ring height	[m]	1
	Ring thickness	[m]	0.12
	Bearings distance	[m]	1.4
Mass properties	Mass	[ton]	9.69
	Momentum of Inertia about longitudinal axis x	[kg m ²]	5.373 10 ³
	Momentum of Inertia about transversal axis y	[kg m ²]	5.373 10 ³
	Momentum of Inertia about axial rotational axis z	[kg m ²]	8.164 10 ³

lateral element is made of S355 steel, and it is forged and machined at a vertical lathe as well, both in the inner and outer side. All the connecting surfaces are chamfered and then welded together with continuous wire welding method.

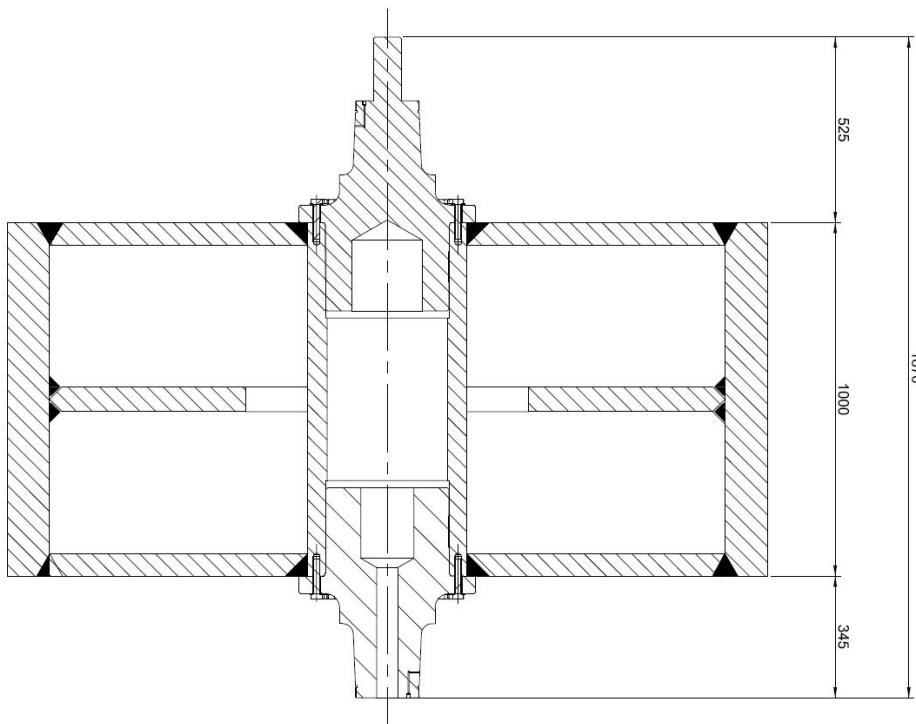


Figure 4.10 The gyroscope: flywheel design section.

The mechanical and geometrical properties of this first unit are presented in Table 4.4. This unit is provided of a vacuum chamber, a sealed case with a low pressure internal environment. This is intended in order to reduce the aerodynamic losses as presented in previous section 2.3.3. The chamber structure receives the mechanical

loads discharged by the radial and thrust bearings of the spinning shaft. It is mounted on the PTO internal shaft, where two radial bearings constraint the y axis rotation, giving the possibility to the frame to rotate only about the x internal precession axis. Thus, the flywheel is mounted on a frame and only the rotation around the x axis is unconstrained. The other degree of freedom are blocked and the inertial torques are exchanged with the floater structure through the supporting structure. In next Figure 4.11 a section of the overall unit is presented.

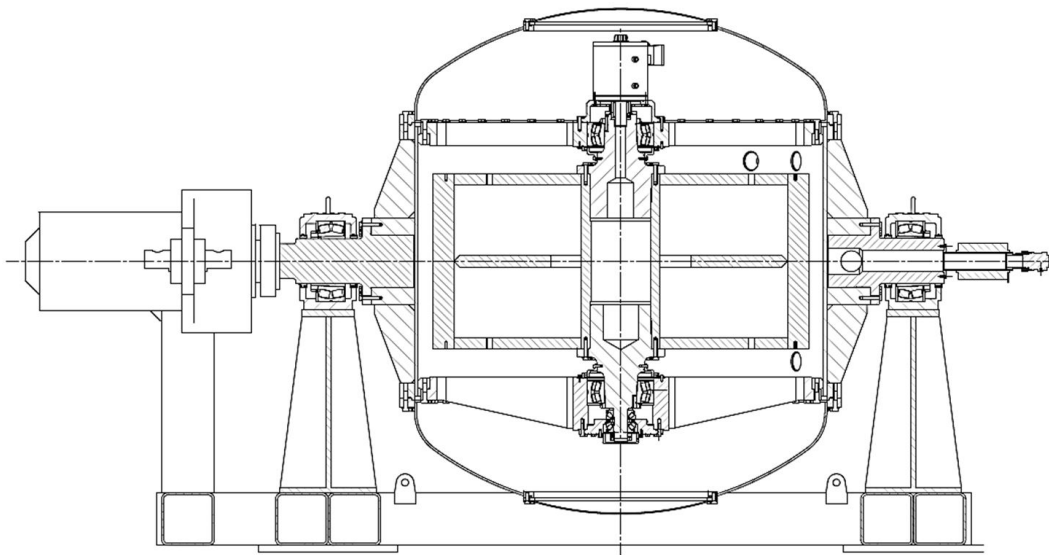


Figure 4.11 The gyroscope: section of the first unit.

Some pictures taken in A.R.I.S. showing specific steps of the assembly procedure are presented in Figure 4.12. Operations start from the vacuum chamber lateral element. This is machined and the two shaft arms are mounted on both sides. Also the spoked wheel with the shaft seat is encased on the top side. After this, in the third picture operations for the assembly of the chamber on the main supporting structure are shown. It can be noticed that bearings are going to be enclosed in the respective half plummer block housings. Once the bearings are ready to work, the chamber is slowly accompanied to its stable position, with the spoked wheel on the bottom. In this picture it is possible to see the seat of the flywheel bearings. In next image it is possible to see the red flywheel. The bearings are then mounted and it is inserted into the chamber. In last picture, a view of the overall group without the bottom and top coatings. In order to realize the specified angular momentum the flywheel must be kept in rotation. The component filling this function is the flywheel motor. It is



Figure 4.12 The gyroscope: assembly of the first unit.

Table 4.5 Flywheel motor, SIEMENS 1FW3154-1BP.

Properties group	Quantity	Unit	Value
Mechanics	Rated Speed	[rpm]	750
	Rated Torque	[Nm]	300
	Maximum Torque	[Nm]	600
	Maximum Speed	[rpm]	1700
Electrics	Rated Current	[A]	47.5
	Rated Voltage	[V]	600
	Rated Power	[kW]	23.6
	Maximum Current	[A]	113
Geometry	Main body longitudinal length	[mm]	338
	External diameter	[mm]	310
Mass	Mass	[kg]	143
	Momentum of Inertia of the rotor	[kg m ²]	0.13

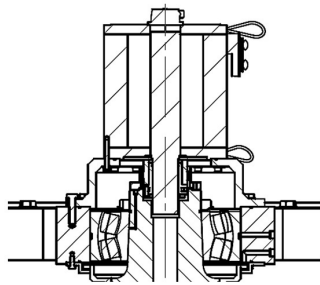


Figure 4.13 The gyroscope: flywheel motor.

an electric brushless torque motor made by Siemens, belonging to the SIMOTICS T-1FW3 family. This electric machine is coupled with the Siemens power electronics hardware SINAMICS S120, giving the possibility to regulate its angular speed. The key technical information about are shown in Table 4.5. A picture of the flywheel motor is shown in Figure 4.13.

The rotation is allowed by a couple of radial and two thrust bearings as showed in Figure 4.14. This configuration is characterised by the use of small thrust bearings working with the axial loads of the flywheel, mainly due to its own weight, thus reducing the power losses. These are mounted on one shaft side tip in order to facilitate maintenance operations. Two radial bearings take up the radial loads due to the gyroscopic inertial torques. These are the most stressed components in the system and usually their working life provides the time of the first return of the device in port. Another strength of this disposition is the avoidance of thermal deformation

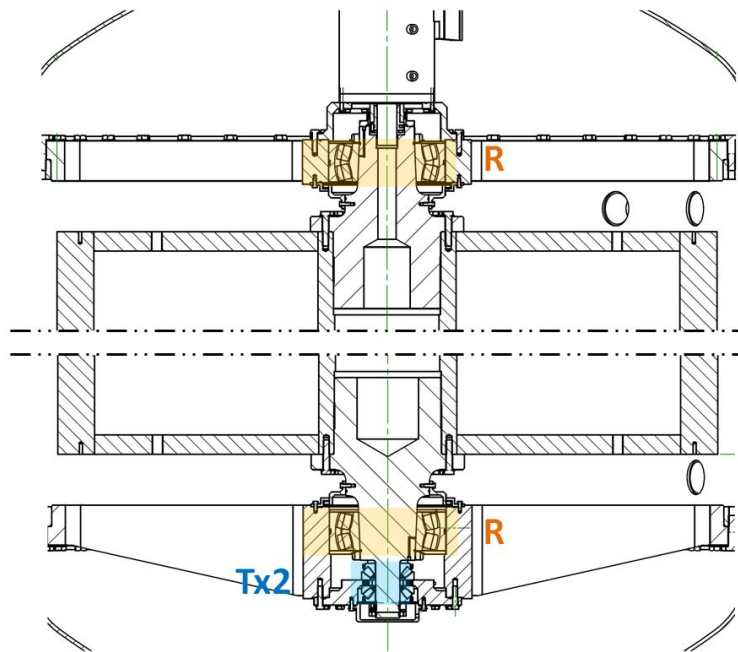


Figure 4.14 The gyroscope: flywheel bearings configuration.

problems. In the design phase it was estimated a 0.5 millimeters axial deformation for the 2 meters shaft in case of 50 degree temperature variation. Such temperatures are expected mainly due to the friction losses of the bearings. For this reason these bearings need a lubricating and cooling actions.

The flywheel bearings lubrication circuit is part of the device overall cooling system that is presented in section 4.7. In general the main concept is taking the heat from the hot spots and to dissipate it with the sea water. Concerning the four flywheel bearings, the topological scheme is presented in Figure 4.15. The main cooling system pumps sends the oil through the rotary hydraulic joint up to each bearing inside the oscillating vacuum chamber. The warm oil is then gathered in enclosed volumes and sucked away by the oil recovery pump via the green lines. The collector receives the all the fluid and the oil is sent back to the cooling system through the rotary hydraulic joint via the yellow line. In Figure 4.16.

The bearings of the internal precession axis have no problem about the temperatures because the rotational speed of this shaft is very low. So they do not occur any type of cooling but they are manually filled with grease.

A more detailed description can be found in [63], [78].

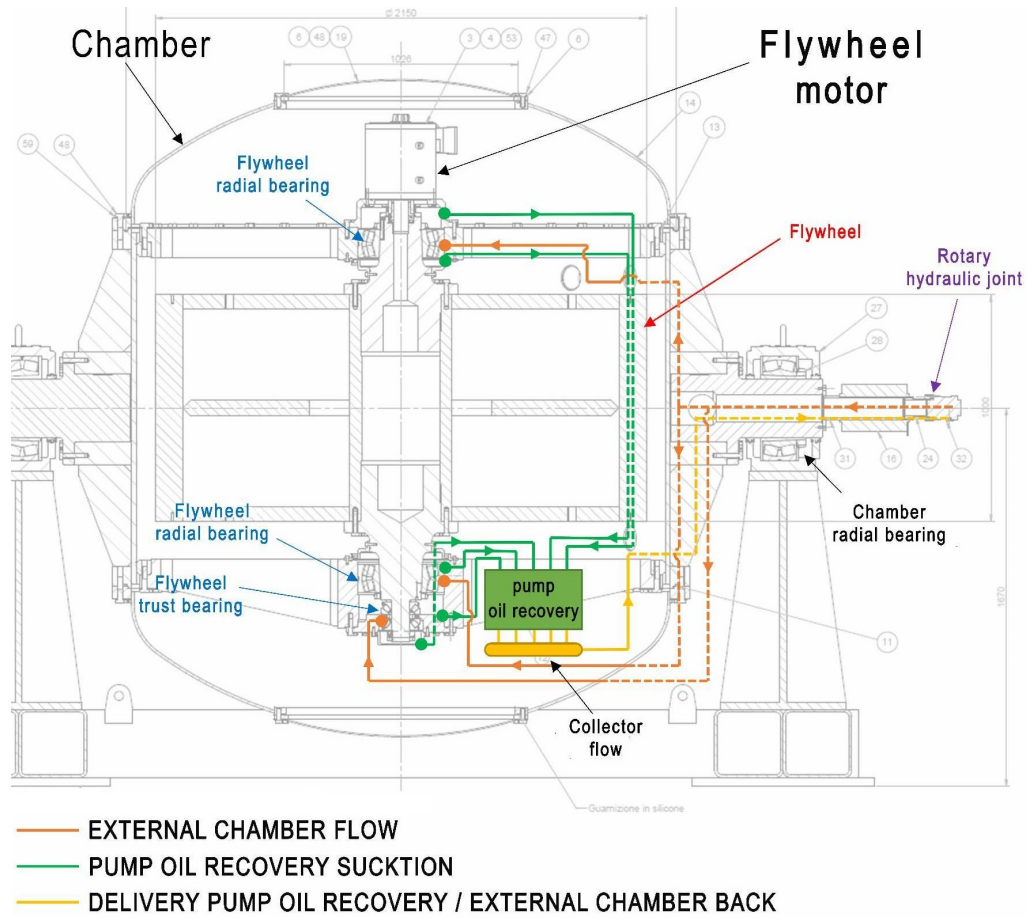


Figure 4.15 The gyroscope: flywheel bearings lubricating system.



Figure 4.16 The gyroscope: flywheel lubricating system, oil recovery pump and rotary hydraulic joint.

4.5 The PTO

The Power Take Off system is completely electric. An electric motor is directly affecting the oscillations of the gyroscopic frame with its torque. It is mounted on the internal precession axis and it is called generator.

The choice of the electric machine is not straightforward, given the oscillatory shape of the power transfer. High torques and low speed are in fact common in wave energy field. For example in this application the incoming waves period is equal to the oscillations of the gyroscopic frame. In particular the PTO load specifications for the two gyroscopic units solution consist of a maximum torque of 70 kNm and a maximum speed of 20 rpm. A gearbox is needed in order to remain in the electrical commercial products context. A 1:10 ratio gearbox by DESCH is mounted for reducing torque and multiplying speed for the generator side.

A Permanent Magnet Synchronous Torque Motor is chosen as generator. It is supplied by SIEMENS, being part of the SIMOTICS series and 1FW3 family. This is operated by a SINAMICS S120, 310A, power electronic module. The Control System is deeply presented in the next Chapter 5.

In Table 4.6 the properties of the generator are presented and in Figure 4.17 a picture of the complete PTO during tests in A.R.I.S. is shown. The gearbox in red is positioned onto the blue main structure. On the left side is connected to the main precession shaft while on the right side the electric machine is installed.

Table 4.6 Generator, SIEMENS 1FW3285-2E.

Properties group	Quantity	Unit	Value
Mechanics	Rated Speed	[rpm]	250
	Rated Torque	[Nm]	4950
	Maximum Speed	[rpm]	440
	Maximum Torque	[Nm]	8150
Electrics	Rated Current	[A]	245
	Maximum Current	[A]	435
	Rated Power	[kW]	130
Geometry	Main body longitudinal length	[mm]	835
	External diameter	[mm]	555
Mass	Mass	[kg]	920
	Momentum of Inertia of the rotor	[kg m ²]	6.02

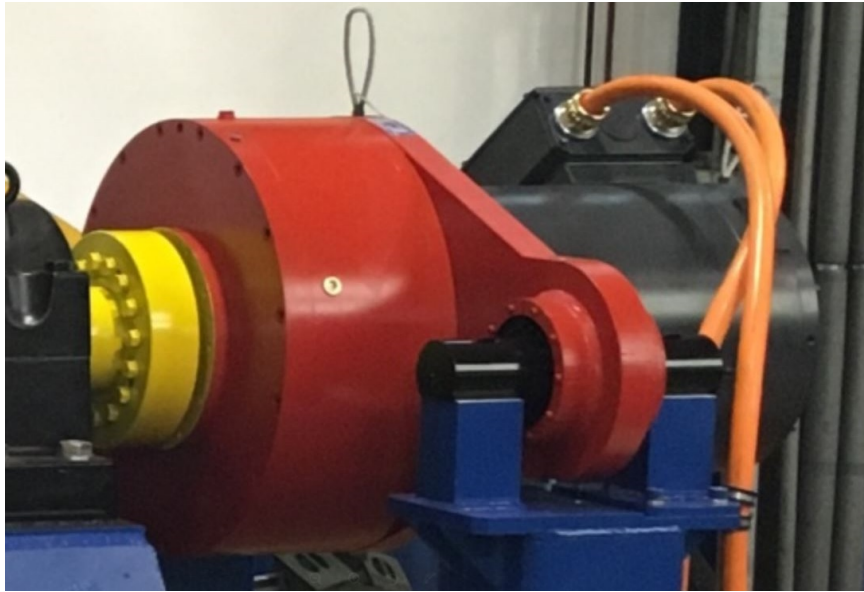


Figure 4.17 The PTO: setup of the first unit in A.R.I.S.

4.6 The Electric System

The electric system is able to smooth the oscillating power coming from the gyroscope into a more continuous electric power flux to be delivered to the grid. The whole system is based on an internal 600V Direct Current (DC) BUS. Some branches with different aims are linked to this main electric power carrier. A conceptual scheme is presented in Figure 4.18, where the DC BUS is at the top.

Starting from the power input, the first branch on the right is that of the PTO. This component converts the mechanical power coming from the precession shaft into an oscillating electric power flux. Its power electronics turns the Alternate Current (AC) electric power coming from the generator into a DC shape and then throws it into the DC BUS. This is the power input for the whole system.

The fundamental function of smoothing the cyclical peaks of power adsorption is realised by the branch with the block of Ultra Capacitors (UC). A series of 5 Maxwell UC with nominal working voltage of 125 V and a capacity of 63F each is used. In this way there is no need of a DC/DC converter changing the voltage for the interface with the BUS.

Also the main internal power consumption sources take the electricity from the DC BUS. The first electric user is the flywheel drive, already introduced in previous section 4.4. Others users are supplied by a DC/AC converter, namely a SINAMICS

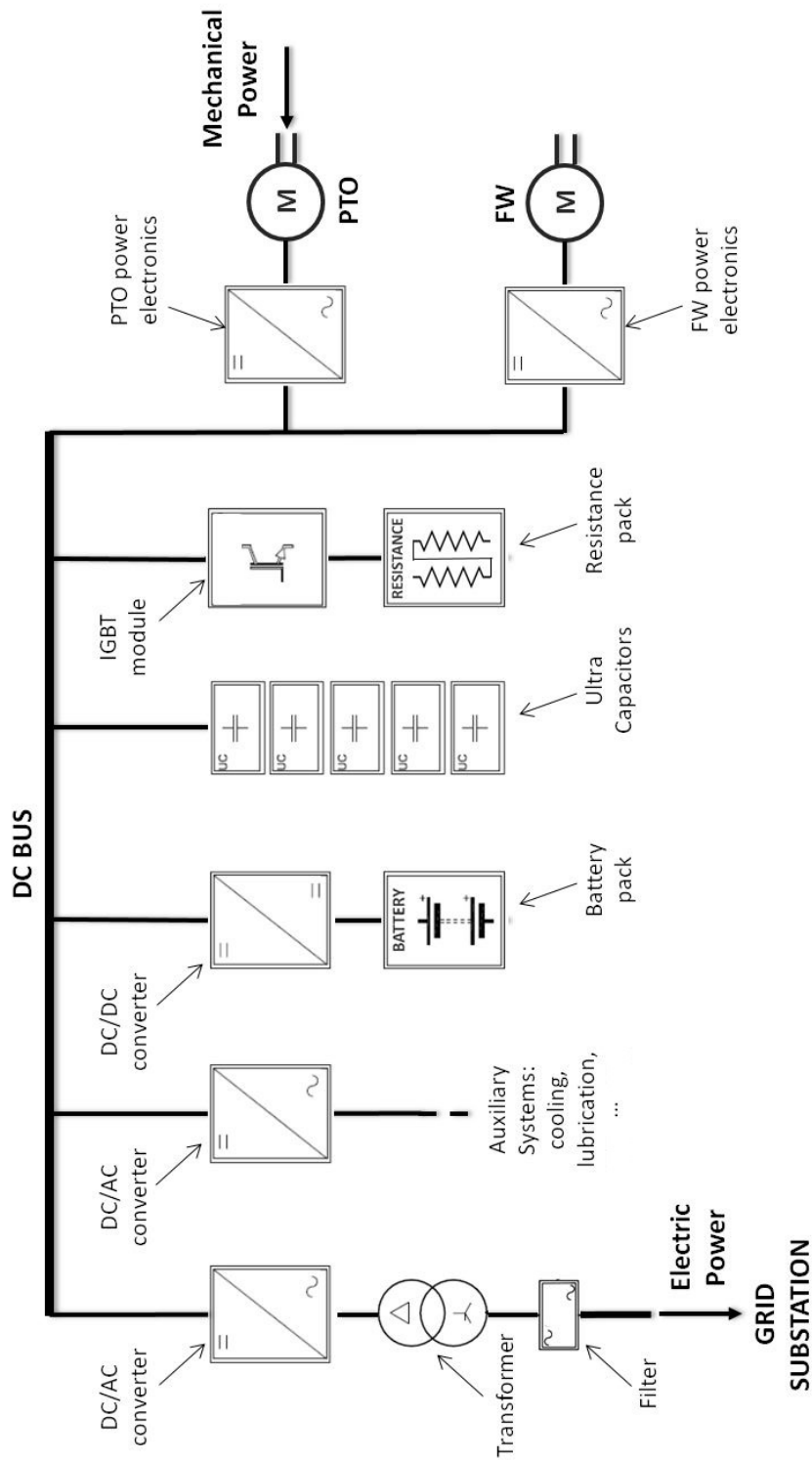


Figure 4.18 The electric system: concept scheme.

S120 45 A module. It receives as input the BUS 600V and gives as output 3AC 400V electric power. A 400V-20kVA transformer by Tenna is used for conditioning with a SINAMICS S120 Basic Line Filter 36 kW filter in series. Some important auxiliary systems onboard, e.g. cooling system, the lubricating system and other minor utilities are supplied with this chain.

A bidirectional DC/DC converter interfaces the DC BUS with the storage onboard. The installed electrical capacity is made of a group of 40 batteries with 12V rated voltage and 100Ah capacity. They are connected in series in order to reach a voltage of 480V. The model is 12 FLB 250 by FIAMM. The code of the converter used is MSc 200A DCDC 700DE. During production mode, its task is to keep the voltage of the DC BUS constant, working with a closed loop proportional controller. An onboard capacity is useful for the functioning in island mode or for safety reasons, when the connection to the grid is interrupted and the system needs to be operated. Moreover all the SCADA and electronics 24V users onboard are connected to the batteries for the supply.

The ISWEC is able to function in two different modes: the island mode and the grid connected mode. The first experimental campaign in 2015 was completely done in the non connected island mode. The start-up of the device and the acceleration of the flywheel unit was done completely thanks to the storage just described.

The power generated during these tests was firstly used for recharging the batteries and then dissipated on resistances. This was possible thanks to a branch whose objective is to control the increase of the DC BUS voltage. An IGBT module checks the DC BUS voltage. If it is higher than some pre-defined thresholds, it links the resistances to the BUS, and the power is dissipated via Joule losses. The IGBT module has been made by Sirius Electronic Systems s.r.l. in collaboration with POLITO and Wave for Energy s.r.l. The resistances pack is represented by 2 Masterwatt 50kW electrical heaters. These are mono-phase DC heaters for sea water, with a rated voltage of 680V.

The last elements to be described are part of the branch of the grid interface. A DC/AC converter works for keeping the voltage of the DC BUS constant, thus drawing power from the DC BUS power and converting it into 900 V AC. It is a SIEMENS SINAMICS Motor Module, the 6SL3325, able to transform the DC 600 V electric power into AC 400 V. Its rated current is 310A and its rated power is 160kW. After a transformer is interposed with galvanic insulation purposes and in order to raise the voltage from AC 400V up to AC 900V. The rated power of this component is 100kVA, thus since this is the last component before the grid, this value also represents the

maximum continuous electric power that can be given by the ISWEC device. A filter is installed on the line in order to improve the quality of the electric power transfer up to the onshore substation.

Some images of the components of the system are presented in Figure 4.19.



Electric Cabinets: DC BUS



Battery Pack



Ultra Capacitors



Electric Resistances, sea water heat exchangers



Electric cabinet. Ultra Capacitors, operator panel and emergency red button, DC/DC converter and a manual switch.

Figure 4.19 The electric system: pictures of components during the SETUP.

4.7 The Cooling System

The cooling system for the ISWEC is a fundamental element, given the high power transfers involved and the relevant heat generated due to friction or Joule effect. Its main objective is to transfer the heat generated inside the device outside to the sea water. In Figure 4.20 a general scheme is presented. There are three main loops with different purposes: the water loop, the glycoled water loop and the lubricant loop. The first loop to be described is the lubricant loop, the inner one. It is composed by two part: one inside the gyroscope vacuum chamber, the other outside. The first has already been described in the gyroscope section (Section 4.4). Briefly, here the fluid vector is lubricant oil, that is pumped starting from the oil reservoir (OL) by two circulating pumps, redundant for safety reasons. The oil then goes into the chamber through the rotating hydraulic joint. It reaches four bearings units, the two radial (RB1,RB2) and the two thrust bearings (TB1,TB2). The oil is then drained and pumped away by a gear oil pump (OP). It passes again through the joint and goes into the oil/glycoled water heat exchanger (HE). After being cooled, the oil starts again the cycle. The second loop to be introduced is the glycoled water loop, the most complex. This closed loop has the responsibility both of re-grigorate the hot oil coming back from the bearings both to cool all the power electronics and all the electric systems. Starting from the glycoled water reservoir (GR), the fluid is pumped by two circulating pumps (CP) and sent to the sea water/glycoled water heat exchanger (HE). After its temperature is lowered, the fluid is sent to two different lines. The first is to the heat exchanger (HE) with the hot oil. From there it is returned to the reservoir. The other line is dedicated to the power electronics. It comprehend a part inside the gyroscope chamber for cooling the flywheel motor (M) and the oil pumps (PM). The water thus has to go through the hydraulic joint. The other line brings the fluid to exchange with the Power Take Off generator and the whole electric panel. The glycoled water is then sent to its committed reservoir. As last loop, the water loop is described. It is the loop that brings the heat outside the device, beyond the hull walls. It is an open loop, since the cooling fluid is the sea water, sucked by two circulating pumps (CP) for safety redundancy reasons. The sea water goes both directly to the resistances electrical heaters (EH), both to the sea water/glycoled water heat exchanger (HE). Once the water is heated, it is thrown into the sea. A picture of the final cooling system group is presented in Figure 4.21.

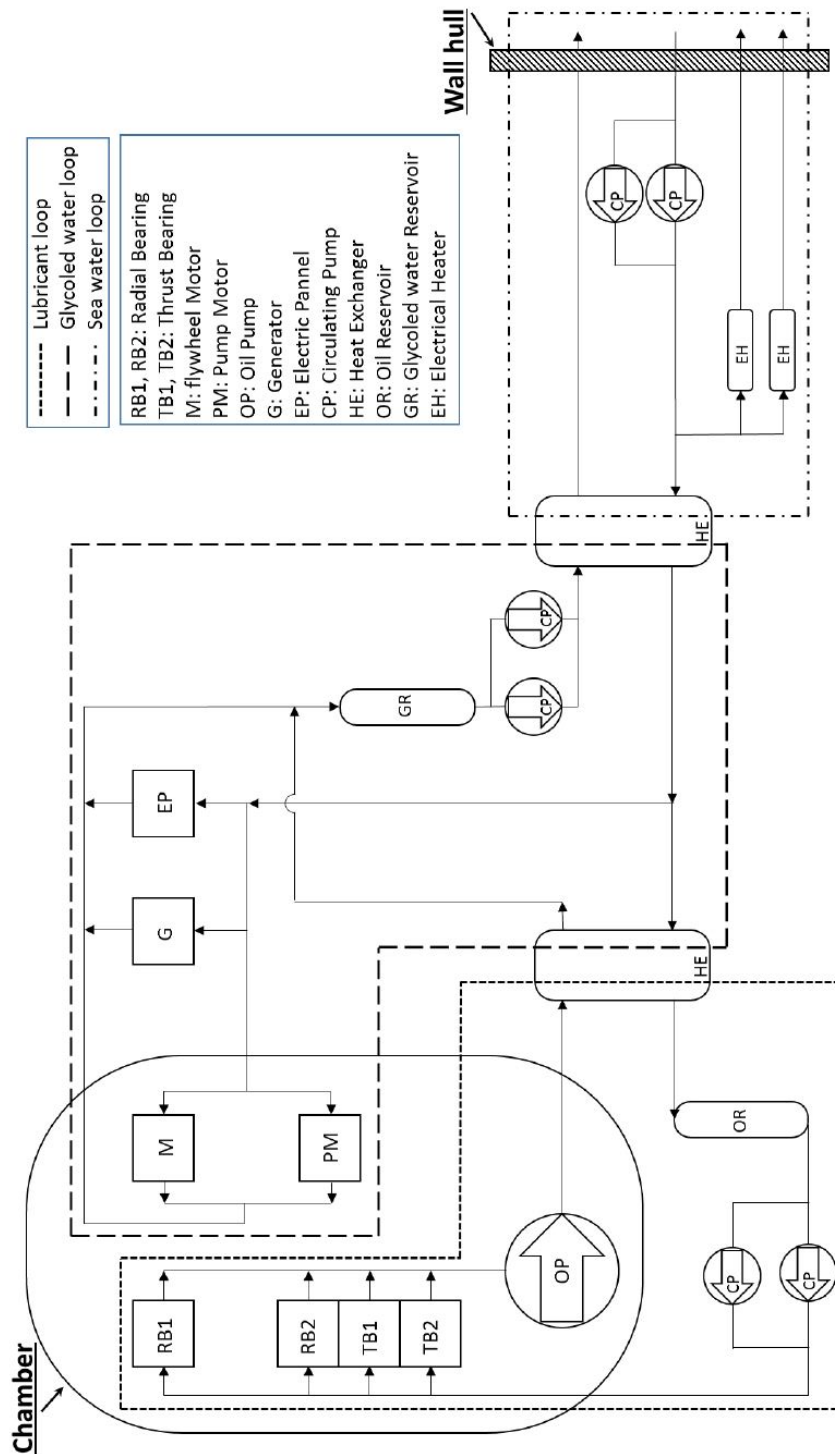


Figure 4.20 The cooling system: scheme.



Figure 4.21 The cooling system: the group in A.R.I.S.

Chapter 5

The SCADA system

5.1 Introduction

The Supervisory Control And Data Acquisition (SCADA) system is the responsible of the overall management of the device and it incorporates all the Human Machine Interface (HMI) components. Objective of this chapter is to introduce the key aspects of the architecture, taking into account the intellectual and industrial properties of Wave for Energy srl.

The design and development of this subsystem of the ISWEC has seen a deep involvement of the candidate, and he has in particular had an important role in the higher level controller. His main activities regarded the design, coding and testing of the PTO set point generation architectures, the development of the system state machine with all its auxiliary automatic strategies, the management of the data communications between the different part of the software, the data acquisition system and the human-machine interface. During this development he has been supervised by the responsible of the SCADA architecture for Wave for Energy srl, Eng. Vincenzo Orlando. The candidate was fully responsible for everything regarding the PTO torque set point generation.

5.2 The SCADA architecture

The overall SCADA architecture functional scheme is illustrated in Figure 5.1. At the top level of the system there is the PLC Master ET 200S. It is the responsible of the inner PROFIBUS data network to which all the different users are connected. The network links the PTO and flywheel CU320 power electronics control units, the cooling system PLC, the compactRIO control system and HMI head hardware, the

components of the electric system described in section 4.6 and the PLC master itself. A customized hardware, the DC BUS manager, is controlled via cRIO and it is interfaced with the Ultra Capacitors via a CAN network. It is the responsible of sequentially activating the electric resistances onboard in case the BUS voltage overcomes some increasing designed thresholds. The cRIO is also directly connected with a number of sensors via RS232 serial communications. Two Inertial Measurements Units (IMU) give information about the floater kinematics, measuring both angular acceleration, velocity and position, both linear accelerations. A Global Positioning System (GPS) sensor provides the absolute position of the device. An UMTS router allows the interface of the cRIO to the internet, ensuring the remote access to the system. In case of a cRIO shutdown, the PLC Master takes the control of the whole structure, leading the system in a safety operation state. In the top right corner of the Figure the blocks are made of discontinuous lines. This indicates that during the first experimental campaign in 2015 this part of the system was not yet installed. Something that must pointed out is that almost all the components are robust off-the-shelf solutions, with standard industrial level reliability. This actually resulted in a very stable system, with very few failures and all due to customized or low-cost components under test.

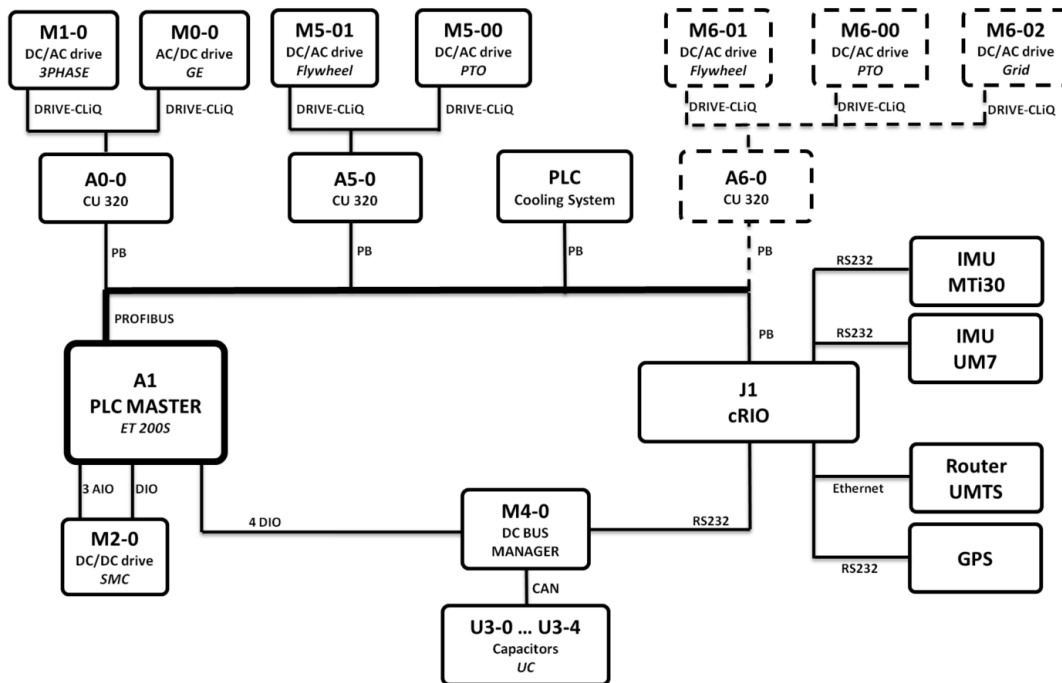


Figure 5.1 Overall SCADA system architecture.

The power generation control hardware is illustrated in Figure 5.2. The information flow is described. The control unit of the PTO electric motor provides the ε and $\dot{\varepsilon}$

measures to the PLC Master. It transmits them to the cRIO always via PROFIBUS. The cRIO elaborates the feedback and returns a T_E torque set value. The PLC Master receives and feed-forwards it to the control unit. The PROFIBUS has a refresh rate of 200 Hz. The cRIO uses the forecasts received from the internet to computing the flywheel speed set.

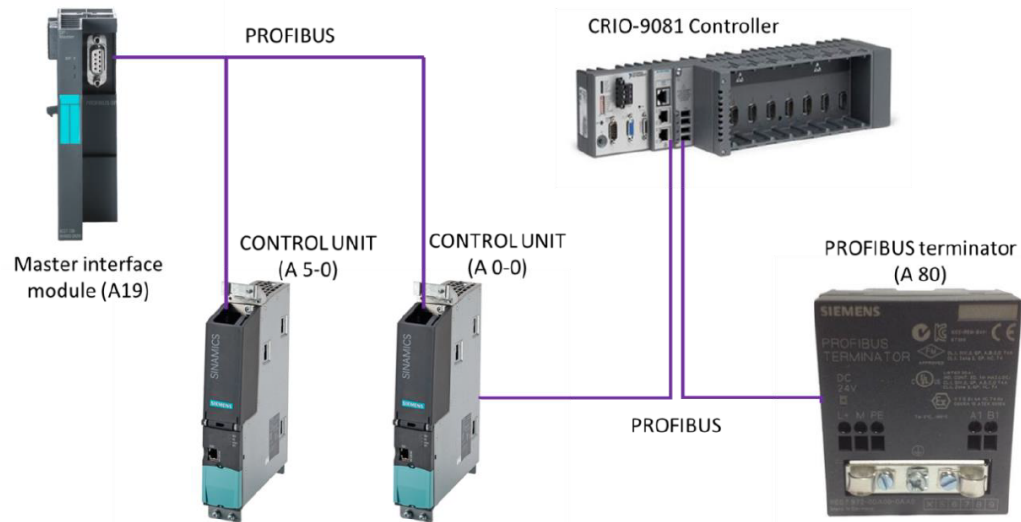


Figure 5.2 Control Hardware. Components directly linked to the power conversion.

The hardware chosen for generating and implementing the control strategies is the National Instrument compactRIO 9081. This has an high-performance multi core system, a built-in VGA display output for an integrated user interface, and a dedicated operating system, the LabVIEW Real-Time OS. It is designed to perform the advanced processing tasks required by complex applications such as rapid control prototyping. It provides high flexibility and performances, suitable for an in-development application as it is ISWEC at this stage. The LabVIEW Real-Time OS is characterized by the possibility to have deterministic execution and reliability in continuous operation environments.

5.3 State Machine and Automatic Operations

One of the main specifications in the development of the device was to require its automatic management. In order to achieve this objective all the possible operational modes has to be identified. The overall software is run onto the cRIO and has been coded in LabVIEW environment. An user interface (UI) is run on a separate PC accessing via LAN network to the cRIO real time platform.

In Figure 5.3 the ISWEC state machine is presented. The first state is the *INIT*. The cRIO sends the start message to the PLC Master that initiates the power up of all the drivers and the cooling system. In this phase the DC BUS voltage is increased up to the nominal working value. The electric motors are not connected to the power source. When the human user triggers the *FIRST START* case with a digital command, the PTO electric motor is controlled to position the angular gyroscope frame in order to obtain a vertical flywheel axis condition. The system is then in the *WAIT* state, ready to be operative. There are two main operating modes: the power production loop (*WAIT,CONTROL,SAFETY*) and the *TESTS* state. The possibility of testing the device has been planned, both for dry tests of the electro-mechanical system both for doing tests after the device is launched. The other working modality is the power generation. This is constituted by three different states and it is a completely automatic system. The control case is the one in which the system is controlled with the power generation strategies proposed in next Chapter 6. When some dangerous conditions for the mechanical or electrical systems are identified, the machine automatically goes into the *SAFETY* state. The procedure is illustrated in section 5.5. After desired conditions are satisfied, the system returns the flywheel axis vertical. After this it passes to *CONTROL* and thus starts again the production phase.

From *TESTS,WAIT* and *CONTROL* it is possible to move directly to the *CLOSE* state, in which the procedure of the controlled shutdown is accomplished.

The human operator has the possibility to bypass the automatic state machine and to force the system into any desired state.

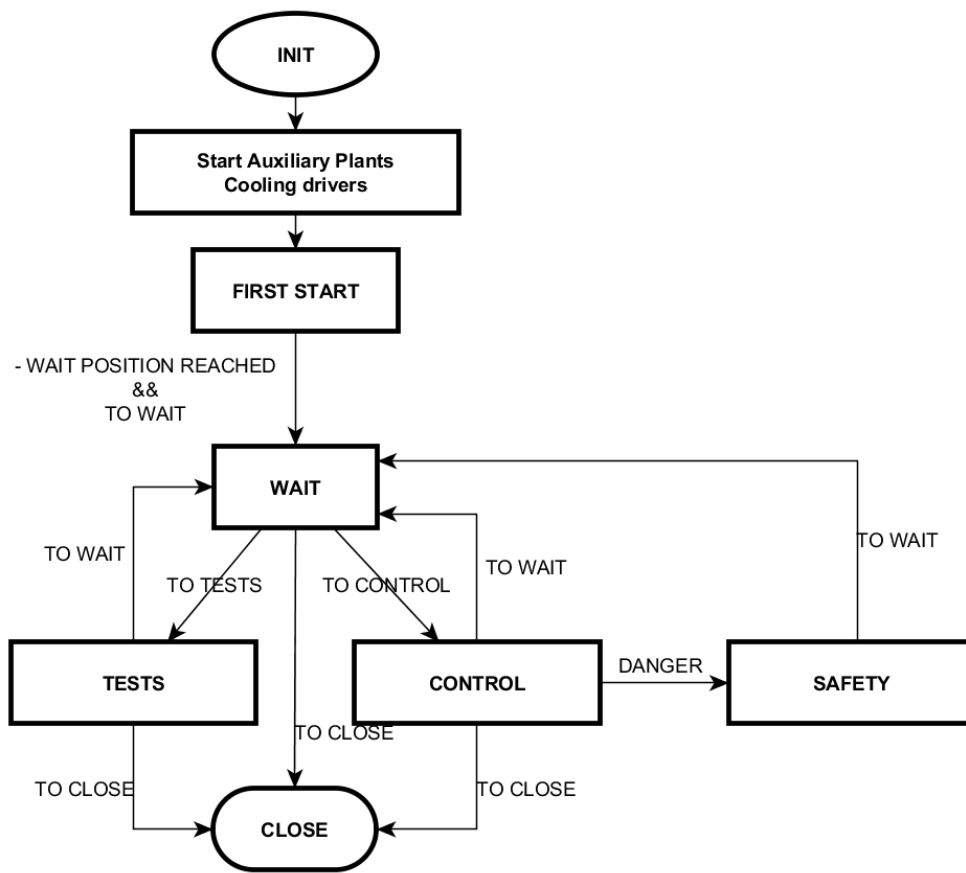


Figure 5.3 The ISWEC state machine.

5.4 PTO electric motor control

Two different and complementary typologies of regulators are controlling the internal gyroscope frame axis of the ISWEC: the angular position control loop and the power adsorption strategy. These different controls acts in different times, depending on the state in which the device is operating.

A position control loop (Figure 5.4) is useful for auxiliary states in which the ε shaft has to be brought at desired angles: $0deg$ for starting the production mode or $90deg$ for the safety case. This control loop consists of a feedback proportional term working on the position error and a derivative/pure damping component proportional to the gyroscope frame axis speed. The second derivative term, with the set-point weighting to zero, has been applied following the application proposed by [3]. The internal precession shaft has in fact a negligible damping and it can be considered a completely, un-damped, inertial system. Weighting to zero the set-point part of the derivative component, the damping action of the system is thus realized by the controller. In this way it is easier to work with higher values of the proportional gain. Another particularity of this system is that during the normal operations in sea, when the flywheel is spinning, the torques exerted by the gyroscopic torques are higher than the maximum available PTO torque. Multiple rate limiter and saturations are introduced in order to avoid the rising of any kind of unstable situation.

The second objective of this controller is the power generation, deeply described in chapter 6. Different strategies aiming to harvest the maximum power from the waves have been numerically studied and will be implemented during the next experimental campaigns.

The transition between the two has been managed using different bump-less strategies in order to avoid undesired torque discontinuities. Both in Simulink and LabVIEW programming environments the provided PID blocks can manage the selected strategies.

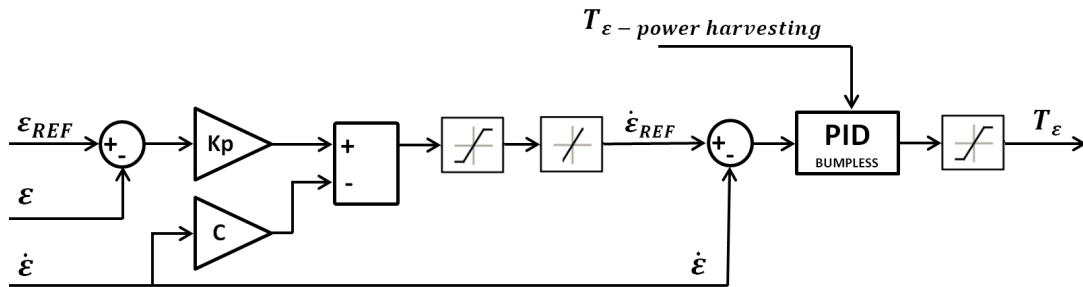


Figure 5.4 Auxiliary position control loop.

5.5 Automatic Management

This section is about the automatic management of the operations during the power production mode and the safety case. The motivations for the safety state and the operations conducted are described.

In the flow diagram of Figure 5.5 the procedures are described as long as the conditions for the transition from one state to the other.

The STATE 0 of the diagram is the *CONTROL* state. The device is harvesting power in the defined normal conditions. A check over the PTO speed and the power is continuously performed, there are in fact two different possible causes of hazard. The first one is related to the PTO speed. If it reaches values higher than the maximum allowed values by the electric drive, in this case 25 rpm , the PTO goes in fault state. The damping action thus is not given to the gyroscope frame shaft. Since the flywheel is spinning this is a very dangerous situation both for the electric and for the mechanical systems. The second hazardous situation happens when the PTO speed is greater than a second lower value, 20 rpm , and the power overcomes a safety threshold. If at least one of these conditions happens the state machine goes into the STATE 1, the *SAFETY*. In this case the position control takes the place of the power generation regulating law. The gyroscope frame ε is brought to the nearest $\pm 90\text{ deg}$ angle. In Figure 5.6 the initial and final positions of the gyroscope frame shaft are represented. After the gyroscope arrives in position a time counter starts, when TIME 1 passes it is returned to the vertical position, the *WAIT* state. After a short period TIME 2 is elapsed, the system returns in the *CONTROL* mode.

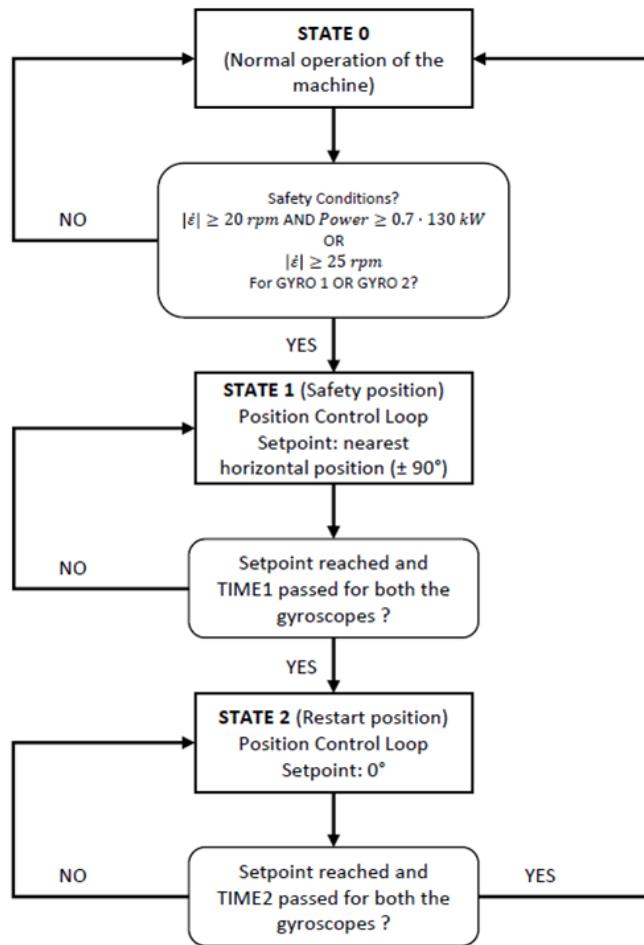


Figure 5.5 Automatic power production operations and safety state. Flow diagram.

PTO internal axis - simplified dynamics:

$$T_\epsilon = I\ddot{\epsilon} + J\dot{\phi}\delta \cos \epsilon$$



$\epsilon = 0^\circ$

Torque Exchange



$\epsilon = 90^\circ$

No Torque Exchange

Figure 5.6 ISWEC Full Scale device. Automatic safety procedure.

5.6 Human Machine Interface

The SCADA communication system communicates with the onshore infrastructure via an internet communication. The monitoring and supervision of the whole device can be performed with a dedicated LabVIEW software. In Figure 5.7 the flows of information is showed. Starting from the right, the interface with sensors and other lower level control hardware is realised with different types of data transmission methods, depending to the different hardwares involved. The cRIO embedded FPGA performs part of these interfacing tasks. Once the information are translated, they are sent to some upper level interpretation and conversion loops: the "MTi" loop receives and conditions the data coming from the Xsens IMU, the "9870 COMMUNICATIONS" the data from the other serial hardware, the UM7 IMU, a GPS and the DC BUS resistances controller hardware. The "PB I/O - COMMS" translates the data received from the PROFIBUS network. All these variables values are updated and written/read in the CVT/CCC Server. These are methods developed in the National Instrument environment for building a TCP/IP client/server communication. All this software is installed in the 9081 cRIO platform. This is then connected to a UMTS Router and the it can be accessed from the internet. On a remote computer, a CVT/CCC Client must be installed, in order to receive and visualize the data online. The user can send information and thus control the device via a AMC communication. An AMC server is installed on the remote computer and is transmitting data to an AMC server installed in the cRIO into the ISWEC. Thus the loop can be closed. Of course, all this flow is not in real time, and the control actions that the user can actuate are parameters update and triggering/digital commands. In order the reduce the data trasmitted via internet, the sample frequency of the visualization is very low, 1 Hz. In this way data communication traffic is reduced.

An image of the User Interface that can be used on a remote computer for monitoring and controlling the ISWEC is shown in Figure 5.8.

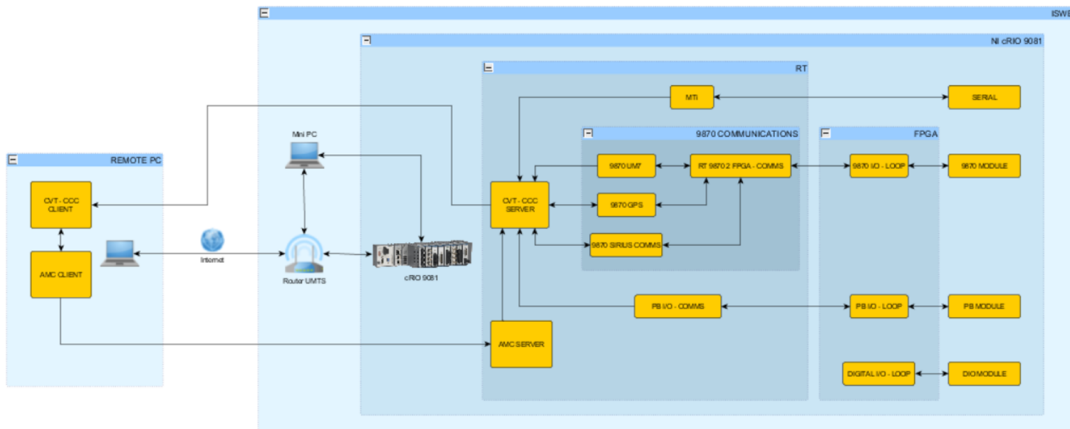


Figure 5.7 SCADA system. Information and DATA flow diagram.

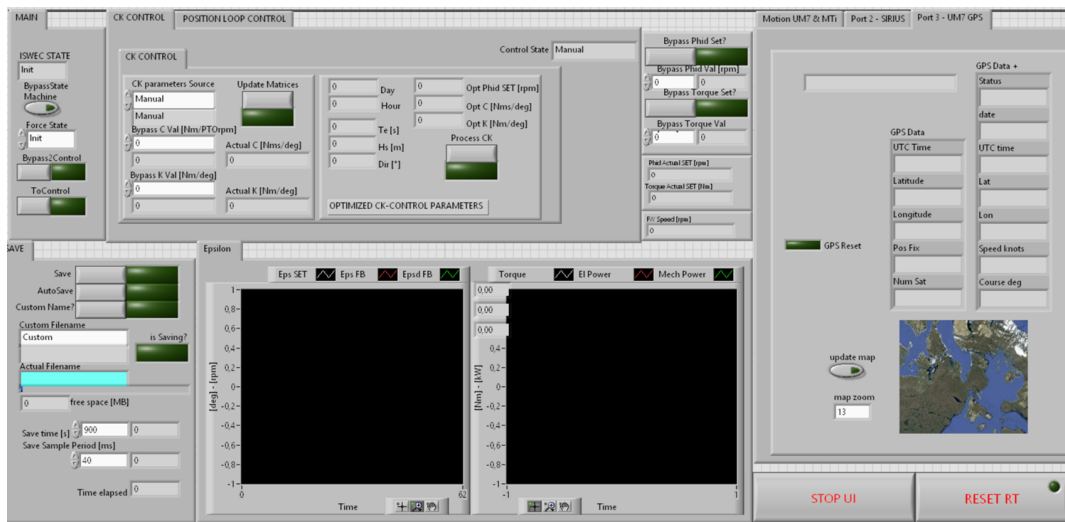


Figure 5.8 SCADA system. User Interface.

5.7 Safety Control

A static nonlinear term is added both to the positioner and the power generating control architectures in order to avoid high PTO shaft speeds. Due to the irregular nature of the wave, it happens that the floater and thus the internal precession axis are over loaded, this causes high PTO speeds and can result in unexpected overcoming of electrical or mechanical limits of the electrical machine.

This term consists in a static additive contribution acting after the power generation/positioner controller has already computed its own output. The output of the controller is saturated at a maximum value. The safety nonlinear term is then added and saturated again, before being given as input to the PTO. The scheme is shown in Figure 5.9. The functioning of this architecture can be better explained looking at the

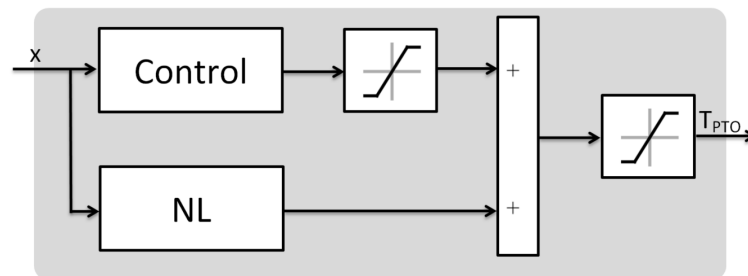


Figure 5.9 Safety control. The control architecture.

shape of the nonlinear term function of which an example can be seen in Figure 5.10. For values of the PTO speed in range I, the term is equal to zero, and thus the control input is the same as the one of the power generation/positioner control. For PTO speed values in range II, the torque action increases linearly, passing from zero to twice the maximum torque allowed by the PTO saturation. In range III, the torque is equal to two times the maximum allowed. This means that, as is clear from Figure 5.9, since the power generation/positioner torque has already been saturated, starting from this PTO speed on, even in the worst case possible, the action given by the PTO is always the maximum possible damping action against the motion. An analytic description

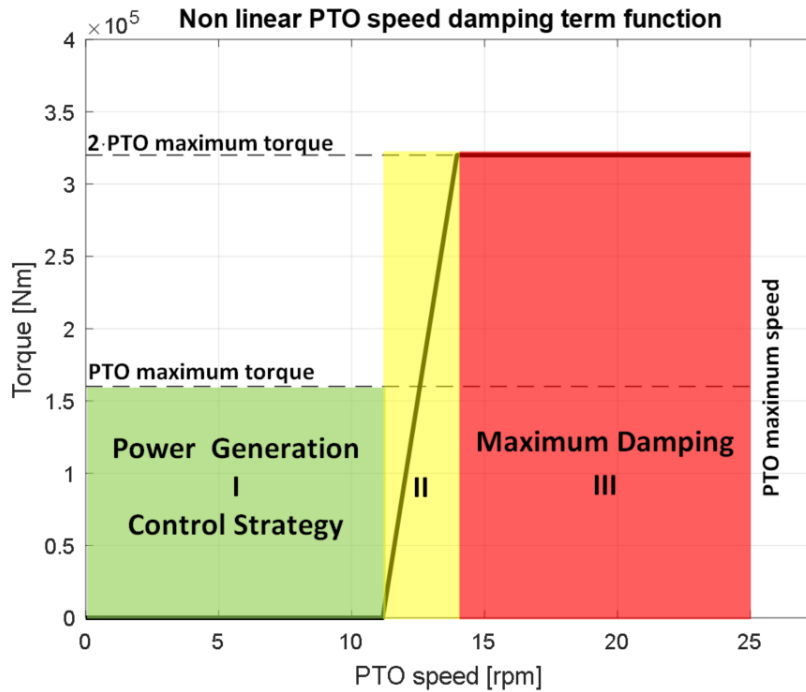


Figure 5.10 Safety control. The static nonlinear term in function of PTO speed.

can be given with a piecewise definition of T_{PTO} :

$$T_{NL}^* = \begin{cases} 0, & \dot{\varepsilon} < \dot{\varepsilon}_{lin} \\ \frac{2T_{PTOmax}}{\dot{\varepsilon}_{damp} - \dot{\varepsilon}_{lin}} (\dot{\varepsilon} - \dot{\varepsilon}_{lin}), & \dot{\varepsilon}_{lin} \leq \dot{\varepsilon} \leq \dot{\varepsilon}_{damp} \\ 2T_{PTOmax}, & \dot{\varepsilon} > \dot{\varepsilon}_{damp} \end{cases} \quad (5.1)$$

Then the torque is elaborated as a damping term: with an opposite sign respect to PTO speed.

$$T_{NL} = -sgn(\dot{\varepsilon}) T_{NL}^* \quad (5.2)$$

Threshold values $\dot{\varepsilon}_{damp}$ and $\dot{\varepsilon}_{lin}$ are computed in order to avoid system oscillations with amplitudes greater than a desired value ε_{max} . In this way the system is robust against wave load peaks.

$$\dot{\varepsilon}_{damp} = \frac{\varepsilon_{max}}{T_e} \quad (5.3)$$

The threshold for linear behavior is heuristically evaluated at 80% of the pure damping value:

$$\dot{\epsilon}_{lin} = 0.8 \dot{\epsilon}_{damp} \quad (5.4)$$

5.8 Forecasts

The use of sea state forecasts is fundamental at this development level. The service for the ISWEC installation in Pantelleria is given by the ENEA-UTMEA italian agency. In Figure 5.11 an example of the output obtained by the analysis is showed. Every day the software automatically download from a FTP server the forecasts for the five following days, with an hour of time interval. For each time step an estimation of the significant wave height, the wave direction and the energy period are provided. These parameters are input for the lookup table with the control parameters scheduled in function of the incoming waves. The development of wave state identification and

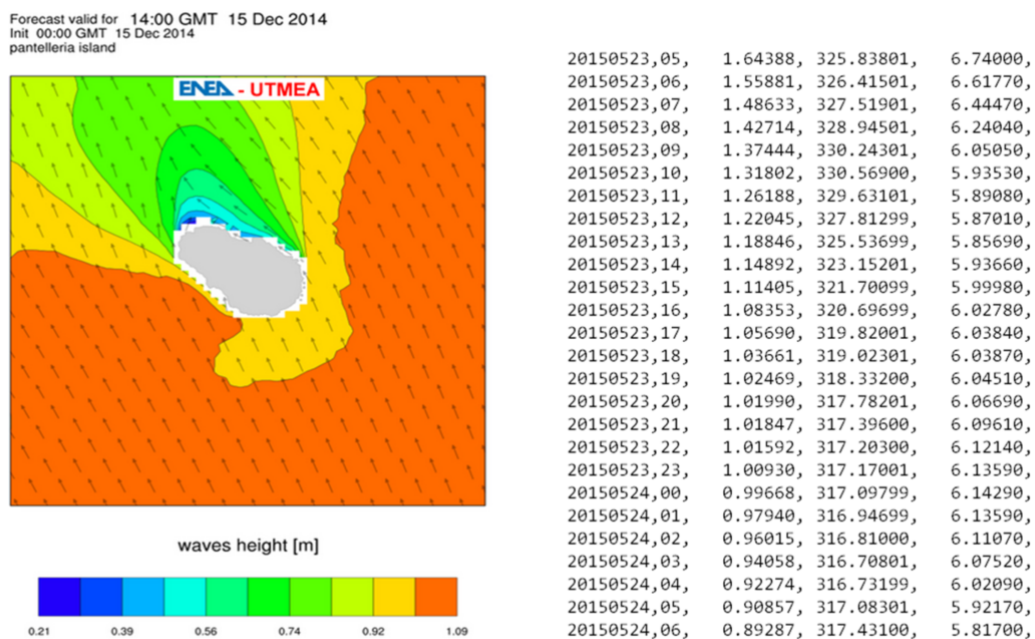


Figure 5.11 Forecasts. An example of study applied to Pantelleria and the received tabulated data.

prediction strategies is one of the main research topics, for the sake of simplification and cost reduction motivations. The effect of the use of forecasts on the regulation of the ISWEC are explored in [13].

Chapter 6

Power Absorption Control

6.1 Introduction

Main aim of this chapter is to present the studies carried out on the regulation control law strategies of the ISWEC device. This is a synthesis of the work performed in last few years by the group and by the candidate. More detailed information can be found in the elaborated literature. References can be found in [19, 14, 15, 103, 13, 100]. In particular the objective is to find the relationship that links some measured states of the device, for example the gyro frame axis position and speed, or the floater kinematics, to the torque exerted by the PTO electric motor on the internal gyro frame shaft. Essentially, the output of the control law is to compute the "best" set torque to be given to the PTO instant for instant. Also the concept of "best" torque is analyzed.

6.1.1 Different Time Levels

The regulator strategies can be categorized differentiating the time scale of their actions. In this way, three main levels can be identified:

- **multihour**. An algorithm takes care of analyzing both historic data and hourly and hourly forecasts in order to decide whether to suspend the power production and decelerate the flywheel or to continue to keep it spinning, thus enabling the power absorption. In the version that went into the sea, it was mainly based upon forecast data, received daily as explained in previous section 5.8. Starting from the expected net power per each incoming hourly defined sea state, the

system evaluates if the overall productivity is positive or negative, taking into account the transient period of decelerating and accelerating the flywheel.

- **hour.** A software hourly reads the foreseen wave energy period and significant height and then gives as output the parameter for the online control law by interpolating over maps. These are tables of optimal parameters in function of the incoming sea state, computed offline by the use of numerical model [15] and some optimization strategies. These strategies consider the productivity, the expected bearings life, the mechanical loads and vibrations over the structure.
- **online.** The online architecture is the one that elaborates the feedback measured by sensors at the hardware working sample frequency and computes the torque reference for the internal PTO electric motor. These are the subject of the current chapter. Other online control software can include the observation and identification of spectral and wave parameters. The main parameter of interest is the incoming wave frequency.

All the possible online strategies have to deal with the constant flywheel speed during the operations in each single hour. So, the first parameter of each control strategy is the flywheel speed. As already mentioned in Chapter 2, the gyroscope coupling terms are linearly proportional to the spinning rate $\dot{\phi}$, the action torque on the internal precession axis is in fact $J\dot{\phi}\dot{\delta}\cos(\varepsilon)$ and the reaction torque over the hull is $J\dot{\phi}\dot{\varepsilon}\cos(\varepsilon)$. Thus, without any precession axis control, with the flywheel in rotation $\dot{\phi} \neq 0$, the system has a stable equilibrium point when the flywheel axis ϕ is horizontal. This angle corresponds to $\varepsilon = \pi/2$, which means that the gyroscope coupling terms in both equations are equal to zero: the PTO is not able to exchange any torque with the floater pitch degree of freedom δ . All the strategies thus also have the responsibility to maintain the flywheel oscillating axis around the vertical direction. This fact has strong implications from a technological point of view, since the power take off system must be able to deal with a reactive power flux.

6.1.2 Online control - Specifications

In literature it is plenty of different control strategies (section 6.4) Seen the applied approach of this thesis and the quite uncommon device analyzed, new online control strategies have been realized. The main specifications for their design are hereafter summarized:

- *Maximization of the adsorbed energy.* First objective is of course the maximization of the net adsorbed energy. During the research phase anyway, can be extremely important to work also with the gross power. In fact, if a control strategy gives relevant results in the gross power production but it is limited by losses coming from a particular subsystem, a technology re-engineering process can be evaluated in order to analyze its improvement or change .
- *Electro-Mechanical physical constraints.* Since the control torque is input of a real system, it must deal with all the limitations present in the application. The PTO electric machine main constraints are torque, speed and power saturations. From a mechanical point of view the constraints are related to power losses or components life. The mechanical losses are mainly due to the action of friction of the flywheel bearings. Consequently the components that have more restrictive requirements about life are the flywheel radial bearings.
- *Smooth torque application.* An important point is to avoid discontinuous applications of torque over the PTO axis. In order to preserve the internal PTO shaft and the gyroscope frame. Vibrations and mechanical stresses have to be limited.
- *Robustness to sea state changes.* Ideally the control architecture must be able to adapt itself and to maximize the power adsorption even if the actual sea state is different to the expected one. This property is difficult to be obtained and it is currently an open point of research in the wave power community. In the following some strategies with a more robust behavior are presented, while productivity is not much affected.
- *Robustness to model uncertainties.* As it is common experience, the hydrodynamic modeling of a WEC is an extremely challenging task. Since all the control strategies go through an offline optimization using numerical models, it can be easily understood that the table where the optimized control parameters are scheduled in function of the sea states can be far from being optimal. Furthermore this property becomes critical when model-based strategies are used. Robustness property is then of high interest and if possible must be evaluated.
- *Easy to tune.* As a result of the two previous specification, a control strategy must have the minimum possible number of control parameters. The smaller is this number the smaller is the quantity of tests to be carried out in order to find

the optimal value. Moreover, the tuning operations into the sea are extremely time consuming.

- *Simplicity.* As a last final remark, a control strategy must be simple. It must be implemented on the device with the available hardware. It must be feasible, low-computational time is required. The use of different feedback measures also can complicate the technological implementation. For example the strategies using the floater pitch value and its rate create the problem of having a stable and completely reliable measure. For example this problem can be solved using redundancy technology and doubling the IMU sensor, at the expenses of the overall system simplicity.

6.1.3 Online control - Classification

In this subsection a classification of the ISWEC online control strategies is presented. The first main distinction is between oscillating and continuous rotation controls. The oscillating controls are those that make the internal PTO precession axis to oscillate around the vertical direction. This oscillations are synchronized with those of the incoming wave. A continuous rotation control keep the PTO precession axis in continuous rotation, and the single revolution happens in a time equal to the incoming wave period. Another differentiation is based on the design and synthesis techniques point of view. Some strategies are model based, so they need a model, in this case linear, of the overall dynamic system. Other are model-less, so they do not require any physics description to be implemented. A last classification of the developed strategy is presented in function of the objective of the control action: resonance conditions, a set point tracking approach or direct power optimization via optimal control are used. In figure 6.1 the control strategies studied and implemented are organized in a table. The first control to be studied is the proportional-derivative control (PD). This consists of an impedance matching technique for the linearized system. It is an oscillating control strategy where a stiffness term keep the flywheel axis oscillating around the vertical position while a damping component enables the power extraction.

A position feedback control opportunely scale the measured pitch values and gives the value as a set point for the internal precession axis (ΔREF). In this way a synchronized oscillating control is realized. A problem in choosing the optimal gains to tune the set point arises.

Model Predictive Control (MPC) has been used in order to have better performances

	Model Based	Model - Less
Oscillating	Linear Quadratic Regulator (LQR)	Proportional-Derivative (PD)
	Model Predictive Control (MPC)	Position Control (deltaREF)
Continuous Rotation	Linear Quadratic Integral Control (LQI)	Speed Control (speedREF)

Objective of the controller		
IMPEDANCE MATCHING	SET-POINT TRACKING	DIRECT POWER OPTIM

Figure 6.1 A proposal of control strategies classification.

for the same set point tracking problem as the previous controller. After the analysis and some optimization of the previous controller, the performances are equivalent. For this reason it will not be presented in the following. For more information see [19].

The last oscillating control strategy developed adopted the optimal control theoretical background. In particular linear quadratic regulator has been used (LQR). The cost function gives the opportunity to directly weight the product of the PTO speed and the PTO torque, thus directly optimizing the power adsorption.

For what concern the continuous rotation control, a model-less and a model based control are presented (speedREF). The model less control takes as reference a speed computed starting from the single identified wave period or even a statistical number given by forecasts as the energy period. The problem is thus seen as a set point tracking one.

The model based continuous rotation control uses instead a formulation of the linear quadratic integral control (LQI), giving always as reference the same as above but also enabling the cross weight of the PTO speed and torque, as for the LQR case.

In this chapter these different control architectures are presented. Time domain simulations with the nonlinear model are done and results are analysed.

6.2 Proportional Derivative (PD) Control

The first control strategy used in the design of the device and implemented in the first experimental campaign is the proportional derivative control, hereinafter referred to as "PD". It consists in the sum of two components. A part proportional to the precession angle ε starting from the zero vertical position and a part proportional to the speed $\dot{\varepsilon}$ of the same axis. Using a mechanical similitude this control can be seen as a spring-damper control, where the first is the stiffness component and the second the damping action. In figure 6.2 the simple scheme of the torque set generation is shown.

The stiffness proportional part implies a reactive power flux. The adsorbed active power is extracted by damping the rotation of the precession axis on which the gyroscope frame is mounted. The very few feedback measures required (PTO position and speed) and the simple architecture, make this system stable and robust, avoiding instabilities in case of highly irregular sea states. Even when the system is subjected to energetic sea states and the PTO goes into torque saturation frequently, the system remains stable. The linearity of PD control is extremely useful for being used in the pre-design phase, in the closed loop frequency domain analysis. In this domain it is possible to design and choose the parameters in order to set the internal mechanical system resonance frequency according to the incoming sea state spectra.

This control law drives the internal precession axis with a stable oscillating behavior.

Technical tips

- The control parameters must keep the internal axis oscillations in a range of $[40\ 60]$ deg in order to have higher enough speed on the internal precession axis for the power conversion and for staying in an area in which there is exchange

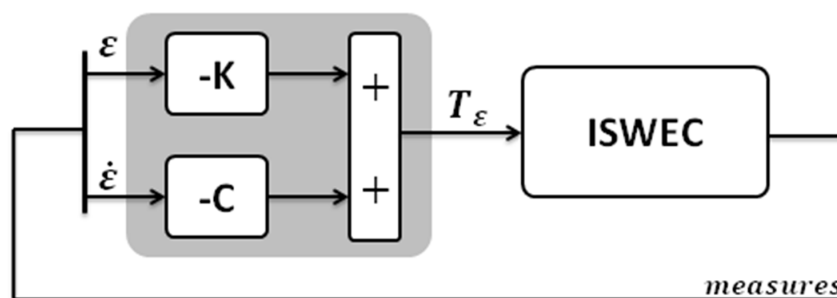


Figure 6.2 Proportional Derivative (PD) control. Simple torque set generation scheme.

of torques between the gyroscope system and the floater. In general, for an oscillating control, the amplitude must be less than 90deg in order to have the gyroscopic torque agreeing with the floater motions.

- When the oscillation crosses the $\pm 180\text{deg}$, an offset of $\mp 180\text{deg}$ is summed to the feedback value, thus the value of the gyroscope frame angle remains into the range $[-180\ 180]\text{deg}$.

Implementation

The hardware implementation of such a strategy is extremely straightforward, since it is a simple feedback law with a couple of gains. It is robust and can work even if all the sensors about the floater motion are offline. It is robust from a technological point of view.

Optimization and Tuning

This control is optimized offline, with the help of numerical simulations. In the version that went into the sea in 2015, a triplet of parameters must be optimized for each sea state: the flywheel speed, the damping and the stiffness parameters. From a perspective of sensitivity on numerical modeling issues, if the model is not particularly good, the parameters are far to be optimal, thus requiring a long tuning phase into the sea. For next experimental campaign, some automatic procedures for parameters selection have been prepared, in order to do this parametric analysis in the least time possible.

6.2.1 Results - Time History Example

An example of time domain simulation of the system working while controlled with a PD control is shown in Figure 6.3. In the top figure the gyroscope frame axis angular position and the floater pitch are plot. The two quantities are synchronized and counter phase. The internal axis has motions of a bigger amplitude. This can also be seen as a sort of gearbox, reducing the torques and increasing the speed with respect to the floater mechanical power. In the second subplot the PTO torque and power are shown. The negative power indicates an adsorption, because the torque given by the electric motor has opposite direction from the precession axis, thus damping its motion. A noticeable quantity of smooth power spent is present, when the PTO is acting as a motor on the internal precession shaft. In the bottom frame, the wave torque over the pitch floater DOF and the pitch angular rate are illustrated. The optimal control theory

of the WECs suggests that they have to be in phase, in order to maximize the power adsorption. With this regulating architecture this property is not guaranteed.

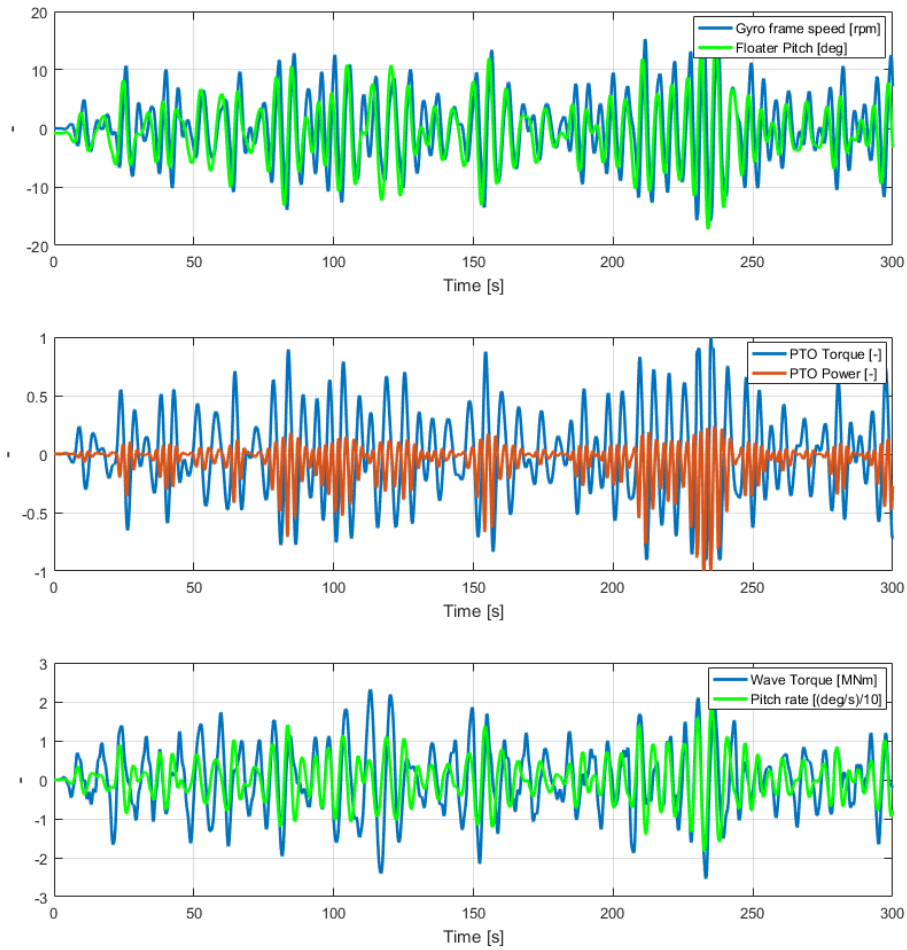


Figure 6.3 PD control. Time history example.

6.3 Model Free strategies

The need for innovative strategies grew in the early stage of the project, when higher reliability, robustness and productivity were searched. Following the specifications presented in section 6.1.2, some new laws were proposed, following numerical and experimental observations of the system behavior. These strategies were in fact elaborated through an approach both analytical and empirical, with a strong applied approach. The idea is to observe the behavior of the system while controlled with proportional-derivative optimized parameters and try to mimic it using a simpler control law. The main concept underlying all the section is the *reduction of the power adsorption maximization problem into a set-point tracking control*. The results obtained are interesting. In the following two control strategies are presented: an oscillating and a continuous rotation control.

6.3.1 Oscillating control

Objective of this feedback position control is to synchronize the pitch, δ , with the gyroscope frame internal precession axis ε . This idea rises from observations of the system while controlled with the proportional-derivative control, in fact to each single oscillation around the pitch DOF corresponds an analogous motion on the internal ε axis, and moreover when this synchronism is lost, the power adsorption is negatively affected and the floater is irregularly damped.

Analytical proof of the objective

The zero-phase between the two oscillations causes a single direction in the power harvesting, from waves to mechanical power. This is sub-optimal for regular waves, but reaches good results comparable with the proportional-derivative control for irregular sea states. The analytic proof of this property is presented. Recalling that the gyroscope frame dynamic equation about the ε axis:

$$T_{\varepsilon PTO} = I_g \ddot{\varepsilon}_{gyro} + J \dot{\phi} \dot{\delta} \quad (6.1)$$

Then, supposing a perfect control action, with a scaling factor equal to 1:

$$\varepsilon_{gyro} = -\delta \quad (6.2)$$

it must be noticed that the sign convention is referred to a particular flywheel spinning direction and for a second gyroscopic group would be opposite ($\dot{\phi}_1 = -\dot{\phi}_2$). The following relationships can be stated:

$$\varepsilon_{gyro} + \delta = 0 \quad \Rightarrow \quad \dot{\varepsilon}_{gyro} + \dot{\delta} = 0 \quad (6.3)$$

Substituting the two last expressions into the precession axis one:

$$T_{\varepsilon PTO} = I_g \ddot{\varepsilon}_{gyro} - J \dot{\phi} \dot{\varepsilon}_{gyro}. \quad (6.4)$$

The equation is translated into frequency domain with the Laplace transform. It is possible to compute the transfer function that links the angular velocity $\dot{\varepsilon}_{gyro}$ to the input control torque $T_{\varepsilon PTO}$.

$$\bar{T}_{\varepsilon PTO} = I_g s \bar{\dot{\varepsilon}}_{gyro} - J \dot{\phi} \bar{\dot{\varepsilon}}_{gyro} \quad (6.5)$$

The mobility transfer function result then to be equal to:

$$\frac{\bar{\dot{\varepsilon}}_{gyro}}{\bar{T}_{\varepsilon PTO}} = \frac{1}{I_g s - J \dot{\phi}} \quad (6.6)$$

Re-formulating this result into classic form, a static gain G_0 and a time constant τ are obtained.

$$\frac{\bar{\dot{\varepsilon}}_{gyro}}{\bar{T}_{\varepsilon PTO}} = G_0 \frac{1}{\tau s - 1} \quad (6.7)$$

Where:

$$G_0 = \frac{1}{J \dot{\phi}} \quad (6.8)$$

$$\tau = \frac{I_g}{J \dot{\phi}} \quad (6.9)$$

Substituting the numerical values of the ISWEC Pantelleria device, the time constant τ can be evaluated. The two inertia values I_g and J have the same order of magnitude, approximately 10^4 . The flywheel angular velocity $\dot{\phi}$, even considering a conservative case, has an order of magnitude of at least 10^1 . The two coefficient can be evaluated:

$$|G_0| \sim 10^{-5} \quad (6.10)$$

$$|\tau| \sim 10^{-1} \text{ s} \quad (6.11)$$

Thus the cutoff frequency of the system is approximately equal to:

$$\omega_{cutoff} = \frac{1}{|\tau|} \sim 10^1 s^{-1}. \quad (6.12)$$

Always in the asymptotic bode diagram, taking into account the phase given by the negative static gain, we can consider the phase to be $\phi = -180 deg$ for lower values of frequency:

$$\omega < \frac{0,1}{|\tau|} \sim 10^0 \quad (6.13)$$

Considering the wave periods of interest, between 3 s and 10 s, it is possible to assume that all incoming waves frequency stays in the range $0.1 Hz < \omega < 0.33 Hz$.

It can be stated that in the range of interest the phase between the PTO torque and the axis speed is always equal to $-180 deg$, so they have opposite sign. Their product will be then always be negative, and the power flux will have the wave to mechanical power direction:

$$P_{PTO} = T_{\varepsilon PTO} \dot{\varepsilon}_{gyro} < 0 \quad (6.14)$$

The architecture

This strategy substantially consists in a position feedback control loop, where the quantity to be controlled is the gyroscope frame angular position. The position set point is computed starting from the measures of the floater pitch motion, obtained with an IMU as presented in previous chapter. Given that the amplitude of δ motions are smaller than those expected for the internal precession axis, a scaling gain must be computed. Various algorithm have been tested, the simpler is hereafter presented. A moving window of pitch sampled point is set, with a time range of about 2 or 3 times the wave energy period of the incoming sea state. From all these samples an evaluation of the current amplitude of the pitch motion is obtained. This value divides the ε amplitude set, numerically identified equal to $45 deg$. The output value is then saturated in order to avoid too small or too big gains and low pass filtered. This is the $K_{\delta 2\varepsilon}$ gain. The gyroscope frame set-point is obtained multiplying the pitch feedback times this gain:

$$\varepsilon_{SET}(t) = -K_{\delta 2\varepsilon}(t) \delta(t) \quad (6.15)$$

The minus sign is needed for having the correct direction. This is the set-point to be followed.

A position control loop is then designed. A simple proportional action elaborates the

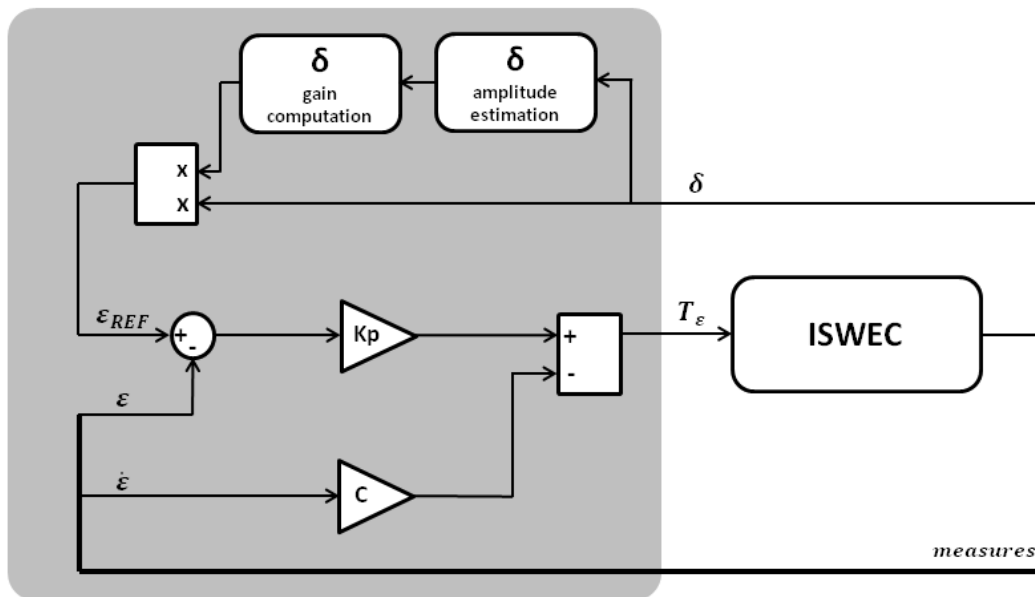


Figure 6.4 DeltaRef control. General architecture.

error between the set and the feedback. In parallel, since the PTO/gyroscope frame axis is mainly inertial and it is poorly damped, a purely damping action is summed. This is proportional to the internal shaft speed $\dot{\epsilon}$.

Technical tips

The same cautions of those used for the proportional-derivative control are used. Another important consideration is following.

- The saturation term after the gain calculus is fundamental: it must limit the highest values in order to avoid unnecessary big internal oscillations in correspondence of small pitch movements.

Implementation

This control scheme requires an inertial measurements unit extremely reliable, in order to obtain continuous and faithful information about the instantaneous pitch position. It is probably the case of evaluating the application of redundancy strategies. Also, an emergency control working without the feedback must be designed, also with a smooth transition between the two.

Optimization and Tuning

This control has to be optimized offline, with the help of numerical simulations. From a perspective of sensitivity on numerical modeling and tuning issues, the number of the parameters to be identified is just a couple for all the sea states, thus requiring a shorter tuning phase into the sea with respect to proportional-derivative control. For

next experimental campaign this control strategy will be tested, in particular for this kind of robustness with respect to different sea states.

6.3.1.1 Results - Time History Example

The behavior of the system controlled with this position controller is illustrated in Figure 6.5. The gyroscope frame position and the floater pitch are synchronized, as requested by the $\dot{\epsilon}_{REF}$ construction. The power adsorption is more unidirectional, almost always adsorbed. Also in this case the wave torque and the pitch angular rate are not always in phase. This only happens in case of longer wave trains and the most energetic ones. In this cases the controller does not interfere with this correct functioning of the dynamic system.

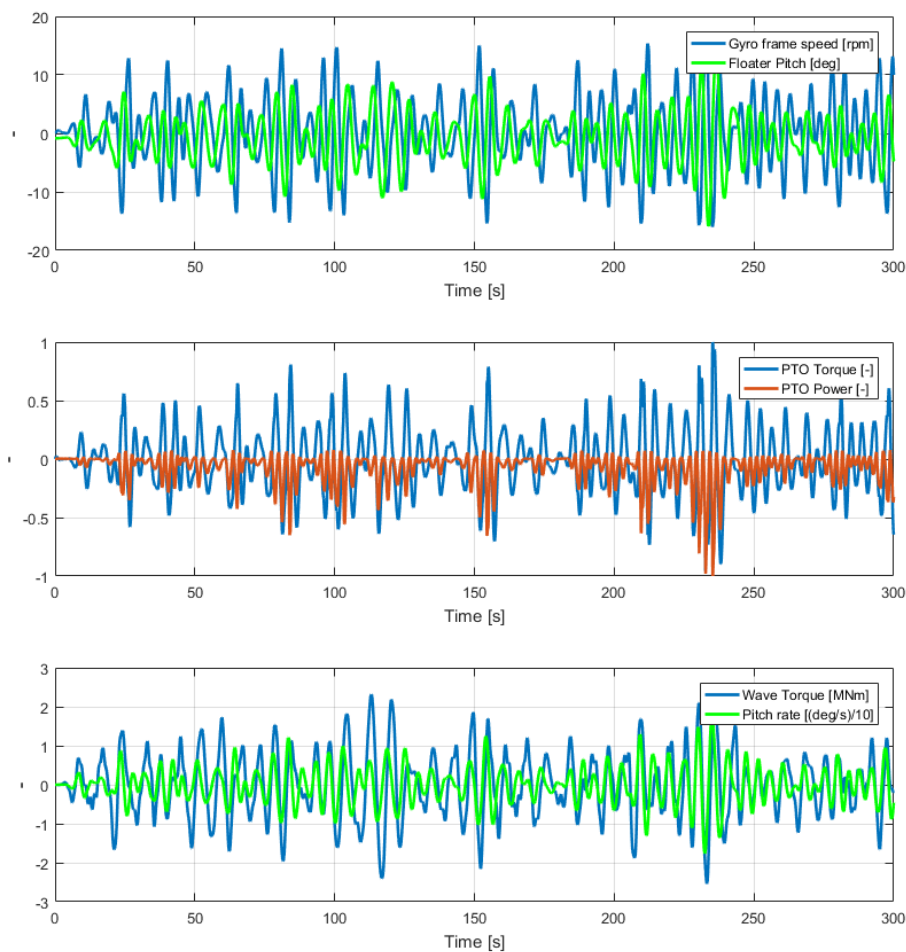


Figure 6.5 DeltaRef control. Time history example.

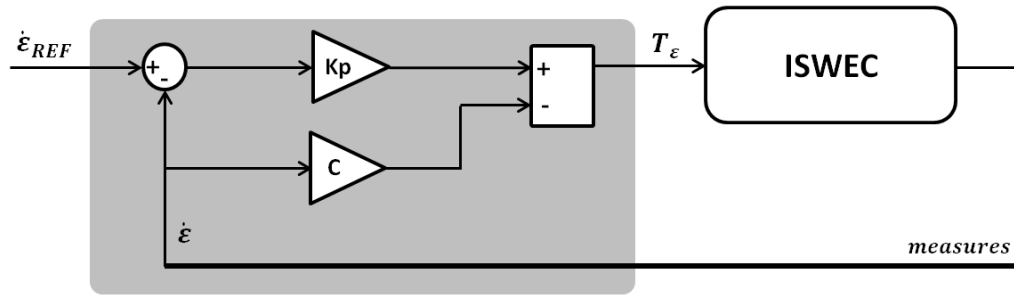


Figure 6.6 SpeedRef control. General architecture.

6.3.2 Continuous Rotation control

The main idea of this strategy is to keep the gyroscope frame in continuous rotation, synchronizing it with the pitch oscillation. This scheme answers to the necessity of having the electric PTO machine working in continuous rotation, thus having higher efficiency. It means that the internal axis makes a complete rotation of $360deg$ for each pitch floater oscillation cycle. This is better shown looking at an example of time history as in Figure 6.6. The reference $\dot{\epsilon}_{SET}$ of the speed feedback control loop is computed starting from a significant frequency of the incoming waves. The wave period can be identified online using autoregressive methods, extended Kalman filters. Some work has been done using this architectures and is presented in [19], [75]. Since the "instantaneous frequency" concept is a bit blurry and dependent of the function assigned to the parameter itself, another method, simpler, has been proposed. It is based on the available forecasts of the incoming sea states. The energy period can be used for computing the speed set in a straightforward manner:

$$\dot{\epsilon}_{SET} = \frac{2\pi}{T_e} \quad (6.16)$$

This set point is then elaborated with a controller very similar to the previous one. A proportional gain elaborates the speed error. In parallel a damping term proportional to the axis speed stabilizes the axis, while enabling the power adsorption.

Technical tips

- This control strategy is quite strong and simple. The synchronization between the two axis is intrinsic into the system, in the sense that the gyroscopic interaction works in order to keep them in phase.

- The proportional gain has to be lower enough to let a slack tracking behavior of the gyroscope frame, otherwise the controller is too tight.

Implementation

The implementation is quite easy. It consists of a simple velocity loop, with only some gains that can be eventually scheduled with respect to the incoming sea states.

Optimization and Tuning

This control has to be optimized offline, with the help of numerical simulations. From a perspective of sensitivity on numerical modeling and tuning issues, the number of the parameters to be identified is just a couple for all the sea states, thus requiring a shorter tuning phase into the sea with respect to proportional-derivative control. For next experimental campaign this control strategy will be tested, in order to check the real benefits on the electric PTO efficiency.

6.3.2.1 Results - Time History Example

In Figure 6.7 an example of a time domain simulation is presented. The speed is kept oscillating around the desired value thanks to the slack proportional gain. The oscillations of the speed enables the power adsorption. This is clear looking at the following picture with the PTO torque and power. It happens that for multiple wave cycles the power is always adsorbed: the gyroscopic inertial torques are accelerating the precession axis. Also in this case there is no guarantee of having the incoming wave torque and the pitch angular rate in phase, as shown in the bottom subplot of the Figure.

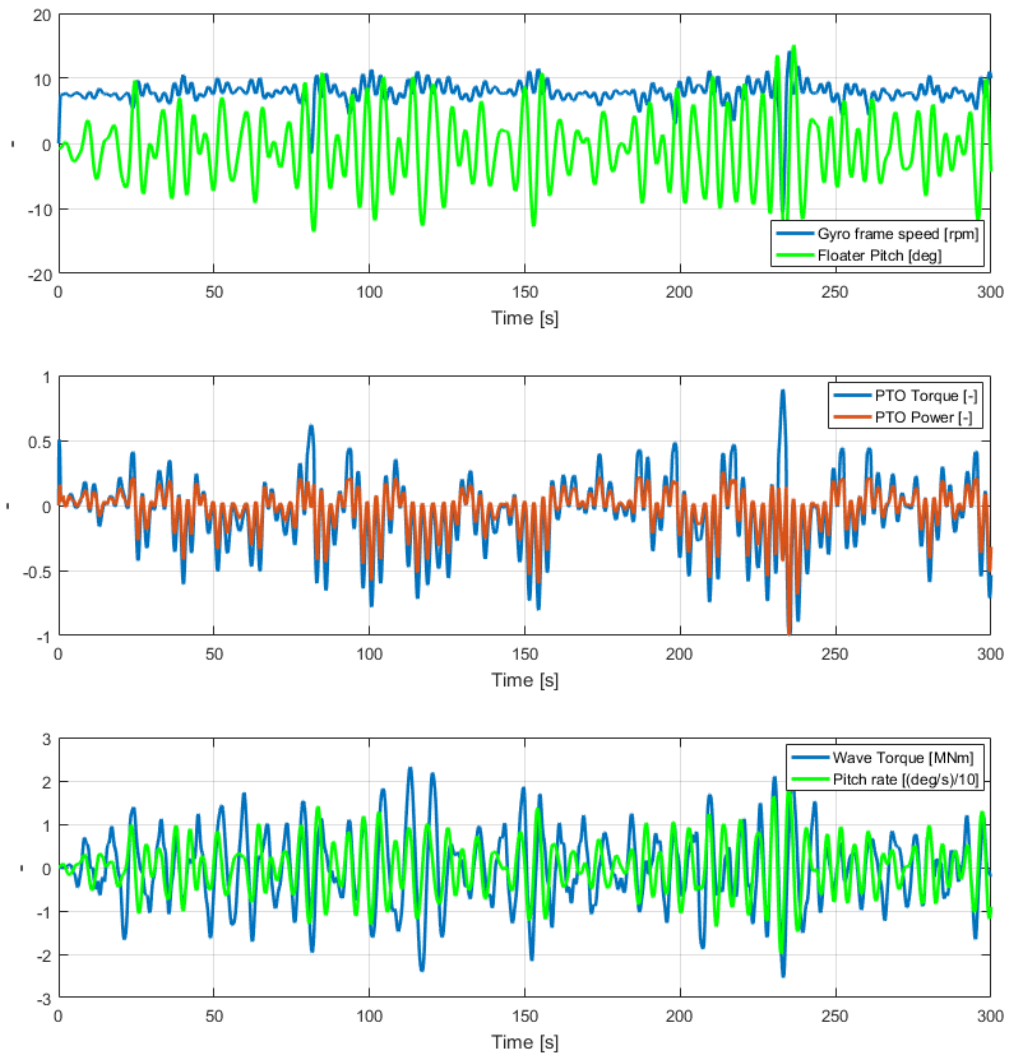


Figure 6.7 SpeedRef control. Time history example.

6.4 The problem of control objective

Control theory usually deals with regulators or set-point tracking problems. A regulator stabilizes a system around a desired state of the system, this can be a position, a voltage, a water level or any other quantity that must be kept the closest possible to a desired value. A set-point tracking problem is a controller that must drive one or more states of a system to follow a desired path in time. A lot of different theories have been proposed to design controllers able to fulfill such specifications. Getting closer to the case study, for wind power the plants are regulated in order to match incoming wind speed with the optimal turbine configuration for that specified continuous or slowly-varying resource. The problem in wave energy field is quite different, because the resource is inherently oscillating and irregular. The problem that has to be faced is to find the "optimal" control objective. Or at least a suitable one.

The problem of optimal power adsorption for a wave energy converter has been studied for a long time in literature [40], [7], [5] and [87] with different kind of hypothesis and for different devices. Some optimal relationships for having the power adsorption of a floating body has been identified [40]. The ISWEC dynamics is quite different because involves an inertial system inside the hull, dynamically linked with the pitch floater DOF by means of the gyroscopic effect, proportional to the pitch angular rate and the internal gyroscope frame rotation rate.

The first approach was to tune the overall resonance frequency of the system by changing the internal axis spring-damping parameters. This is the objective that lead to the design of the proportional-derivative control. Analyzing the functioning of the system when driven with optimal proportional-derivative parameters, the idea of reduction of the power-maximization problem to a simpler one naturally rises. In particular the idea is to design some simple connection between the floater and the inner system. Thus the two previous model free controls: the position oscillating control loop (see analytical proof at section 6.3.1) and the continuous rotation control loop. Both these strategies are set-point tracking architectures. Even if they show an interesting robustness properties with respect to their set-point, the objective, up to the productivity, still they do not present any explicit reference to the power adsorption optimization, the real final objective of this technology.

Optimal control theory makes available some tools giving the opportunity to directly optimize the power adsorption. It has been in fact widely used in wave power

field in a lot of its different applications: linear, nonlinear, constrained and others (see next section 6.5). In the present work the simple linear steady state case of a linear quadratic regulator and a linear quadratic integral regulator are used. They are introduced in the second part of the chapter.

6.5 Model Based strategies: Optimal Control

In the wide theoretical world of optimal control, a lot of different implementations and formulations can be used. Time-varying matrices formulation, known disturbance, wave model augmentation, linear quadratic Gaussian regulator and receding horizon represent interesting techniques used in wave energy ([87], [22], [2]) and are worth to be explored further for the study and optimization of the ISWEC power production capabilities.

6.5.1 Time Varying Linear Quadratic Regulator and Known Disturbance

As first example of application and for showing the potential of these theories, a time varying linear quadratic regulator with the matrix weighting the state/input product is used. In this way it is possible to introduce into the cost function the product between the PTO speed state and the PTO torque control input, i.e the adsorbed power.

The system under control has controllable input and the future disturbance is known. For the ISWEC application, this means that we are optimizing the power adsorbed while keeping the gyroscope around the vertical position, given that the complete wave torque $d(t)$ in the future are known. The problem is theoretically proved and then solved.

The system is written in linearized state space form as shown in 2.43:

$$\dot{\mathbf{X}}(t) = \mathbf{A}(t)\mathbf{X}(t) + \mathbf{B}(t)u(t) + \mathbf{W}(t)d(t) \quad (6.17)$$

where $u(t)$ is the PTO gyroscope frame torque and $d(t)$ is the wave torque in time. The performance index is defined with the following:

$$\mathbf{J}(t) = \frac{1}{2} \mathbf{X}^T(T) \mathbf{S}(T) \mathbf{X}(T) + \frac{1}{2} \int_{t_0}^T \begin{bmatrix} \mathbf{X}^T(\tau) & u^T(\tau) \end{bmatrix} \begin{bmatrix} \mathbf{Q}(\tau) & \mathbf{V}(\tau) \\ \mathbf{V}(\tau) & \mathbf{R}(\tau) \end{bmatrix} \begin{bmatrix} \mathbf{X}(\tau) \\ u(\tau) \end{bmatrix} d\tau \quad (6.18)$$

Using Pontryagin's minimum principle, it is possible to obtain the optimal control law that find the optimality solution accordingly to the cost function of the previously formulated problem in the time interval $[t_0, T]$.

$$u(t) = -\mathbf{R}^{-1}(t) [(\mathbf{V}^T(t) + \mathbf{B}^T(t)\mathbf{K}(t)) \mathbf{X}(t) + \mathbf{B}^T(t)g(t)] \quad (6.19)$$

where $\mathbf{K}(t)$ and $g(t)$ are the feedback control action and are computed as hereafter shown.

disturbance independent term

This term is dependent on the type of the cost function.

$$-\dot{\mathbf{K}}(t) = \mathbf{K}(t)\mathbf{A}(t) + \mathbf{A}^T(t)\mathbf{K}(t) - \mathbf{S}^T(t)\mathbf{R}(t)\mathbf{S}(t) + \mathbf{Q}(t) \quad (6.20)$$

with:

$$\mathbf{S} = \mathbf{R}^{-1}(t) (\mathbf{V}^T(t) + \mathbf{B}^T(t)\mathbf{K}(t)) \quad (6.21)$$

and with initial state:

$$\mathbf{K}(T) = \mathbf{S}(T) \quad (6.22)$$

Since the known state of this differential equation is the final one, it must be solved by backward time integration. According to this, the sign of 6.20 must change when the integration is performed.

disturbance dependent term

The disturbance term is function of the cross weight of states and the disturbance matrix.

$$-\dot{g}(t) = [\mathbf{K}(t)\mathbf{M}(t) - \mathbf{P}(t)] g(t) + \mathbf{K}(t)\mathbf{W}(t)d(t) \quad (6.23)$$

with

$$\mathbf{M} = -\mathbf{B}(t)\mathbf{R}^{-1}(t)\mathbf{B}^T(t) \quad (6.24)$$

$$\mathbf{P} = -\mathbf{A}^T(t) - \mathbf{V}(t)\mathbf{R}^{-1}\mathbf{B}^T(t) \quad (6.25)$$

and with the initial state:

$$g(t) = 0 \quad (6.26)$$

Since the known state is the final one, this equation must be computed time integrating backward in time. According to this, the sign of 6.23 must change when the integration is performed.

The results obtained with this kind of control strategy are shown in Figure 6.8. The weighting parameters are designed with the criteria explained in next section 6.5.2. The outcomes are extremely interesting and show the potential of optimal control theories applied to the ISWEC system. Some considerations are hereafter proposed. Looking at the third plot on the bottom of the figure the floater pitch angular rate is in phase with the wave torque acting on the same floater DOF. This condition is known to be the optimal condition for the power transfer from the wave to the floater. This optimal condition is realized while the PTO gyroscope frame angular position is in phase with the floater pitch motion. This makes the power adsorption unidirectional from the floater to the PTO system, as also proved in previous section 6.3.1.

This control presents multiple practical and theoretical issues to be solved before it can be used in the real environment (linear model, constraints, the incoming wave, among the principals). A simplified architecture has been then found, as is explained in section 6.5.2.

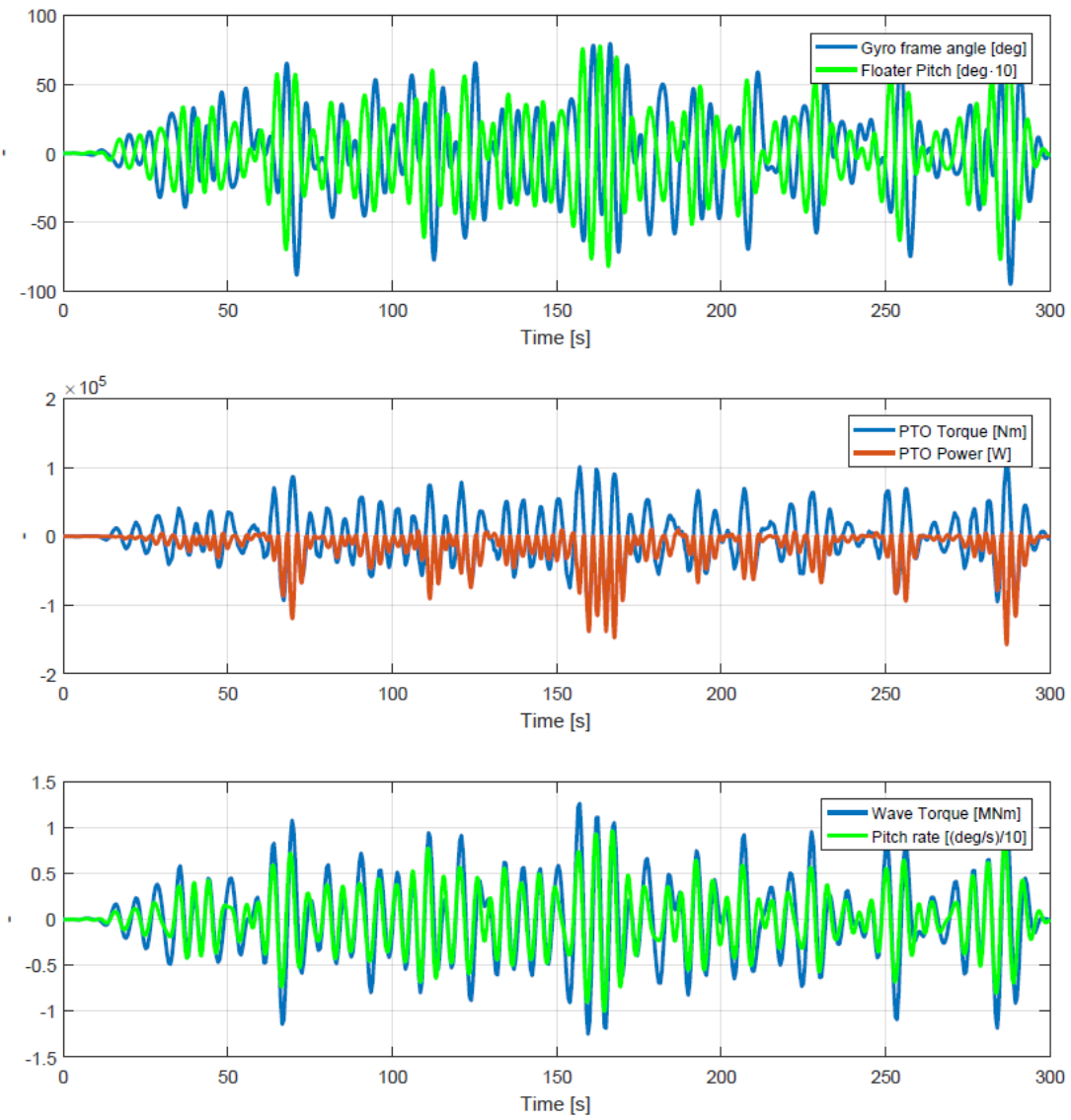


Figure 6.8 Optimal control with known wave disturbance. Time history example.

6.5.2 Oscillating Linear Quadratic Regulator

The infinite-horizon continuous time Linear Quadratic Regulator (LQR) [65, 4] is used as a frame for the design of the feedback control law. In order to keep the problem formulation as simple as possible, the unknown wave disturbance input is not modeled, and it is not part of the design. Gain scheduling is used for overcome problems with the trigonometric nonlinearity caused by the gyroscopic effect ($\dot{\phi} \delta \cos \varepsilon$).

6.5.2.1 Linear Quadratic Regulator

The application of the steady state LQR for the ISWEC is presented. The first equation is the continuous time linear time invariant state space model. The second equation is the quadratic cost function. It is minimized offline in the design phase. It must be noticed that the time interval of the computation of the integral begins in $t = 0$ and finishes in $t = \infty$. This is different from the previous version, shown in section 6.5.1. The problem to be solved is then written in 6.27: the cost function J must be minimized while the constraints imposed by the dynamic system are fulfilled.

$$\begin{cases} \dot{\mathbf{X}}(t) = \mathbf{A}\mathbf{X}(t) + \mathbf{B}u(t) \\ J(\infty) = \int_0^{\infty} [\mathbf{X}^T(\tau) u(\tau)] \begin{bmatrix} \mathbf{Q} & \mathbf{N} \\ \mathbf{N} & R \end{bmatrix} \begin{bmatrix} \mathbf{X}(\tau) \\ u(\tau) \end{bmatrix} d\tau \end{cases} \quad (6.27)$$

In the particular case of the LQR oscillating control for the ISWEC:

$$\begin{bmatrix} \dot{\varepsilon} \\ \varepsilon \\ \dot{\delta} \\ \delta \\ \rho_{rv1} \\ \vdots \\ \rho_{rvn} \\ T_{PTO} \end{bmatrix}^T \begin{bmatrix} q_{11} & 0 & 0 & \cdots & 0 & n_1 \\ 0 & q_{22} & 0 & \cdots & 0 & 0 \\ 0 & 0 & 0 & \cdots & 0 & 0 \\ \vdots & \vdots & \vdots & \ddots & \vdots & \vdots \\ 0 & 0 & 0 & \cdots & 0 & 0 \\ n_1 & 0 & 0 & \cdots & 0 & r \end{bmatrix} \begin{bmatrix} \dot{\varepsilon} \\ \varepsilon \\ \dot{\delta} \\ \delta \\ \rho_{rv1} \\ \vdots \\ \rho_{rvn} \\ T_{PTO} \end{bmatrix} \quad (6.28)$$

then the cost function can be expanded in the form:

$$J = q_{11}\dot{\varepsilon}^2 + q_{22}\varepsilon^2 + 2n_1\dot{\varepsilon}T_{PTO} + rT_{PTO}^2 \quad (6.29)$$

where

q_{11} quadratic damping cost term. Useful for the stabilization the system and damping the motions of the PTO axis.

q_{22} quadratic stiffness cost term. Useful for keeping the system oscillating around the vertical position ($\varepsilon = 0$).

n_1 power weighting term. This weight the product of $\dot{\varepsilon}$ and $T_{\varepsilon PTO}$. Since it is a minimization problem $n_1 > 0$.

r PTO torque action cost term. It is used to limit the control action.

The steady state optimal solution of the optimization problem previously stated is given by the solution of an Algebraic Riccati Equation (ARE) in matrix variable \mathbf{S} (costate matrix).

$$\mathbf{A}^T \mathbf{S} + \mathbf{S} \mathbf{A} - (\mathbf{S} \mathbf{B} + \mathbf{N}) \mathbf{R}^{-1} (\mathbf{B}^T \mathbf{S} + \mathbf{N}^T) + \mathbf{Q} = 0 \quad (6.30)$$

After the solution of the previous equation is found, the Feedback Kalman gain \mathbf{K} is then computed as:

$$\mathbf{K} = \mathbf{R}^{-1} (\mathbf{B}^T \mathbf{S} + \mathbf{N}^T) \quad (6.31)$$

The PTO torque elaborated by the controller starting from the measure and observation of the instantaneous state has then the analytical relationship:

$$u(t) = T_{\varepsilon}(t) = -\mathbf{X}(t) \mathbf{K} \quad (6.32)$$

Figure 6.9 presents the overall control architecture. The feedback gain is function of ε because it is scheduled around several linearization points of the precession axis, as explained in next section 6.5.2.3.

6.5.2.2 Objective function parameters design

In optimal control theory the design of cost function parameters is a delicate step. Since the objective of the control represents the customized part of the design. The approach hereafter adopted is to scale all the weighting parameters of the cost function in order to have a particular ratio with the maximum PTO torque. The components in \mathbf{Q} are fundamental for the stabilization and oscillating behavior of the system and they

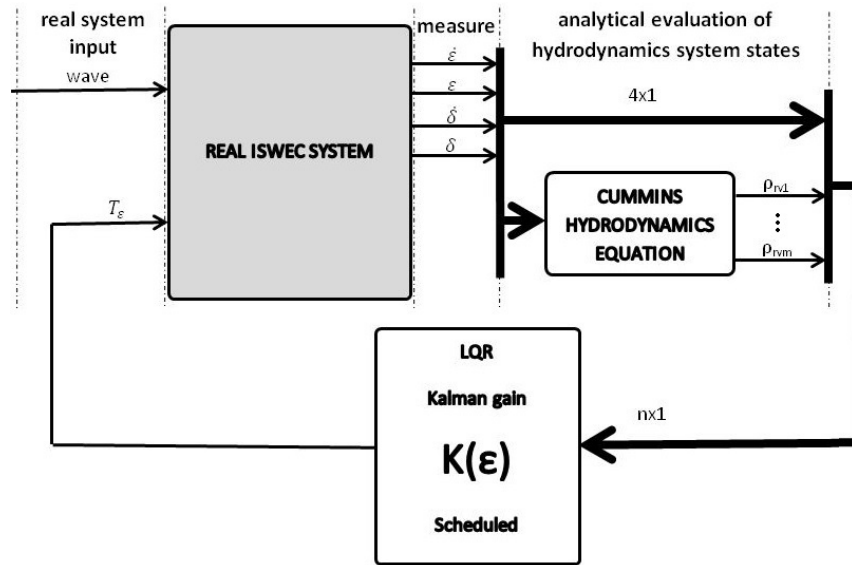


Figure 6.9 Overall LQR architecture

are scaled starting from the maximum expected values of PTO velocity and position, and their square are dividends of the maximum PTO torque. The scalar element in \mathbf{R} gives information about the quantity of regulating action desired. It is of a inferior order of magnitude with respect to the others cost function elements. The important state/input coupling matrix element in \mathbf{N} is the parameter weighting the power. It is set to be K_N times PTO maximum torque divided per an estimate of two times the maximum power. All these are deeply described in the following.

Q - Inner States matrix design The two coefficients in this matrix are the in a way analogous to those of the PD control, even if they are acting on the square of the respective states values. q_{22} is responsible of the regulation of the flywheel axis angular position around the vertical axis while q_{11} is quadratically weighting the PTO speed damping the motion in order to dynamically stabilize the system.

Damping quadratic weight

$$q_{11} = \frac{T_{max}}{\dot{\epsilon}_{max}^2} \quad (6.33)$$

with $\dot{\epsilon}_{max} = \dot{\epsilon}_{maxPTO}/K_{safety}$ and where the maximum torque is defined as:

$$T_{max} = T_{PTOmax} \tau \cdot \#gyroscopes \quad (6.34)$$

Stiffness quadratic weight

$$q_{22} = \frac{T_{max}}{\epsilon_{max}^2} \quad (6.35)$$

with T_{max} defined as before.

R - Input matrix design This term must not influence the optimization of the torque law but has to be enough to avoid extra use of PTO torque action. The idea is that the system have to work smoothly with the maximum torque available, even exceeding the threshold of the maximum PTO torque. The torque and speed constraints given by the electro-mechanical PTO are managed with the nonlinear term presented in previous chapter 5. This hypothesis can be formulated as follows:

$$\begin{aligned} T_{max} &\gg T_{max}^2 r \\ \frac{T_{max}}{T_{max}^2} &\gg r \end{aligned} \quad (6.36)$$

if it is desired at least one order of magnitude of difference:

$$r = \frac{T_{max}}{T_{max}^2 10^2} \quad (6.37)$$

N - Inner States/Input matrix design This is the matrix that gives the possibility to weight the product of the PTO speed and the PTO torque. The mechanical power thus enters the optimization process.

$$\begin{aligned} K_N T_{max} &= 2 \dot{\epsilon}_{max} T_{max} n_1 \\ n_1 &= \frac{K_N T_{max}}{2 \dot{\epsilon}_{max} T_{max}} \end{aligned} \quad (6.38)$$

6.5.2.3 Gain Scheduling

The feedback control law used applies only to linear time invariant systems. The dynamic of the ISWEC, as seen in equation 2.36, has at least one trigonometric nonlinear term, the inertial gyroscopic coupling between internal PTO precession axis and the pitch floater DOF is in fact dependent on the ϵ values.

Since the system dynamics is relatively slow and smooth, and the system is intrinsically stable, the feedback Kalman gain obtained from the previous analysis can be scheduled as a function of the instantaneous value of ϵ precession axis and varied according to it. Figure 6.10 shows some different positions around which the system matrix can be linearized.

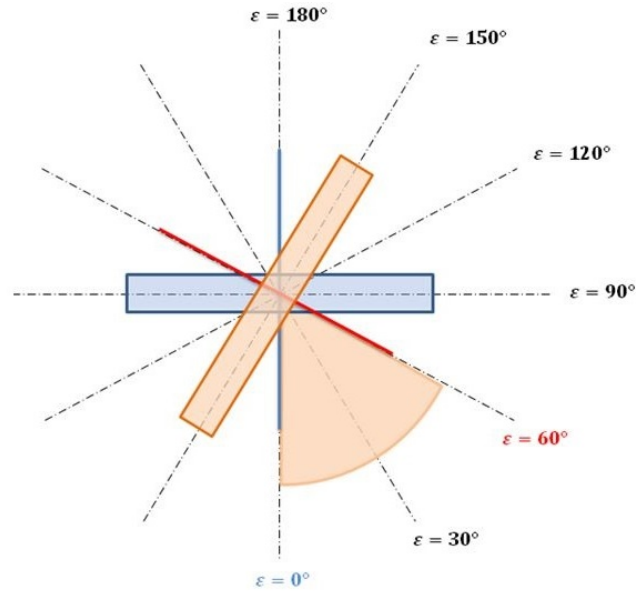


Figure 6.10 Gyroscope at different angular position for gain scheduling.

More analytically, in equation (6.39) \mathbf{A} matrix is rewritten explicating the nonlinear term. It is then linearized around each of these positions, for each linearization point the Kalman feedback gain is computed. Since the nonlinear function is even, only the right half of the plane must be used in the design ($0 < \varepsilon \pi$).

$$\mathbf{A} = \begin{bmatrix} 0 & 0 & \frac{J_g \dot{\phi} \cos(\varepsilon)}{I_g} & 0 & \dots \\ 1 & 0 & 0 & 0 & \dots \\ -\frac{J_g \dot{\phi} \cos(\varepsilon)}{I_{eq} + \mu_{\infty}} & 0 & 0 & -\frac{K_w}{I_{eq} + \mu_{\infty}} & \dots \\ 0 & 0 & 1 & 0 & \dots \\ \vdots & \vdots & \vdots & \vdots & \ddots \end{bmatrix} \quad (6.39)$$

The control Kalman gain matrices need then to be aggregated together. In order to have a smooth transition between them in the whole ε range, it is divided in at least than 10 arcs. The feedback \mathbf{K} matrices are then linearly combined by interpolation (see Figure 6.11 and equation (6.40)).

$$k_j(\varepsilon) = \frac{k_j(\varepsilon_{i+1}) - k_j(\varepsilon_i)}{(\varepsilon_{i+1} - \varepsilon_i)}(\varepsilon_i - \varepsilon) + k_j(\varepsilon_i) \quad (6.40)$$

Here $k_j(\varepsilon_i)$ is the element j of the feedback gain vector, and $i, i + 1$ represent two adjacent linearization angles.

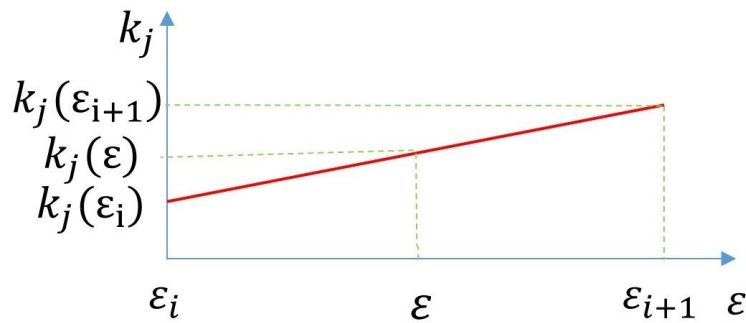


Figure 6.11 Interpolation method for j -th element k_j at generic position ε in the interval $[\varepsilon_i, \varepsilon_{i+1}]$ subsequent linearization points

The implementation of the gain scheduled controller results then in a lookup table with these n linearization feedback Kalman gains.

6.5.2.4 Results - Time History Example

The LQR control effects over the ISWEC overall dynamics are presented in Figure 6.12. The gyroscope frame internal precession axis is synchronized and counter phase with the floater pitch angle. There is not a computed gain for the amplitude of the oscillations, but the ε axis motions are governed by the K_N value entering the optimal control cost function. The effects of this parameter are better illustrated in following section. The PTO torque and power are presented, and more reactive power seems to be present if compared to the DeltaRef model-free control. Also in the last subplot, the wave incoming torque and the floater pitch angular speed are more phased, resembling a bit the time varying optimal control with known waves.

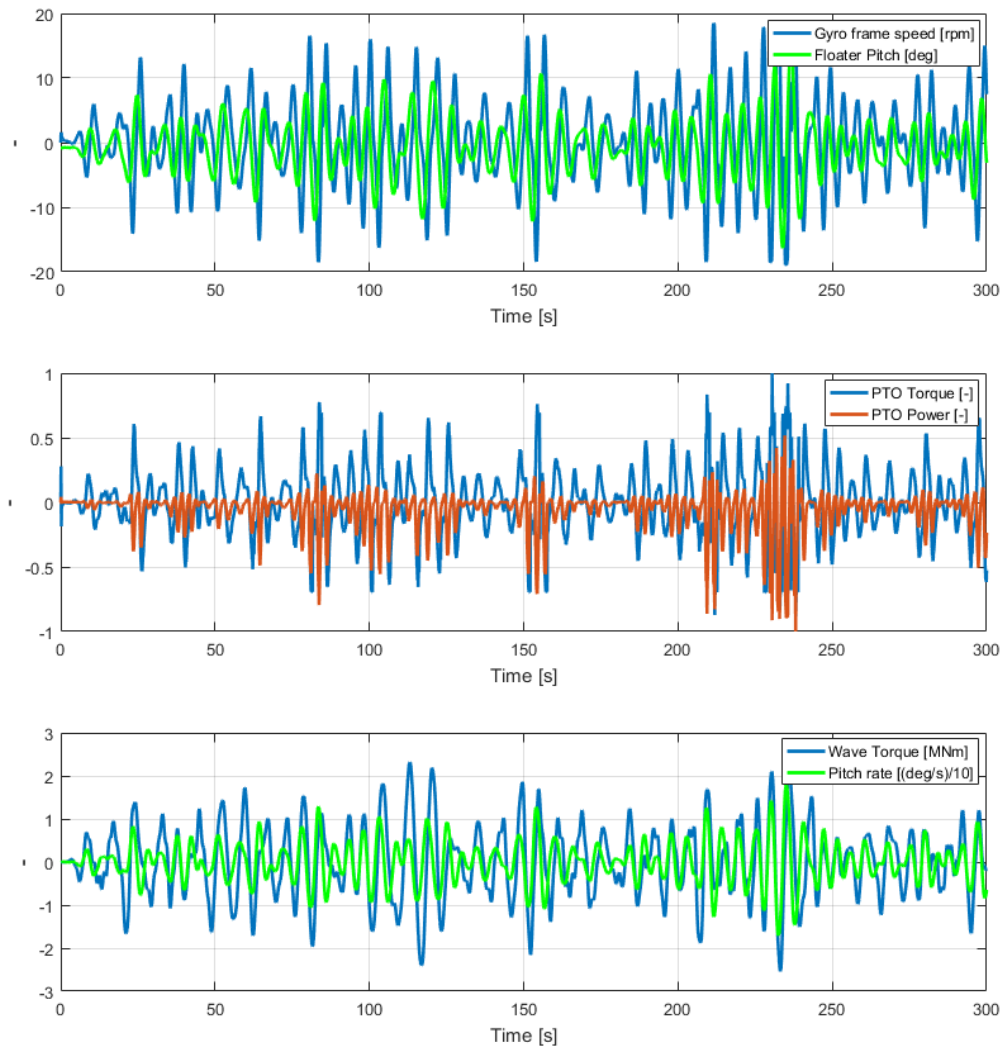


Figure 6.12 LQR control. Time history example.

6.5.2.5 Results - The effect of power weight

The aim of this subsection is to investigate the effect of the power weight parameter multiplier K_N , showed in equation (6.38). This term is linearly proportional to the final power term used in the objective cost function. The higher K_N is, the more the system dynamics is induced to have an increased power absorption behavior and becomes unstable.

In order to assess how K_N influences the power absorption, time domain simulations with the same wave input were carried on, while K_N is the only parameter to be changed, from a very small value of 1 up to 40. The forcing wave chosen for the analysis has an energy period $T_e = 6.5s$ and a significant amplitude $H_s = 2.5m$.

The results of this analysis are shown in Figures 6.13 to 6.15.

In each figure the same time interval is presented for four different values of K_N : 1, 5, 15, 40.

In Figure 6.13, wave elevation and internal PTO precession axis position are plotted. For small values of the power weighting coefficient, the regulating behavior given by the \mathbf{Q} states matrix of the LQR is predominant, keeping the gyroscope frame ε shaft with limited amplitude and low velocity. For higher values of K_N , the system presents larger oscillations, until reaching a maximum value of amplitude, less than $100deg$. This effect is due to the intervention of the nonlinear term, which can be seen better in Figure 6.14. Moreover, the maximum PTO speed in all simulations is ensured to be always less than the maximum allowed value. In this figure the wave force acting on the pitch DOF, the pitch angular rate and the internal PTO precession axis speed are reported. In this time series group it can be noticed that for small values of the power parameter the PTO internal motion is a smooth curve. For higher values, the maximum speed is heavily limited by the nonlinear term. It can be noticed that as for the case of the optimal control with known future wave disturbance, the internal axis motion and the floater pitching motion are in phase. This happens even if the controller does not take into account in its design phase about the wave. It is in fact not modeled. This causes the controlled system to have a pure damping nature for the floater, at least for values of K_N that does not make the nonlinear control act. This is particularly clear in Figure 6.15. The pure damping action of this control law can be seen from the power time histories for small values of K_N . Despite this, when the magnitude of this parameter increases and the nonlinear term appears, some reactive component is required in order to keep the PTO shaft synchronized with the floater motions.

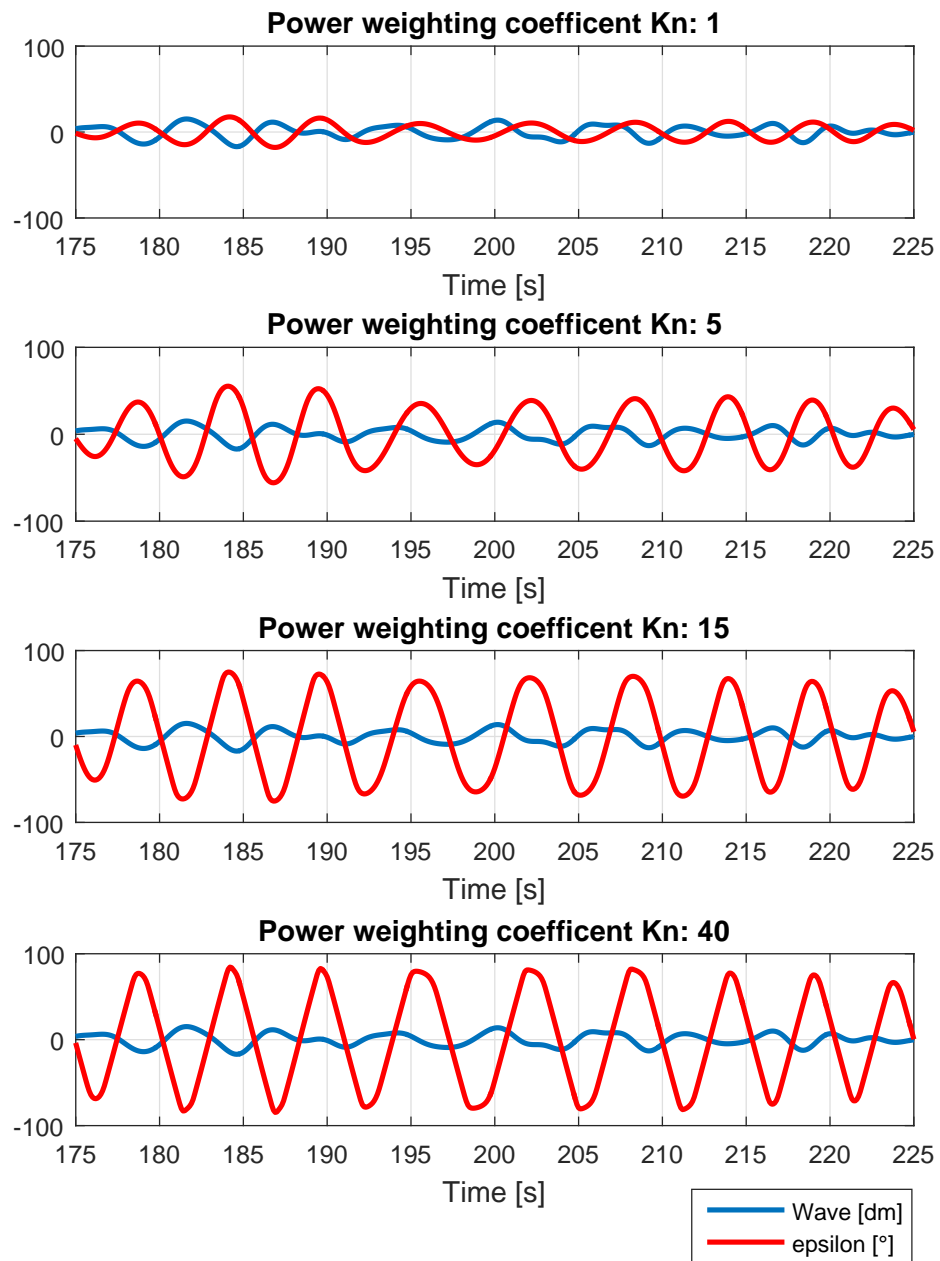


Figure 6.13 Time histories. Effect of K_N . Wave elevation and internal precession gyroscope frame axis position.

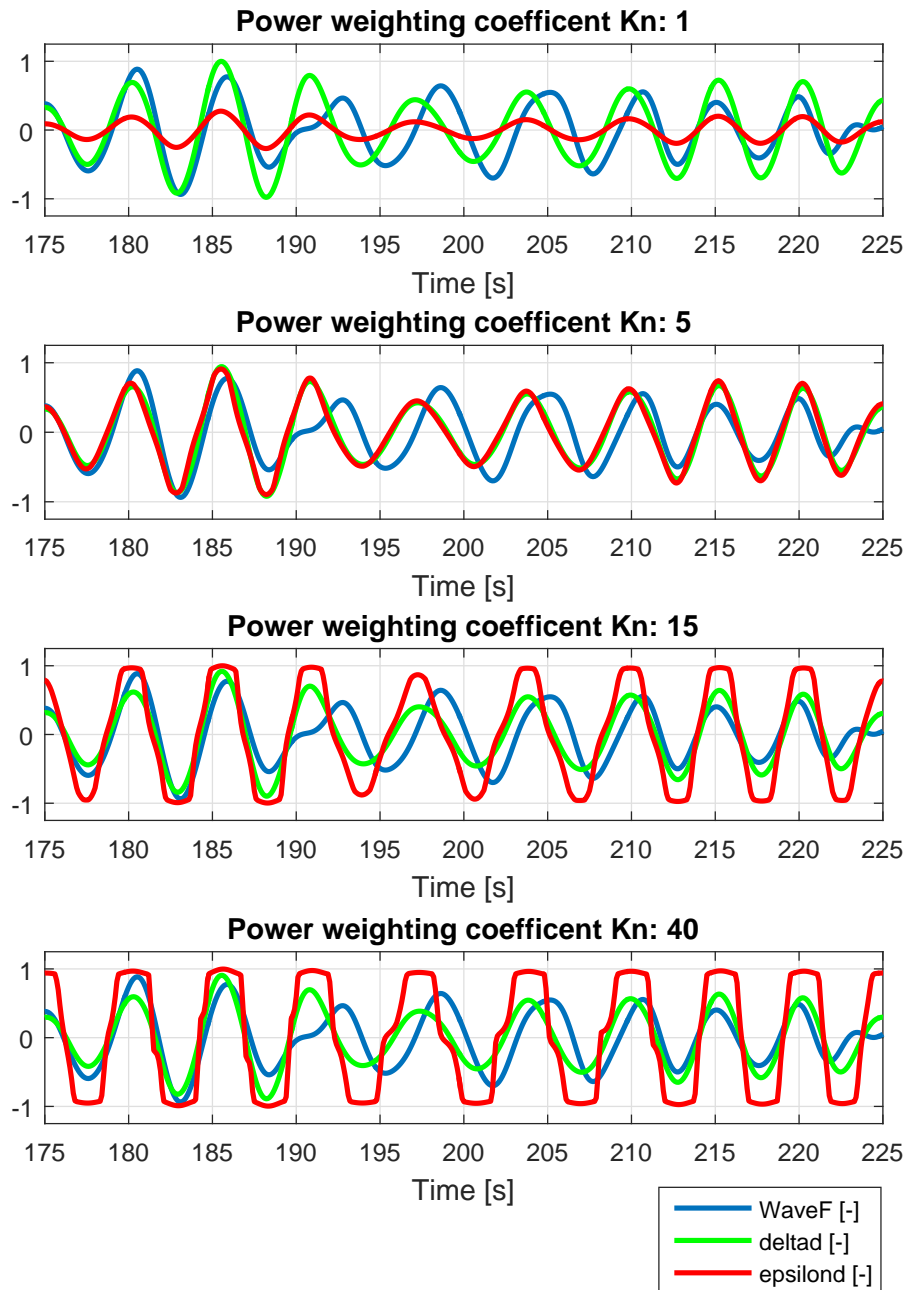


Figure 6.14 Time histories. Effect of K_N . Dimensionless scaled wave force, pitch rotational speed and internal precession gyroscope frame axis speed.

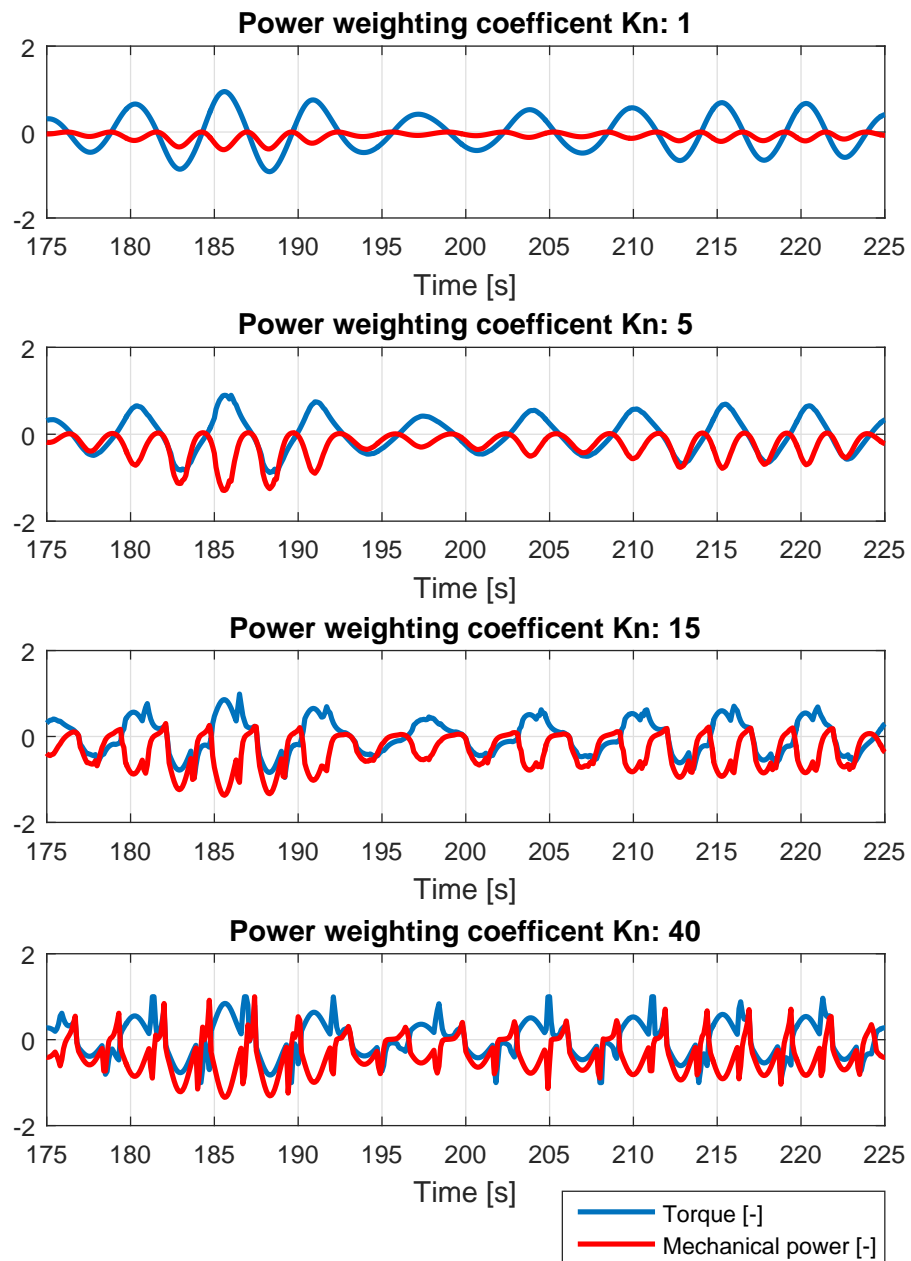


Figure 6.15 Time histories. Effect of K_N . Dimensionless scaled PTO torque and mechanical power.

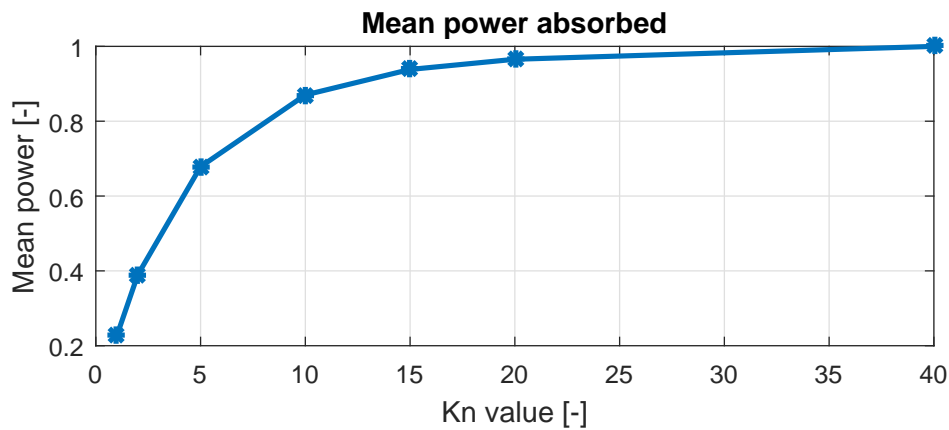


Figure 6.16 Effect of K_N . Dimensionless scaled mean torque power in function of changing K_N

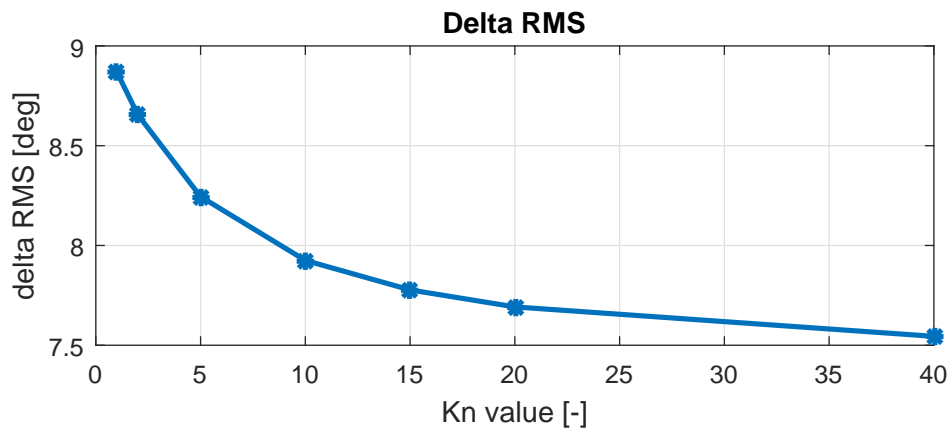


Figure 6.17 Effect of K_N . RMS of pitch in function of changing K_N

In Fig.6.16 the consequences of power weight on mean absorbed power are presented. The higher the constant is, the higher the damping of the floater pitching motion (Fig.6.17), the higher is the power absorption. The intervention of the nonlinear term, giving a maximum range of motion to the gyroscope system, causes the performances to converge to a maximum.

K_N is chosen in order to maximize the mean absorbed power and to reduce sudden variations on the torque given by the nonlinear term.

An additional state is defined for a single input - single output tracking. Its derivative is equal to the error between the reference gyroscope frame speed and its actual value.

$$\dot{\xi} = \dot{\epsilon} - \dot{\epsilon}_{REF} \quad (6.43)$$

and the ξ state is thus defined as an integral:

$$\xi(t) = \int_0^t [\dot{\epsilon}(\tau) - \dot{\epsilon}_{REF}(\tau)] d\tau \quad (6.44)$$

The new state space formulation can be re-elaborated as follows:

$$\begin{bmatrix} \dot{\mathbf{X}} \\ \dot{\xi} \end{bmatrix} = \begin{bmatrix} \mathbf{A} & \mathbf{0} \\ \mathbf{C} & \mathbf{0} \end{bmatrix} \begin{bmatrix} \mathbf{X} \\ \xi \end{bmatrix} + \begin{bmatrix} \mathbf{B} \\ \mathbf{0} \end{bmatrix} u + \begin{bmatrix} \mathbf{0} \\ -\mathbf{I} \end{bmatrix} \dot{\epsilon}_{REF} \quad (6.45)$$

Thus, if a Kalman gain K is designed in order to stabilize the current augmented system, then $\dot{z} = 0$ and $\dot{\epsilon}_{REF} = \dot{\epsilon}_{FB}$.

The designed control law is slightly different from previous presented LQR. It is a constant vector multiplying the

$$u(t) = -\mathbf{K}^* \mathbf{X}^*(t) \quad (6.46)$$

The system of equations to be optimized is thus:

$$\begin{cases} \dot{\mathbf{X}}^*(t) = \mathbf{A}^* \mathbf{X}^*(t) + \mathbf{B}^* u(t) + \mathbf{B}_{REF} \dot{\epsilon}_{REF}(t) \\ J(\infty) = \int_0^\infty [\mathbf{X}^{*T}(\tau) u(\tau)] \begin{bmatrix} \mathbf{Q}^* & \mathbf{N}^* \\ \mathbf{N}^* & \mathbf{R}^* \end{bmatrix} \begin{bmatrix} \mathbf{X}^*(\tau) \\ u(\tau) \end{bmatrix} d\tau \end{cases} \quad (6.47)$$

The weight matrix of the LQI oscillating control for the ISWEC is:

$$\begin{bmatrix} \dot{\epsilon} \\ \dot{\delta} \\ \delta \\ \rho_{rv1} \\ \vdots \\ \rho_{rvn} \\ T_{PTO} \\ \xi \end{bmatrix}^T \begin{bmatrix} q_{11} & 0 & \cdots & 0 & n_1 & 0 \\ 0 & 0 & \cdots & 0 & 0 & 0 \\ \vdots & \vdots & \vdots & \ddots & \vdots & \vdots \\ 0 & 0 & \cdots & 0 & 0 & 0 \\ n_1 & 0 & \cdots & 0 & r & 0 \\ 0 & 0 & \cdots & 0 & 0 & q_{n+1,n+1} \end{bmatrix} \begin{bmatrix} \dot{\epsilon} \\ \dot{\delta} \\ \delta \\ \rho_{rv1} \\ \vdots \\ \rho_{rvn} \\ T_{PTO} \\ \xi \end{bmatrix} \quad (6.48)$$

It can be computed the following expression:

$$J = q_{1,1} \dot{\epsilon}^2 + 2n_1 \dot{\epsilon} T_{PTO} + r T_{PTO}^2 + q_{n+1,n+1} \xi^2 \quad (6.49)$$

where

$q_{1,1}$ quadratic damping cost term. Useful for the stabilization the system and damping the motions of the PTO axis.

n_1 power weighting term. This weight the product of $\dot{\epsilon}$ and $T_{\epsilon PTO}$. Since it is a minimization problem $n_1 > 0$.

r PTO torque action cost term. It is used to limit the control action.

$q_{n+1,n+1}$ quadratic cost term of the speed error integral. Useful for keeping the system in continuous rotation.

The synthesis of the controller is then realized with the Matlab®function *lqi*.

The architecture of this feedback controller is presented in Figure 6.18.

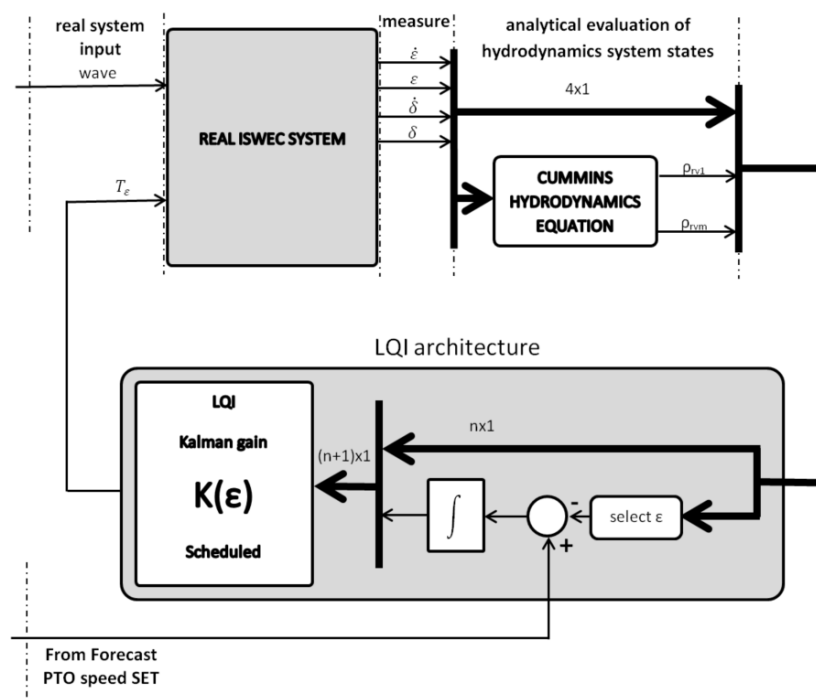


Figure 6.18 Overall LQI architecture

6.5.3.2 Anti Wind-Up technique

The problem of integral wind-up is well known in control theory. This brings instability into the system. In order to avoid this phenomenon in this speed control loop several methods can be implemented. In this paragraph the taken choice is described.

The scheme is presented in Figure 6.19. A saturation is connected in series with the integrator and it is limiting the signal ξ , integral of the speed error $\dot{\xi}$. The subtraction of the saturated signal $\bar{\xi}$ and ξ is multiplied per a proportional gain and it is summed to the input $\dot{\xi}$ of the integral.

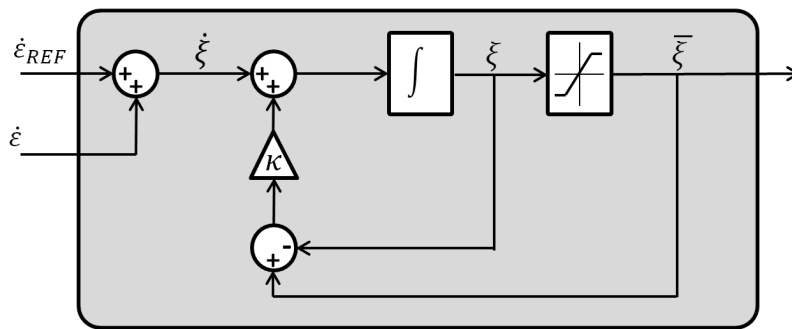


Figure 6.19 Anti Windup Strategy scheme

6.5.3.3 Gain Scheduling

The same gain scheduling technique of 6.5.2.3 is applied. In this case this solution is even more important, because of the system makes complete rotations at every wave cycle.

6.5.3.4 Results - Time History Example

An example of time history is presented in Figure 6.20. In the top graph, the floater pitch motion is in green. The Gyro frame speed has a mean value equal to the desired set and the oscillations are caused by the presence of the power weight coefficient in the optimal control cost function. In the second plot the PTO torque and power are presented. They are synchronous, since the speed is always greater than zero. There are several moments in which the PTO is working as motor (the power is positive). In the last figure, the wave torque and pitch angular rate are shown. This architecture does not guarantee the phase.

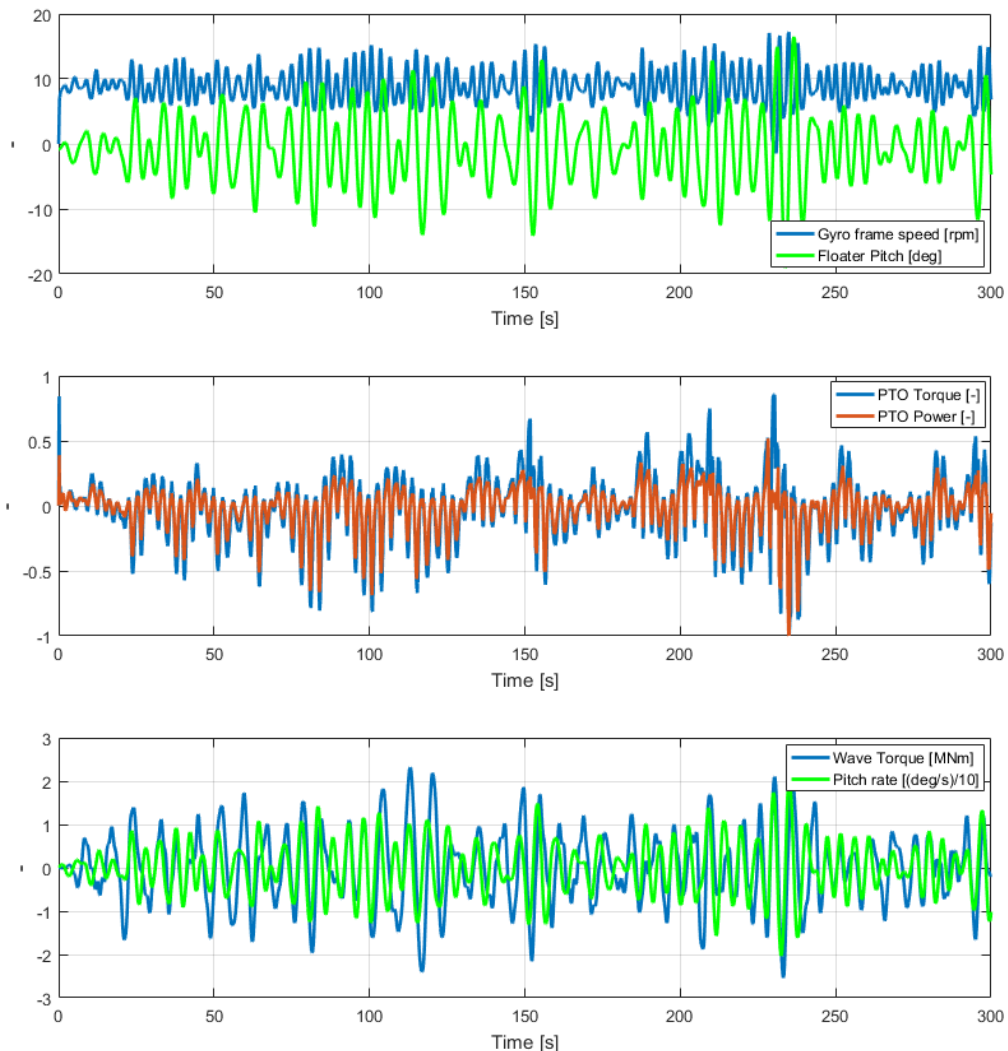


Figure 6.20 LQI control. Time history example.

6.5.3.5 Results - The effect of power weight

The effect of the power weight coefficient in the design cost function is definitely clear in Figure 6.21. Four increasing values of K_N : 1, 5, 15, 40 have been used for the design of a controller for the same wave and the same flywheel speed. The destabilizing effect is clear: the more the parameter is, the more amplitude are the speed oscillations. From the second picture 6.22, it can be seen that for higher values of K_N the power adsorption properties increase (the power tends to be more negative). In last Figure 6.23 it is again explicitated that this control does not take into account for the optimization the presence of the wave torque acting over the pitch floater DOF.

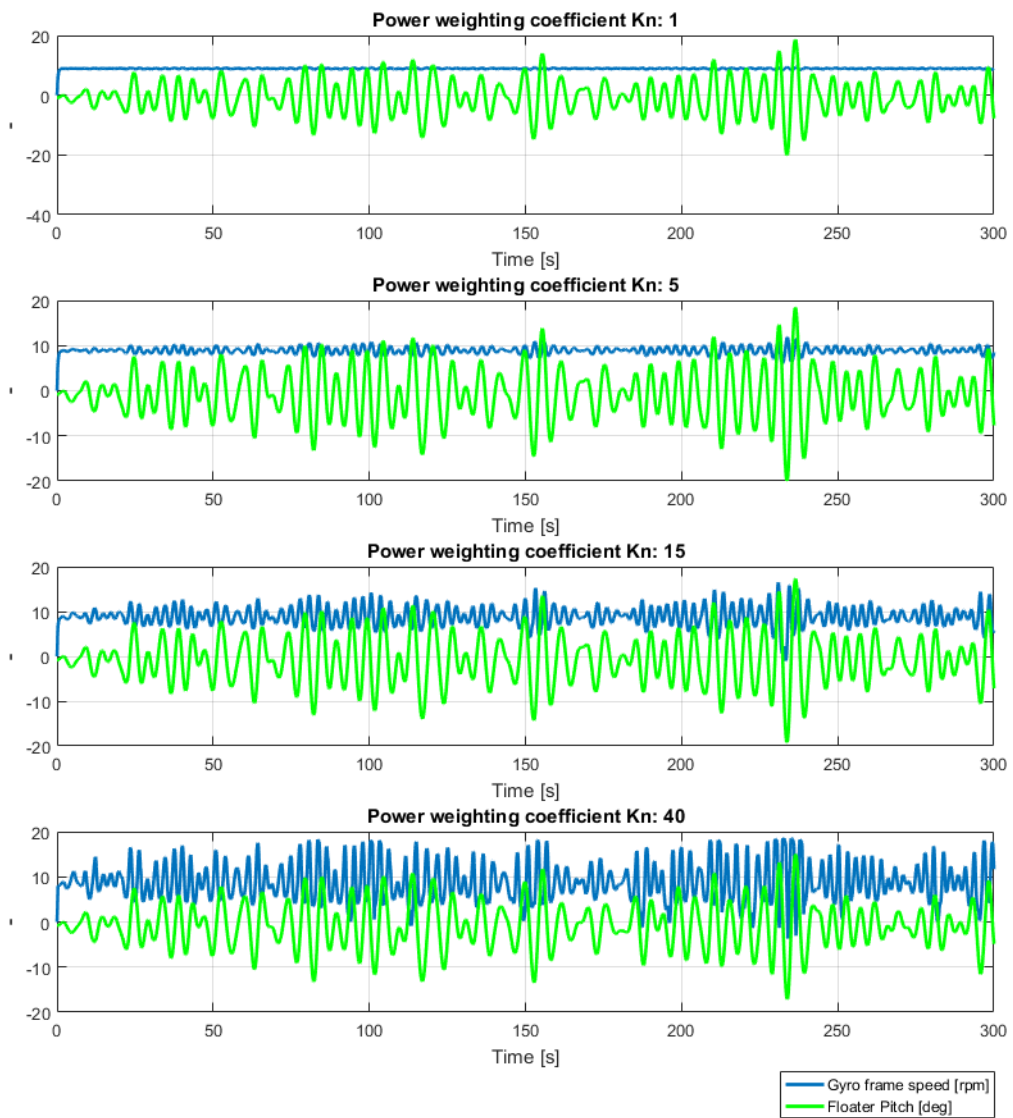


Figure 6.21 Time histories. Effect of K_N . Floater pitch and internal precession gyroscope frame axis speed.

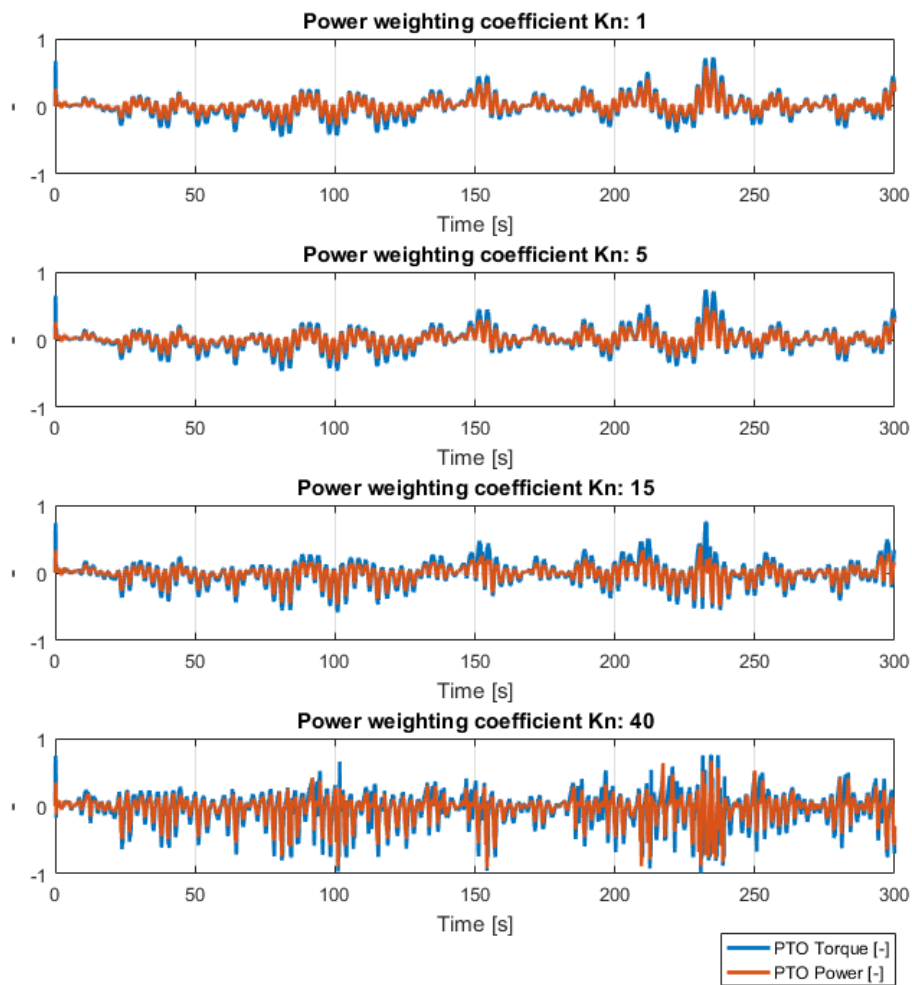


Figure 6.22 Time histories. Effect of K_N . Dimensionless scaled scaled PTO torque and mechanical power.

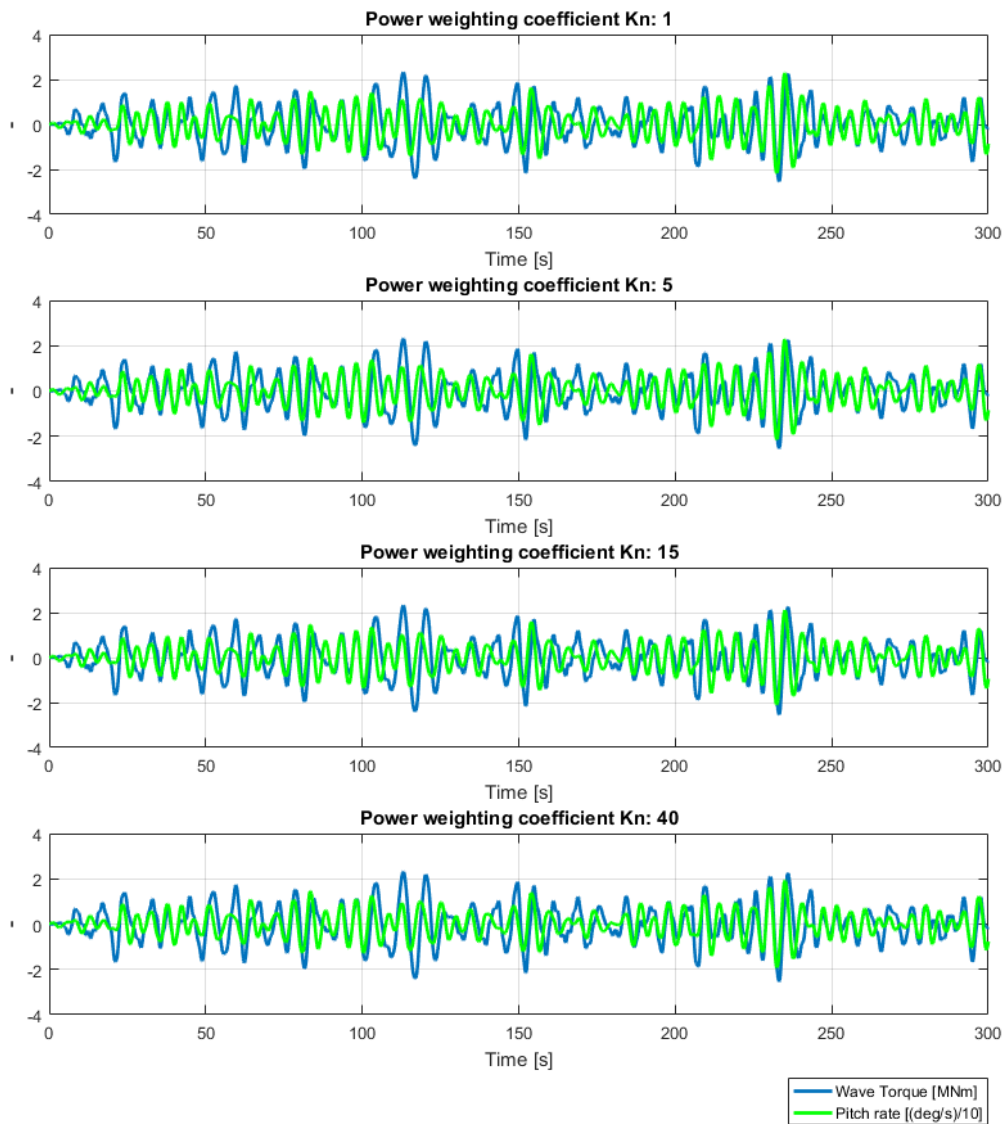


Figure 6.23 Time histories. Effect of K_N . Wave force and floater pitch angular rate.

6.6 Power Production Comparison

A comparison about the power production realized by the controllers in different sea states conditions is performed in order to assess the performances of the control strategies presented in the chapter.

Two different ways of choosing the optimal configuration of parameters are used: the maximization of the net power and the optimization of the gross power. The first method is used in order to evaluate the performances of the device in the installation site and to compute the productivity of the WEC. The second method is interesting because it can show the influence of the different strategies in the power adsorption principle, and maybe lead to a different design of some of the components causing the main power losses: the PTO system, the bearings and the gyroscope.

6.6.1 Optimization via Time Domain simulations

First step for the analysis is to choose the set of waves objective of the simulations. In Figure 6.24 the eight waves from Pantelleria installation site environment are shown. In Table 6.1 the energy period and significant height are shown according with the wave identification number.

The set of parameters for each control architecture is different. In the following description it is illustrated, along with the overall number of simulations and the estimated computational time.

- **PD Control** The control parameters are three: the damping coefficient, the stiffness coefficient and the flywheel speed.

Damping coefficient: [5000 : 5000 : 30000] *Nms/rad* - 6 values.

Wave ID	T_e [s]	H_s [m]
1	5.5	0.5
2	6.5	0.5
3	5.5	1.5
4	6.5	1.5
5	7.5	1.5
6	6.5	2.5
7	7.5	2.5
8	8	3.25

Table 6.1 Selected wave state for comparison.

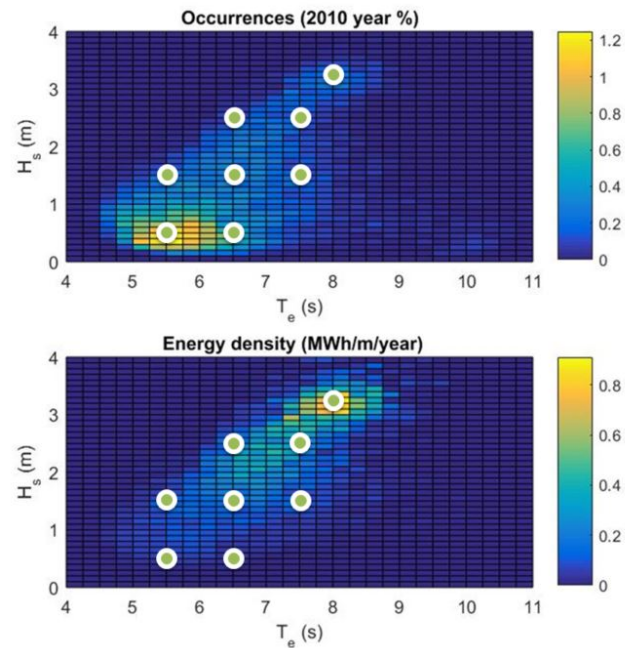


Figure 6.24 Pantelleria, Italy. Occurrences and energy scatter table for 2010. Selected wave states for the comparison.

Stiffness coefficient: $[5000 : 5000 : 35000] Nm/rad$ - 7 values.

Flywheel speed: $[50 : 50 : 500] rpm$ - 10 values.

The total number of simulation for each sea state is thus $6 \times 7 \times 10 = 420$.

Multiplying it by the number of waves to be studied, 8, the overall number of simulations is 3360.

Since the single simulation of a 900s wave lasts 50s, the overall CPU time required for the whole grid to be simulated is about 47hours.

- **DeltaRef Control** The control parameters objective for this optimization are two: the desired nominal amplitude and the flywheel speed.

Nominal Amplitude: $[40 : 5 : 60] deg$ - 5 values.

Flywheel speed: $[50 : 50 : 500] rpm$ - 10 values.

The total number of simulation for each sea state is thus $5 \times 10 = 50$.

Multiplying it by the number of waves to be studied, 8, the overall number of simulations is 400.

Since the single simulation of a 900s wave lasts 50s, the overall CPU time required for the whole grid to be simulated is about 6hours.

- **SpeedRef Control** The control parameters objective for this optimization are two: the damping parameter and the flywheel speed.

Damping parameter: $[5000 : 5000 : 35000]$ Nms/rad - 7 values.

Flywheel speed: $[50 : 50 : 500]$ rpm - 10 values.

The total number of simulation for each sea state is thus $7 \times 10 = 70$.

Multiplying it by the number of waves to be studied, 8, the overall number of simulations is 560.

Since the single simulation of a 900s wave lasts 50s, the overall CPU time required for the whole grid to be simulated is about 8hours.

- **Oscillating LQR Control** The control parameters objective for this optimization are two: the power weighting coefficient and the flywheel speed.

Power Weighting Parameter, K_N : $[5 : 2.5 : 20]$ - 7 values.

Flywheel speed: $[50 : 50 : 500]$ rpm - 10 values.

The total number of simulation for each sea state is thus $7 \times 10 = 70$.

Multiplying it by the number of waves to be studied, 8, the overall number of simulations is 560.

Since the single simulation of a 900s wave lasts 50s, the overall CPU time required for the whole grid to be simulated is about 8hours.

- **Continuous Rotation LQI Control** The control parameters objective for this optimization are two: the desired nominal amplitude and the flywheel speed.

Power Weighting Parameter, K_N : $[10 : 5 : 40]$ - 7 values.

Flywheel speed: $[50 : 50 : 500]$ rpm - 10 values.

The total number of simulation for each sea state is thus $7 \times 10 = 70$.

Multiplying it by the number of waves to be studied, 8, the overall number of simulations is 560.

Since the single simulation of a 900s wave lasts 50s, the overall CPU time required for the whole grid to be simulated is about 8hours.

Looking at the overall time required for the optimization, it is clear how the number of free parameter is a fundamental quantity that enters in the definition of an "optimal control" strategy. Less number of parameter implies less time during the optimization and therefore the sea tuning phase.

All the previous illustrated configurations of parameters have been simulated using the numerical models presented in Chapter 2, using a gridding approach. The results of the analysis are presented in the following sections.

6.6.2 Results - Net Power optimization

The first optimization method is to maximize the net adsorbed power. For each control strategy the configuration that maximize this index is found. In the following Figures, for each sea state, identified with the wave ID, some quantities of interest are shown. Through the observation of such synthetic results, it is possible to draw some suggestion about their quality and optimality.

In first Figure 6.25, the adimensionalised net power adsorbed is showed. For all the waves the PD control registers the best performances. The oscillating controls, both model-based and model-free are following. The LQR in averages -7.01% and the DeltaRef -13.9% for the waves 3 : 8. The continuous rotation control is worst in both cases. Moreover, the continuous rotation control is not able to work in small height sea states and the device must be powered off. The main reason for which the continuous rotation control is performing bad can be understood looking at Figure 6.26: the losses are almost the double with respect to any other oscillating control strategy. An interesting information is also that both the LQR and the DeltaRef oscillating controls cause less losses on the bearings system with respect to the PD. In particular the LQR in the case of small waves height (less intervention of the nonlinear term) losses are definitely less. In the case of PTO power losses presented in Figure 6.27 the continuous rotation controllers are performing worse than the oscillation ones. This can be due to the motor power required for keeping the system in rotation even in case of irregular phase forces changes. The LQR PTO losses are bigger than the DeltaRef control. For what concern the last Figure 6.28, it can be noticed that the torque rms is the most constant quantity. Only the DeltaRef control seems to require less torque with respect to the others. It is in fact synchronized with the floater motions, and thus the PTO is never working counter-phase with the gyroscopic torque.

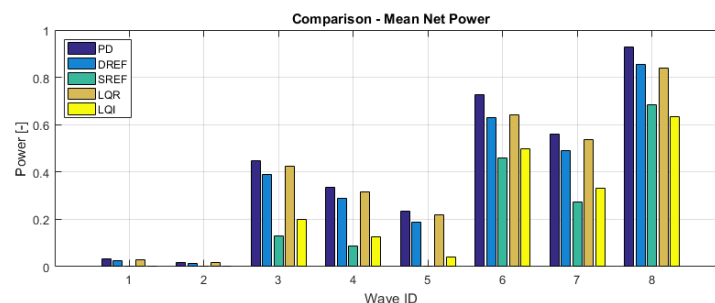


Figure 6.25 Adimensionalised mean net adsorbed power. Sea states describing Pantelleria site.

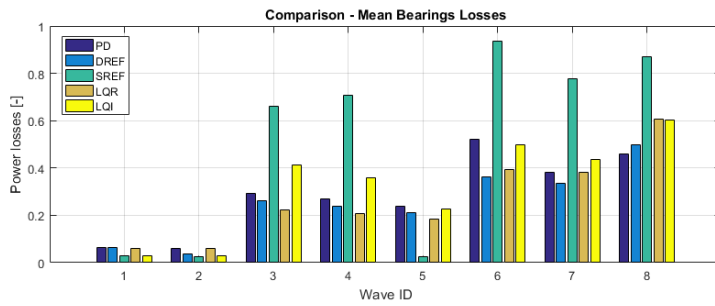


Figure 6.26 Adimensionalised mean bearing losses. Sea states describing Pantelleria site.

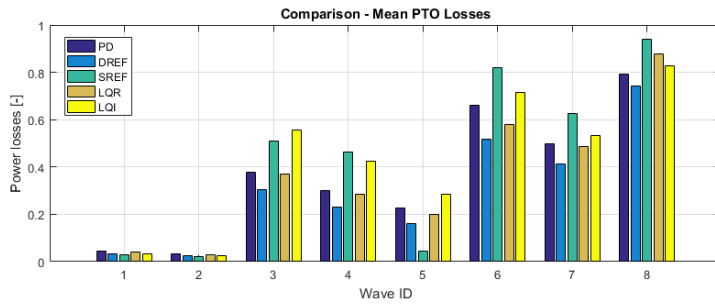


Figure 6.27 Adimensionalised mean PTO losses. Sea states describing Pantelleria site.

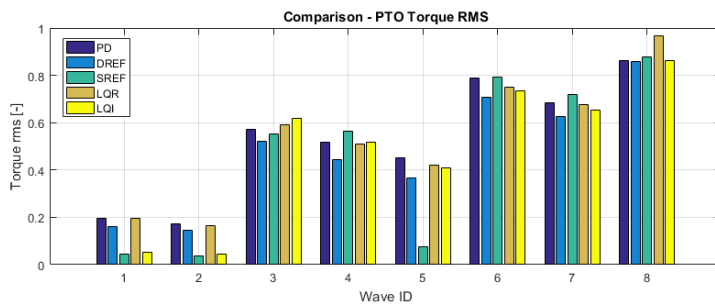


Figure 6.28 Adimensionalised PTO torque RMS. Sea states describing Pantelleria site.

6.6.3 Results - Gross Power Optimization

The second method of optimization is to maximize the adsorbed gross power (Figure 6.29). Even if this can't be used in the computation of the productivity, it can be useful to work with this perspective in order to understand what are the phenomena involved in the power conversion and what are the conversion capabilities of the floater, remembering that it is the first power conversion instrument. The architecture that maximizes the power adsorption is the PD, the proportional-derivative, control. The second architecture, the LQR, has a percentage difference from it of -11.04% and the DeltaRef of -17.29% , always on waves 3:8. Meanwhile the gross production for different strategies is not so different, looking at the bearings losses in Figure 6.30 the situation changes. The continuous rotation control strategies bearings losses are almost the double with respect to the others, and both the model-based and the model-less oscillating controls cause less losses on the flywheel bearings. The PTO losses are shown in Figure 6.31. The oscillating strategies always present high values of PTO losses, this time almost equal to those of the PD. The oscillating strategies present lower values. For what concern the PTO torque it is difficult to draw conclusions, since all the values have about the same values.

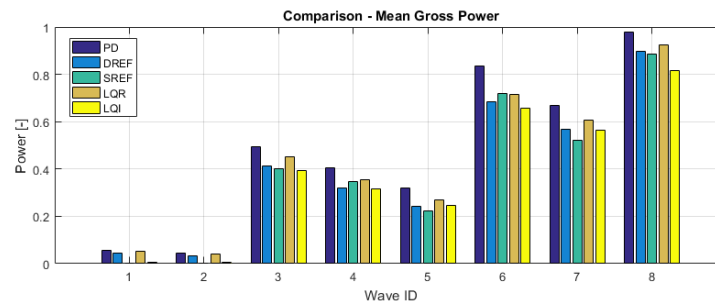


Figure 6.29 Adimensionalized mean gross adsorbed power. Sea states describing Pantelleria site.

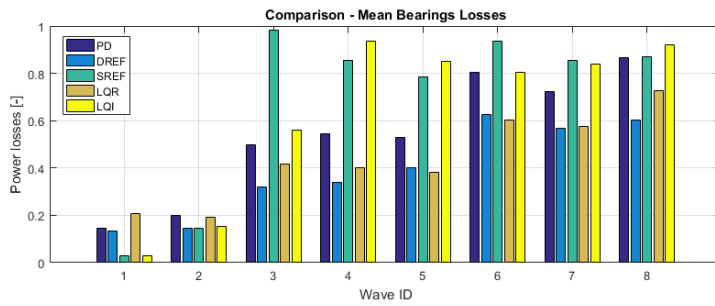


Figure 6.30 Adimensionalized mean bearing losses. Sea states describing Pantelleria site.

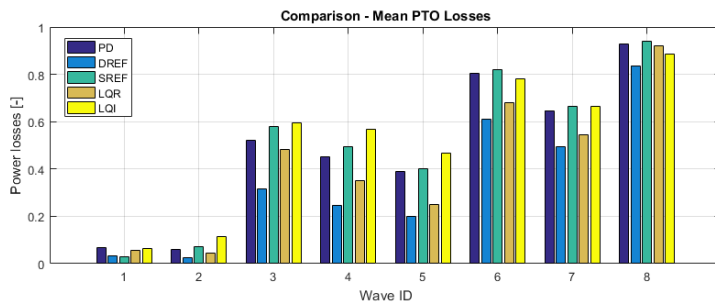


Figure 6.31 Adimensionalized mean PTO losses. Sea states describing Pantelleria site.

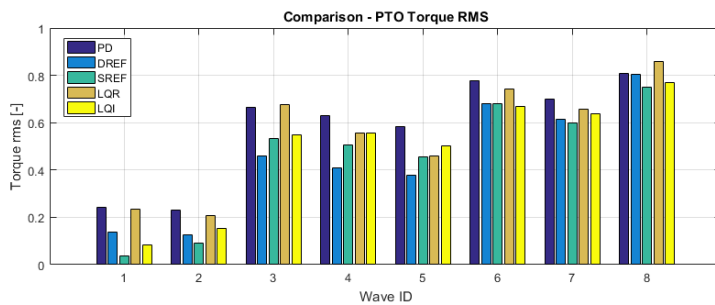


Figure 6.32 Adimensionalized PTO torque RMS. Sea states describing Pantelleria site.

6.7 Conclusions

In this section the conclusion of the whole study about the possible approaches for controlling the ISWEC are presented. At the end some possible developments are advised.

The first point must deal with the productivity. The most productive architecture is the PD, the proportional-derivative control. This technologically robust architecture reaches the best performances with the numerical environment. Following, the oscillating control strategies are not so far and the continuous rotation give the least interesting values of adsorbed power.

Another interesting point is that in the case of a gross power optimization, all the strategies reach similar values. This can be a clue that the limit of the first conversion step are reached. If so, the objective of the control has to be also to simplify the problem.

The simplification of the problem comes in two different ways: the development of less sensitive strategies with respect to the modeling errors and the reduction of control parameters, for reducing the optimization and tuning time. The first objective is reached with model-free strategies, the second with the model-based optimal control applications. The results obtained are interesting and satisfactory in the cases of oscillating controls.

The continuous rotation strategies are performing worse with respect to others but, since their main problem is in the bearings losses, it is possible to state that with a new ISWEC design focused on the problem could make them competitive.

Some synthetic conclusions are represented in following Figures 6.33,6.34 and 6.35.

	Model Based	Model - Less
Oscillating	Linear Quadratic Regulator (LQR)	Proportional-Derivative (PD)
	Model Predictive Control (MPC)	Position Control (deltaREF)
Continuous Rotation	Linear Quadratic Integral Control (LQI)	Speed Control (speedREF)

Productivity

GOOD
 MODERATE
 BAD

Figure 6.33 Control strategies comparison. Productivity.

As a last remark, some hints for a further research activity.

In this thesis the continuous rotation strategies have just a constant speed reference.

	Model Based	Model - Less
Oscillating	Linear Quadratic Regulator (LQR)	Proportional-Derivative (PD)
	Model Predictive Control (MPC)	Position Control (deltaREF)
Continuous Rotation	Linear Quadratic Integral Control (LQI)	Speed Control (speedREF)

Number of parameters to be optimized per single sea state:

1	2	3
---	---	---

Figure 6.34 Control strategies comparison. Number of free parameters.

	Model Based	Model - Less
Oscillating	Linear Quadratic Regulator (LQR)	Proportional-Derivative (PD)
	Model Predictive Control (MPC)	Position Control (deltaREF)
Continuous Rotation	Linear Quadratic Integral Control (LQI)	Speed Control (speedREF)

Expected robustness to numerical model uncertainties

GOOD	MODERATE	BAD
------	----------	-----

Figure 6.35 Control strategies comparison. Robustness against modeling and forecasts errors.

More intelligent and adaptive algorithm have been studied and tested (autoregressive methods and Kalman filters for identifying the pitch average oscillating period) but the performances were basically not varying. This can be due both to the correct use of the speed reference both to the "instantaneous frequency" definition itself.

The introduction of an estimation of the forcing wave is required. As seen in the section about optimal control with know waves, section 6.5.1, in optimal conditions the floater pitch rate is in phase with the wave forces. In all the strategies studied afterward this result was not reached. The development of strategies taking into account the waves could improve the performances of model-based optimal controls. An MPC implementation of the control of the time varying LQR could be the best solution, especially for oceanic more linear devices.

The introduction of the wave force could also be interfaced with model-less strategies, slightly changing their objective.

Chapter 7

Experimental Campaign: 2015

7.1 Introduction

The full scale ISWEC device designed for the Pantelleria site was launched and installed in August 2015. The first experimental campaign period was from August up to December 2015, then the system was taken into port for system upgrades. During this testing period the key components and the working principles were tested in real sea environment. The sea tests have been a key step in the development of the concept, an unique opportunity to verify the technology and to face the real environment issues. In this chapter the first experimental campaign is described.

7.2 The installation progress

During the first installation the system was tested in an uncompleted configuration. Aim of this section is to report the progress of the installation at the time.

- **Mooring System** The bow mooring system was completely installed. This is the first architecture designed for the device, since it is designed to allow the system to passively self-align with the incoming wave front.
- **Floater** The floater was complete but no electric cable and no aft mooring interfaces were predisposed.
- **Gyroscopes** Only the vacuum chamber gyroscope was installed. The second group was during its production and assembly phase. In place of the second unit, in order to balance the floater, a concrete block was allocated.

- **Electric Infrastructure** The electric cable and the interface to the island grid were not built yet. The power production was dissipated during the harvesting phase. This was anyway a significant problem, because the system had to be switched on, with a gyroscope group only, and the flywheel had to be accelerated using the electric batteries on-board.

7.3 Experimental data

Data log operations were managed by the cRIO 9081, as explained in section 5.6. The logged quantities are summarized in the following Table 7.1.

Two time histories examples are presented in following Figures 7.1, 7.2. The first is taken from the first days after the installation and the hydrodynamic behavior of the floater can be seen. The second is a time interval in which the ISWEC was powered on, an the torques and power fluxes can be seen. The first picture shows some data recorded the 8th of August 2015 at 8:30 am. The sea state was characterized by an energy period of 4.42 s and a significant height of 0.55 m with a power density of 0.66 kW/m. Both the flywheel and PTO electric drives were switched off, in fact their signals are equal to zero. The floater is pitching quite a lot, if compared to the very low wave height. Something that can be immediately seen is that the hull is rolling as well. This can be due to multiple factors. First of all, even if in tank tests, with directional waves, the scaled devices were almost completely not rolling, the roll stiffness is still quite low. In case of a not perfect alignment or of multi-directional waves, this can result in relevant oscillations about this axis. The problem of misalignment was particularly acute in correspondence of small energetic and ample waves, when the wave itself can't push enough the floater in order to align it. Moreover, already during the mooring system installations, the problem of intense transversal currents arose.

Table 7.1 All the logged data and system parameters.

<i>Low Sampling Period (0.1s)</i>	<i>High Sampling Period (10s)</i>	<i>When requested by the User</i>
Floater movements, PTO axis position, speed, PTO torque and power, Flywheel speed, Overall electrical power, PTO electrical power	GPS position, Ultra Capacitor temperatures, Cooling system temperatures	The "Expert list", all the parameters of the machines.

This impact was undervalued, but it still cannot be neglected for the least energetic sea states.

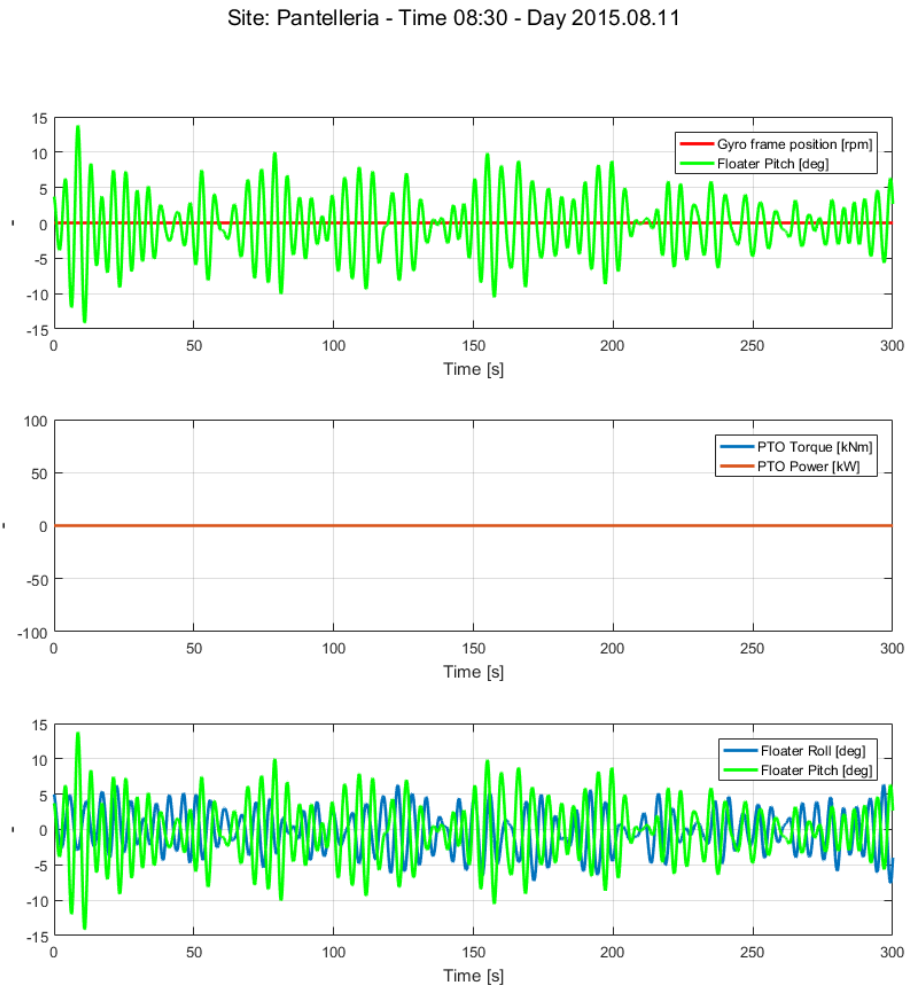


Figure 7.1 Experimental data. Pantelleria. Example of the floater kinematics with conversion system off.

The second time history presented in Figure 7.2 is of the 20th of November 2015 at 09:58 pm. The incoming waves had an energy period of 6.83 s and a significant height of 2.58 m with a power density of 22.27 kW/m. In this case the device was powered on and the flywheel speed in the time interval shown was set to 200 rpm. In the top graph the internal gyroscope frame axis and the floater pitching motion are plotted. Starting from the floater, its pitch motion is relevant and exceed the value of 10 deg multiple times. This happens even if the flywheel and the PTO are working for damping the system motions. The gyroscope frame axis is oscillating with an amplitude of 50 deg.

After 250s the automatic machine moves to the *safety* case. The flywheel rotation axis is set to be horizontal thus avoiding the exchange of gyroscopic torques. After some seconds it is moved back to zero and then the harvest phase restarts. In the second plot the PTO torque and speed are presented. The torque was here saturated to the nominal torque of the electric motor, in order to avoid hazards. The electric power adsorbed by the PTO is represented in red. It can be noticed that even if the system is choked (one gyroscope, maximum torque at nominal, reduced flywheel speed) and no tuning phase was previously preformed, the system is producing and the conversion concept works well also into the sea environment. In the third graph, the floater roll motion is added to the pitch. It can be noticed that the system has a relevant roll motion. This suggests that some more deep analysis has to be carried out about the planar hypothesis of the hydrodynamic model.

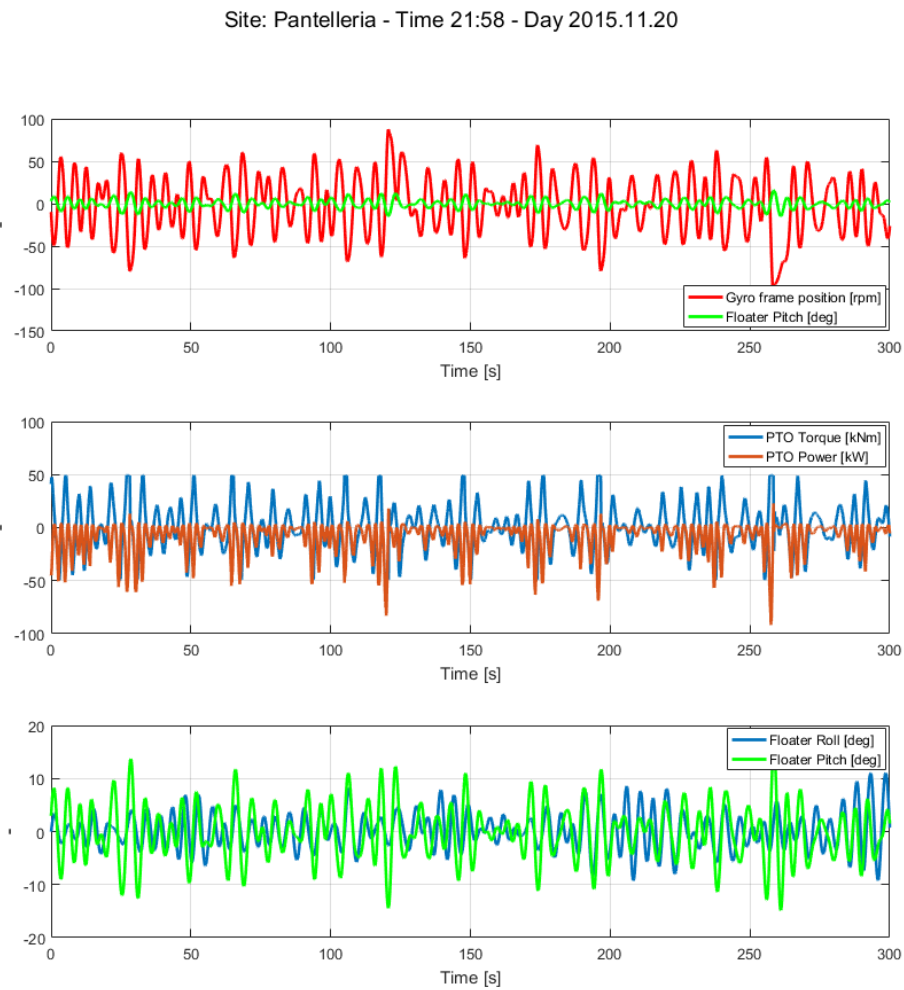


Figure 7.2 Experimental data. Pantelleria. Example of the floater and conversion system behaviour.

7.4 Validation

The first use of experimental data was for numerical models validation. Starting from the PTO technology, going through the mechanical model up to the most challenging phenomenon, the floater hydrodynamic interaction with the sea surface. All the comparisons presented in this chapter deals with the wave power conversion concept technology. The validation of mechanical losses, plant losses and others auxiliary systems is not addressed.

7.4.1 Controller and PTO

The first part to be validated is the controller technology. The controller action, the PTO torque, is analysed. In the second part a validation of the quasi-static modeling approach of the PTO drive is performed. The experimental and the simulated mechanical and electric power fluxes are compared.

As shown in Figure 7.3, the time histories of the experimental kinematics of the internal gyroscope frame axis are given as input to the controller block of the numerical model. The simulated resulting torque is given as input with the PTO speed to the losses subsystem. In this block the static relationship explained in section 2.3.4 is implemented in a look-up-table. Then both the simulated torque and the PTO losses are saved. In post-processing the simulation results are compared with the experimental data.

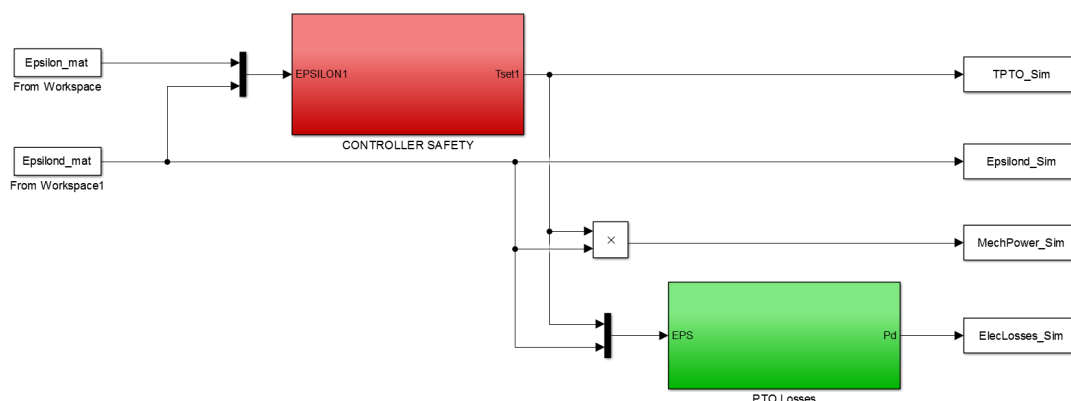


Figure 7.3 Experimental data. Pantelleria. Example of the floater and conversion system behaviour.

Looking at the comparison proposed in Figure 7.4, in the top left corner graph the experimental and simulated torque are plot. For all the tests the rms error between the PTO feedback torque and the PTO simulated one stays in the range of $\pm 1\%$. This very small error can be easily justified by the very slow dynamics of the actuation required, due to the slow oscillations of the system. In the top right corner the experimental gyroscope frame position and speed shown. These are several order of magnitude slower than the sum of the drive and PTO electric actuation system. In the bottom left the comparison between power fluxes is proposed. Both the mechanical and electrical power are well described by the model. The average values of these quantities in the time range proposed, $[240\ 260]$ s, are reported in Table 7.2.

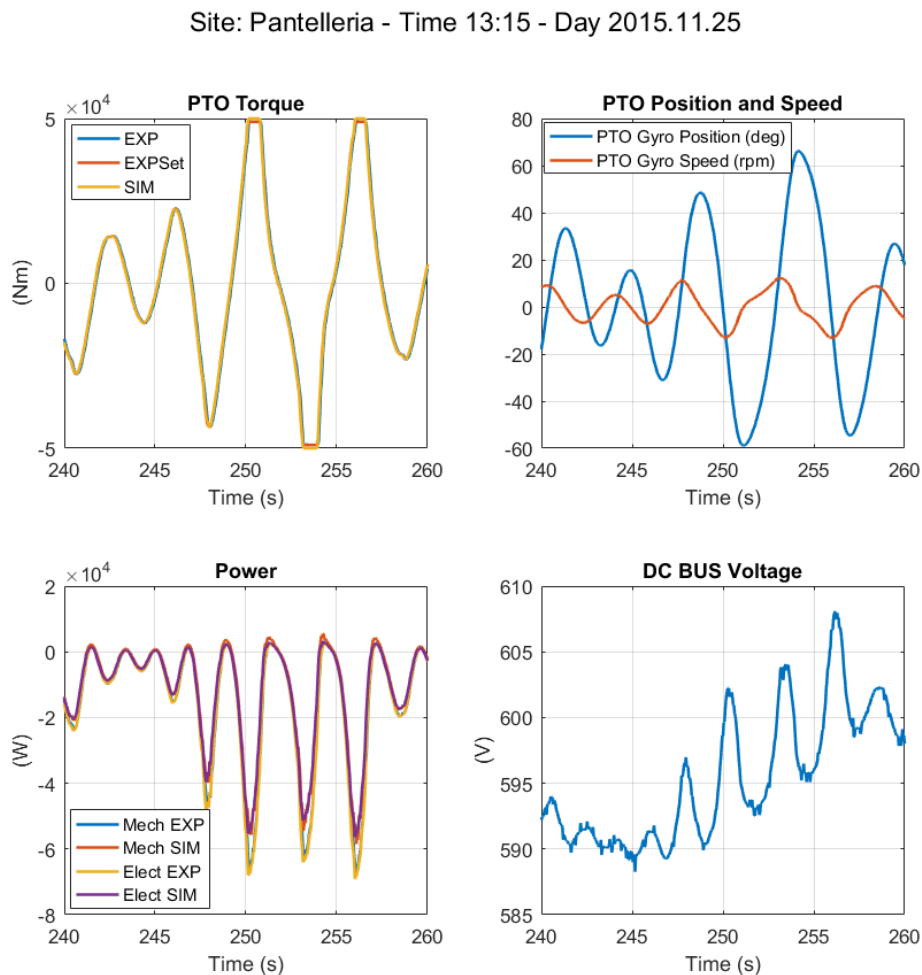


Figure 7.4 Experimental data. Pantelleria. Example of the floater and conversion system behaviour.

Table 7.2 Pantelleria. Experimental and simulated comparison. 25th November 2015. Average power fluxes of [240 260] s range.

25 th November 2015			
Average Mechanical Power	[kW]	Average Simulated Power	[kW]
Experimental	-14.9	Experimental	-12.0
Simulated	-15.6	Simulated	-12.4

Also the power fluxes modelization is acceptable and can be considered validated in this condition. It must be noticed the behavior of the voltage over the DC BUS, continuously increasing during the most intense power adsorption cycles.

An unmodelled phenomenon with respect to the full scale sea device is in fact the system protection for DC BUS overvoltage conditions. This happens when the system is working correctly and it is adsorbing considerable power. In the final installation, the DC BUS will be controlled by the grid DC/AC inverter that will deliver more power to the grid. In the 2015 experimental campaign anyway, this safety control happened to act multiple times, and its effect must be described. In Figure 7.5 an example of such situation is presented. When the system is producing well, the gyroscope internal shaft has the correct phase with respect to the floater motions and the wave incoming torque, the system have a good adsorption response. The DC BUS accumulates energy and its voltage rises. A safety controller ask the systems to position around the horizontal position and the power adsorption is interrupted. At the present stage, this electric capacitance is not modeled, and in fact there are big differences both in torque actuation and in power fluxes around these points. These differences must be taken into account while analyzing the results of the next sections.

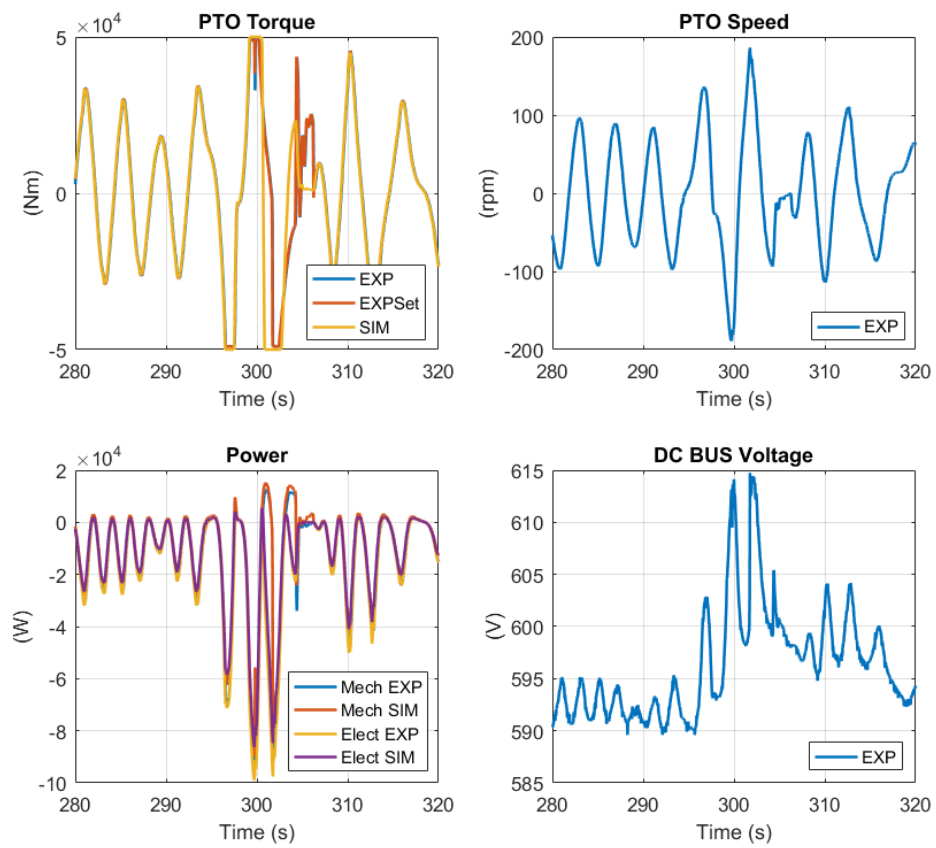


Figure 7.5 Experimental data. Pantelleria. Experimental and simulation comparison. Over-voltage protection system effect.

7.4.2 Mechanics

The second step in the validation has been the verification of the internal overall electro/mechanical system. The floater motions have been given as kinematic input to the mechanical simulation system, in analogy with the floater hydrodynamic modeling. The reaction torque computed by the model is sinked. For what concern the internal gyroscope frame axis, it is controlled in position by the controller subsystem, already validated in the previous section 7.4.1. In Figure 7.6 the scheme is presented.

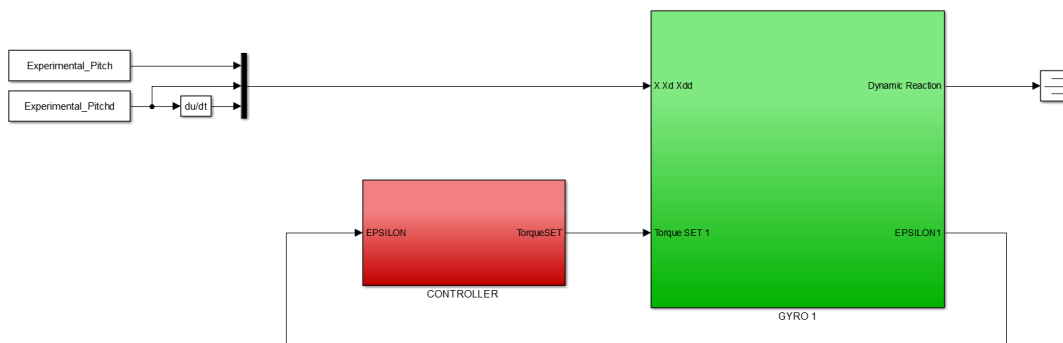


Figure 7.6 Experimental data. Pantelleria. Example of the floater and conversion system behaviour.

An example of the analysis carried out for one sea state is hereafter described. The data from the 28th of November 2015 at 04:03 pm is used. The results are shown in Figure 7.7 and their synthetic description is in Table 7.3. The correlation of the overall system numerical model is again very good. However some differences especially in amplitude can be seen already at the kinematics level. This discrepancy affects the torque given by the control and, for error propagation, it is amplified in the PTO mechanical power evaluation. In any case, the power is still simulated accurately. A quantitative evaluation can be given through the computation of the rms error for the gyroscope frame axis position and speed, and the PTO torque. Also the percentage difference between the average adsorbed power in simulation and experiments is a key factor for evaluating the performances of the model. For this data set, the rms errors are all below the 6% threshold. The average power is overestimated by the model of about the 16%.

The same analysis has been repeated for all the data sets analyzed. Since in some cases the control system was corrupted and the internal gyroscope frame axis was uncontrolled, causing multiple complete rotation around ε , all the tests with an this phenomena have been neglected. The results of the analysis are proposed in Figure 7.8.

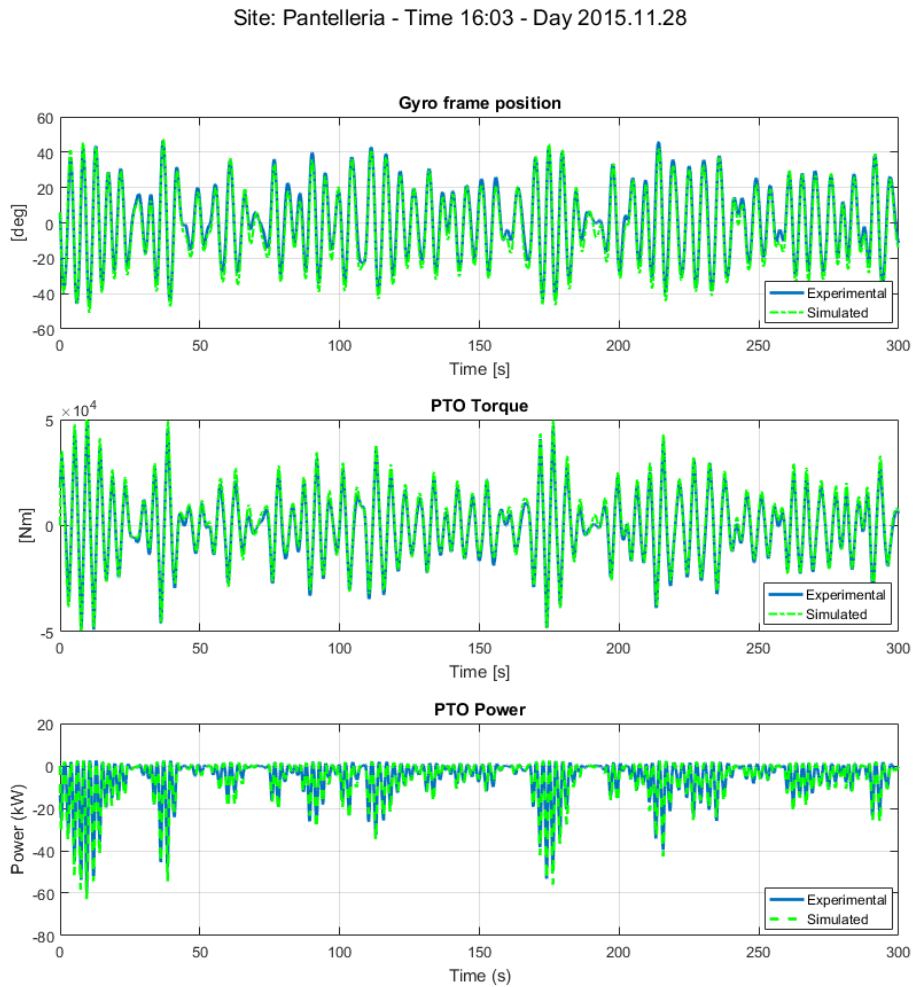


Figure 7.7 Electro-mechanical system validation. Single wave internal system quantities comparison. Time histories.

Since for all the data sets the simulation is overestimating the motions and the power, a next possible step could be to identify a dissipative term for the internal precession shaft.

A conclusion that can be drawn from this analysis is that the internal model of the ISWEC is quite accurate and with some upgrades could bring reliable results about the estimation of loads and the productivity of the device. These two facts are fundamental for the model-based design approach used, especially for the future developments of the system.

Table 7.3 Electro-mechanical system validation. Single wave internal system quantities comparison (Site: Pantelleria - Time 16:03 - Day 2015.11.28). Synthetic results.

Test number 44	Experimental	Simulated	Relative Error
ϵ_{rms}	19.99 deg	20.99 deg	5.02%
$\dot{\epsilon}_{rms}$	4.20 rpm	4.39 rpm	4.64%
$Torque_{gyro,rms}$	15.2 kNm	16.1 kNm	5.95%
$Power_{mechanical,mean}$	5.23 kW	6.08 kW	16.2%

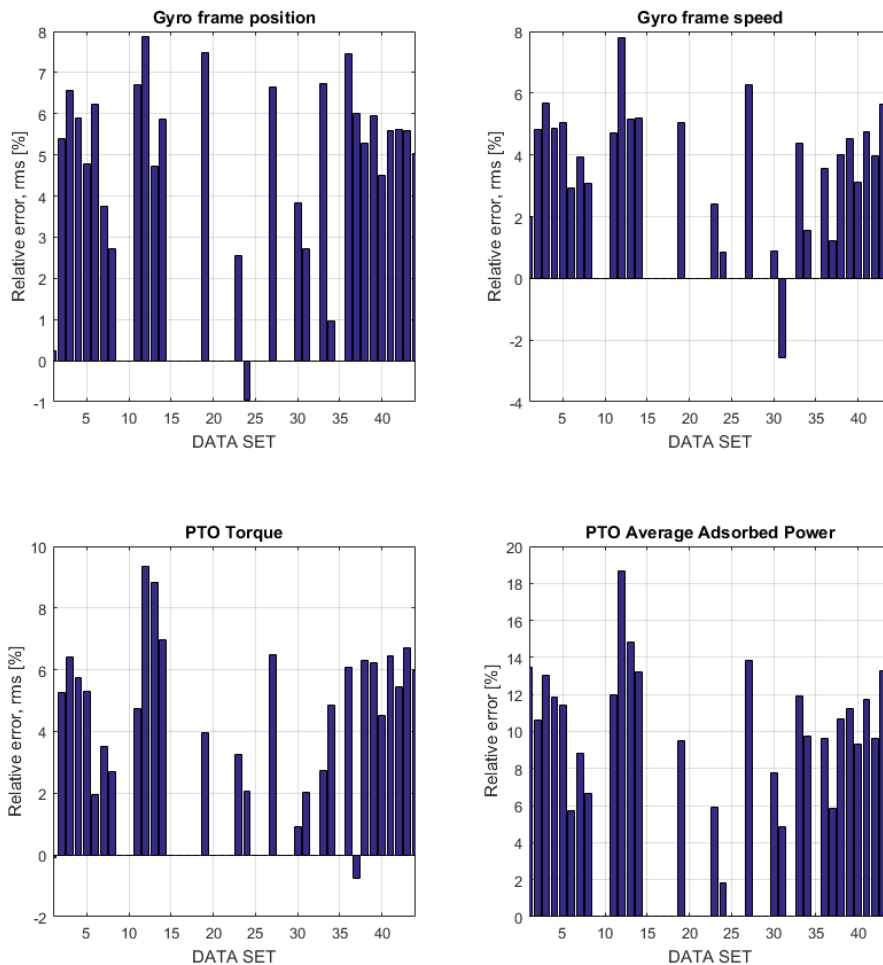


Figure 7.8 Electro-mechanical system validation. Data Set synthetic results.

7.4.3 Hydrodynamics

The validation of the hydrodynamic modeling is the most challenging part in the overall wave energy technology domain. First step in the analysis of the results, is to

review some of the design assumptions used for the hydrodynamic interaction.

The system main assumptions:

- *Self-aligning mooring system* The system is able to passively self orientate with respect to the main wave front.

and the model main hypothesis

- *Planar model* The hydrodynamic main effects can be described with a 2D approximation of the floating device motions.
- *Currents* The effect of the subsea currents is negligible if compared with the mean drift forces due to the waves.
- *Directionality* The sea states are thought as mainly unidirectional for the Pantelleria installation site.

Immediately afterwards the sea installation the system broadly oriented in the correct direction, showing the same behaviour that the scale prototypes already had in the simpler tanks environment. When the sea states became more energetic and a visible wavefront occurred, it was clear that not always the system was completely oriented. It sometimes had a misorientation with respect to the forward direction, sometimes even of relevant angles. As first intervention, the installation and arrangement of the sea state and currents sensor was predisposed. The information of currents was in fact not working at the time. As a further action, the design of an aft mooring capable of keeping the system oriented toward the prevailing direction started. Anyway this unforeseen phenomenon must be taken into account during the comparison analysis of the experimental data. The results are in fact partial and there is not the complete required data.

Three data set have been used for the comparison. They are presented in Table 7.4. Each single test record is 20 minutes long. The first set is characterized by waves with a wave energy period near $4s$, the second close to $5.5s$ and the third of about $6.5s$. The wave height is increasing with the period, describing the common sea states present in Pantelleria. In all these configuration the internal electro-mechanical system was powered off, so the hydrodynamic interaction between the floater and the sea can be verified.

In Table 7.5 some synthetic results about the comparison between the experimental and simulated kinematics of the floater are presented. Thinking at the planar modeling,

Table 7.4 Data set used for a first hydrodynamic comparison between experimental and numeric data. Site: Pantelleria, Year: 2015.

<i>26th October 2015</i>				
<i>Test ID</i>	<i>Time</i>	<i>En. Period [s]</i>	<i>Sign. Height [m]</i>	<i>Power Density [kW/m]</i>
1	10:22	4.06	0.59	0.69
2	11:22	4.31	0.60	0.76
3	12:22	4.14	0.67	0.92
4	13:22	4.26	0.72	1.07
5	14:22	4.27	0.64	0.86
<i>21th November 2015</i>				
<i>Test ID</i>	<i>Time</i>	<i>En. Period [s]</i>	<i>Sign. Height [m]</i>	<i>Power Density [kW/m]</i>
6	13:22	5.58	1.54	6.49
7	14:22	5.51	1.41	5.36
8	15:22	5.62	1.45	5.81
<i>30th November 2015</i>				
<i>Test ID</i>	<i>Time</i>	<i>En. Period [s]</i>	<i>Sign. Height [m]</i>	<i>Power Density [kW/m]</i>
9	10:22	6.33	2.20	14.96
10	11:22	6.53	2.68	23.02
11	12:22	6.57	2.30	17.01
12	13:22	6.41	2.22	15.48
13	14:22	6.48	2.05	13.29
14	15:22	6.51	1.97	12.37

only the pitch and heave DOFs are examined. This is due to the fact that the surge motion is very difficult to be logged from one hand, and on the other the overall modeling of the mooring system and the subsea currents is quite complex. Another DOF processed is the roll. For each of these three states, the rms value of the experimental time series associated with the test is proposed. Simulations only give the results of the pitch and heave. The relative error of the simulations with respect to the real data is computed.

The first two data set to be examined are the 26th of October and the 30th of November. During these tests the device was likely oriented in the correct way. The environmental situation can be portrayed as in Figure 7.9. The floater experienced a roll motion, even if smaller with respect to the pitch. This behavior does not happen during unidirectional tank tests, and is probably due to some transversal wave component coupled with the small hydrostatic roll restoring forces. The second degree of freedom of interest, the most important for the power conversion, is the pitch. The rms error between experiments and numeric results is quite low. In average it is below the 10% threshold. This result for these two data set can be considered as good. Looking

Table 7.5 Results of the hydrodynamic comparison between experimental and numeric data. Site: Pantelleria, Year: 2015.

<i>26th October 2015</i>							
<i>Test ID</i>	<i>Roll rms [deg]</i>		<i>Pitch rms [deg]</i>		<i>Heave rms [m]</i>		
	<i>EXP</i>	<i>EXP</i>	<i>SIM</i>	<i>Rel. Error</i>	<i>EXP</i>	<i>SIM</i>	<i>Rel. Error</i>
<i>1</i>	0.93	2.42	2.40	-0.8%	0.122	0.104	-14.8%
<i>2</i>	0.90	2.52	2.55	1.2%	0.116	0.113	-2.6%
<i>3</i>	0.94	2.34	2.40	2.5%	0.110	0.105	-4.6%
<i>4</i>	0.98	2.48	2.40	-3.2%	0.108	0.104	-3.7%
<i>5</i>	0.96	3.08	2.71	-12.0%	0.146	0.116	-20.6%
<i>21th November 2015</i>							
<i>Test ID</i>	<i>Roll rms [deg]</i>		<i>Pitch rms [deg]</i>		<i>Heave rms [m]</i>		
	<i>EXP</i>	<i>EXP</i>	<i>SIM</i>	<i>Rel. Error</i>	<i>EXP</i>	<i>SIM</i>	<i>Rel. Error</i>
<i>6</i>	2.66	3.80	4.37	15.0%	0.350	0.305	-12.9%
<i>7</i>	2.65	3.53	4.41	24.9%	0.357	0.317	-11.2%
<i>8</i>	2.75	3.82	5.16	35.1%	0.380	0.384	1.1%
<i>30th November 2015</i>							
<i>Test ID</i>	<i>Roll rms [deg]</i>		<i>Pitch rms [deg]</i>		<i>Heave rms [m]</i>		
	<i>EXP</i>	<i>EXP</i>	<i>SIM</i>	<i>Rel. Error</i>	<i>EXP</i>	<i>SIM</i>	<i>Rel. Error</i>
<i>10</i>	2.64	5.24	5.97	13.9%	0.57	0.54	-5.3%
<i>11</i>	2.51	4.73	5.37	13.5%	0.50	0.54	8.0%
<i>12</i>	2.29	5.15	5.43	5.4%	0.47	0.49	4.3%
<i>13</i>	2.16	5.42	5.28	-2.6%	0.46	0.52	13.0%
<i>14</i>	2.18	5.49	5.28	-3.8%	0.45	0.46	2.2%

at the situation for the heave, it seems that in general for small period and height the model is underestimating it, meanwhile for higher values it is overestimating. This analysis is of course qualitative, since a more extensive campaign has to be carried out.

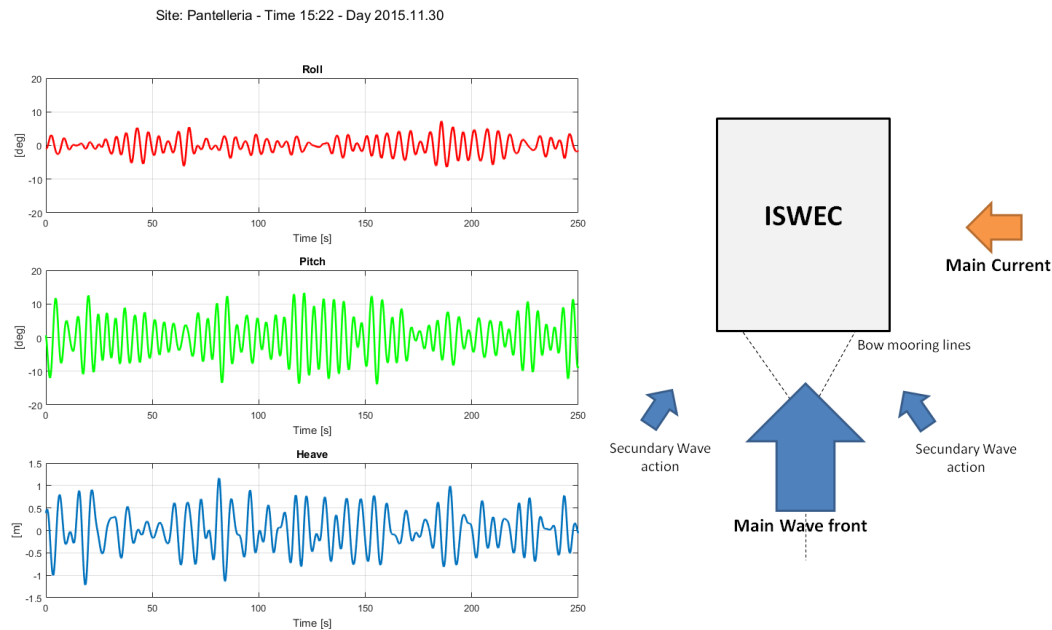


Figure 7.9 ISWEC sea environment installation. The wave incoming front force is predominating. The planar hypothesis are verified. Site: Pantelleria - Time 15:22 - Date: 2015.11.30

Another interesting observations can come looking at the data coming from the 21st of November. The wave with Test ID 7 is shown in Figure 7.10. Looking at the bigger relative error especially in pitch, it can be inferred that in this case the model is not enough for describing the phenomenon. Usually when simulations results are not matching, there are bigger roll motions even comparable with the order of magnitude of pitch. In the case of this set, this can be seen both from the synthetic results of the table both looking at the time history in figure. In this cases it is possible to state that the planar model is not enough and that forces caused by unmeasured currents or three dimensional waves could cause misalignment that change the interaction between the floater and the wave front. This situation is schematically represented in Figure 7.10.

Two kind of solutions are explored in order to deal with this issue: a systemic solution and a modeling one. The first idea is about upgrading the mooring system with an aft mooring architecture, designed to keep the ISWEC oriented in a specified

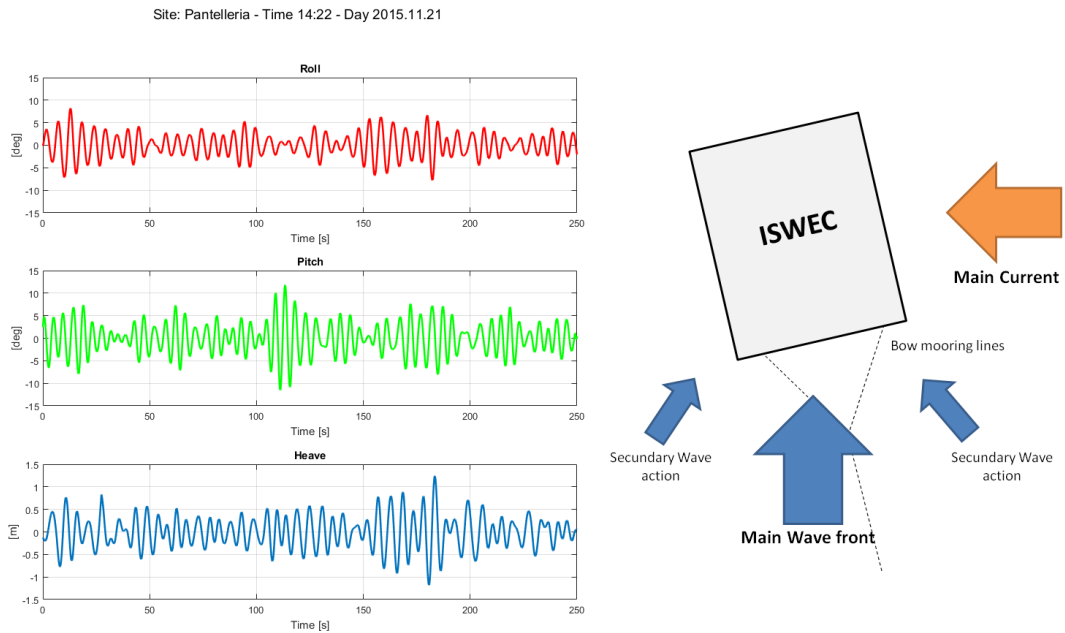


Figure 7.10 ISWEC sea environment installation. The wave incoming front force is predominating. The planar hypothesis are verified. Site: Pantelleria - Time 14:22 - Date: 2015.11.21

direction. This solution is showed in Figure 7.11 and should partially solves the problem while involving the loss of mooring self-alignings property.

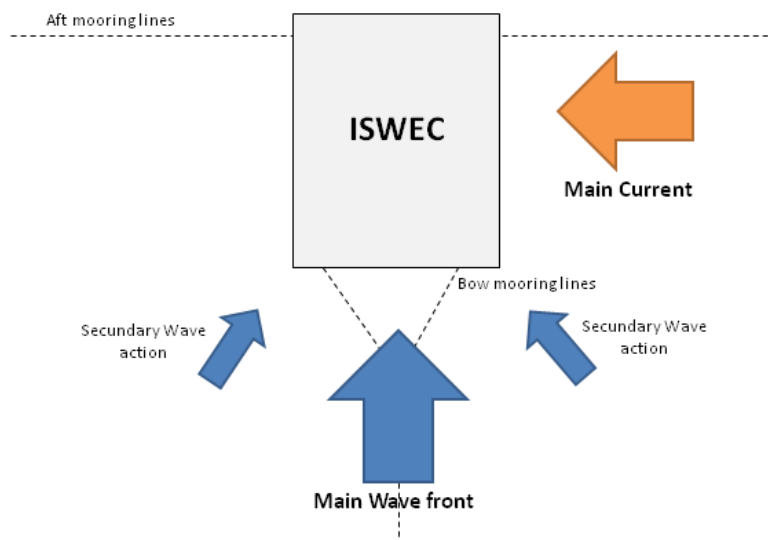


Figure 7.11 A proposed aft mooring architecture for solving the issues of misalignment in an high directional site.

Table 7.6 Data set used for a first wave to mechanical power comparison between experimental and numerical data. Site: Pantelleria, Year:2015.

Test ID	Day	Time	En. Period [s]	Sign. Height [m]	Pow. Density [kW/m]
1	7 Oct 2015	11:22	4.87	1.13	3.06
2	7 Oct 2015	12:22	4.95	1.14	3.12
3	20 Nov 2015	14:22	6.19	2.11	13.44
4	20 Nov 2015	15:24	6.20	2.30	16.02
5	27 Nov 2015	11:32	7.95	3.88	58.63
6	27 Nov 2015	17:22	7.83	3.45	45.73
7	27 Nov 2015	18:22	7.50	3.43	43.27
8	27 Nov 2015	20:26	7.24	3.24	37.19
9	28 Nov 2015	15:32	6.01	1.76	9.16

On the other hand the development of a full 6D simulation environment is started, in order to assess how important could be to consider these effects in the model-based design phase.

7.4.4 Wave To Mechanical Power

Last part in this first comparison between the experimental and simulated data is to assess the performances of the overall conversion system: from the waves up to the mechanical power adsorbed by the PTO. The following data set are completely free of any safety procedure. A time history of the wave elevation is taken from the AWAC installed near the ISWEC installation point. This experimental wave profile is used for generating the generalized forces acting as power input of the 3 DOF freedom model. The model complete of all its part is then run and some synthetic results are shown in next Tables 7.6, 7.7 and 7.8. The 9 waves chosen are quite heterogeneous: they have different periods and wave heights, representing the different waves states present in the occurrences scatter table of Pantelleria.

The first table of results to be examined is about the hydrodynamic behavior of the floater. It can be seen that for higher and more energetic sea states the performances of the model worsen. This can be seen especially for the pitch, where the error of the rms value can reach up to 40%.

The second table of results is about the internal mechanical system and the PTO. The absolute values of average adsorbed power have been protected for industrial reasons, anyway the final error of the model can be appreciated. The range of values

Table 7.7 Results of the wave to power comparison. Floater hydrodynamic quantities.

Test ID	Roll rms [deg]		Pitch rms [deg]		Heave rms [deg]		
	EXP	EXP	SIM	Rel. Error	EXP	SIM	Rel. Error
1	1.78	3.86	3.67	-5%	0.28	0.32	17%
2	1.71	3.65	3.72	2%	0.26	0.32	27%
3	2.44	5.05	5.15	2%	0.49	0.54	9%
4	2.82	4.91	5.55	13%	0.57	0.58	2%
5	4.12	5.78	6.87	19%	0.78	0.97	25%
6	3.70	4.84	6.12	26%	0.81	0.87	7%
7	4.00	5.13	6.34	24%	0.78	0.86	10%
8	3.67	4.64	6.48	40%	0.79	0.82	4%
9	3.33	3.58	4.36	22%	0.42	0.47	11%

Table 7.8 Results of the wave to power comparison. Electro-mechanical system quantities and power.

Test ID	Gyroscope frame angle rms [deg]			Flywheel Speed [rpm]	Avg Mechanical Power [kW]
	EXP	SIM	Rel. Error	EXP = SIM	Rel. Error
1	15.03	15.02	0%	159	-1%
2	14.53	15.15	4%	159	7%
3	15.50	16.94	9%	118	13%
4	20.17	24.31	20%	146	35%
5	30.60	34.12	11%	219	16%
6	24.76	30.15	22%	219	50%
7	25.07	30.22	21%	216	32%
8	22.56	30.21	34%	214	70%
9	18.20	21.59	19%	185	47%

varies considerably, and the model over-predict performances for the most energetic sea states. The flywheel speeds to be used have been low in this first experimental campaign. This was due to the absence of any connection to the grid and the sub-optimal performances of the floater with one gyroscope unit only.

The results can be rearranged in function of power density, wave significant height or energy period order. Their linear trend of experimental and simulations data are also plot. Looking and comparing the the experimental and simulation results, it can be stated that the simulations are overestimating the power production for most powerful waves. Anyway an higher number of tests is required in order to quantitatively assess this phenomenon.

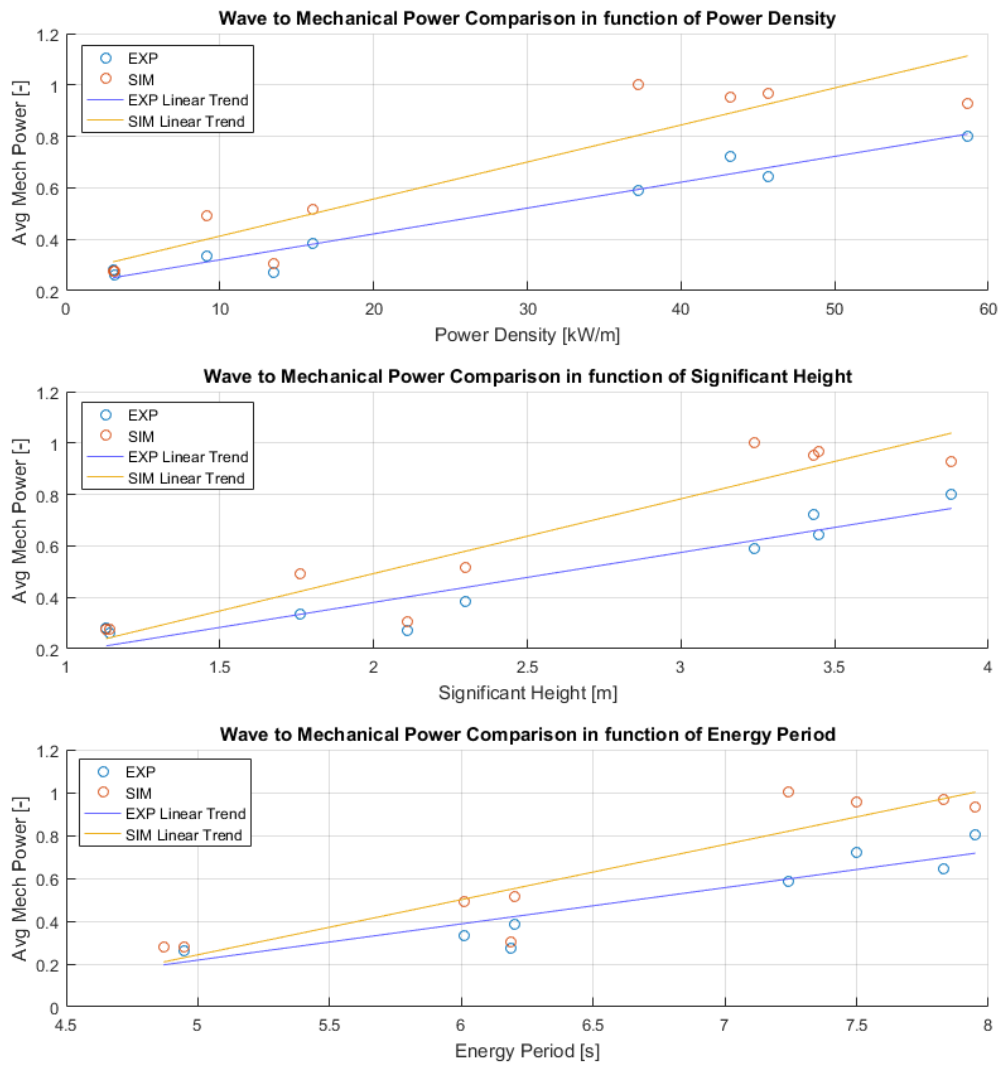


Figure 7.12 Results of the wave to power comparison. Electro-mechanical system quantities and power.

7.5 Final Comments

The numerical model has been compared and a first validation has been carried on. The main subsystems have been individually studied and then analyzed together in the last section about the wave to mechanical power analysis. In general the results are satisfactory and the final synthetic results are consistent.

Anyway some comments can be made for further developments. The numerical model developed is reliable especially for what concerns the hydrodynamic part. But the performances degrade when the internal gyroscope system is powered on and it is in working conditions. This fact has to be deeply analyzed, both looking at the different interaction that the floater establishes with the sea surfaces and the internal mechanical system, in particular with the identification of the internal gyroscope frame shaft damping components.

From the hydrodynamic modeling point of view, the planar model has to be better studied and maybe upgraded. The addition of non-linear Froude-Krylov forces could improve the description given by the model.

Some improvements of the mooring system modeling and the related experimental acquisition of relevant mooring system data have to be planned.

In conclusion, the model can be seen as a good tool for the computation of the productivity in an installation site during the model based design, in order to compute and obtain the specification useful for the pre-design and detailed design of the device.

Chapter 8

Conclusions

During the PhD program, the ISWEC full scale device for Pantelleria (Sicily) was assembled and launched. Activities of different nature have been carried out by the candidate: the development and upgrade of different numerical models, the design and implementation of the prototype SCADA software, the direct involvement in tank and sea experimental campaigns, the prototypes setup, their operations and the analysis and post-processing of gathered data. Finally, theoretical research activities have been carried out: these concerned innovative power harvesting control strategies applied to the ISWEC.

Looking at main outcomes of the experimental activities, it is possible to briefly list some major enhancements concerning the system comprehension and its mathematical description. Looking at the impact of the HMRC tank hydrodynamic tests, the identification of a quadratic viscous term has been particularly relevant. In fact it gave the opportunity of overcoming the problems related to resonances phenomena of the previously-used fully-linear hydrodynamic model. Also, the comparison between this data and the numerical simulations provided the foundations for developing a complete hydrodynamic planar model. The challenge of having the ISWEC device operating in Pantelleria has been an exciting opportunity to test and verify the working hypothesis used for years by the group during the technology development. The 2015 experimental campaign and its results enabled a first assessment of the performances of the hydrodynamic planar approach and the validation of the overall electro-mechanical system, including the quasi-static PTO efficiency maps. The results of this comparison are definitely promising: despite the inner simplifications of the design procedure, the presented model-based design approach revealed to be consistent and viable solution for the design of a wave energy converter technology.

The SCADA system, the safety algorithms and the automatic state machine performed correctly during tests, without any major failure or problem. They proved to be a reliable architecture for monitoring and remotely controlling the device. The ISWEC successfully went through the first start and it was possible to control the device via a dedicated user interface software. The data acquisition software also accomplished its task, avoiding any kind of information loss.

From a first data analysis it seems that the planar model is not sufficient for the description of the three dimensional irregular sea environment. Also currents are not taken into account. A more accurate description and modeling approach has to be discussed and implemented, always taking into account the specification of low computational resources, required for a model-based design approach.

From a technology evaluation point of view, it is still difficult to fully evaluate the technology. Sea tests verified its working principle but the data gathered at the moment is not enough for a complete validation and assessment of the ISWEC performances. Nonetheless, some system upgrades have been discussed and a few have already been integrated in the current ISWEC design: a gyroscope without the vacuum chamber and an aft mooring with viscous-elastic lines are the main novelties to be introduced. Looking at the research activities about the ISWEC power harvesting control strategies, some interesting conclusions have been stated. The advantages and weaknesses of each regulating strategy have been identified and classified. An interesting result is that after the numerical optimization phase, for what concern the gross productivity, all the strategies return very similar values of power adsorption capabilities. This suggests that the maximum possible floater conversion capabilities have been reached. The developed strategies have nonetheless different characteristics. The robustness with respect to different sea states is studied, since it is believed to drastically reduce the time requested for tuning the control system parameters of the ISWEC at sea. During next experimental phases the pitch position control loop strategy is proposed to be tested. This is chosen because of its simplicity and robustness properties.

During the three years and a half of research, experiences and efforts, several aspects of the whole project development have been considered and analyzed. Many of these could not practically be fitted into this thesis, being sensitive for Wave for Energy srl from the industrial property point of view or simply because of their incompleteness. Focusing on the latter, it is possible to outline some research activities and further work that deserve to be explored.

Starting from the modeling part, the first future step will be the introduction of a

non-linear Froude–Krylov force calculation, using the instantaneous wetted surface, both for the planar and 6DOF numerical models. Thinking at the experience into the sea, in order to deal with sea currents, also some innovative mooring architectures have to be investigated. Looking at the design procedure, it would be useful to analyze the feasibility of the introduction of the several power losses terms at the very first steps of the design procedure: in this way it could be possible to extend the range of analyzed system configurations, and to find innovative solutions. An example of new solution arised from the early analysis of the ISWEC working principle is the introduction of the eccentric mass on the gyroscope frame in order to reduce the PTO electric motor usage and thus its size (costs) [10]. For what concern the control system, the main further expected activities concern the integration and testing into the sea of the several proposed algorithms. The major expected result is the verification of the robustness of the model-free oscillating controller. The last major research path is related to the identification of the current and incoming sea states starting from on-board measurements. In this way the technology would be completely autonomous, independent from the forecasts provided by third party institutions.

As a final remark, a personal comment about the ISWEC technology. I think that this conversion principle is interesting and must be further explored. Even if the Pantelleria full scale prototype is the first version of the device, it already shows all the potentialities of the technology. Main objective now is to maximize the impact of the experiences gathered during the sea tests both for the industrial and the research partners of the project.

Bibliography

- [1] Abraham, E. and Kerrigan, E. [2013], ‘Optimal active control and optimization of a wave energy converter’, *IEEE Transactions on Sustainable Energy* **4**(2), 324–332.
URL: <http://dx.doi.org/10.1109/TSTE.2012.2224392>
- [2] Andersen, P., Pedersen, T., Nielsen, K. and Vidal, E. [2015], Model predictive control of a wave energy converter, in ‘IEEE conference on control applications (CCA) - Sidney, NSW, Australia’, pp. 1540–1545.
URL: <https://dx.doi.org/10.1109/CCA.2015.7320829>
- [3] Astrom, K. and Hagglund, T. [2005], *Advanced PID Control*, 1st edn, ISA - The Instrumentation, Systems, and Automation Society, Research Triangle Park, NC 27709 (USA).
- [4] Athans, M. and Falb, P. L. [1966], *Optimal Control: An Introduction to the Theory and Its Applications*, McGraw-Hill Book Company, New York (USA).
- [5] Babarit, A. and Clément, A. [2006], ‘Optimal latching control of a wave energy device in regular and irregular waves’, *Applied Ocean Research* **28**(2), 77 – 91.
URL: <http://dx.doi.org/10.1016/j.apor.2006.05.002>
- [6] Babarit, A., Guglielmi, M. and Clément, A. H. [2009], ‘Declutching control of a wave energy converter’, *Ocean Engineering* **36**(12-13), 1015–1024.
URL: <http://dx.doi.org/10.1016/j.oceaneng.2009.05.006>
- [7] Bacelli, G. and Ringwood, J. [2015], ‘Numerical optimal control of wave energy converters’, *IEEE Transactions on Sustainable Energy* **294 - 302**(2), 294–302.
URL: <https://dx.doi.org/10.1109/TSTE.2014.2371536>
- [8] Benbouzid, H. and Benbouzid, M. [2014], Ocean wave energy extraction: Up-to-date technologies review and evaluation, in ‘International Power Electronics and Application Conference and Exposition’, Shangai (China), pp. 338–342.
URL: <https://dx.doi.org/10.1109/PEAC.2014.7037878>
- [9] Bilgen, E. and Boulos, R. [1973], ‘Functional dependence of torque coefficient of coaxial cylinders on gap width and reynolds numbers’, *ASME Journal of Fluids Engineering* **95**(1), 122–126.
URL: <https://dx.doi.org/10.1115/1.3446944>
- [10] Bonfanti, M., Sirigu, S., Bracco, G., Passione, B., Vissio, G., Pozzi, N. and Mattiazzo, G. [2017], Application of a passive control technique to the iswec, in A. Lewis, ed., ‘Proceedings of the Twelfth European Wave and Tidal Energy Conference’, EWTEC, University College Cork (Ireland), pp. 1137–1 – 1137–8.

- [11] Bracco, G. [2010], ISWEC: a gyroscopic wave energy converter, PhD thesis, Politecnico di Torino (Italy).
- [12] Bracco, G., Cagninei, A., Casassa, M., Giorcelli, E., Giorgi, G., Mattiazzo, G., Passione, B., Poggi, D., Raffero, M. and Vissio, G. [2014], 'Modeling and optimization of a wave energy converter using ANSYS AQWA', In: ANSYS User Group Meeting. pp. 79-86.
- [13] Bracco, G., Carillo, A., Giorcelli, E., Liberti, L., Mattiazzo, G., Prudentino, E., Sannino, G. and Vissio, G. [2015], Use of wave forecast for the regulation of ISWEC, in 'In Proceedings of the European Wave and Tidal Energy Conference EWTEC', Nantes (France), pp. 10B3-4-1 10B3-4-6. ISSN: 2309-1983.
- [14] Bracco, G., Casassa, M., Giorcelli, E., Giorgi, G., Mattiazzo, G., Passione, B., Raffero, M. and Vissio, G. [2015], *Application of sub-optimal control techniques to a gyroscopic Wave Energy Converter*, Renewable Energies Offshore, Taylor & Francis Group, London (UK), pp. 265-269.
URL: <https://dx.doi.org/10.1201/b18973-39>
- [15] Bracco, G., Giorcelli, E., Giorgi, G., Mattiazzo, G., Passione, B., Raffero, M. and Vissio, G. [2015], Performance assessment of the full scale ISWEC system, in 'Industrial Technology (ICIT), 2015 IEEE International Conference', Seville (Spain), pp. 2499-2505.
URL: <https://dx.doi.org/10.1109/ICIT.2015.7125466>
- [16] Bracco, G., Giorcelli, E. and Mattiazzo, G. [2008], One degree of freedom gyroscopic mechanism for wave energy converters, in 'ASME - International Design Engineering Technical Conferences and Computers and Information in Engineering Conference', Vol. 2, New York (USA), pp. 895-902.
URL: <https://dx.doi.org/10.1115/DETC2008-49847>
- [17] Bracco, G., Giorcelli, E. and Mattiazzo, G. [2011], 'Isvec: A gyroscopic mechanism for wave power exploitation', *Mechanism and Machine Theory - Elsevier* **46**, 1411-1424.
URL: <http://porto.polito.it/id/eprint/1847623>
- [18] Bracco, G., Giorcelli, E., Mattiazzo, G., Orlando, V. and Raffero, M. [2015], 'Hardware-in-the-loop test rig for the ISWEC wave energy system', *Mechatronics, Elsevier* **25**, 11 - 17.
URL: <https://dx.doi.org/10.1016/j.mechatronics.2014.10.007>
- [19] Bracco, G., Giorcelli, E., Mattiazzo, G., Passione, B., Prudentino, E., Raffero, M. and Vissio, G. [2015], Application of linear model predictive control to the ISWEC, in G. Soares, ed., 'Renewable Energies Offshore', Taylor & Francis Group, pp. 257-264.
URL: <https://doi.org/10.1201/b18973-38>
- [20] Bracco, G., Giorcelli, E., Mattiazzo, G., Pastorelli, M. and Taylor, J. [2009], ISWEC: design of a prototype model with a gyroscope, in 'International Conference on Clean Electrical Power (ICCEP)', Capri (Italy), pp. 57-63.
URL: <https://dx.doi.org/10.1109/ICCEP.2009.5212081>

- [21] Bracco, G., Vissio, G., Giorcelli, E., Valério, D. and Beirao, P. [2016], ISWEC control tuning: Lessons learned, in C. Soares, ed., '2nd International Conference on Renewable Energies Offshore - RENEW', Taylor & Francis Group, Lisbon (Portugal), p. 427–434.
URL: <https://dx.doi.org/10.1201/9781315229256-52>
- [22] Brekken, T. [2011], On model predictive control for a point absorber wave energy converter, in 'IEEE PowerTech', Trondheim (Norway), pp. 1–8.
URL: <https://dx.doi.org/10.1109/PTC.2011.6019367>
- [23] Brito e Melo, A. and Luis Villate, J. [2016], OES 2016 annual report, Technical report, Ocean Energy Systems (OES).
URL: <https://report2016.ocean-energy-systems.org/>
- [24] Bucher, R., Jeffrey, H., Bryden, I. and Harrison, G. [2016], 'Creation of investor confidence: The top-level drivers for reaching maturity in marine energy', *Renewable Energy, Elsevier* **88**, 120 – 129.
URL: <https://dx.doi.org/10.1016/j.renene.2015.11.033>
- [25] Budal, K. and Falnes, J. [1975], 'A resonant point absorber of ocean-wave power', *Nature - Nature Publishing Group* **256**, 478–479.
URL: <http://dx.doi.org/10.1038/256478a0>
- [26] Childs, P. [2010], *Rotating flow - 1st Edition*, Butterworth-Heinemann, London (UK).
- [27] Clerici, A., ed. [2016], *World Energy Perspective - Variable Renewables Integration in Electricity Systems: How to Get it Right*, World Energy Council, London (UK).
- [28] Commission, E. [2011], 'MARINET (MARine Renewables Infrastructure Network Technologies) project'. EU Seventh Framework Programme for research. Timeline 2011 to 2015. Funded under: FP7-INFRASTRUCTURES. Project ID: 262552.
- [29] Cox, P., Betts, R., Jones, C., Spall, S. and Totterdell, I. [2000], 'Acceleration of global warming due to carbon-cycle feedbacks in a coupled climate model', *Nature - Nature Publishing Group* **408**, 184–187.
URL: <https://dx.doi.org/10.1038/35041539>
- [30] Crowley, T. J. [2000], 'Causes of climate change over the past 1000 years', *Science - American Association for the Advancement of Science* **289**(5477), 270–277.
URL: <http://science.sciencemag.org/content/289/5477/270>
- [31] Cruz, J. [2008], *Ocean Wave Energy - Current Status and Future Perspectives*, Green Energy and Technology, Springer-Verlag Berlin Heidelberg, New York (USA).
- [32] Cummins, W. [1962], The impulse response function and ship motions, Technical Report 1661, Navy Department, David Taylor Model Basin, Maryland (USA).
URL: <http://hdl.handle.net/1721.3/49049>

- [33] De Chowdhury, S., Nader, J., Sanchez, A. and Manasseh, R. [2015], ‘A review of hydrodynamic investigations into arrays of ocean wave energy converters’, *arXiv* pp. 1–58.
URL: <https://arxiv.org/abs/1508.00866>
- [34] Drew, B., Plummer, A. and Sahinkaya, M. [2009], ‘A review of wave energy converter technology’, *Proceedings of the Institution of Mechanical Engineers, Part A: Journal of Power and Energy* **223**(8), 887–902.
URL: <http://dx.doi.org/10.1243/09576509JPE782>
- [35] Elhanafi, A., Fleming, A., Macfarlane, G. and Leong, Z. [2017], ‘Numerical hydrodynamic analysis of an offshore stationary–floating oscillating water column–wave energy converter using CFD’, *International Journal of Naval Architecture and Ocean Engineering - Elsevier* **9**(1), 77 – 99.
URL: <http://www.sciencedirect.com/science/article/pii/S2092678216304290>
- [36] European Commission [2012], ‘Communication from the commission to the european parliament, the council, the european economic and social committee and the committee of the regions: *Blue Growth, opportunities for marine and maritime sustainable growth*’, EU Publication Office.
- [37] European Commission [2017], ‘DTOcean project - (design and optimization tool for ocean arrays)’. EU Seventh Framework Programme for research, technological development and demonstration under grant agreement no 60859.
URL: <http://www.dtocean.eu/DTOcean-project>
- [38] European Commission - Directorate General for Maritime Affairs and Fisheries [2014], *Blue Energy - Action needed to deliver on the potential of ocean energy in European seas and oceans by 2020 and beyond*, EU publication Office.
URL: <https://dx.doi.org/10.2771/32703>
- [39] Falcao, A. [2010], ‘Wave energy utilization: A review of the technologies’, *Renewable and Sustainable Energy Reviews - Elsevier* **14**(3), 899 – 918.
URL: <http://dx.doi.org/10.1016/j.rser.2009.11.003>
- [40] Falnes, J. [2005], *Ocean Waves and Oscillating Systems - Linear Interactions Including Wave-Energy Extraction*, Cambridge University Press, Cambridge (UK).
- [41] Falnes, J. and Løvseth, J. [1991], ‘Ocean wave energy’, *Energy Policy - Elsevier* **19**(8), 768 – 775.
URL: [http://dx.doi.org/10.1016/0301-4215\(91\)90046-Q](http://dx.doi.org/10.1016/0301-4215(91)90046-Q)
- [42] Faltinsen, O. [1990], *Sea Loads on Ships and Offshore Structures*, Cambridge University Press, Cambridge (UK).
- [43] Folley, M., ed. [2016], *Numerical Modelling of Wave Energy Conversion - 1st Edition*, Academic Press, Massachusetts (USA).
- [44] *FORESEA (Funding Ocean Renewable Energy through Strategic European Action) project* [n.d.]. funded by Interreg NWE (North-West Europe) programme, Lead Partner Organisation The European Marine Energy Centre Limited (EMEC), Timeline 2016-2019.

- URL:** <http://www.nweurope.eu/projects/project-search/funding-ocean-renewable-energy-through-strategic-european-action/>
- [45] Fossen, T. [2011], *Handbook of Marine Craft Hydrodynamics and Motion Control*, first edn, John Wiley & Sons Ltd, New Jersey (USA).
- [46] Fusco, F. and Ringwood, J. [2010], ‘Short-term wave forecasting for real-time control of wave energy converters’, *Sustainable Energy, IEEE Transactions* **1**(2), 99–106.
URL: <https://dx.doi.org/10.1109/TSTE.2010.2047414>
- [47] Google Maps [2017]. www.google.maps.com, [Accessed: 14/07/2017].
- [48] Gunn, K. and Stock-Williams, C. [2012], ‘Quantifying the global wave power resource’, *Renewable Energy - Elsevier* **44**, 296 – 304.
URL: <https://dx.doi.org/10.1016/j.renene.2012.01.101>
- [49] Hals J., Falnes J., M. T. [2010], ‘Constrained optimal control of a heaving buoy wave-energy converter’, *Journal Offshore Mechanics and Arctic Engineering - ASME* **133**(1), 011401 1–15.
URL: <https://dx.doi.org/10.1115/1.4001431>
- [50] Holmes, B. [2003], Ocean energy: Development and evaluation protocol. part 1: Wave power., Technical report, HMRC - Marine Institute, Cork (Ireland).
- [51] Hong, Y., Waters, R., Boström, C., Eriksson, M., Engström, J. and Leijon, M. [2014], ‘Review on electrical control strategies for wave energy converting systems’, *Renewable and Sustainable Energy Reviews - Elsevier* **31**, 329 – 342.
URL: <http://www.sciencedirect.com/science/article/pii/S1364032113008022>
- [52] Honkasalo, N. [2015], Power statistics and trends: The five dimensions of the energy union, Techno-economical report, Eurelectric, Brussels (Belgium).
URL: <http://www.eurelectric.org>
- [53] Hoskin, R. and Nichols, N. [1986], Latching control of a point absorber, in ‘3rd International Symposium on Wave, Tidal, OTEC and Small Scale Hydro Energy’, The Fluid Engineering Centre, Bedford (UK), pp. 317–330.
- [54] International Energy Agency [2016], *Key world energy statistic - 2016*, OECD/IEA, Paris (France). [Accessed: 13/07/2017].
URL: <https://www.iea.org/publications/freepublications/>
- [55] Jones, C., Magalen, J. and Roberts, J. [2014], WEC array effects on wave, current and sediment circulation: Monterey bay, CA, Technical report, Sandia National Laboratories, California (USA). SAND 2014-17401.
- [56] Kassem, A. M., Besheer, A. H. and Abdelaziz, A. Y. [2015], ‘A linear quadratic gaussian approach for power transfer maximization of a point absorber wave energy converter’, *Electric Power Components and Systems - Taylor and Francis* **43**(8-10), 1173–1181.
URL: <http://dx.doi.org/10.1080/15325008.2015.1010048>

- [57] Keane, K. [2017], ‘Last turbine for first full-scale floating offshore wind farm installed [online]’, *BBC News*. Available from: <http://www.bbc.com/news/uk-scotland-north-east-orkney-shetland-40947146> [Accessed: 18/08/2017].
- [58] Kempener, R. and Neumann, F. [2014a], Ocean thermal energy conversion. technology brief, Technical report, International Renewable Energy Agency, Abu Dhabi (UAE).
URL: <http://www.irena.org/DocumentDownloads/Publications/>
- [59] Kempener, R. and Neumann, F. [2014b], Tidal energy. technology brief, Technical report, International Renewable Energy Agency, Abu Dhabi (UAE).
URL: <http://www.irena.org/DocumentDownloads/Publications/>
- [60] Kempener, R. and Neumann, F. [2014c], Wave energy. technology brief, Technical report, International Renewable Energy Agency, Abu Dhabi (UAE).
URL: <http://www.irena.org/DocumentDownloads/Publications/>
- [61] Korde, U. A. [2016], *Hydrodynamic Control of Wave Energy Devices*, Cambridge University Press, Cambridge (UK).
URL: <https://dx.doi.org/10.1017/CBO9781139942072>
- [62] Lagarias, J., Reeds, J., Wright, M. and Wright, P. [1998], ‘Convergence properties of the nelder-mead simplex method in low dimensions.’, *SIAM Journal of Optimization* **9**, 112–147.
URL: <https://doi.org/10.1137/S1052623496303470>
- [63] Lange, R. [2015], FTA and FMEA applied to ISWEC, Master’s thesis, Politecnico di Torino (Italy).
- [64] Levine, W. S., ed. [2010], *The Control Handbook, Second Edition*, Electrical Engineering Handbook, Taylor & Francis - CRC Press, New York (USA).
URL: <https://dx.doi.org/10.1201/b10382>
- [65] Lewis, F. L., Vrabie, D. L. and Syrmos, V. L. [2012], *Optimal Control of Continuous-Time Systems, in Optimal Control*, John Wiley & Sons, Inc., Hoboken, NJ (USA), chapter 3, pp. 110–176.
URL: <http://dx.doi.org/10.1002/9781118122631.ch3>
- [66] Li, Y. and Yu, Y. [2012], ‘A synthesis of numerical methods for modeling wave energy converter point absorbers’, *Renewable and Sustainable Energy Reviews - Elsevier* **16**(6), 4352–4364.
URL: <https://dx.doi.org/10.1016/j.rser.2011.11.008>
- [67] López, I., Andreu, J., Ceballos, S., de Alegría, I. M. and Kortabarria, I. [2013], ‘Review of wave energy technologies and the necessary power-equipment’, *Renewable and Sustainable Energy Reviews - Elsevier* **27**, 413 – 434.
URL: <http://dx.doi.org/10.1016/j.rser.2013.07.009>
- [68] Mattiazzo., G. and Giorcelli, E. [2007], Mathematical model of a energy converter from sea waves, in ‘World Energy Congress’, Rome (Italy).

- [69] Medhaug, I., Stolpe, M., Fischer, E. and Knutti, R. [2016], ‘Reconciling controversies about the global warming hiatus’, *Nature - Nature Publishing Group* (545), 41–47.
URL: <https://dx.doi.org/10.1038/nature22315>
- [70] Mofor, L., Goldsmith, J. and Jones, F. [2014], Ocean energy. technology readiness, patents, deployment status and outlook, Technical report, International Renewable Energy Agency, Abu Dhabi (UAE).
URL: <http://www.irena.org/DocumentDownloads/Publications/>
- [71] Paparella, F., Monk, K., Winands, V., Lopes, M., Conley, D. and Ringwood, J. [2015], ‘Up-wave and autoregressive methods for short-term wave forecasting for an Oscillating Water Column’, *IEEE Transactions on Sustainable Energy* 6(1), 171–178.
URL: <http://dx.doi.org/10.1109/TSTE.2014.2360751>
- [72] Pecher, A. [2016], *Experimental Testing and Evaluation of WECs*, Vol. 7 of *Ocean Engineering and Oceanography*, Springer, chapter 9, pp. 221–260.
URL: https://dx.doi.org/10.1007/978-3-319-39889-1_9
- [73] Penalba, M., Giorgi, G. and Ringwood, J. V. [2017], ‘Mathematical modelling of wave energy converters: A review of nonlinear approaches’, *Renewable and Sustainable Energy Reviews - Elsevier* 78, 1188 – 1207.
URL: <http://www.sciencedirect.com/science/article/pii/S1364032116308784>
- [74] Perez, T. and Fossen, T. [2008], ‘Time- vs. frequency-domain identification of parametric radiation force model for marine structures at zero speed’, *Modeling, Identification and Control: A Norwegian Research Bulletin* 29(1), 1–19.
URL: <https://dx.doi.org/10.4173/mic.2008.1.1>
- [75] Petruzzi, C. [2016], Control of a gyroscopic wave energy converter, Master’s thesis, Politecnico di Torino (Italy).
- [76] Pinkster, J. [1980], Low Frequency Second Order Wave Exciting Forces On Floating Structures, PhD thesis, Delft University of Technology, Delft (Netherlands).
- [77] Pozzi, N., Castino, A., Vissio, G., Passione, B., Sirigu, S., Bracco, G. and Mattiazzo, G. [2017], Experimental validation of different hydrodynamic modelling techniques applied to the ISWEC, in A. Lewis, ed., ‘Proceedings of the Twelfth European Wave and Tidal Energy Conference’, EWTEC, University College Cork (Ireland), pp. 1110–1–1110–10. ISSN: 2309-1983.
- [78] Raffero, M. [2014], Design of a Wave Energy Converter - a case of application: ISWEC, PhD thesis, Politecnico di Torino (Italy).
- [79] Raffero, M., Bracco, G., Passione, B., Vissio, G., Mattiazzo, G. and Giorcelli, E. [2015], Identification of the hydrodynamic parameters of a wave energy converter, in ‘In Proceedings of the European Wave and Tidal Energy Conference EWTEC’, Nantes (France), pp. 09C1–3–1 09C1–3–10. ISSN: 2309-1983.
- [80] Raffero, M. and Vissio, G. [2015], ISWEC hydrodynamic model validation, Technical report, MARINET Infrastructure Access Report.
URL: www.marinet2.eu/wp-content/uploads/2017/04/ISWEC_HMRC.pdf

- [81] Retes, M. P., Giorgi, G. and Ringwood, J. [2015], A review of non-linear approaches for wave energy converter modelling, *in* 'In Proceedings of the European Wave and Tidal Energy Conference EWTEC', European Wave and Tidal Energy Conference 2015, Nantes (France), pp. 08C1–3 1–10.
- [82] Ringwood, J., Bacelli, G. and Fusco, F. [2014], 'Energy-maximizing control of wave-energy converters: The development of control system technology to optimize their operation', *IEEE Control Systems* **34**(5), 30–55.
URL: <https://dx.doi.org/10.1109/MCS.2014.2333253>
- [83] Salter, S. [1974], 'Wave power', *Nature - Nature Publishing Group* (249), 720–724.
URL: <https://dx.doi.org/10.1038/249720a0>
- [84] Saupe, F., Gilloteaux, J.-C., Bozonnet, P., Creff, Y. and Tona, P. [2014], Latching control strategies for a heaving buoy wave energy generator in a random sea, *in* '19th IFAC World Congress', Vol. 47, Cape Town, (South Africa), pp. 7710 – 7716.
URL: <http://www.sciencedirect.com/science/article/pii/S1474667016428272>
- [85] Schlichting, H. and Gersten, K. [1987], *Fluid mechanics*, Pergamon Press, New York (USA).
- [86] Scruggs, J. [2011], Multi-objective optimal causal control of an ocean wave energy converter in random waves, *in* 'IEEE Oceanic Engineering Society - OCEANS Conference', Waikoloa, HI (USA), pp. 1–6.
URL: <https://dx.doi.org/10.1016/j.apor.2013.03.004>
- [87] Scruggs, J., Lattanzio, S., Taflanidis, A. and Cassidy, I. [2013], 'Optimal causal control of a Wave Energy Converter in a random sea', *Applied Ocean Research - Elsevier* **42**, 1–15.
URL: <https://dx.doi.org/10.1016/j.apor.2013.03.004>
- [88] Secretariat REN21 [2017], *Renewables 2017 Global Status Report*, REN21, Paris (France).
- [89] Sharkey, F., Conlon, M. and Gaughan, K. [2012], Practical analysis of key electrical interfaces for wave energy converter arrays, *in* '4th International Conference on Ocean Energy ICOE', Dublin (Ireland).
- [90] Sirigu, S. A., Vissio, G., Bracco, G., Giorcelli, E., Passione, B., Raffero, M. and Mattiazzo, G. [2016], 'ISWEC design tool', *International Journal of Marine Energy* **15**, 201 – 213. Selected Papers from the European Wave and Tidal Energy Conference 2015, Nantes (France).
URL: <http://dx.doi.org/10.1016/j.ijome.2016.04.011>
- [91] Sirigu, S., Vissio, G., Bracco, G., Dafnakis, P., Passione, B., Pozzi, N. and Mattiazzo, G. [2017], A performance assessment methodology for floating pitching WEC arrays, *in* A. Lewis, ed., 'Proceedings of the Twelfth European Wave and Tidal Energy Conference', EWTEC, University College Cork (Ireland), pp. 1109–1–1109–8. ISSN: 2309-1983.

- [92] Sørensen, B. [1991], 'A history of renewable energy technology', *Energy Policy - Elsevier* **19**(1), 8 – 12.
URL: <http://www.sciencedirect.com/science/article/pii/030142159190072V>
- [93] Theodorsen, T. and Regier, A. [1944], Experiments on drag of revolving disks, cylinders, and streamline rods at high speeds, Technical Report NACA-TR-793, National Advisory Committee for Aeronautics. Langley Aeronautical Lab, Langley Field, VA (USA).
- [94] Thomas, C., Cameron, A., Green, R., Bakkene, M., Beaumont, L., Collingham, Y., Erasmus, B., de Siqueira, M. F., Grainger, A., Hannah, L., Hughes, L., Huntley, B., van Jaarsveld, A., FMidgley, G., Miles, L., Ortega-Huerta, M. A., Peterson, A. T., Phillips, O. L. and Williams, S. E. [2004], 'Extinction risk from climate change', *Nature - Nature Publishing Group* (427), 145–148.
URL: <https://dx.doi.org/10.1038/nature02121>
- [95] Tollefson, J. [2014], 'Power from the oceans: Blue energy', *Nature - Nature Publishing Group* **508**, 302 – 304.
URL: <http://dx.doi.org/10.1038/508302a>
- [96] Tucker, M. and Pitt, E., eds [2001], *Waves in Ocean Engineering*, Vol. 5 of *Elsevier Ocean Engineering*, 1st edn, Elsevier Science, New York (USA).
- [97] Turkenburg, W., Arent, D., Bertani, R., Faaij, A., Hand, M., Krewitt, W., Larson, E., Lund, Mehos, M., Merrigan, Mitchell, C., Moreira, J., Sinke, W., Sonntag, V., Thresher, B., VanSark, W. and Usher, E. [2012], *Global Energy Assessment - Toward a Sustainable Future*, Cambridge University Press, Cambridge (UK) and New York, NY (USA) and the International Institute for Applied Systems Analysis, Laxenburg (Austria), chapter 11 - Renewable Energy.
URL: <http://doi.org/10.1017/CBO9780511793677>
- [98] United Nations [1992], 'United nations framework convention on climate change'. 1771 UNTS 107; S. Treaty Doc No. 102-38; U.N. Doc. A/AC.237/18 (Part II)/Add.1; 31 ILM 849, [Accessed: 16/07/2017].
URL: <https://unfccc.int/resource/docs/convkp/conveng.pdf>
- [99] United Nations [1998], 'Kyoto protocol to the united nations framework convention on climate change'. UN Doc FCCC/CP/1997/7/Add.1, [Accessed: 18/07/2017].
URL: <https://unfccc.int/resource/docs/convkp/kpeng.pdf>
- [100] Valério, D., Beirao, P., Vissio, G., Bracco, G. and Mattiazzo, G. [2016], Tuning a linear quadratic regulator for point absorber wave energy converters, in C. G. Soares, ed., '2nd International Conference on Renewable Energies Offshore - RENEW', Taylor & Francis Group, p. 421–426.
URL: <https://dx.doi.org/10.1201/9781315229256-51>
- [101] Vissio, G., Passione, B., Di Carlo, C., Bracco, G., Giorcelli, E., Mattiazzo, G., Raffero, M. and Sirigu, S. [2015], ISWEC design tool, in 'In Proceedings of the European Wave and Tidal Energy Conference - EWTEC', Nantes (France), pp. 09B1–3–1 09B1–3–9. ISSN: 2309-1983.

- [102] Vissio, G., Passione, B., Hall, M. and Raffero, M. [2015], Expanding ISWEC modelling with a lumped-mass mooring line model, *in* 'In Proceedings of the European Wave and Tidal Energy Conference EWTEC', Nantes (France), pp. 09B1-4-1 09B1-4-9. ISSN: 2309-1983.
- [103] Vissio, G., Valério, D., Bracco, G., Beirao, P., Pozzi, N. and Mattiazzo, G. [2017], 'ISWEC: linear quadratic regulator oscillating control', *Renewable Energy - Elsevier* (103), 372-282.
URL: <https://10.1016/j.renene.2016.11.046>
- [104] Wang, L., Isberg, J. and Tedeschi, E. [2018], 'Review of control strategies for wave energy conversion systems and their validation: the wave-to-wire approach', *Renewable and Sustainable Energy Reviews - Elsevier* **81**(1), 366 – 379.
URL: <http://www.sciencedirect.com/science/article/pii/S136403211731016X>
- [105] WMO [1998], *Guide to Wave Analysis and Forecasting*, number WMO-No.702, 2nd edn, Secretariat of the World Meteorological Organization, Geneva (Switzerland).
- [106] Wolgamot, H. and Fitzgerald, C. [2014], 'Nonlinear hydrodynamic and real fluid effects on wave energy converters', *Proceedings of the Institution of Mechanical Engineers, Part A: Journal of Power and Energy - SAGE* **229**(7), 772-794.
URL: <https://doi.org/10.1177/0957650915570351>